Investigation of the heat transfer enhancement effects of nanofluids in process heating and cooling.

A thesis

submitted in fulfilment

of the requirements for the degree

of

Doctor of Philosophy in Engineering

at

The University of Waikato

by

ABDUL KAGGWA

THE UNIVERSITY OF
WAIKATO
Te Whare Wānanga o Waikato

2022

“Mukutya katonda ensibuko y’amagezi gyegasookera”.

Mukama katonda oli w’abuyinza! N’eyanzizza neyanzegge. Ebyawandiikibwa bigamba nti “abamanyi tebenkana n’abatamanyi” era bbajajjaffe b’alugera nti “obutasoma buluma bukulu”.

Mukama katonda nannyini ggulu n’ensi eno, n’eyanzizza nnyo olwobuwanguzi bwontusizaako.

Ayi mukama katonda! nkusaba okusoma kuno, n’amagezi gompadde awamu nebyo byonna ebirungi byenjize biyambe, era bibeere byamugaso nnyo eri nze kamwa koogera, amakagaange, abantu bange n’ensi yonna okutwaliza awamu.

Ndi mufirika, munnaUganda, Omuganda asibuka e Masaka-Bukomansimbi, ekyalo kiguŋŋumika.

Rose Naluyima

Maama omulungi anzala, Mukama akuwe ekiwumulo ekyemirembe.

Abstract

The global energy system faces a dual challenge; the need for more energy and less carbon emission. Out of the 50 billion tonnes of greenhouse gases emitted each year, 24.2 % comes from energy use in industries such as processing and manufacturing that require constant heating and cooling. Heat transfer improvements in heating and cooling industries cause energy saving thus reducing operational costs, increase the operational life of heat transfer systems and reducing greenhouse gas emissions. While nanofluids usage in heat exchangers presents a critical step for emission reduction, several factors including instability of suspended nanoparticles, the effect of a surfactant on physical property measurements and combining nanofluids with inserts have not been adequately assessed.

This thesis investigates the use of highly conductive nanofluids as a potential alternative to conventional working fluids with low thermal conductivity, such as water, currently used in heat exchangers for heating and cooling systems. A distinguishing feature of this study is the consideration of the effect of surfactants on the stability of nanofluids, the physical properties of the nanofluids and the thermal performance of the nanofluids. The use of nanofluids in combination with hiTRAN® heat transfer inserts was also investigated.

Activated carbon (C), copper oxide (CuO) and alumina (Al_2O_3) nanoparticles were suspended in distilled water (H_2O) and Ethylene glycol (EG). Surfactants were added including sodium dodecyl benzene sulfonate (SDBS), cetyltrimethyl ammonium bromide (CTAB), sodium lauryl sulphate (SDS) and Arabinogalactan (ARB) to create 20 combinations of nanofluids.

ARB as a surfactant kept C/H_2O and CuO/EG nanofluid stable for 29 days. Whereas CTAB and SDBS surfactants kept C/H_2O and Al_2O_3/H_2O nanofluids stable for 17 and 11 days respectively. Viscosity results showed that in some cases the surfactant caused a slight increase in viscosity and in some cases viscosity decreased. Thermal conductivity results showed that it is difficult to get repeatable measurements, and that may explain why there is such variation in the reported literature.

Out of the 20 combinations of nanofluids prepared, Al_2O_3/H_2O, C/H_2O/CTAB and CuO/H_2O/ARB combinations of nanofluids were selected because they were relatively stable with low viscosity, and were tested with and without hiTRAN® inserts in a double-pipe heat exchanger test rig. The experimental data was subsequently used in the

evaluation of nanofluids overall heat transfer coefficients, pressure drop, friction factor and thermal performances. In terms of heat transfer enhancement, the individual effects of nanofluids and inserts appeared to be additive. However, the pressure drop of the inserts was significantly greater than the nanofluids. The system with both nanofluids and inserts was able to achieve higher heat transfer coefficients at lower Reynolds numbers than the system without inserts; however, with inserts the Reynolds numbers that could be achieved were lower than for the system without inserts. As a consequence, when the system was operated at full pumping speed nanofluids with inserts yielded similar heat transfer coefficients compared to nanofluids alone.

The C/H_2O/CTAB nanofluid consistently had the best performance of the three nanofluids considered both with and without inserts, and it is believed that with higher concentrations of nanoparticles, C/H_2O/CTAB could achieve greater than 100 % thermal performance values. However, during nanofluids testing, it was difficult to reuse and replace nanofluids. Cleaning and removing all the nanoparticles in the test-loop was practically challenging because there was more sedimentation mostly for Al_2O_3/H_2O nanofluid which had no surfactant.

Acknowledgements

First of all, I thank my Chief supervisor, Associate Prof. James K. Carson, for the support and guidance throughout this PhD. I also thank my co-supervisors Dr. Martin J. Atkins, Dr. Amir H. Tarighaleslami and Prof. Michael R. Walmsley; Your support toward this thesis is greatly appreciated.

I must acknowledge the University of Waikato for the award of a three years Doctoral Scholarship. Finance-wise this was a huge great peace of mind.

I would also like to take this opportunity to thank Mr. Martin Gough and Dr.-Ing. Peter Droegemueller from Calgavin LTD for providing the tube inserts.

I greatly acknowledge the numerous other staff members, both technical and administrative, at the University of Waikato that have helped during the course of my doctorate and thank them for their efforts. A big thank you goes to all my friends at the University of Waikato, the list is too long to mention each by name but you know who you are.

To my distant relatives in Uganda and friends in several countries across the globe, thanks for the interesting conversations that sometimes boosted my morale.

Lastly but most certainly not least I have to thank my wonderful, incredible wife Ssu for taking good care of our son Yan-Lee Kaggwa; and giving me all the time that I needed to focus on this PhD. The last few years of this PhD study have not only been emotionally draining on me, but also on you, so I thank you for being my sounding board and supporting me unconditionally.

List of Publications

This research has produced articles listed below; published in scientific journals.

A. Kaggwa., J.K. Carson., M. Atkins., M. Walmsley. The effect of surfactants on viscosity and stability of activated carbon, alumina and copper oxide nanofluids. Mater. Today Proc. 18, 510–519 (2019). doi:10.1016/j.matpr.2019.06.240

A. Kaggwa., J.K. Carson. Developments and future insights of using nanofluids for heat transfer enhancements in thermal systems : a review of recent literature. Int. Nano Lett. (2019). doi:10.1007/s40089-019-00281-x

A. Kaggwa, J.K. Carson, M. Atkins, M. Walmsley, 2018, *Physical Properties and Rheological Characteristics of Activated Carbon Nanofluids with Varying Filler Fractions and Surfactants*, Applied Mechanics and Materials, vol. 884, pp. 58-65, doi 10.4028/www.scientific.net/AMM.884.58

Table of Contents

Abstract i
Acknowledgements iii
Table of Contents v
List of Figures x
List of Tables xv
Nomenclature xvii
Chapter 1 Introduction 1
1.1 Introduction 1
1.2 Research Aims 3
1.3 Thesis Structure 4
Chapter 2 Literature Review 5
2.1 Introduction 5
2.2 Background of Nanofluids 6
2.3 Potential applications of Nanofluids 8
2.3.1 Electronics cooling 8
2.3.2 Automobile industry 8
2.3.3 Boilers and Nuclear reactors 8
2.3.4 Oil filled space heaters 9
2.3.5 Solar Application 9
2.3.6 Nanorefrigerants 10
2.3.7 Biomedical applications 13
2.4 Preparation of nanofluids 13
2.5 Mechanism of heat transfer enhancement in nanofluids. 14
2.6 Thermophysical-properties of nanofluids 16
2.6.1 Thermal conductivity 16
2.6.2 Viscosity 19
2.7 Inserts with nanofluids in heat exchangers 21
2.8 Current challenges of Nanofluids as a heat transfer fluid 24
2.9 Conclusion 26
Chapter 3 Preparation and Stability Assessment of Nanofluids 28

3.1 Introduction 28
3.2 Nanofluid preparation 28
3.2.1 Nanomaterials. 29
3.2.2 Base fluids 30
3.2.3 Surfactant selection. 30
3.2.4 Preparation process 31
3.3 Stability measurements 32
3.3.1 Zeta-potential 32
3.3.2 UV-vis spectroscopy 33
3.3.3 Electron microscopy 33
3.3.4 Sedimentation 34
3.4 Measurement procedure 34
3.5 Results and discussion 35
3.6 Conclusion 38
Chapter 4 Physical property measurement of nanofluids 40
4.1 Introduction 40
4.2 Viscosity 41
4.2.1 Measurements and data analysis 41
4.2.2 Results and Discussion 43
4.3. Thermal conductivity 48
4.2.3 Measurement procedure of nanofluid using a probe. 50
4.2.4 Measurement procedure of nanofluids using TC-30™ device 56
4.2.5 Results and Discussion 57
4.3 Selection of nanofluids tested for heat transfer in the rig. 59
4.4 Density 60
4.4.1 True density of nanoparticles 60
4.4.2 Density of water/surfactant mixtures 60
4.5 Specific heat capacity 62
4.6 Conclusion 63
Chapter 5 Instrumentation, Experimental set-up and Heat transfer Measurements 65
5.1 Introduction 65
5.2 Experimental setup 66
5.3 Instruments and devices. 67

5.3.1 Double pipe heat exchangers. 67
5.3.2 Rig support Stand 68
5.3.3 Cooling Source 68
5.3.4 Heating Source....69
5.3.5 Temperature measurement....70
5.3.6 Pumps 70
5.3.7 Flow measurement....71
5.3.8 Differential pressure measurement 71
5.3.9 Data logger....71
5.4 Experimental procedure 74
5.4.1 Raw data processing 74
5.5 Calculations for heat transfer analysis 76
5.5.1 Uncertainty analysis....78
5.6 Performance evaluation of nanofluids....79
Chapter 6 Experimental evaluation of the performance of Al_2O_3/H_2O, C/H_2O/CTAB and CuO/H_2O/ARB nanofluids. 83
6.1 Introduction 83
6.2 Water as a base case. 85
6.2.1 Heat transfer....86
6.2.2 Pressure Drop....90
6.3 Nanofluids 91
6.3.1 Al_2O_3/H_2O nanofluid 92
6.3.2 CuO/H_2O/ARB Nanofluid 94
6.3.3 C/H_2O/CTAB Nanofluid 95
6.4 Comparison of heat transfer, pressure drop and friction factor of nanofluids to water 97
6.4.1 Heat transfer of nanofluids compared to water....97
6.4.2 Friction factor and pressure drop of nanofluids and water 98
6.5 Practical Challenges associated with nanofluids....100
6.6 Performance evaluation of Al_2O_3/H_2O, C/H_2O/CTAB and CuO/H_2O/ARB nanofluids 101
6.7 Conclusion....104
Chapter 7 Experimental heat transfer evaluation of nanofluids combined with hiTRAN® inserts. 105
7.1 Introduction 105

7.2 hiTRAN® inserts 106
7.2.1 Installation of hiTRAN® inserts in heat exchangers 106
7.3 Water combined with inserts 108
7.3.1 Heat transfer 108
7.3.2 Pressure drop 109
7.4 Nanofluids 110
7.4.1 Al_2O_3/H_2O nanofluid and inserts 110
7.4.2 CuO/H_2O/ARB nanofluids and inserts 112
7.4.3 C/H_2O/CTAB nanofluids and inserts 113
7.5 Comparison of heat transfer, pressure drop and friction factor of nanofluids with inserts to water with inserts 114
7.5.1 Heat transfer of nanofluids with inserts compared to water with inserts 114
7.5.2 Friction factor and pressure drop of nanofluids with inserts and water with inserts 115
7.6 Comparison of heat transfer, pressure drop and friction factor of nanofluids combined with inserts, and without inserts 116
7.6.1 Heat transfer of nanofluids with and without inserts 116
7.6.2 Pressure drop and friction factor of nanofluids with and without inserts 118
7.7 Thermal performance of Al_2O_3/H_2O, C/H_2O/CTAB and CuO/H_2O/ARB nanofluids combined with inserts 120
7.8 Comparison of heat transfer, pressure drop and thermal performance at full pumping speed. 121
7.9 Conclusion 124
Chapter 8 Conclusions and recommendations 125
8.1 Conclusions 125
8.2 Contributions 127
8.3 Recommendations for future work 128
References 129
Appendix A Published Articles 154
Appendix B Characterisation and physical property measurements 155
B.1 Introduction 155
B.2 Stability 155
B.3 Viscosity 156
B.4 Specific heat capacity 160
Appendix C Experimental devices and calibration 163

C.1 Introduction....163
C.2 Thermocouples....163
C.3 Flow meters....165
C.4 Pressure differential transmitter....166
C.5 Heat exchanger....167
C.6 Rig support stand construction....169
Appendix D Measurement procedure....170
D.1 Introduction....170
D.2 Data procedure and processing....170
D.3 Uncertainty analysis....173
D.4 Uncertainty in heat transfer rate measurements....174
D.5 Uncertainty in overall heat transfer measurements....175
D.6 Uncertainty in friction factor....176
D.7 Standard operation procedure....177

List of Figures

Figure 1.1 Primary energy demand and carbon emissions 1

Figure 1.2 World population prospects 2

Figure 2.1 Thermal Conductivity of some heat transfer materials 6

Figure 2.2(a) Thermal conductivity as a function of nanoparticle volume fraction 11

Figure 2.3 Methods of nanofluids preparation. 14

Figure 2.4 Free body diagram of particle (P.2) neglecting thermophoresis force. 15

Figure 2.5 Nanoparticle interaction under the cross coupling of thermal motion and electric field. 15

Figure 2.6 The effect of nanoparticle concentration on thermal conductivity using different models 19

Figure 2.7 The effect of nanoparticle concentration on viscosity using different models 20

Figure 2.8 Common types of inserts used to enhance heat transfer. 22

Figure 2.9 Suspension and stability of nanoparticles. 25

Figure 2.10 Structure of nanoparticle in the base fluid. Molecules of the liquid (1) can form a specific, highly ordered layer (2) near the nanoparticle surface (3). 25

Figure 3.1 Transmission electron microscopic (TEM) images of (a) activated carbon, (b) copper oxide and (c) alumina nanoparticles 29

Figure 3.2 Nanofluids preparation process. 32

Figure 3.3 Fresh stable nanofluid on the day of preparation (a) and (b) variation of sediment height after time. 34

Figure 3.4 Samples of nanofluid with varying surfactants immediately after preparation. 35

Figure 3.5 Samples of nanofluid with varying surfactants after 30 days. 36

Figure 3.6 Stability timeline of nanofluids with water as base fluid. 37

Figure 3.7 Stability timeline of nanofluids with ethylene glycol as base fluid. 38

Figure 4.1 Viscometer and water bath. 41

Figure 4.2 The effect of surfactants on viscosity measurements of nanofluids with EG as base fluid at $T = 25°C$. 43

Figure 4.3 Viscosity measurements as a function of shear rate for nanofluids with water as base fluid at $T = 25$ °C. 45

Figure 4.4 A comparison of viscosity measurements on the day of preparation and seven weeks later for: (a) C/H_2O, (b) CuO/H_2O and (C) Al_2O_3/H_2O nanofluids. 47

Figure 4.5 A comparison of measured thermal conductivity of Al_2O_3/H_2O nanofluid 49

Figure 4.6 A comparison of measured thermal conductivity of CuO/H_2O nanofluid 49

Figure 4.7 Thermal conductivity probe. 50

Figure 4.8 Schematic diagram of the thermal sensor probe. 51

Figure 4.9 An electric circuit diagram of TP08 thermal sensor housed in the box. 52

Figure 4.10 Schematic diagram of thermal conductivity measurement. 52

Figure 4.11 full set of 4 replicates in one measurement, (b) the first test out of 4, (C) selected data range based on the variance to determine final thermal conductivity 54

Figure 4.12 A comparison between measured thermal conductivity and literature values of deionized water and ethylene glycol using transient hot-wire technique. 55

Figure 4.13 Unidirectional (a) and (b) planar directional heat transfer 56

Figure 4.14 Thermal conductivity measurements procedures using TC-30™ device. 56

Figure 4.15 A comparison of measured thermal conductivity of Al_2O_3/H_2O nanofluid 58

Figure 4.16 A comparison of measured thermal conductivity of CuO/H_2O nanofluid 59

Figure 4.17 Density measurements of ARB surfactants. 61

Figure 4.18 Density measurements of CTAB surfactants. 61

Figure 4.19 Sample preparation process to measure specific heat capacity in DSC 62

Figure 5.1 Schematic diagram of the closed flow loop 66

Figure 5.2 Schematic diagram (a) and (b) real double pipe heat exchangers. 67

Figure 5.3 Rig support stand and its dimensions. 68

Figure 5.4 Cold water tank 69

Figure 5.5 Composition of the thermal tank including: (a) heating coil (b) installed coil inside the tank (c) insulated tank 69

Figure 5.6 Thermocouple calibration (a) water bath method and (b) ice point method. 70

Figure 5.7 (a) DAQ 34970A and (b) 20 channel armature multiplexer module. 72

Figure 5.8 Front and back view of the real experimental rig. 73

Figure 5.9 Recorded raw data from the logger 75

Figure 5.10 Processed data belonging to similar tube-side flow rate (50.0 l/min)..... 76

Figure 6.1 A comparison of experimental Nusselt number against Reynolds number for Al_2O_3/H_2O nanofluid..... 84

Figure 6.2 Measured tube and shell-side overall heat transfer coefficients for water 86

Figure 6.3 Comparison between h_i measured and predicted. 88

Figure 6.4 Shows h_o calculated from U_i when Gnielinski correlation is used for h_i 89

Figure 6.5 Comparison between U_i Measured and that predicted using h_o from Dirker et al. proposed correlation and h_i from Gnielinski correlation. 89

Figure 6.6 Test results for measured and predicted data of friction factor. 91

Figure 6.7. Heat transfer of Al_2O_3/H_2O nanofluids compared to water 92

Figure 6.8. A comparison of heat transfer present results for Al_2O_3/H_2O nanofluid with that from Sonowane et al. 93

Figure 6.9. Pressure drop and friction factor of Al_2O_3/H_2O compared to deionised water. 94

Figure 6.10. Heat transfer of CuO/H_2O/ARB nanofluids compared to water 94

Figure 6.11. Pressure drop and friction factor of CuO/H_2O/ARB compared to water 95

Figure 6.12. Heat transfer of C/H_2O/CTAB nanofluids compared to water 96

Figure 6.13. Pressure drop and friction factor of C/H_2O/CTAB compared to water. 96

Figure 6.14. Comparison of nanofluid heat transfer enhancement to deionized water 97

Figure 6.15 Friction against Reynolds number for nanofluids 98

Figure 6.16. Effect of Pressure drop on nanofluids compared to water 99

Figure 6.17 Thermal performance of nanofluids calculated using Web and Kim's method. 101

Figure 6.18 Thermal performance of nanofluids calculated directly using measured heat transfer and friction factor ratios. 102

Figure 7.1. hiTRAN® inserts. 106

Figure 7.2. hiTRAN® insert and the tools used during installation process 107

Figure 7.3 Installed insert in a heat exchanger. 108

Figure 7.4. A comparison of U_i before and after the installation of inserts 109

Figure 7.5. Measured pressure drop and calculated friction factor for water combined with inserts 109

Figure 7.6. A comparison pressure drop and friction factor for water before and after installation of inserts 110

Figure 7.7. Heat transfer of Al_2O_3/H_2O nanofluids with inserts compared to water with inserts 111

Figure 7.8. Pressure drop and friction factor of Al_2O_3/H_2O with inserts compared to deionised water with inserts. 111

Figure 7.9. Heat transfer of CuO/H_2O/ARB nanofluids with inserts compared to water with inserts 112

Figure 7.10. Pressure drop and friction factor of CuO/H_2O/ARB with inserts compared to water with inserts. 112

Figure 7.11. Heat transfer of C/H_2O/CTAB nanofluids with inserts compared to water with inserts. 113

Figure 7.12. Pressure drop and friction factor of C/H_2O/CTAB with inserts compared to water with inserts. 113

Figure 7.13. Heat transfer results of nanofluids with inserts. 114

Figure 7.14 Friction factor against Reynolds number for nanofluids combined with inserts. 115

Figure 7.15 Pressure drop versus Reynolds number for nanofluids combined with inserts. 116

Figure 7.16. Combined heat transfer results for nanofluids with and without inserts. 117

Figure 7.17 Friction factor for nanofluids combined with and without inserts 118

Figure 7.18. Pressure drop for nanofluids combined with and without inserts 119

Figure 7.19 Thermal performance of nanofluids combined with inserts. 120

Figure 7.20 A comparison between thermal performance of nanofluids combined with and without inserts. 121

Figure 7.21 Maximum *U* at full pumping speed for nanofluids combined with and without inserts 122

Figure 7.22 Maximum pressure drop at full pumping speed for nanofluids combined with and without inserts 122

Figure 7.23 Maximum thermal performances achieved at full pumping speed for nanofluids combined with and without inserts 123

Figure B.1 Stability timeline (a) and (b) samples of nanofluid with varying surfactants after 40 days. 156

Figure B.2 Viscosity as a function of linear velocity. 157

Figure B.3 The effect of shear rate on hexane and water carbon nanofluids. 157

Figure B.4 Comparison of shear stress against shear rate of nanofluids with various surfactants at T=25 °C. 159

Figure B.5 Differential scanning calorimeter. 160

Figure B.6 Effect of activated carbon nanoparticles and surfactant on heat capacity (a) and (b) enhancement ratio as a function of temperature. 161

Figure B.7 Specific heat capacity measurements for surfactants (a) and (b) nanoparticles using a DSC 162

Figure C.1 Plotted graphs indicating thermocouple gain and offset from calibration. 164

Figure C.2 Tube side flow meter calibration 165

Figure C.3 Annulus side flow meter calibration 166

Figure C.4 Comparison between measured and gauge pressure 167

Figure C.5 Temperature profile for counter-current flow in the heat exchanger. 168

Figure C.6 Rig support stand and its dimensions. 169

Figure D.1 Configuration of channels on DAQ 171

Figure D.2 Exportation of data prior to processing. 172

Figure D.3 Excel spreadsheet with processed data 173

Figure D.4 The energy balance ratio of the test closed-loop for the testing system. ... 175

List of Tables

Table 2.1 Passive and active heat transfer enhancement techniques 5

Table 2.2 A summary of research on nanorefrigerants. 12

Table 2.3 Summary of nanofluids empirical models of thermal conductivity 18

Table 2.4 Summary of nanofluids empirical models of viscosity 21

Table 2.5 Summarised studies on inserts and nanofluids in double pipe heat exchanger. 23

Table 3.1 Physical characteristics of nanoparticles produced and supplied by NanoAmor. 29

Table 3.2 Physico-chemical properties of base fluids. 30

Table 3.3 Physico-chemical properties of surfactants 31

Table 3.4 Concentration of nanoparticles in nanofluids. 32

Table 4.1 Viscosity of Ethylene glycol based nanofluids with various surfactants 44

Table 4.2 Viscosity of water based nanofluids with various surfactants 44

Table 4.3 Average relative viscosity of nanofluids immediately after preparation and seven-week later 46

Table 4.4 Measured thermal conductivity using the Hukseflux™ TP08 needle Probe 57

Table 4.5 Measured thermal conductivity using the Thermtest TC-30™ device 57

Table 4.6 Density measurements of nanoparticles 60

Table 4.7 Measured specific heat capacity of nanoparticles and surfactants. 63

Table 5.1 Heat exchanger dimensions 67

Table 5.2 Summary of apparatus accuracy 78

Table 5.3 Estimated uncertainties from primary measurements and derived quantities 79

Table 6.1 purchased cost of nanoparticles and analytical grade surfactants 103

Table 7.1 Heat transfer improvement of nanofluids combined with inserts compared to water with inserts at Re = 61777 114

Table 7.2. Heat transfer improvement of nanofluids compared to water at Re = 61777 117

Table 7.3. Pressure drop and ratio for similar fluid with and without inserts at Re = 61777 119

Nomenclature

A	Surface area (m^2)
Avg	Average
bf	Base fluid
C_p	Specific heat capacity (kJ/kg.K)
D	Tube diameter (m)
E	Enhancement ratio
f	friction factor
h	convective heat transfer coefficients ($kW/m^2.K$)
i	inside
J	Chilton-Colburn factor
k	thermal conductivity ($kW/m^2.K$)
l	tube length (m)
LMD	Log-mean temperature difference
$\dot{m}$	mass flow rate (kg/s)
n	rotational speed (rpm)
nf	nanofluid
Nu	Nusselt number
o	Outside
P	Particle
Pr	Prandtl number
$\dot{Q}$	heat transfer rate (kW)
r	radius (m)
Re	Reynolds number
Stdev	Standard deviation
T	temperature (°C)
TM	Trade-mark
U	overall heat transfer coefficient ($kW/m^2.K$)
V	Velocity (m/s)
ΔP	Pressure drop (kPa)

ΔT	temperature difference (°C)
ϕ	volume concentration of nanoparticles
ω	Angular velocity
β	Viscosity index
φ	Thermal efficiency
λ	Pumping power
η	Thermal efficiency (Web and Kim)
$\%$	Percentage
δ	tube wall thickness (mm)
γ	Shear rate (s^{-1})
ρ	Density (kg/m^3)
μ	Viscosity (Pa.s)
∂	Uncertainty

Chapter 1
Introduction

1.1 Introduction

The increasing global demand for more energy and reducing the use of fossil fuels (see Fig. 1.1) that contribute to greenhouse gas emissions has led to discussions on climate change. The 2010 United Nations Climate Change Conference (UNCCC) concluded that global warming cannot be avoided, only mitigated (Michonski and Levi 2010) in order to maintain global temperature rise below 2 °C. Five years later, the 2015 Paris Agreement (UNFCCC. Conference of the Parties (COP) 2015) revised the earlier 2010 agreement; sighting that the 2 °C reduction target was insufficient, and that a 1.5 °C target is required in order to keep the emissions levels low by 2030.

The present statistics show that out of the 50 billion tonnes of greenhouse gases emitted each year, 24.2 % comes from energy use in industries that require constant heating and cooling such as processing and manufacturing industries (Ritchie and Roser 2020). Moreover, a continuously rising trend in population (see Fig. 1.2) (World Bank 2020), emerging economies (IMF 2019) and energy consumption (Ritchie 2014; BP 2020b; U.S. Energy Information Adminstration n.d.). Therefore, reducing carbon emissions strongly relies on innovations and advances from intensifying Research and Development (R&D) activities in energy technologies, heat transfer and energy efficiency.

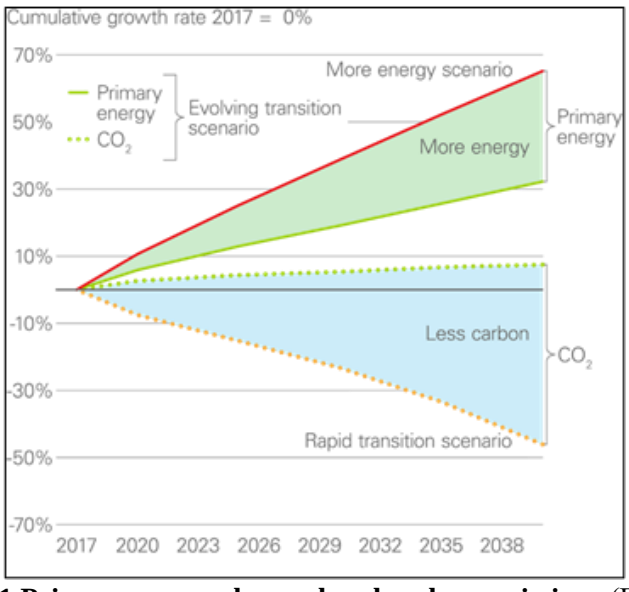

Figure 1.1 Primary energy demand and carbon emissions (BP 2020a)

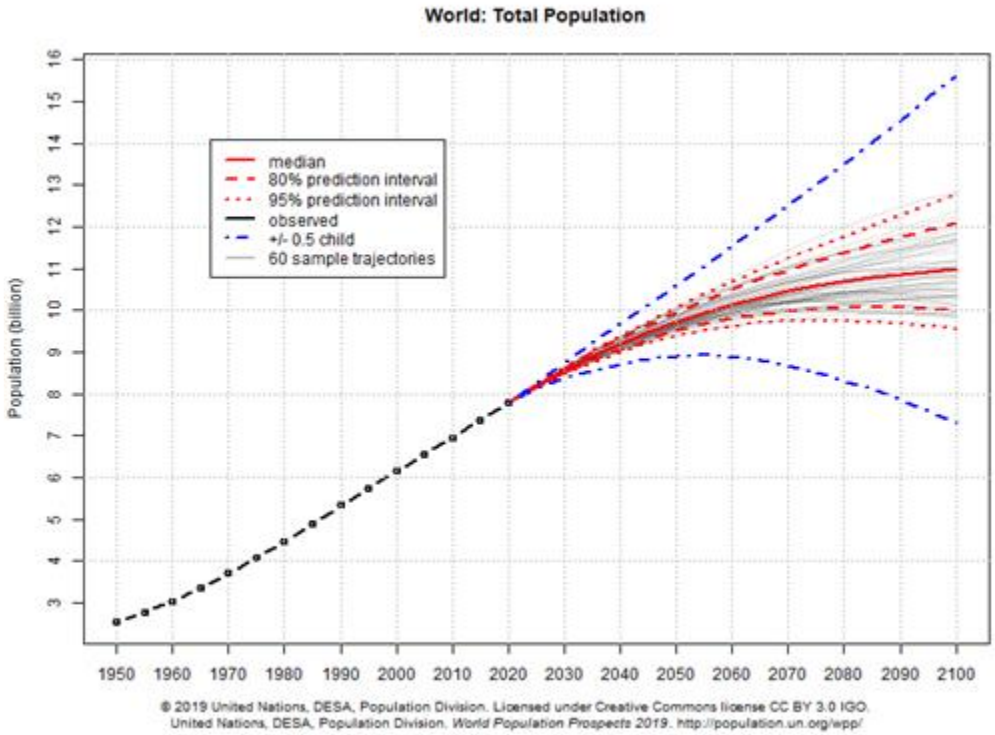

Figure 1.2 World population prospects (United Nations 2020)

Heating and cooling is one of the most prioritised needs of many industrial technologies and applications. Based on the rate of heat transfer equation ($Q = h * A * \Delta T$) that determines the performance of most heat transfer systems, it explains that heat transfer improvement can be possible by increasing: (1) heat transfer area 'A', (2) temperature 'ΔT', and (3) heat transfer coefficients 'h'. However, increasing the heat transfer area and the temperature difference will automatically result in bulkiness of the heat exchangers size and weight, and an increase in power input respectively; resulting in high operating costs.

To that end, various technologies have been used to increase heat transfer coefficients including: enhanced surfaces (grooved, rough, extended and treated), coiled devices, Swirl flow devices, and the most recent being additives for liquids (Webb and Kim 2006).

Conventional heat transfer fluids such as air, water, ethylene glycol, and oil show very low thermal conductivity compared to solids. Therefore, the suspension of solid nanoparticles has led to the renewed interest of nanofluids, an active area of research with a target of optimising heat transfer systems using engineered fluids (Choi Argonne, IL (United States). Energy Technology Division] 1998).

Nanofluids are heat transfer working fluids composed of nanosized solid particles and conventional base fluids. This combination yields significant magnitude of thermal

conductivity that further enhance heat transfer coefficients and the performance of heat exchangers in thermal systems (Sarit K. Das et al. 2007).

In addition, several types of inserts including; twisted tape, wire coil static mixer ribs/baffles, winglet and customised wire matrix inserts such as hiTRAN® inserts may be used to achieve heat transfer enhancement (Webb and Kim 2006). The nature and geometric design of installed inserts in heat exchanger and their geometric design produce strong vortices, intense secondary flow and great disturbance to boundary layers which increases the heat transfer coefficients significantly (Sheikholeslami, Gorji-Bandpy, and Ganji 2015; Keklikcioglu and Ozceyhan 2018).

Therefore, the development of new highly conductive and sustainable heat transfer fluids coupled with inserts technologies is of primary importance for heat transfer enhancements. The advances made in heating or cooling in industrial devices and systems in general, cause energy saving and heat transfer improvement, reduce operational costs and increase the operational life of heat transfer systems, thus reducing emissions and global warming in general.

1.2 Research Aims

The fact that surfactants play a fundamental role to keep nanoparticles in suspension, what is not yet clear is their impact on thermal properties such as viscosity and thermal conductivity. Whilst little quantitative heat transfer analysis has been carried out on combinations of nanofluids with twisted tape or wire coil inserts, no previous study has investigated matrix type of inserts (hiTRAN® inserts) with nanofluids. Also, no controlled studies have been reported about the reproducibility of nanofluids. Therefore, the primary aim of this thesis is to compare and evaluate various combinations of nanofluids composed of different nanoparticles, base fluids and surfactants. This will assist to:

i. Identify optimal pairing(s) of nanoparticles, base fluid and surfactants with optimal thermo-physical properties which show the highest thermal conductivity with minimal increase in viscosity.
ii. Measure thermal and rheological properties of selected combinations of nanofluids.

iii. Perform heat transfer enhancements in an experimental test closed flow loop composed of double pipe heat exchangers with and without inserts.

iv. Understand the long-term behaviour of nanofluids. For example, long-term stability and replicability of viscosity measurements; which are relevant for practical application conditions such as repeated heating or cooling cycles.

1.3 Thesis Structure

This thesis has been divided into 8 chapters, with the main research findings being presented in Chapter 3, 4, 6 and 7. The first chapter began with a brief statement of the context of the work as well as the objectives and methodology. Chapter 2 is the literature review, Chapter 3 assesses the stabilising effect of surfactants on nanofluids, Chapter 4 focused on measurement of physical properties of nanofluids, Chapter 5 described the construction of the test rig, Chapter 6 covered the thermal performance of selected nanofluids, Chapter 7 covered the performance of nanofluids with hiTRAN® inserts. Finally, Chapter 8 summarises the major findings of this study and touches on recommendations where future research could be directed.

Chapter 2

Literature Review

2.1 Introduction

As society makes attempts to combat climate change and provide sustainable energy access for all. It is important to provide solutions that will improve energy stability and efficiency to reduce global warming.

The knowledge and understanding of heat transfer is important for the design of a wide range of industrial, commercial and domestic processes and appliances, including chemical processing, air conditioning and refrigeration, solar energy production and conversion, oil and gas industries and electronics cooling. In thermal engineering, the improvement in the thermal performance of systems is termed 'heat transfer enhancement'. Over the past decade, several techniques have been proposed as ways of enhancing heat transfer (Khaled et al. 2010; Léal et al. 2013; Sheikholeslami, Gorji-Bandpy, and Ganji 2015). These techniques have been classified as passive or active (Table 2.1).

The difference between these two techniques of heat transfer enhancement is: Passive methods requires no external power; but, modified surfaces of fluid flow or adjusted geometry of the heat exchanger to increase thermal efficiency. On contrast, active techniques require energy addition to improve heat transfer of the systems. It is reported (Keklikcioglu and Ozceyhan 2018) that providing external energy in most applications is complicated and not easy; thus limiting the use of active techniques in scientific fields.

Table 2.1 Passive and active heat transfer enhancement techniques (Grassi and Testi 2006)

Passive	***Active***
Additives for liquids (nanofluids)	Mechanical aids
Rough surfaces	Surface vibration
Extended surfaces (fins)	Fluid vibration
Displaced enhancement devices (inserts)	Electrostatic fields
Swirl flow devices (inserts)	Injection
Coiled tubes	Suction
Surface tension devices	Jet impingement
Treated surfaces	

The aim of this chapter is to review the advancements made toward heat transfer enhancements in thermal systems; using a passive technique (introducing solid nanoparticles into liquids) to improve thermal conductivity.

Since the thermal conductivity of solids may be several orders of magnitude higher than the thermal conductivities of conventional heat transfer fluids such as water (H_2O), oil or ethylene glycol (EG) (see, Fig. 2.1), the addition of highly conducting solid particles to a fluid has the potential to increase the effective thermal conductivity of the fluid.

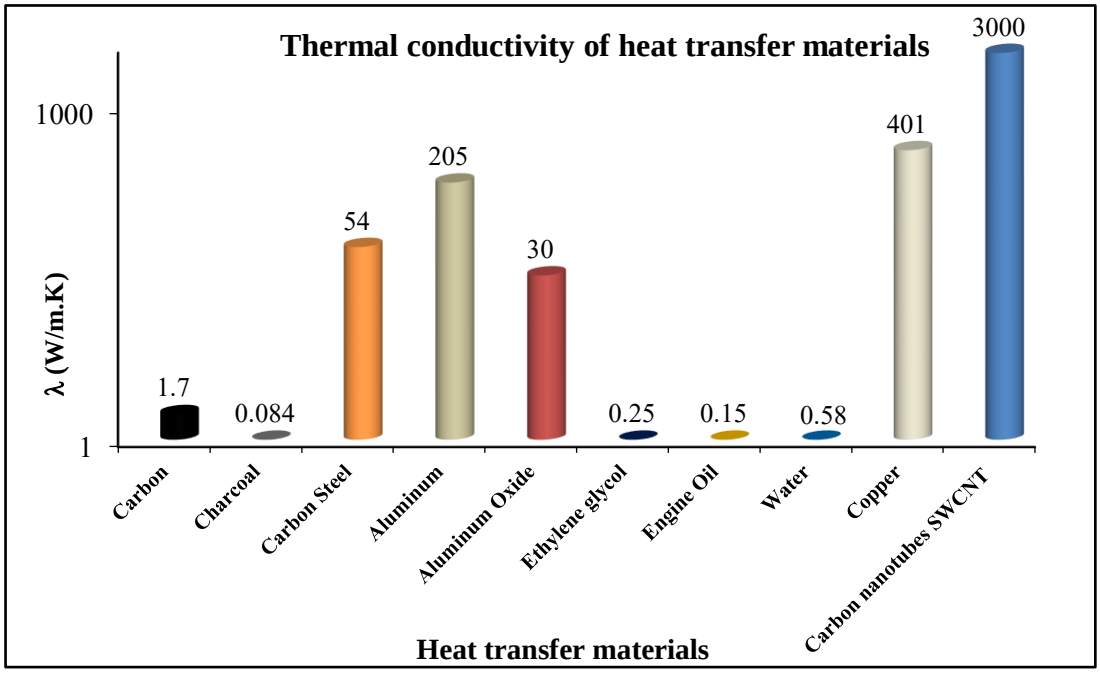

Figure 2.1 Thermal Conductivity of some heat transfer materials (Ho, Powell, and Liley 1968; Engineering ToolBox n.d.; R. H. Perry, Green., and Maloney. 1998)**.**

2.2 Background of Nanofluids

Suspension of solid objects in traditional fluids is not a recent phenomenon. In fact, it started many years ago with experiments carried out by Maxwell in 1873 (Maxwell 1892). In his work, he suspended milli and micro-metre rather than nano-metre sized particles in heat transfer fluids with the objective of improving their thermophysical properties. His results yielded significant thermal conductivity increases but also several problems such as lack of stability and increased viscosity. These challenges put a pause on the investigation for several years. It wasn't until 1956 after the famous talk of Richard

Feynman '*there's plenty of room at the bottom*' (Feynman 1960) that Tanuguchi (Tanuguchi 1974) come up with the term ***'Nano-Technology'*** in 1974.

A decade later (1985), Argonne National Laboratory (ANL) started a research program entitled '*Advanced Fluids*' focusing on advancing energy transmission fluid technology in large scale heating and cooling systems. Under this program (Choi Argonne, IL (United States). Energy Technology Division] 1998), several tests were conducted employing a number of options such as downscaling micro-channel diameters from 0.15 m to 50.0 μm and using micrometre-sized particles. However, they found that micro-sized particles wear out pipes, pumps and clog in microchannels. Therefore, they could not be used in practical heat transfer equipment.

In 1993 Choi (S K Das et al. 2007) proposed the use of a suspension of nano-meter sized particles in heat transfer fluids. Choi's tests presented much better results than milli- or micro-meter sized particles particularly in terms of stability and thermal conductivity.

At an international mechanical engineering congress in 1995, Choi and Eastman coined the term ***"nanofluids"*** (S. U. S. Choi and Eastman 1995a) where they presented results of suspended copper nanoparticles in water. Their investigations revealed that the thermal conductivity of the fluid was enhanced by a factor of 1.5 and 3.5 compared to water at volume fractions of 5 % and 20 % respectively. Further experiments with copper nanoparticles in acidified ethylene glycol showed apparently anomalous increases in thermal conductivity (Eastman et al. 2001). However, they also observed that the thermal conductivity of copper/ethylene-glycol nanofluids decreased with time, which was most likely due to agglomeration and/or sedimentation of the nanoparticles.

Similar encouraging results were observed by other researchers and subsequently the use of nanofluids for heat transfer enhancement became a very active area of research (Alawi, Sidik, and Kherbeet 2015; Kasaeian, Eshghi, and Sameti 2015). However, to date it does not appear that nanofluids have received widespread usage outside the research environment. In practice the usage of nanoparticles in heat transfer equipment still faces a number of challenges arising from issues such as (1) lack of stability of the nanofluids, (2) high variation on reported physical properties and heat transfer enhancement effects in the literature, (3) lack of understanding about the mechanisms and forces that act on the nanoparticles during and after suspension. These issues have slowed the process of standardisation and formulation of nanofluid technology.

2.3 Potential applications of Nanofluids

Nanofluids have demonstrated their potential to replace convectional working fluids in heat transfer systems. This has created opportunities to develop effective heat transfer systems and equipment across various industrial applications.

2.3.1 Electronics cooling

The cooling of microprocessors in computers and data centers is still a technical challenge because of ever-increasing heat loads that in turn reduce the performance and reliability of electronic devices. Nanofluids have demonstrated the capability of increasing heat rejection rates in electronics cooling applications (Ali et al. 2019; Sohel Murshed and Nieto de Castro 2017).

2.3.2 Automobile industry

The growing demand for hybrid electric vehicles (HEV) inevitably raises thermal management issues. In heavy duty vehicles such as trucks, larger radiators increase frontal areas, resulting in additional aerodynamic drag and increased fuel consumption (S K Das et al. 2007). Therefore, nanofluids have a great potential for use as engine coolant in radiators. For instance, it is reported (Heris et al. 2014) that a heat transfer coefficient enhancement of about 55 % was registered when 0.8 vol% concentration of CuO nanoparticles were suspended to a mixture (50/50) of water and ethylene glycol base fluid. Similarly, SiO_2 nanofluid with 1-2 vol.% concentrations enhanced heat transfer rate up to 50% compared to pure water (Adnan M Hussein, Bakar, and Kadirgama 2014).

In another study (Nieh, Teng, and Yu 2014), results showed that the heat dissipation capacity and the efficiency factor of the Al_2O_3 nano-coolant were higher than the mixture of ethylene glycol/water base fluid by 25.6 %.

2.3.3 Boilers and Nuclear reactors

Most boilers use large amount of heat from burning either natural liquified gas (LNG) or coal to convert water to high temperature steam, which is transported for district heating or required in manufacturing and processing, or power generation industry.

Nanofluids have the potential to replace pure water which in turn increase heat flow rates at reduced energy costs (Kamel et al. 2018).

In the nuclear industry, nanofluids can be employed as a coolant that circulates past the reactor core to absorb the heat resulted from nuclear fission; then carried away from the reactor and then used to generate steam which in turn runs through steam turbines to drive ship and submarine propellers or turn electrical generators.

In the power generation and transmission sector, nanofluids have the potential to replace the conventional oil as a coolant in transformers thus leading to increased heat rejection, reduced size and weight of transformers.

2.3.4 Oil filled space heaters

These are portable units in households popular for domestic heating. Environmental-wise, space heaters involve no burning fuels or coal; the working fluid in the reservoir is electrically heat, and the transfer of heat occurs through the fins by convection to warm the required space. Nanofluids have the potential to enhance the tradition oil normally used in these units because of its relatively high specific heat; capable to store thermal energy in such a small volume for longer periods.

2.3.5 Solar Application

Solar energy stands out as a primary means of reducing global carbon emissions to the Earth's atmosphere. Lewis et al. (Lewis et al. 2005) observed that more energy from sunlight strikes the Earth in one hour (4.3 × 1020 J) than all the energy consumed on the planet in a year (4.1 × 1020 J). They added that 120,000 TW of radiation arrives at the surface of the Earth, far exceeding human needs even in the most aggressive energy demand scenarios. However, many solar capture devices suffer from relatively low collection efficiencies. Recent studies (Colangelo et al. 2013; Alim et al. 2013) indicate that nanofluids can be used specifically to boost their performance of solar energy conversion systems where the optical and thermal performance is low.

Kabeel et al. (Kabeel, El-Said, and Abdulaziz 2015) investigated a thermal solar water heater with Al_2O_3/H_2O nanofluid in forced convection, and their results showed an increased solar collector efficiency of 11 % for 3 % nanoparticle concentration. An enhancement of 21 % in average heat transfer coefficient was reported by Ebrahimnia et

al. (Ebrahimnia-Bajestan et al. 2016) after conducting laminar flow convective heat transfer experiments of water-based TiO_2 nanofluid flowing through a uniformly heated tube.

Al-Waeli et al. (Al-Waeli et al. 2017) conducted an experimental investigation of SiC/H_2O nanofluid as a working fluid for a photovoltaic/thermal (PV/T) system. They concluded that the thermal conductivity was enhanced by up to 8.2 % for the temperature range of 25 - 60 °C, and the thermal efficiency of the collector was increased by up to 100.19 % compared to the efficiency when water was used as the working fluid.

Luo et al. (Luo et al. 2017) investigated thermal energy storage enhancement of a binary system of molten salt nanoparticles. They observed 4.71 % enhancement of the total storage capacity over a temperature range of 160 to 300 °C. Their results also indicated an improvement in specific heat of the nano-salt by 11.48 %.

With these promising results, it seems likely that solar energy capture devices may be one of the first applications to have the wide spread uptake of nanofluids technology, although the stability of nanofluids remains a significant barrier (Gorji and Ranjbar 2017).

2.3.6 Nanorefrigerants

The refrigeration industry is progressively making efforts to replace traditional refrigerants with ones that have less impact on the environment. However, studies on potential replacements such as R1234ze or R1234yf or R450A have indicated that they have lower heat transfer performance than the refrigerants they are intended to replace (Kaggwa and Wang 2016; Mendoza-Miranda et al. 2016). Therefore, the suspension of solid nanoparticles in poorly performing refrigerants (‘nanorefrigerant’) can enhance refrigeration system performance. Several experimental and numerical investigations (Arslan 2017; Sharif et al. 2017; Lim, Azmi, and Yusoff 2016; Nair, Tailor, and Parekh 2016) have concluded that nanorefrigerants improve energy efficiency, and the overall system performance. For instance, Fig. 2.2 indicates that the thermal conductivity and heat transfer of nanorefrigerant (CuO/R-134a) is higher than R-134a alone (Fadhilah, Marhamah, and Izzat 2014). Moreover, R-134a has a high global warming potential and is being phased out of use as a refrigerant. However, potential replacements such as R-1234yf or R-1234ze have low thermal conductivity. Therefore, suspending nanoparticles in R-1234yf or R-1234ze can enhance their thermal conductivity.

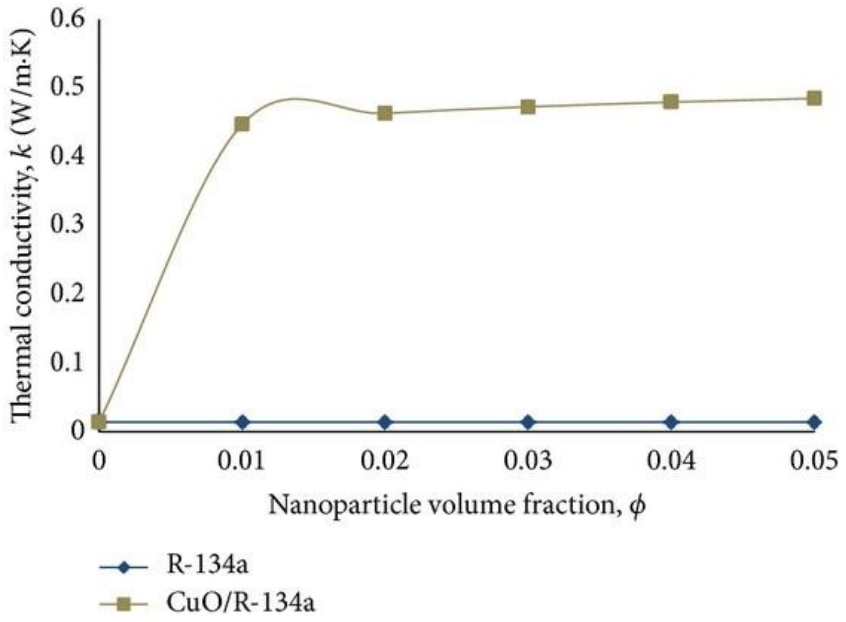

Figure 2.2(a) Thermal conductivity as a function of nanoparticle volume fraction (Fadhilah, Marhamah, and Izzat 2014)**.**

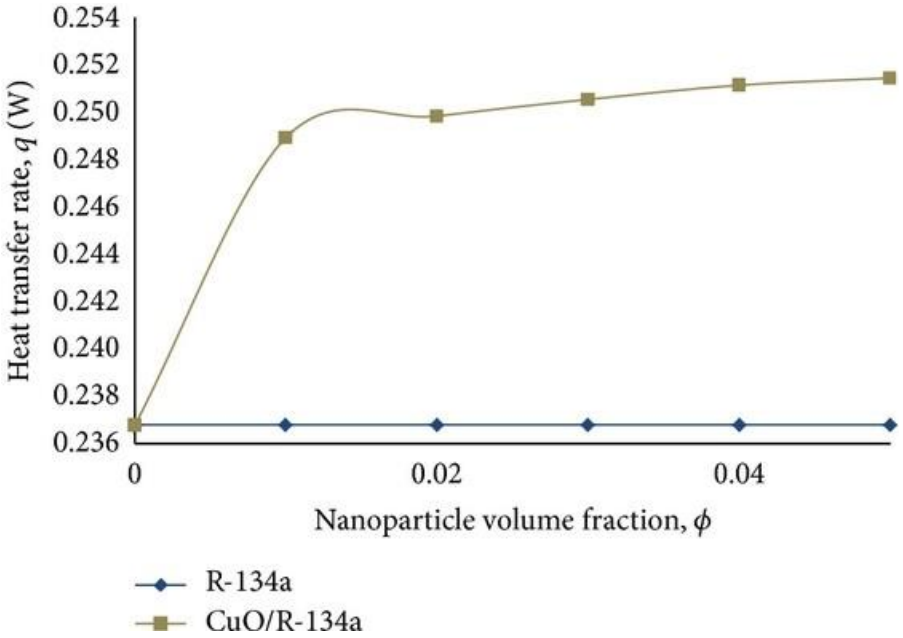

Figure 2.2(b) Heat transfer rate as a function of nanoparticle volume fraction (Fadhilah, Marhamah, and Izzat 2014)**.**

Sanukrishna et al. (Sanukrishna, Vishnu, and Jose Prakash 2017) dispersed copper oxide nanoparticles in R-134a and polyalkylene glycol. Their results revealed 12.67 % increase in thermal conductivity and a flow boiling heat transfer enhancement of 37 %.

The coefficient of performance (COP) of nanorefrigerant was 7.5 % higher than pure refrigerant.

However, Lin et al. (Lin et al. 2017b) carried out an experiment to evaluate the degradation of a nanolubricant-refrigerant mixture during continuously alternating condensation and evaporation processes. They discovered that changing the lubricant and nanoparticles mass fraction in nanolubricant degrades the mixture by 28 – 77 % after 20 cycles for nanoparticle concentrations of 0.2 - 1.0 %, heating and cooling temperature of 50 – 80 $^{\circ}$C and 5 –15 $^{\circ}$C respectively. They concluded that degradation would be reduced by low heating and cooling temperatures, and low nanoparticle concentrations.

Lin et al. (Lin et al. 2017a) conducted an experiment using TiO_2 nanoparticles and concluded that only a small fraction of the total number of nanoparticles circulated by migration from the mixture to the vapour with the refrigerant dry-out process.

Lee et al. (J. Lee and Mudawar 2007a) carried out an assessment on the effectiveness of nanofluids for single and two-phase in micro-channels. They concluded that nanoparticles should not be used in two-phase micro-channel due to the clustering phenomenon that propagates upstream to fill the entire channel thus preventing coolant from circulation and causing catastrophic failure of the system. Additional results on nanorefrigerant investigations has been summarised in Table 2.2.

It appears, therefore, that the use of nanofluids in two-phase flows have more technological hurdles to overcome than for single-phase applications.

Table 2.2 A summary of research on nanorefrigerants.

Author	***Nanorefrigerant***	***Results***
Lim et al. (Lim, Azmi, and Yusoff 2016)	Al_2O_3 / water-EG	Convective heat transfer coefficient enhanced by 25.4%
Redhwan et al. (Redhwan et al. 2017)	Al_2O_3 / PAG SiO_2 / PAG	Enhancement was 1.04 times higher than the base lubricant
Wang et al. (K. J. Wang, Ding, and Jiang 2006)	Al_2O_3 / R-22	Nanoparticles can enhance the heat transfer characteristic of the refrigerant, and the bubble size diminishes and moves quickly near the heat transfer surface.
Jiang et al. (Weiting Jiang, Ding, and Peng 2009)	CNT-R-113	Measured thermal conductivities of four kinds of 1.0 vol. % CNT– R113 nanorefrigerant increase to 82%, 104%, 43% and 50%, respectively.
Tazarv et al. (Tazarv et al. 2016)	TiO_2 / R-141B	Enhancement of convective heat transfer coefficient and higher vapour qualities.

2.3.7 Biomedical applications

The biomedical industry and research institutions (Bhardwaj and Kaushik 2017) have progressively gained interest in the usage of nanofluids including drug delivery for cancer treatment (D. Yang et al. 2009), surface and subsurface defect sensors (Mahendran and Philip 2013).

2.4 Preparation of nanofluids

Nanoparticles used in nanofluids range in size from 1 nm to 100 nm and have different shapes such as nanospheres (spherical), nanoreefs, nanoboxes, nanoclusters and nanotubes. Some studies (S. L. Lee et al. 2016; Harikrishnan et al. 2017; H. Chen et al. 2009; Deepak Selvakumar and Dhinakaran 2016) have concluded that the morphology of nanoparticles is defined during synthesis, and that the average size of nanoparticles plays a significant role in the enhancement of thermal conductivity, which is the primary factor for heat transfer enhancement.

There are two popular methods used in the preparation of nanofluids: the single-step method and the two-step method (Babita, Sharma, and Gupta 2016) as shown in Fig. 2.3. The single-step method involves the production of nanoparticles and suspension of the particles into the base fluid simultaneously. For example, the nanoparticles may be formed by condensation from the vapour phase directly into the heat transfer liquid. This method has the advantage of producing minimal nanoparticle agglomeration; however, it is characterised by high costs, and is therefore likely to be infeasible on an industrial scale. In addition, physical vapour condensation or direct evaporation are most likely to happen (Babita, Sharma, and Gupta 2016). By contrast, in the two-step method, nanoparticles are produced in a separate process before being dispersed in the base fluid (Haddad et al. 2014). Stabilising agents such as surfactants can be added to lower the interfacial forces between the nanoparticles and base fluid molecules. Subsequently, the solution may be mixed using mechanical devices such as homogeniser, stirrer and ultrasonicator. The two-step method appears to have received the most widespread use, since it is generally less labour-intensive and more cost effective (Haddad et al. 2014; Sidik et al. 2014; Li et al. 2009).

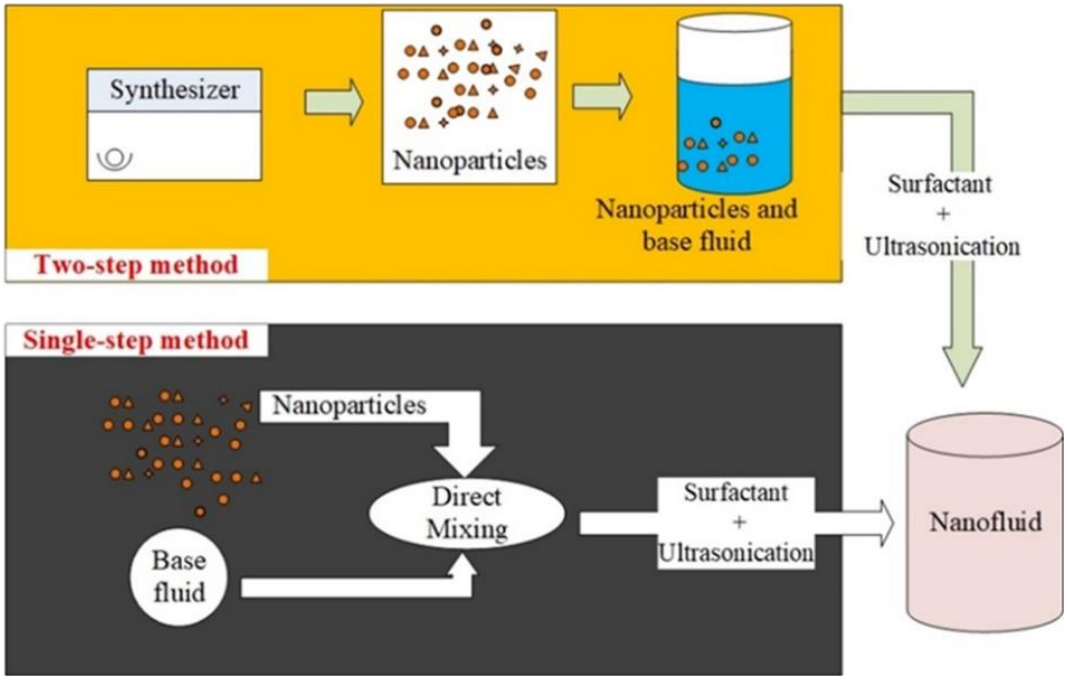

Figure 2.3 Methods of nanofluids preparation.

2.5 Mechanism of heat transfer enhancement in nanofluids.

Maxwell (Maxwell 1892) proposed a model for determining the electrical conductivity of a dispersion of spheres in a continuous medium that has subsequently been applied successfully to the prediction of thermal conductivities of heterogeneous materials (Hamilton and Crosser 1962; Carson et al. 2005). Maxwell's model and derivatives may be thought of as 'classic theory' for thermal conductivity modelling (S. Lee et al. 1999a). However, the rise in popularity of nanofluids has largely been due to reports of experimentally determined thermal conductivities being many times higher than those predicted by classic theory (Xing, Yu, and Wang 2016; Weixue Jiang et al. 2017). In the open literature, there does not appear to be any single theory that can explain the apparently anomalous heat transfer enhancement effects in nanofluids that have been reported by some researchers (Eastman et al. 2001; Leong et al. 2018). However, a variety of mechanisms have been proposed. For instance, in a review of metal-oxide nanoparticles Suganthi et al. (Suganthi and Rajan 2017) concluded that Brownian motion plays a significant role in increasing thermal conductivity of nanofluids, in which the stochastic movement of nanoparticles in a fluid depends on temperature, diameter of the particles and viscosity of the fluid. Farzaneh et al. (Farzaneh et al. 2016) suggested that in addition to Brownian-motion, nanoparticles once suspended also experience drag,

thermophoresis, London-Van der Waals and electric double layer forces. The study added that a combination of inter-particle Van der Waals and electric double layer forces (Fig. 2.4) produces a combined force called "DLVO", (Derjaguin–Landau–Verwey and Overbeek) which, together with other forces play a significant role in the mechanism of heat transfer in nanofluids.

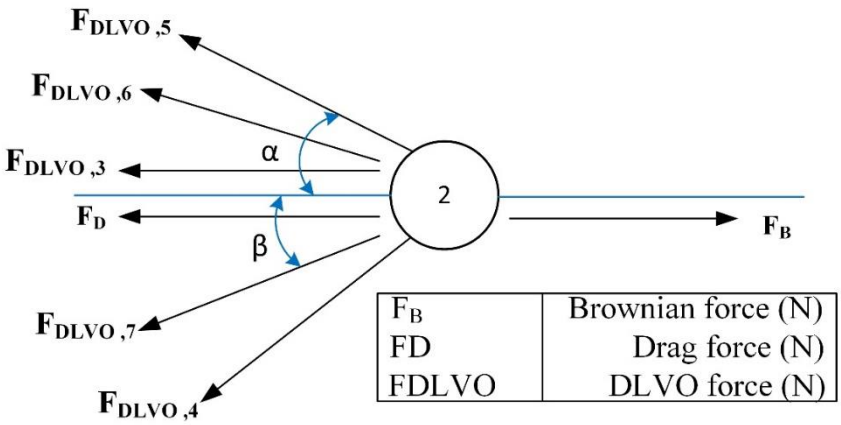

Figure 2.4 Free body diagram of particle (P.2) neglecting thermophoresis force (Farzaneh et al. 2016)**.**

Kang et al. (Kang and Wang 2017) proposed a mechanism based on the cross coupling of thermal and electric transports in nanofluids. They explained that due to the fact that nanoparticles have surface charges, a varying electric field can be generated to accompany the particle thermal motion. Therefore, the base fluid is heated by the nanoparticles through molecular collision such that nanoparticles may be considered as an internal heat source (see Fig. 2.5).

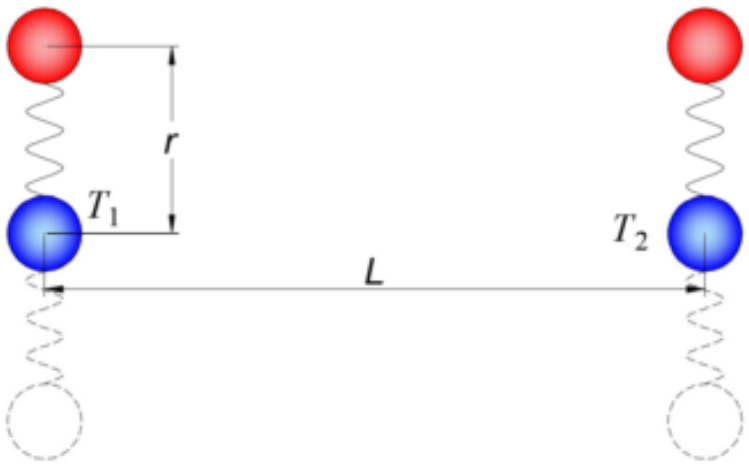

Figure 2.5 Nanoparticle interaction under the cross coupling of thermal motion and electric field (Kang and Wang 2017)**.**

Sanukrishna et al. (Sanukrishna, Vishnu, and Jose Prakash 2017) reported that the mechanism of molecular layer formation inside evaporator tubes during evaporation could be the reason for heat transfer enhancement in two-phase flow boiling. However, to date none of these theories have been used to produce models that can accurately predict heat transfer enhancement across a wide range of applications.

Saha and Paul (Saha and Paul 2014) conducted a numerical analysis of the heat transfer behaviour of water based Al_2O_3 and TiO_2 nanofluids in a circular pipe under the turbulent flow condition. They claimed that smaller nanoparticles with higher velocity move faster than the large particles, and thus reduce the possibility of collision with each other. They continued to report that smaller diameter of nanoparticles will be more in number in comparison with large diameter of nanoparticles and will make a contact with the neighbouring fluid over a greater surface area. As a result, this will help in increasing the viscosity and thermal conductivity which result in the enhancement of heat transfer

However, latest development in colloids science believe that several unique characteristic to nanofluids (the timescales of the motion of particles and fluid affect the heat transfer) (Michaelides 2013) and changes in the properties of nanofluids have a strong implication on thermal dispersion and the motion of nanoparticles in the flowing nanofluid; thus, affecting the level of heat transfer enhancements (T. J. Choi et al. 2018).

2.6 Thermophysical-properties of nanofluids

Any heat transfer model requires accurate physical property data. The physical properties that affect conduction and convection include thermal conductivity, specific heat capacity, density and viscosity. For specific heat capacity and density, it is often assumed that a weighted arithmetic mean of the components' (i.e., base fluid and nanoparticle) densities or specific heat capacities can provide accurate predictions of the nanofluids density or specific heat capacity. However, determining the thermal conductivity and viscosity of nanofluids is not as straightforward.

2.6.1 Thermal conductivity

Thermal conductivity is the most studied transport property in nanofluids, as it is commonly assumed that the significant increase in heat transfer rates observed with nanofluids is primarily caused by the increased thermal conductivity. For nanofluids,

common thermal conductivity measurement methods include the transient hot-wire method (Duangthongsuk and Wongwises 2009) or the thermal property analyser (Kannaiyan et al. 2017).

Hemmat Esfe et al. (Hemmat Esfe et al. 2014) studied the thermal efficiency, defined as thermal conductivity divided by viscosity of ferromagnetic nanoparticles suspended in ethylene glycol. They focussed on the effect of particle size, temperature and concentration to determine the thermal conductivity and viscosity of the nanofluids with volume fractions up to 3 % in the temperature range of 26 – 55 $^{\circ}$C. Their results showed that the thermal efficiency of nanofluids increased with an increase in the temperature and solid volume fraction. They also concluded that the optimum particle size depended on the flow regime (i.e., the laminar vs. turbulent).

Deepak et al. (Deepak Selvakumar and Dhinakaran 2016) developed a model to predict the thermal conductivity of nanofluids based on particle size distribution and multi-level homogenization. They mainly focused on the effects of Brownian motion, interfacial layer formation and particle clustering. Similarly, Lee et al. (S. L. Lee et al. 2016) reported that thermal efficiency of nanofluids was improved by increasing particle size and temperature. However, particle size variation was more noticeable than temperature variation for thermal conductivity and viscosity measurements.

Ueki et al. (Ueki et al. 2017) conducted an experiment on thermophysical properties of carbon-based nanofluids. They found that carbon black and carbon nanopowder enhanced thermal conductivity by 7 % and 19 % respectively. They concluded that nanoparticle geometry and temperature both influenced thermal conductivity.

Lenin and Joy (Lenin and Joy 2017) reported that the critical concentration for thermal conductivity enhancement varies with the surfactant used, possibly due to the difference in the degree of aggregation of the nanoparticles and conformation of the surfactant molecules on the nanoparticle's surface. They added that base fluids with lower thermal conductivity and dielectric constant showed larger enhancement in the thermal conductivity relative to base fluids.

Hussein et al. (A.M. Hussein, Kadirgama, and Noor 2016) found the effect of volume fraction, temperature, and diameter on friction is not clearly elaborated in the literature, yet it is vital for developing correlations of thermal properties of nanoparticles. Shekarian et al.(Shekarian, Tarighaleslami, and Khodaverdi 2014) reviewed the effective parameters on the nanofluid thermal conductivity.

A large number of thermal conductivity models have been proposed (examples shown in Table 2.3), some of which consider the morphology of nanoparticles while others assume that all particles are spherical and introduce a variety of (mostly empirical) constants. Therefore, it is difficult to know which model should be used for a particular nanofluid. To demonstrate, a comparison of predictions from the models of Pak and Cho (Pak and Cho 1998), Buongiorno et al. (Buongiorno 2006), Maiga et al. (Maïga et al. 2004) and Mintsa et al.(Mintsa et al. 2009) in Fig. 2.6 shows significant differences in model predictions.

Table 2.3 Summary of nanofluids empirical models of thermal conductivity (k is thermal conductivity, ϕ is volume fraction)

Author	***Empirical model***	***Remarks***
Maxwell (Maxwell 1892)	$K_{nf} = \left[\frac{K_p + K_{bf} + 2\phi\left(K_p - K_{bf}\right)}{K_p + K_{bf} + \phi\left(K_p - K_{bf}\right)} \right] K_{bf}$	volume fraction of solid spherical particles
Pak and Cho (Pak and Cho 1998)	$K_{nf} = \left(1 + 7.74\phi\right) K_{bf}$	Depends on sphererical and non-spherical particles
Maiga et al.(Maïga et al. 2004)	$K_{nf} = \left(1 + 4.97\phi^2 + 2.72\phi\right) K_{bf}$	Considered spherical particles.
Boungiorno (Buongiorno 2006)	$K_{nf} = \left(1 + 2.92\phi - 11.99\phi^2\right) K_{bf}$	Titania sphererical and non-spherical particles
Mintsa et al.(Mintsa et al. 2009)	$K_{nf} = \left(1 + 1.7\phi\right) K_{bf}$	-

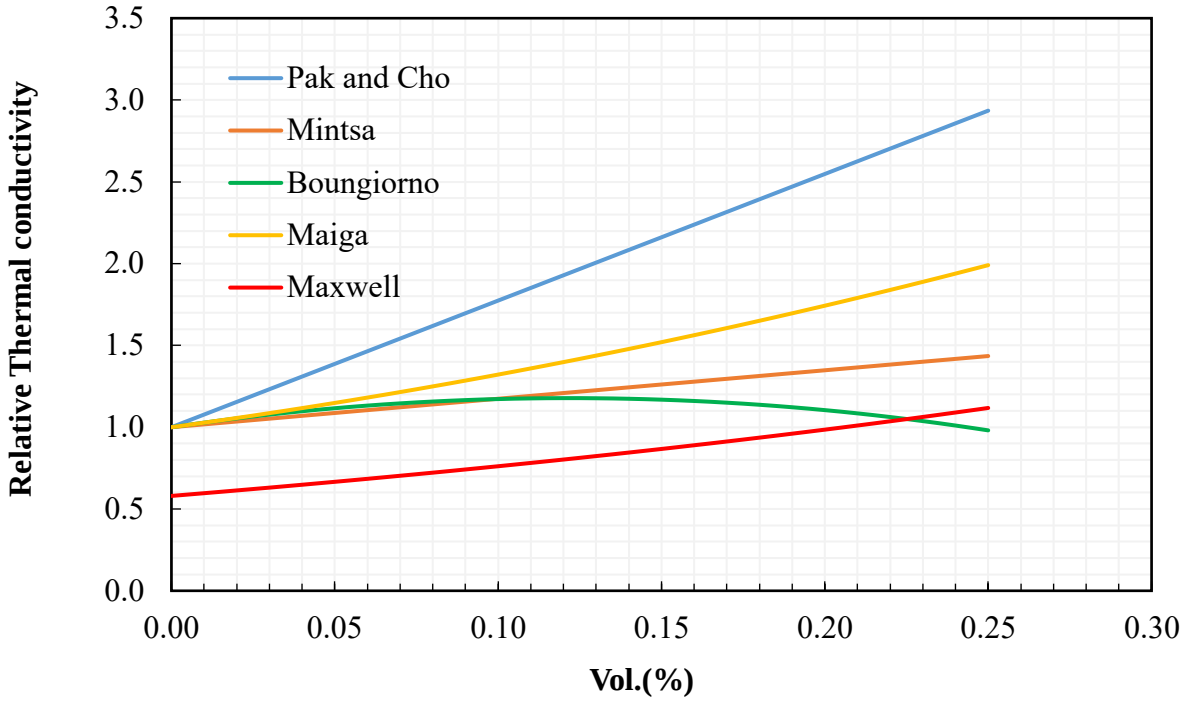

Figure 2.6 The effect of nanoparticle concentration on thermal conductivity using different models (Maxwell 1892) (Pak and Cho 1998; Maïga et al. 2004; Buongiorno 2006; Mintsa et al. 2009)**.**

2.6.2 Viscosity

In their landmark paper, Choi and Eastman (S. U. S. Choi and Eastman 1995a) assumed that the addition of nanoparticles would not significantly affect the viscosity of the nanofluids, however, this is not necessarily the case. For example, Namburu et al. (Namburu et al. 2007) measured the viscosity of copper oxide nanoparticles dispersed in a mixture of ethylene glycol and water and found that the viscosity of 6.12 % volume concentration of the nanofluids was four times the viscosity of the base fluid. They concluded that the viscosity of nanofluids increases with increasing amounts of nanoparticles. Similarly, Hemmat et al. (Hemmat Esfe and Saedodin 2014) found that the viscosity of zinc-oxide/ethylene glycol nanofluids increased considerably with particle volume concentration, as did Mariano et al. (Mariano et al. 2015) and Yu et al. (W. Yu et al. 2009), who also made the point that heat transfer enhancement effects of the nanofluid was offset by the increased pumping power requirements.

It is also possible that the addition of nanoparticles and/or surfactants may cause the nanofluids to behave in a non-Newtonian manner, even though the base fluid may be Newtonian. While Mariano et al. (Mariano et al. 2015) reported that the viscosity of the

nanofluids is 'nearly independent' of the shear rate, Kaggwa et al.(Abdul et al. 2018) observed that the viscosity of carbon-water nanofluids decreased with an increase in shear rate and the viscosity of carbon-hexane nanofluids increased with the increase in shear rate.

It can be difficult to model the viscosity of nanofluids. To illustrate, Fig. 2.7 shows different viscosity models, the popular Einstein (Einstein 1906) model for mixture viscosity compared to the Krieger-Dougherty (Krieger and Dougherty 1959), Brinkman (Brinkman 1952), Batchelor (Batchelor 1977) and Mooney (Mooney 1951) models for nanofluids that produce widely differing predictions. The discrepancy among predictions may be due to a number of factors. For example, Einstein (Einstein 1906) assumed the particles to be rigid, uncharged and devoid of any attractive forces and in low concentration, whereas Krieger and Dougherty (Krieger and Dougherty 1959) considered the full range of particle volume fractions, the influence of aggregation and the formation of interfacial layers.

As with thermal conductivity, the viscosity of nanofluids remains an area requiring further investigation, particularly as the effect of the surfactant on viscosity is not always taken into consideration or reported in viscosity studies.

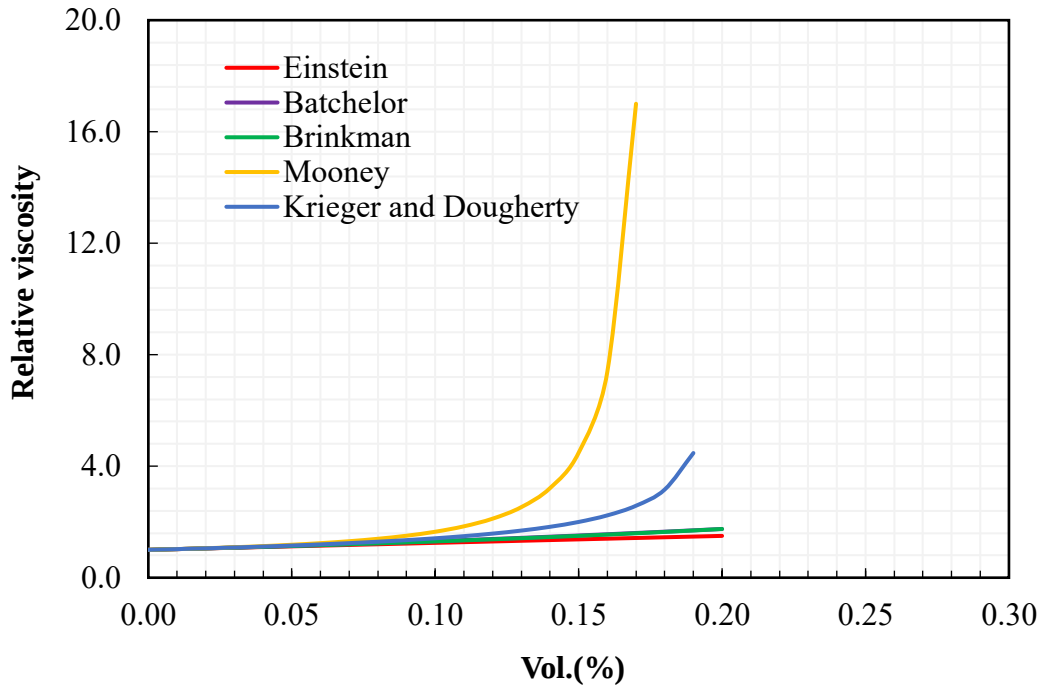

Figure 2.7 The effect of nanoparticle concentration on viscosity using different models (Einstein 1906; Krieger and Dougherty 1959; Brinkman 1952; Batchelor 1977; Mooney 1951)

Table 2.4 Summary of nanofluids empirical models of viscosity (μ is viscosity, ϕ is volume fraction)

Author	*Empirical model*	*Remarks*
Einstein (Einstein 1906)	$\mu_{nf} = (1 + 2.5\phi)\mu_{bf}$	Infinite dilution of spherical, and rigid nanoparticles devoid of any attractive forces.
Mooney (Mooney 1951)	$\mu_{nf} = \exp[\frac{2.5\phi}{1-(\phi/\phi_m)}]\mu_{bf}$	Einstein's model extended to apply to a suspension of finite concentration
Brinkman (Brinkman 1952)	$\mu_{nf} = [\frac{1}{(1-\phi)^{2.5}}]\mu_{bf}$	Modified Einstein model of spherical particles extended up to 4% volume concentration
Batchelor (Batchelor 1977)	$\mu_{nf} = (1 + 2.5\phi + 6.2\phi^2)\mu_{bf}$	Considered large nanoparticle concentration up to 10%
Krieger and Dougherty (Krieger and Dougherty 1959)	$\mu_{nf} = \left(1 - \frac{\phi}{\phi_m}\right)^{-\eta\phi_m} \mu_{bf}$	Considered the full range of particle volume fraction.

2.7 Inserts with nanofluids in heat exchangers

When fluid flows through a plain smooth tube, the fluid nearest the wall experiences frictional drag forces which has the effect of slowing down the fluid at the wall (Thome 2004). As a result, this reduces the tube-side heat transfer coefficient and consequently, the performance of the heat exchanger significantly. A variety of inserts including twisted tape, wire coil static mixer ribs/baffles and winglet inserts (see Fig. 2.8) may be used to achieve heat transfer enhancement (Webb and Kim 2006). The nature and geometric design of installed inserts in heat exchanger produce strong vortices, intense secondary flow and great disturbance to boundary layers which increases the heat transfer coefficients significantly.

Although some research has been carried out on nanofluids in conjunction with various types and designs of inserts as summarised in Table 2.5, what is not yet clear is the impact of free space between each node. Unlike hiTRAN® inserts with a matrix geometrical design, most studied inserts are regularly spaced. It is reported that swirl flow decays faster due to free space between nodes (Smith Eiamsa-ard, Thianpong, and Promvonge 2006). Therefore, the free space between each node is not put in consideration

for heat transfer and friction factor. Similar to wire coil inserts where the continuous swirl flow is generally interrupted by periodic wire coil space.

To date, it appears that there is no quantitative analysis that specifically combines matrix inserts (hiTRAN®) and nanofluids.

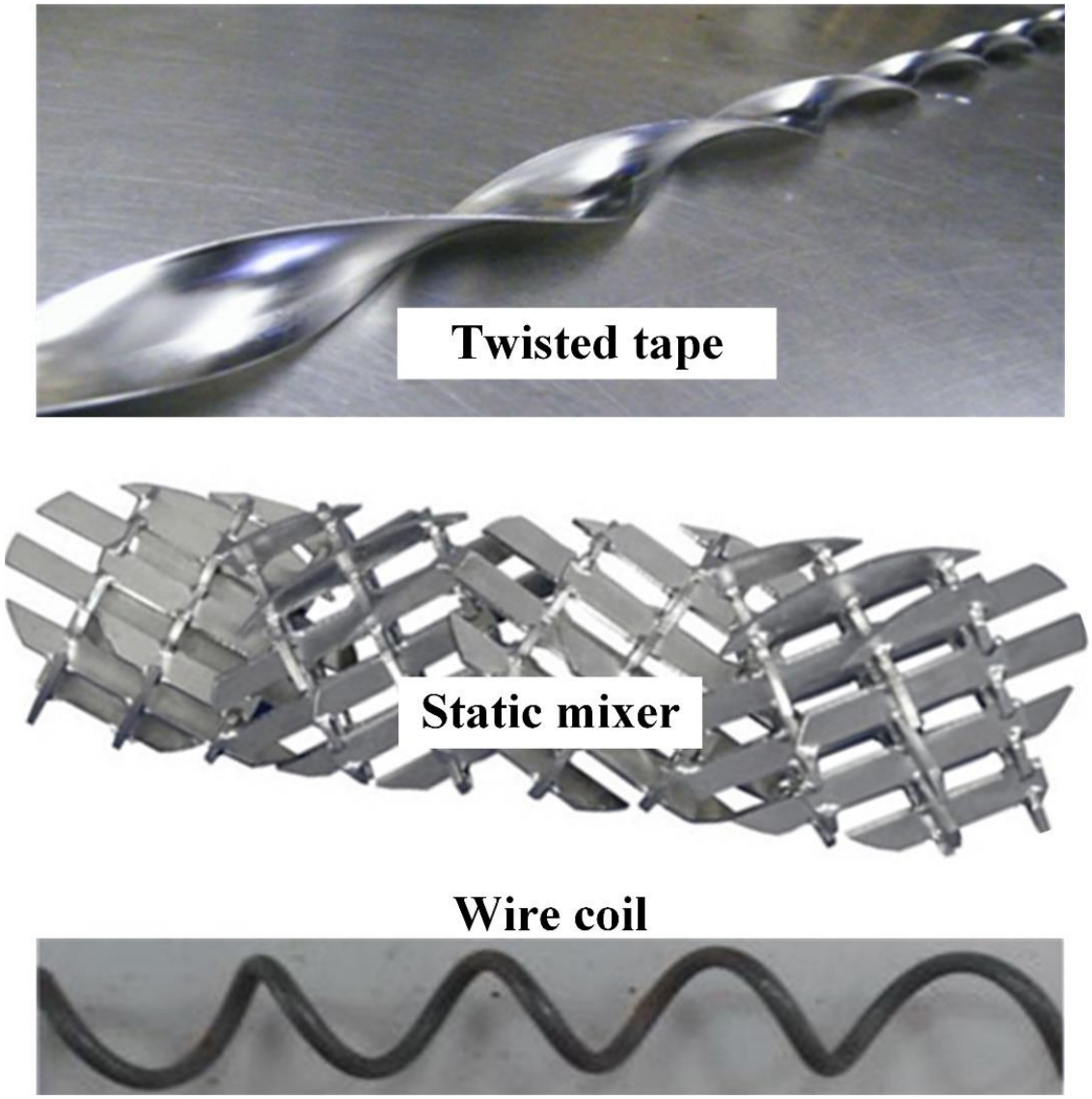

Figure 2.8 Common types of inserts used to enhance heat transfer.

Table 2.5 Summarised studies on inserts and nanofluids in double pipe heat exchanger.

Author	***Type of inserts and working fluids***	***Results***
Sundar et al.(Syam Sundar et al. 2017)	Wire coil and Fe_3O_4/H_2O nanofluid	32.03% enhancement in Nusselt number with a friction penalty of 1.162 times compared to water.
Hazbehian et al.(Hazbehian et al. 2016)	Twisted tape and TiO_2/Polyvinyl alcohol nanofluids	The thermal performance factor increased up to 1.75 times. The average Nusselt number and friction factor in the tube were 50–130, and 30–95 % higher than those in the plain tube; 90–220 and 100–270 % when the working fluid is nanofluid, respectively.
Promvonge et al.(Promvonge 2008)	Conical rings and air	The thermal performance of 0.96–1.07 and friction factor ranging from 68.62–70.25 was registered.
Yudav et al. (Yadav 2009)	Twisted tape and H_2O	40% increase in heat transfer coefficients with pressure penalty of 1.3-1.5 times, compared to plain heat exchanger was observed.
Eiamsa et al.(S. Eiamsa-ard, Kiatkittipong, and Jedsadaratanachai 2015)	Overlapped dual twisted tapes and TiO_2/ H_2O nanofluids	Heat transfer rates were enhanced up to 89% with friction factor of 5.43 times. The thermal performance was 1.13 times as compared to plain tube.
Akpinar et al. (Akpinar and Bicer 2005)	Helical wires and H_2O	An augmentation of up to 2.64 times in Nusselt number alongside an increase of up to 2.74 times in friction factor compared to the smooth tube was observed.
Choudhari et al.(Choudhari and G 2013)	Wire coil and H_2O	Enhancement of 1.58 times as compared to plane tube was achieved. Friction factor found to be increasing with the decreasing pitch of coil wire insert.

2.8 Current challenges of Nanofluids as a heat transfer fluid

Despite the promising heat transfer enhancement potential observed by many researchers, there are several barriers to widespread implementation in industrial settings. Nanoparticles are not cheap and there is no standard price at present (for example, at the time of writing, 100 g of the widely studied alumina or copper oxide nanoparticles from supplier (A) cost US$492.00 and US$80.00 respectively (Nanostructured and amorphous Materials Inc. 2019), and from supplier (B) cost US$59.00 and US$189.00 (US Research Nanomaterials n.d.) respectively). In addition, it seems that the properties of nanoparticles differ according to the manufacturer, which adds to the uncertainty of physical property data. Equally important, some nanomaterials are toxic and therefore extra measures taken in preparation increase production cost. Mahian et al (Mahian et al. 2013) explained that challenges such as the high cost of nanoparticles, instability and agglomeration, pumping power and pressure drop, erosion and corrosion of components make nanofluid usage commercially unattractive. However, they concluded that the general application of nanofluids is still in its infant stages and therefore, future investigations will increase the potential applications of nanofluids.

Yang et al. (L. Yang et al. 2017) explained that factors such as particle parameters (particle type, loading, size and shape) and environmental parameters (base fluid, pH value, temperature and the standing time) influence thermal conductivity. These factors and as well as preparation methods could be significant causes of the discrepancy in thermal conductivity enhancement reported in the literature.

The sedimentation of nanoparticles over time (Fig. 2.9) is still a major challenge (Aref et al. 2017; W. Chen et al. 2017; L. Chen et al. 2008; Timofeeva, Moravek, and Singh 2011) that needs to be overcome before there can be widespread uptake of nanofluids (Colangelo et al. 2013). Simple methods have been proposed such as adding stabilising agents (surfactants) to the base fluid before the suspension of nanoparticles to lower the interfacial forces between the fluid molecules and the nanoparticles. However, even with the addition of surfactants there is no guarantee of permanent stability.

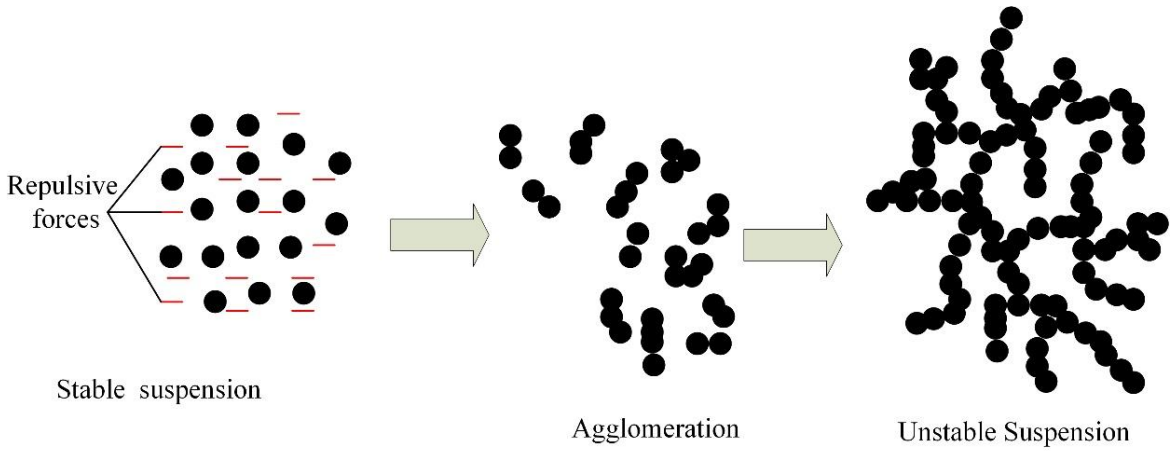

Figure 2.9 Suspension and stability of nanoparticles.

Nanofluids experience a number of effective forces during and after suspension such as drag, thermophoresis, Brownian, Van der Waals and electric double layer forces. Interfacial layers (Fig. 2.10) can build bridges between nanoparticles within the base fluid molecules, reducing their effectiveness (Sizochenko et al. 2017). This is a major challenge with no solution currently cited in the literature yet is one of the primary factors that many researchers think contributes to aggregation and subsequent sedimentation (Pal 2014; Machrafi and Lebon 2016; Pinto and Fiorelli 2016).

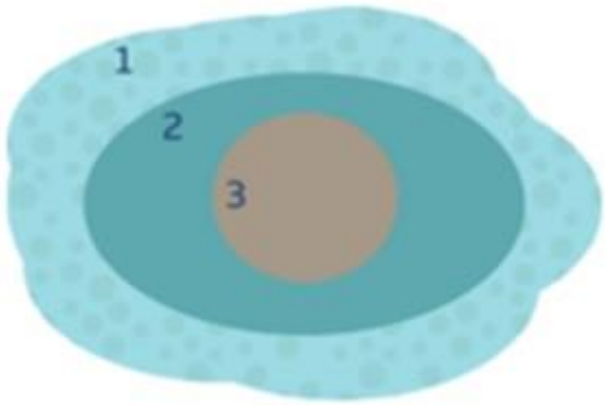

Figure 2.10 Structure of nanoparticle in the base fluid. Molecules of the liquid (1) can form a specific, highly ordered layer (2) near the nanoparticle surface (3).[66].

Yu et al. (F. Yu et al. 2017) suggested that a systematic summary of dispersing strategies of nanofluids in thermal applications is needed to provide general guidelines on the preparation and characterization of stable thermal nanofluids, and also to help bridge the gap between researchers in different disciplines.

Despite the fact that the field of nanofluids is still in the infancy, the future of nanofluids seems promising. Significant efforts continue to be devoted to theoretical and experimental studies in order to improve the general performance and potential applications of nanofluids. For instance, efforts are being made to reduce the production costs of nanofluids by developing large-scale production methods (Haddad et al. 2014; Hooman Yarmand, Azim Ataollahi, Oshkour Samira, Gharehkhani Seyed Farid, Seyed Shirazi, Siamak Pilban, Jahromi Mehran, Sookhakian, Saeid and Salim Newaz Kazi, Wan Jefrey 2015), and to improve the stability of nanofluids (Devendiran and Amirtham 2016; Fuskele and Sarviya 2017).

Furthermore, little experience can be found regarding pilot scale or full-scale plants. Numerous publications can be found, e.g., for solar thermal absorbers. No information is however to be found about high temperature, high pressure and long-term behaviour of nanofluids in such systems. Hence, besides basic research it is of great importance to expand studies to real application test environments. Besides the technological advance nanofluids can cause, safety issues need to be pursued with the same effort. What impact can nanoparticles of different materials, shape and size have on the human body?

The critical technical breakthroughs in industrial-scale production of nanofluids necessary to bring nanofluids to commercialization are expected to be achieved through continued support of nanofluid R&D and collaboration with industrial partners.

2.9 Conclusion

The use of nanofluids in a wide range of applications appears to be growing steadily. However, currently it appears that material scientists and chemists perform most investigations of nanofluids characterisation, whereas thermal and mechanical engineering researchers carry the experiments on the application of nanofluids, and there is not always close collaboration or communication between the two groups, which may contribute to the lack of agreements of results. The following major conclusions are drawn from this review of the literature:

- Nanofluids have a wide range of potential applications for heat transfer enhancement, including this present study (single-phase cooling /heating).
- There are wide ranges in heat transfer enhancement and physical property data for similar nanofluids reported in the literature.

- Customized tube inserts of various geometry and design employed in heat exchangers with nanofluids increase heat transfer coefficients as well as friction penalty.

This chapter has reviewed some historically major milestones toward the concept of nanofluids. In addition, the production, mechanisms and models of nanofluids have been reviewed. The performance, potential applications and benefits of nanofluids toward heat transfer enhancements have been addressed. Finally, the challenges toward the applicability of nanofluids in heat transfer systems have been addressed.

In the next chapter, what follows is the preparation and stability assessment of various combinations of nanofluids for the current study.

Chapter 3
Preparation and Stability Assessment of Nanofluids

3.1 Introduction

In Chapter 2, sedimentation of suspended nanoparticles over time was reviewed as a major challenge (Aref et al. 2017; W. Chen et al. 2017; L. Chen et al. 2008; Timofeeva, Moravek, and Singh 2011) that needs to be overcome before there can be widespread uptake of nanofluids. Nanoparticles in nanofluids show a tendency to agglomerate and later sediment at the bottom because of the big difference in density between the nanoparticles and the base fluid (Sánchez-Coronilla et al. 2017; Kouloulias, Sergis, and Hardalupas 2016; F. Yu et al. 2017; Harikrishnan et al. 2017). However, surfactants are capable of improving stability (Harikrishnan et al. 2017).

This chapter will discuss the preparation and observation of stability of various combinations of nanofluids and surfactants; and, the most stable nanofluids will be considered for heat transfer enhancement evaluation in a test rig.

The following questions will be addressed:

(1) Is there a combination of nanoparticles, base fluid and surfactant that can be prepared to improve stability of nanofluids for heat transfer single-phased applications?

(2) What is the best approach to assess stability of these nanofluids?

3.2 Nanofluid preparation

In this study, the two-step method of nanofluid preparation (Chapter 2, Fig. 2.3) was adopted because it is generally less labour-intensive and more cost effective (Haddad et al. 2014; Sidik et al. 2014; Li et al. 2009); and appears to be the most widely used technique.

3.2.1 Nanomaterials.

Early studies on nanofluids for improving heat transfer rates concentrated on two particular materials; copper oxide (S. U. S. Choi and Eastman 1995b; Eastman et al. 2001) and aluminium oxide (Masuda H., Ebata A. 1993; Xie et al. 2002; El Bécaye Maïga et al. 2005). Currently, there is a wide range of nanomaterials (Devendiran and Amirtham 2016) that have been studied and can be used to make nanofluids. In this thesis, activated carbon, copper oxide and alumina were selected to make nanofluids because of their affordability and physical characteristics (see Table 3.1) such as the large specific surface area which is capable of increasing the contact area between liquid molecules and nanoparticles.

Table 3.1 Physical characteristics of nanoparticles produced and supplied by NanoAmor (Nanostructured and amorphous Inc. 2019)**.** (Thermal conductivity data not provided by manufacturer).

Nanomaterial	***Average particle size* (nm)**	***Density* ($kg.m^{-3}$)**	***Specific surface* area ($m^2.kg^{-1}$)**	***Purity* (%)**
Activated carbon	50	500	500000	99.5
Copper Oxide	30 - 50	6315	13100	99.0
Alumina	20 - 30	3950	180000	99.97

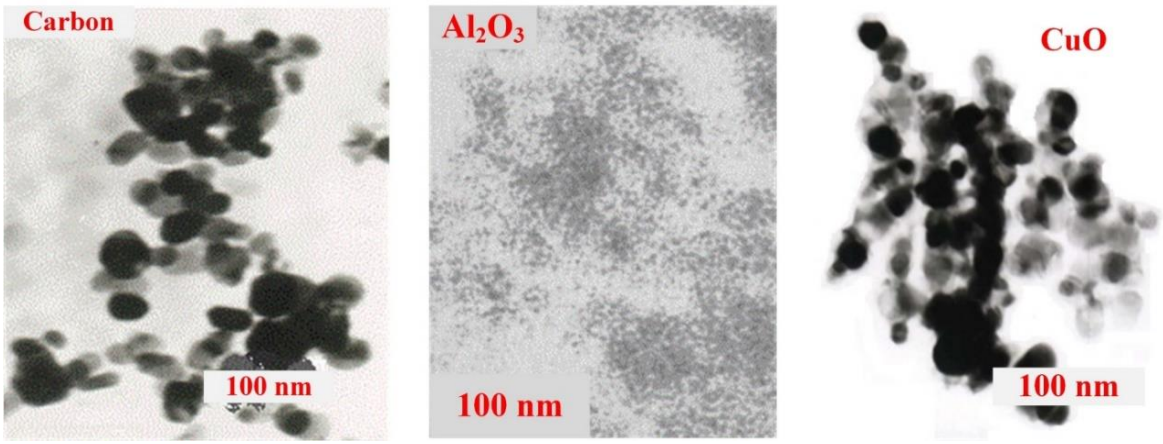

Figure 3.1 Transmission electron microscopic (TEM) images of (a) activated carbon, (b) copper oxide and (c) alumina nanoparticles (Nanostructured and amorphous Inc. 2019)**.**

3.2.2 **Base fluids**

Water (H_2O) is the most commonly used base fluid to make nanofluids because it is cheap, non-toxic, and above all its thermal conductivity is comparatively high compared to other tradition fluids. Besides water, ethylene glycol (EG) is also popular in nanofluids investigations because it has a high boiling point and low melting point compared to water. The physico-chemical properties of water, and ethylene glycol are shown in Table 3.2.

Table 3.2 Physico-chemical properties of base fluids.

Base fluid	***Formula***	***Density*** **(kg/m^3)**	***Boiling point*** **(ÁC)**	***Thermal conductivity*** **(W.m.K)**
Water	H_2O	997	100	0.60
Ethylene glycol	$C_2H_6O_2$	1110	197.3	0.25

3.2.3 Surfactant selection.

The fact that nanoparticles have higher densities than most base fluids means that suspended nanoparticles are most likely to sediment after preparation. Surfactants are capable of improving the stability of nanofluids because they reduce the interfacial tension between the base fluid molecules and the suspended nanoparticles (Manilo et al. 2018; Duangthongsuk and Wongwises 2009). Effective surfactants induce repulsive forces between suspended particles, and cause hydrophobic surfaces to behave like hydrophilic surfaces (Mahbubul 2019).

A selection of low toxicity and cost-effective surfactants including sodium lauryl sulphate (SDS), cetyltrimethyl ammonium bromide (CTAB), sodium dodecyl benzene sulfonate (SDBS) and Arabinogalactan (ARB) (P. K. Das et al. 2018) were investigated for use as stabilizing agents. Their high melting point (Table 3.3) and solubility with base fluids were considerable interests to preparing stable nanofluids that will be later used in a closed-loop rig to investigate heat transfer enhancements.

Table 3.3 Physico-chemical properties of surfactants

Surfactant	*Class*	*Formula*	*Melting point (°C)*
ARB	neutral	$C_{20}H_{36}O_{14}$	200 - 204
SDBS	anionic	$CH_3(CH_2)_{11}C_6H_4SO_3Na$	204 - 207
CTAB	cationic	$C_{19}H_{42}BrN$	237 - 243
SDS	anionic	$NaC_{12}H_{25}SO_4$	206

3.2.4 Preparation process

Nanoparticles were weighed and then added in sample bottles containing base fluid (water or ethylene glycol). Subsequently, 2 g of surfactant was added followed by stirring and ultra-sonication with Qsonica (Q500) sonicator Fig. 3.2. Ultra-sonication causes mechanical vibration that creates microscopic bubbles. The bubbles cycle into the solution, collapse and break apart the molecules thus forming homogenous and stable solutions. Based on recommendations of Lin et al. (Lin, Peng, and Ding 2015), nanofluids were kept under ultra-sonication for 1 hour with the micro-tip probe amplitude and the pulse set to 20% and 10 seconds respectively.

The volume concentration of nanoparticles 'ϕ' was calculated using Eqs. 3.1 and 3.2 for nanofluids with or without surfactants respectively; where 'm' denotes mass, 'ρ' is the density. Subscripts 's' indicate surfactant, 'p' and 'b' symbolise (nano) particle and base fluid respectively.

$$\phi = \frac{\left(m_p/\rho_p\right)}{\left(m_p/\rho_p\right) + \left(m_{bf}/\rho_{bf}\right) + \left(m_s/\rho_s\right)} \tag{3.1}$$

$$\phi = \frac{\left(m_p/\rho_p\right)}{\left(m_p/\rho_p\right) + \left(m_{bf}/\rho_{bf}\right)} \tag{3.2}$$

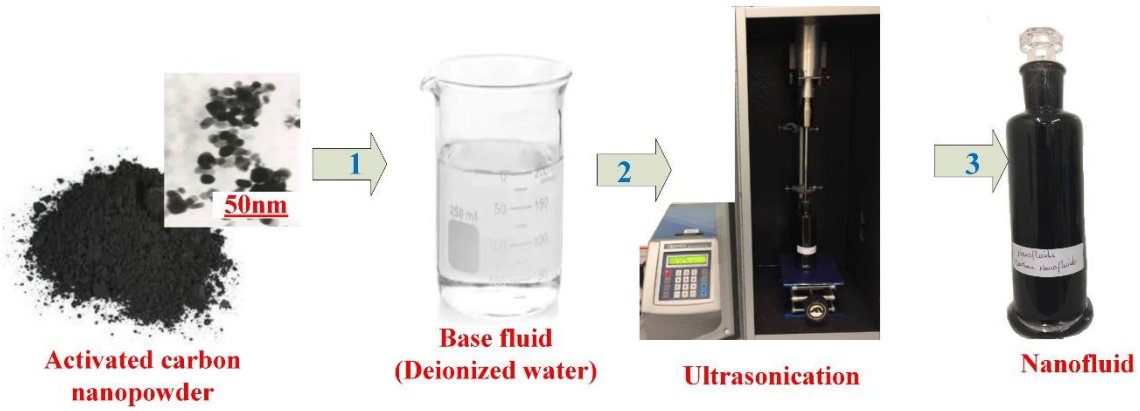

Figure 3.2 Nanofluids preparation process.

Table 3.4 Concentration of nanoparticles in nanofluids.

Nanofluid	*Base fluid (l)*	*Nanoparticles (kg)*	*Volume concentration (vol. %)*
C/H_2O	0.04	0.002	1.45
C/EG	0.04	0.002	1.59
CuO/H_2O	0.04	0.002	0.75
CuO/EG	0.04	0.002	0.82
Al_2O_3/H_2O	0.04	0.002	1.23
Al_2O_3/EG	0.04	0.002	1.35

3.3 Stability measurements

Several approaches have been used to evaluate the stability of nanofluids with the methods differing from one another based on the type or application of the nanofluids. The advantages and disadvantages of these techniques are summarised below.

3.3.1 Zeta-potential

This method determines stability by measuring how fast suspended nanoparticles move in an applied electric field. However, it is reported (Nanocomposix 2012) that the technique has the following disadvantages:

- it cannot be applied to highly conductive nanofluids, because the movement of conductive ions leads to electrode polarization and degradation

- data quality is reduced at very high concentrations because the sample absorbance diminishes the intensity of the scattered light and multiple scattering events
- the instrument requires sufficient light scattering events in order to calculate a Zeta potential value accurately
- The calculation that determines Zeta potential can be affected by the unknown solution properties such as viscosity and temperature.

Moreover, when quantitative results of zeta-potential and that of the sedimentation test were compared the conclusion was zeta-potential value cannot represent the suspension stability of nanofluids (Kim et al. 2015).

3.3.2 UV-vis spectroscopy

A strong light beam passes through a sample to a photodetector from which stability is evaluated as the amount of UV-visible light absorbed or scattered before and after passing through the sample. However, Ghadimi et al. (Ghadimi, Saidur, and Metselaar 2011) highlighted that this method is unsuitable for highly concentrated or dark coloured nanofluids because it leads to high absorbance of incident light and diminishes the intensity of scattered light which reduces the quality of data.

3.3.3 Electron microscopy

This technique involves either a scanning or transmission electron microscope (SEM/TEM) from which an electronic beam is scanned over a sample and transmitted through a sample to create images and relevant information about the sample. However, while this approach provides relevant data on morphology and particle size, the information on stability is generally insufficient. In addition, it only evaluates a small sample; and the measurement accuracy depends on the contrast of the sample relative to the background (Celine 2012).

3.3.4 Sedimentation

One of the questions posed in the beginning of this chapter was, “What is the best approach to assess stability of nanofluids?”. Having mentioned many shortcomings from these other stability techniques (Zeta-potential, UV-vis spectroscopy and electron microscopy), the sedimentation technique where stability is determined by measuring the height of a supernatant as a function of settling time appears to have less limitations; Many experts (Kouloulias, Sergis, and Hardalupas 2016; Ramin Ranjbarzadeh et al. 2018; Shao et al. 2015) now believe that this approach is simple, inexpensive and provides accurate visual results using photographs compared to other techniques. Therefore, this method was used to assess the stability of nanofluids throughout this thesis.

3.4 Measurement procedure

Immediately after preparation, nanofluid samples were placed on a flat table. A ruler was placed vertically close to the sample bottle to measure the height of sediment over a period of 30 days. At the same time as a height measurement was made, photographs were taken as illustrated in Fig. 3.3.

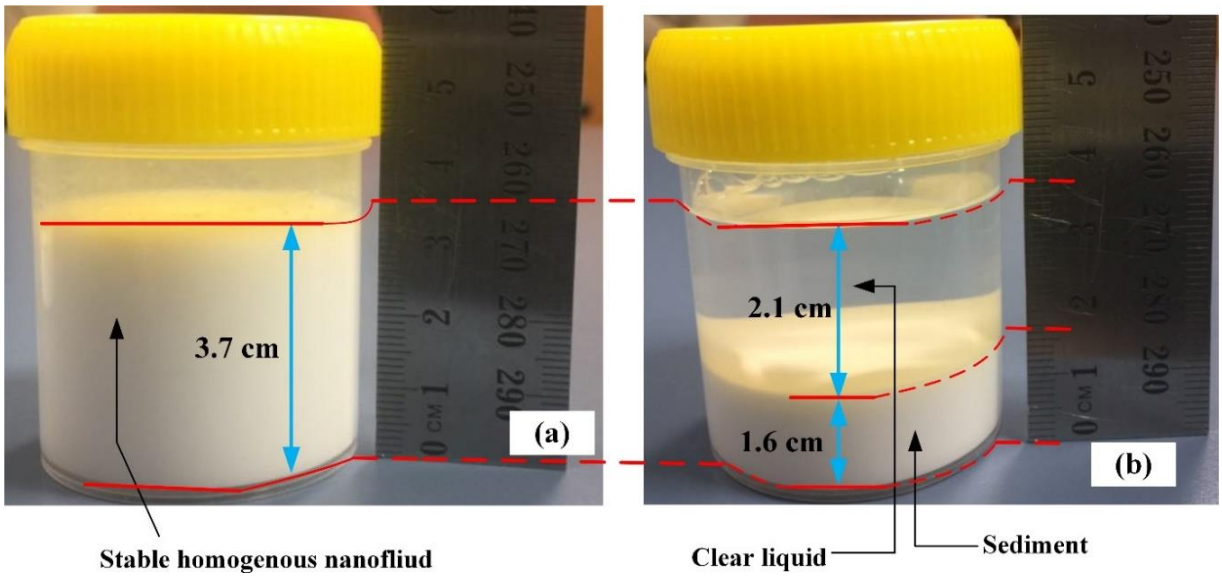

Figure 3.3 Fresh stable nanofluid on the day of preparation (a) and (b) variation of sediment height after time.

3.5 Results and discussion

A comparison between Figs. 3.4 and 3.5 shows that ARB as a surfactant maintained the stability of C/H_2O, CuO/H_2O and CuO/EG nanofluids for 29, 19 and 29 days respectively, longer than other surfactants. This might have happened because the structure of ARB allows complete solubility, excellent dispersion and stability over a wide range of concentrations (D'Adamo 1996; Mucalo et al. 2002)

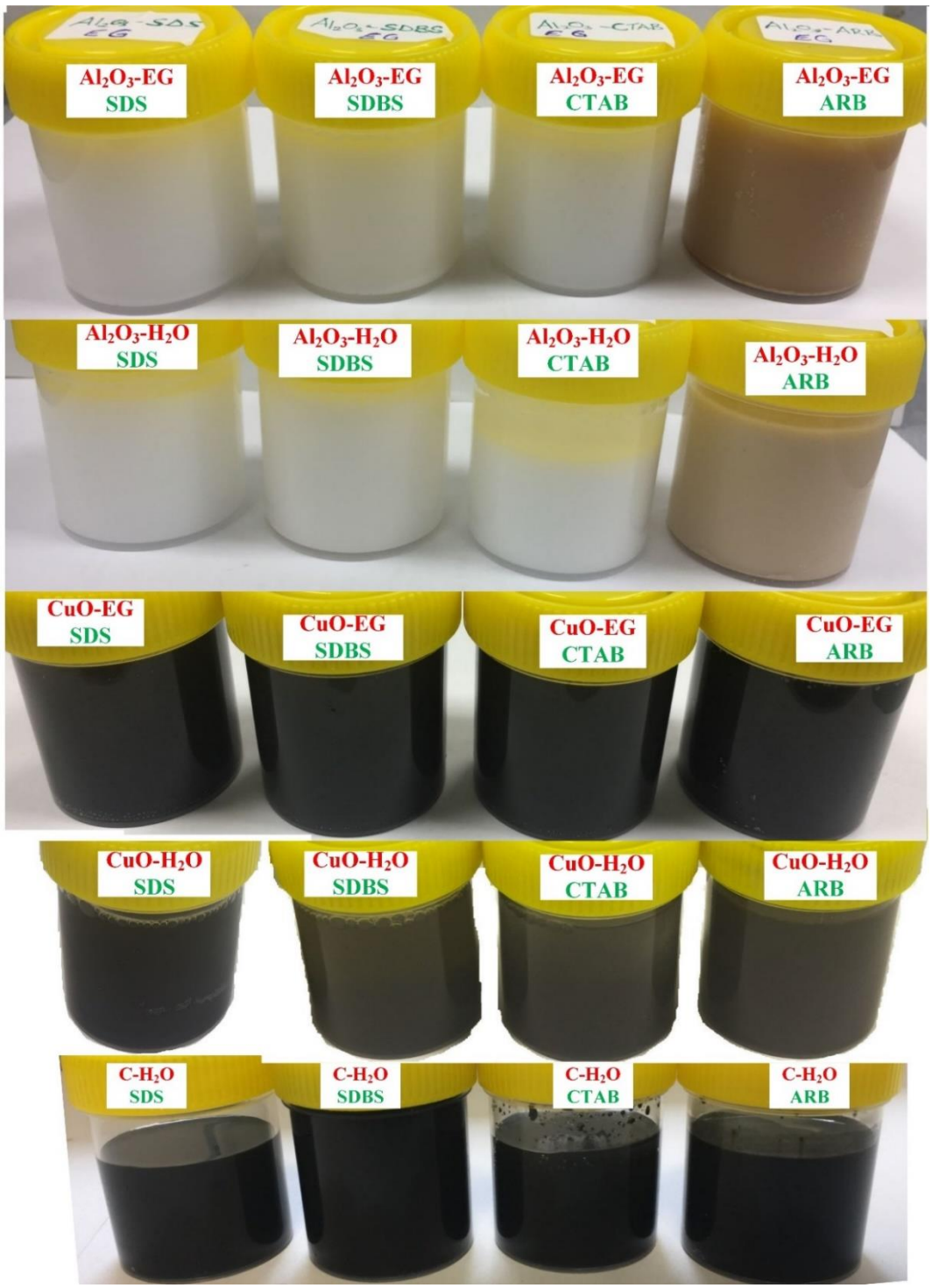

Figure 3.4 Samples of nanofluid with varying surfactants immediately after preparation.

Figure 3.5 Samples of nanofluid with varying surfactants after 30 days.

Shin et al. (Shin, Premkumar, and Geckeler 2008) pointed out that neutral surfactants (Table 3.3) can easily interact with the surfaces of nanoparticles which may enhance the binding and surface coverage of nanoparticles to molecules. For that reason, it is probable that the interaction of anionic (SDBS and SDS) and cationic (CTAB) surfactants with surfaces of C/H_2O and CuO/EG nanofluids might have been weakened, thus leading to lower stability times except for C/H_2O nanofluid with CTAB that lasted for 17 days.

Figure 3.6 shows that CTAB and SDS sustained the stability of C/H_2O nanofluid for 17 and 10 days respectively longer than SDBS that lasted for only 2 hours. Hakiki et al. (Hakiki, Maharsi, and Marhaendrajana 2015) stated that when the surface coverage by the surfactants increases, the surface free energy decreases and the surfactants start aggregating into micelles. Surprisingly, SDBS maintained stability of Al_2O_3/H_2O nanofluid for 11 days compared to CuO/H_2O and C/H_2O nanofluids stability that lasted for 3 and 2 hours respectively.

It has been suggested that surface tension increases as nanoparticle size increases (Zhu et al. 2011; Munyalo and Zhang 2018). For this reason, the time that nanoparticles stayed in suspension might have been reduced because of the difference in the average particle size of C and CuO compared to Al_2O_3 (Table 3.1). The adsorbed surfactant is degraded by the increased attractive charges between particles, thereby reducing the time nanoparticles stay in suspension.

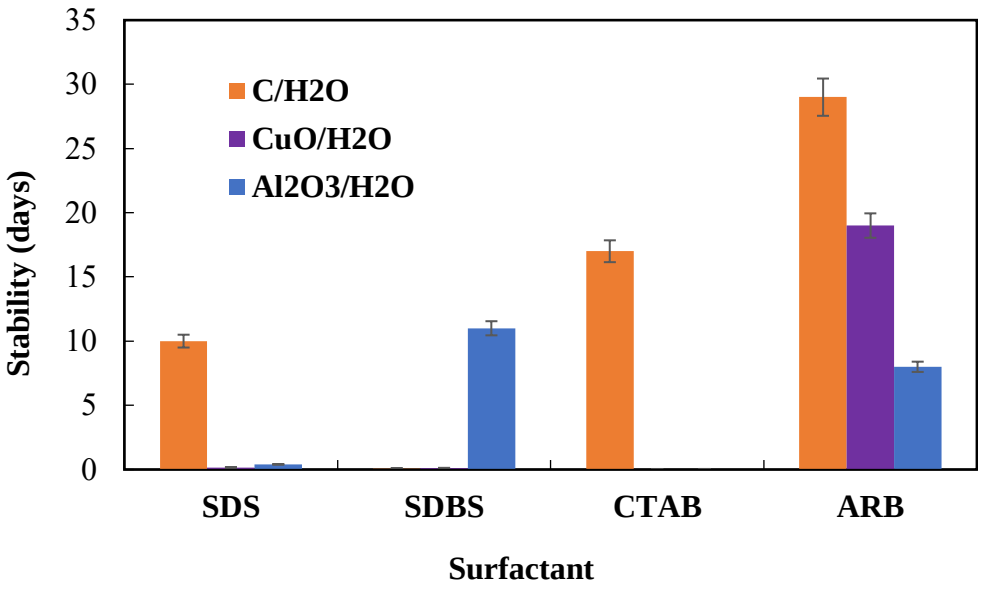

Figure 3.6 Stability timeline of nanofluids with water as base fluid.

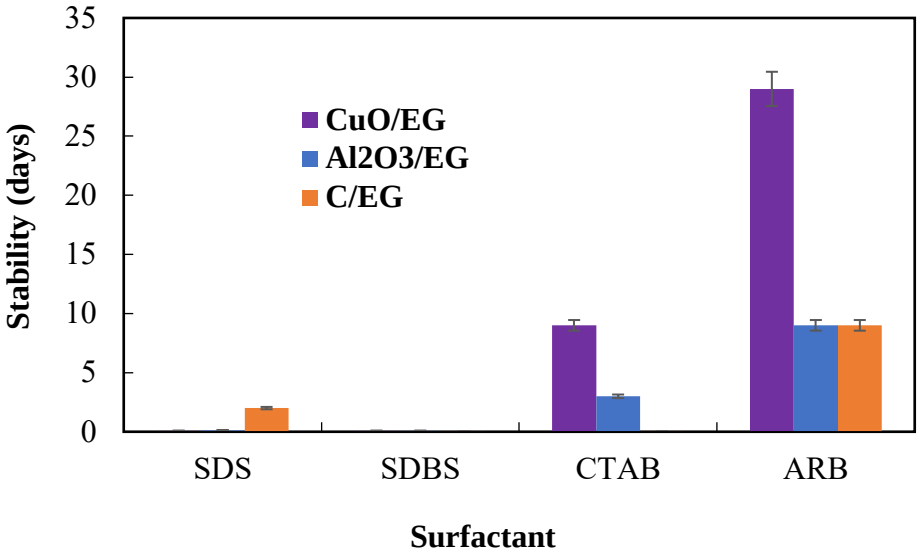

Figure 3.7 Stability timeline of nanofluids with ethylene glycol as base fluid.

In the beginning of this Chapter, the first question that was asked was, "Is there a combination of nanoparticles, base fluid and surfactant that can be prepared to improve stability of nanofluids for heat transfer single-phased applications?". The answer is, there is no permanent stability of nanofluids based on all combinations of nanofluids prepared and observed over a period of 30 days. However, some combinations of nanofluids including C/H_2O/ARB, CuO/EG/ARB, C/H_2O/CTAB and Al_2O_3/H_2O/SDBS were stable for more than 10 days compared to the rest of the combinations of nanofluids.

3.6 Conclusion

The aim of this chapter was to evaluate the stability of nanofluids with various surfactants and select the most stable nanofluids for heat transfer enhancement evaluation in a test rig. The findings are:

- After time, nanoparticles agglomerate and later sediment at the bottom of the vessel to form a thick solution regardless of any combination of either surfactant or base fluid. However, ARB as a surfactant presented the best stability within the period of 29 days for C/H_2O and CuO/EG. CTAB showed better stability of C/H_2O for 17 days. Al_2O_3/H_2O nanofluid remained stable for 11 days with SDBS surfactant.

- It is still a challenge to build-up a standard evaluation stability technique; to account for properties of nanofluid as a whole; targeting specifically surface

modifications of suspended nanoparticles and liquid molecules in a single measurement or evaluation.

This chapter has detailed the preparation process and stability assessment of nanofluids with various surfactants. The next chapter will discuss physical property measurement of nanofluids including viscosity, thermal conductivity, density and specific heat capacity. Thereafter, a clear assessment will be conducted, and the outcomes from the next chapter together with stability conclusions made in this chapter will lead to a selection of combinations of nanofluids to be tested for heat transfer in the rig.

Chapter 4

Physical property measurement of nanofluids

4.1 Introduction

In Chapter 2, it was reviewed that thermal conductivity and viscosity of nanofluids remains an area requiring further investigation, particularly as the effect of the surfactant on physical properties is not always taken into consideration.

The conclusions in Chapter 3 showed that stability of nanofluids, as assessed, by the sedimentation method, was significantly affected by the presence of a surfactant; however not all surfactants worked equally well with each nanoparticle/base-fluid pairing.

Density, specific heat capacity, thermal conductivity and viscosity of nanofluids all depend on nanoparticle concentration; however, thermal conductivity and viscosity are volumetric properties (i.e., the measured property will be affected by the spatial distribution of the nanoparticles) whereas density and specific heat capacity are not. Previous studies have shown that the density, viscosity and thermal conductivity of nanofluids increases with increasing nanoparticle concentration (Devendiran and Amirtham 2016; Sezer, Atieh, and Koç 2019). In some cases, it has been reported that specific heat capacity increases (Tiznobaik and Shin 2013; Yarmand et al. 2016; Ghazvini et al. 2012) or decreases (J. Lee and Mudawar 2007b; Kulkarni et al. 2008; Pandey and Nema 2012) with nanoparticle concentration.

The aim of this chapter is to assess the impact of surfactants on physical properties of nanofluid focusing mainly on volumetric properties (viscosity and thermal conductivity) because these two properties are inherently more difficult to measure.

First, viscosity for wide range of nanofluid combinations will be measured, which will then lead to a selection of nanofluid combinations whose thermal conductivity, density and specific heat capacity will be assessed. Finally, conclusion will be made for selection of nanofluids combinations to be tested for heat transfer in a closed test loop. The questions yet to be answered here are:

(1) What is the impact of surfactants on physical properties of nanofluids?

(2) Can the viscosity measurements of nanofluids be replicated after a period of time?

(3) Why is there so much variability in the reported thermal conductivity measurements?

4.2 Viscosity

4.2.1 Measurements and data analysis

Viscosity is measured by either monitoring the movement of fluid through a channel subject to shear forces (dynamic viscosity), or by observing the time required for a given volume of liquid to flow through a capillary or restriction (kinematic viscosity) (Stewart 2016a).

In this study, combinations of nanofluid samples whose viscosity was tested were prepared in the similar fashion as described in Chapter 3 with similar quantities of nanoparticles and surfactants for both base fluids (distilled water and Ethylene glycol).

Viscosity was measured using an Anton-Paar digital viscometer (DV - 1P) Fig. 4.1. This viscometer measured the torque created by the rotation of a spindle at constant speed from which dynamic viscosity was obtained as a value proportional to the measured torque (Paar and Viscometers 2006). Dynamic viscosity measurements '$\mu_{measured}$' were later compared to the viscosity of distilled water to obtain relative viscosities '$\mu_{relative}$' as

$$\mu_{relative} = \frac{\mu_{measured}}{\mu_{water}} \tag{4-1}$$

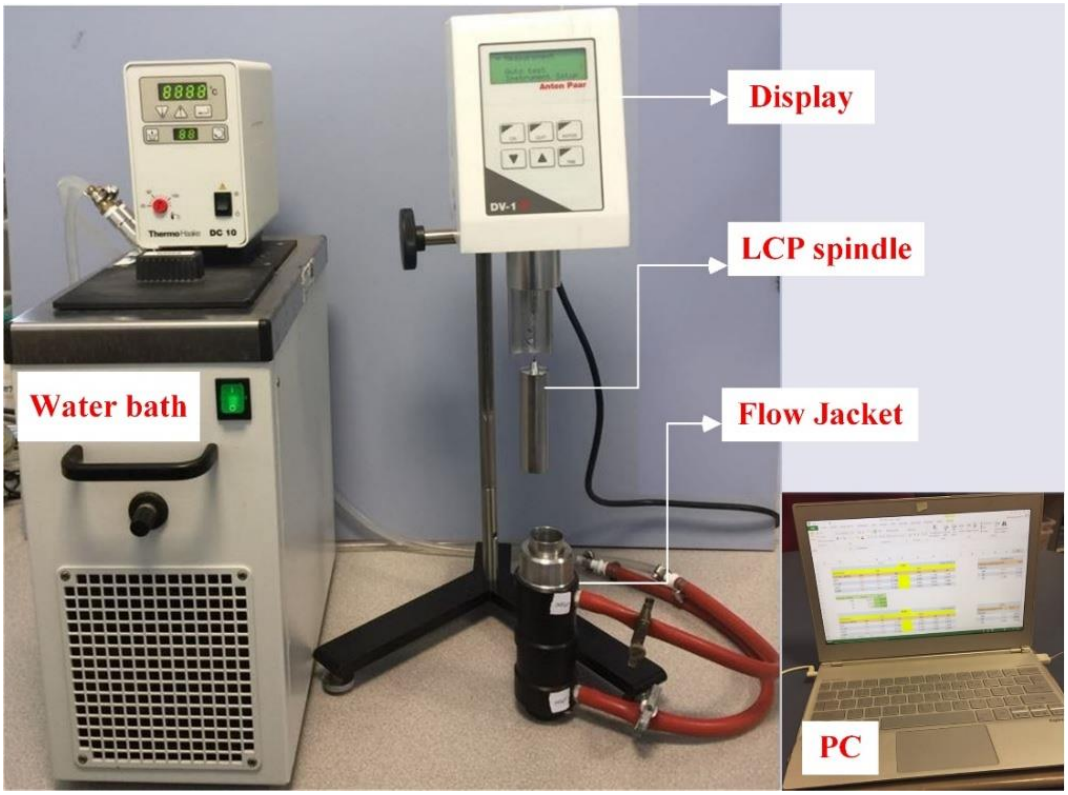

Figure 4.1 Viscometer and water bath.

Prior to starting measurements, the flow jacket that housed the sample chamber was connected to a water bath flow loop to maintain steady nanofluid sample temperatures. The low viscosity adapter 'LCP spindle' was used throughout the entire investigation because it allows accurate measurements for the viscosity ranges expected for nanofluids, as suggested by the user's manual (Paar and Viscometers 2006).

The viscometer spindle had three choices of rotational speeds: 30, 50 and 100 revolutions per minute (rpm). The viscometer accuracy and repeatability of the full-scale range of the measurements values was stated by the manufacturer to be ± 1 % and ± 0.2 % respectively [20]. The water bath was set at 25 °C, and the spindle was lowered into the sample chamber. Thereafter, the viscometer was levelled for accurate measurements. For each viscosity measurement, three viscosity readings were recorded with a minute time interval between each reading.

Distilled water being a Newtonian fluid was used as a reference to study the impact of shear rate on viscosity measurements of nanofluids. This is because Newtonian fluids are preferred in thermal systems; they have constant viscosity at a particular temperature and pressure; and are independent of shear rate (Stewart 2016b).

Shear rate '$\dot{\gamma}$' was calculated using Eqs. 4.2 – 4.4. Where 'V' is the linear velocity, 'n' is the rotational speed (rpm), 'ω' and 'r' are the angular velocity and the radius of the sample chamber and the spindle denoted with subscripts 'c' and's' respectively.

$$V = \omega r \tag{4-2}$$

$$\omega = 2\pi n \tag{4-3}$$

$$\dot{\gamma} = \frac{\omega r_s}{r_c - r_s} \tag{4-4}$$

4.2.2 Results and Discussion

A percentage index '$\beta_{\%}$' defined by (Eq. 4.5) was used to determine the magnitude of viscosity where μ_a is the average relative viscosity of nanofluid with surfactant divided by μ_b relative viscosity of nanofluid with no surfactant.

$$\beta_{\%} = \left(\frac{\mu_a}{\mu_b} - 1\right) 100 \tag{4-5}$$

The viscosity of nanofluids with ethylene glycol (EG) as a base fluid exceeded the range that the viscometer can measure at speeds above 30 rpm, so only results at this speed are presented. Figure 4.2 shows the viscosities of nanofluids with the combinations of three nanoparticles and four surfactants, along with control samples that did not have surfactant, measured at 30 rpm. The most significant increase in viscosity due to the presence of surfactants, was registered from SDS and CTAB surfactants in C/EG nanofluid with an increase of 63 % and 67.5 % respectively. ARB yielded the least increase in viscosity for C/EG and Al_2O_3/EG nanofluids as shown in Table 4.1. SDS registered the least enhancement of 6.5 % for CuO/EG nanofluid.

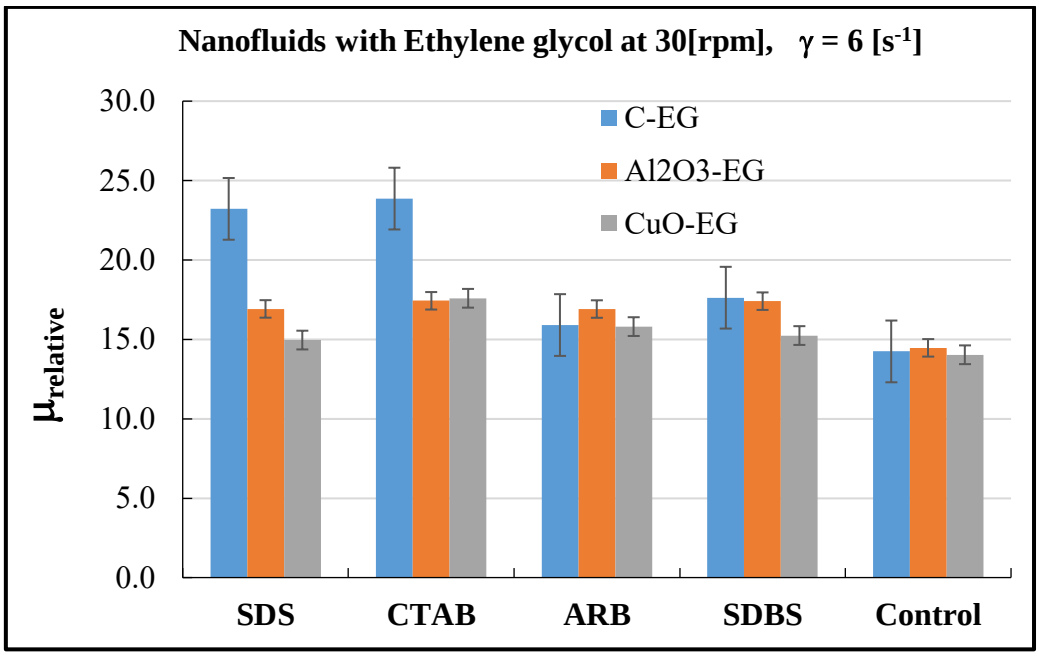

Figure 4.2 The effect of surfactants on viscosity measurements of nanofluids with EG as base fluid at *T* = 25ÁC.

Table 4.1 Viscosity increase (%) of Ethylene glycol based nanofluids with various surfactants

	Viscosity increase (%)		
Surfactant	***C/EG***	***Al_2O_3/EG***	***CuO/EG***
SDS	63.04	16.95	6.59
CTAB	67.58	20.48	25.35
ARB	11.67	16.89	12.65
SDBS	23.76	20.32	8.63

Table 4.2 Viscosity increase (%) of water based nanofluids with various surfactants

	Viscosity increase (%)		
Surfactant	***C/H_2O***	***Al_2O_3/H_2O***	***CuO/H_2O***
SDS	22.81	121.49	34.83
CTAB	6.43	334.71	17.22
ARB	119.30	107.44	7.31
SDBS	11.70	17.36	21.19

Figure 4.3a demonstrates that the viscosity of C/H_2O nanofluid was independent of shear rate regardless of any surfactant used. However, ARB that presented the best stability (Chapter 3) for keeping nanoparticles in suspension for more than 20 days showed a remarkable increase in viscosity with an enhancement of 119.3 % compared to C/H_2O nanofluid with no surfactant. Moreover, Fig. 4.3b illustrates that the addition of CTAB and ARB created a shear thickening behaviour for CuO/H_2O nanofluids whereas the viscosity of nanofluids with SDS and SDBS seemed to be independent of shear rate. Equally important, a slight increase of 15 % in viscosity of CuO/H_2O nanofluid with SDS compared to the nanofluid without surfactant was noticed.

CTAB increased the viscosity of Al_2O_3/H_2O nanofluid by 251.3 % (Fig. 4.3c). Shear thinning behaviour can be clearly noticed specifically at low values of shear rate between 5 to 10 s^{-1}. It is known that cationic surfactants like CTAB possess positive charges on their hydrophilic end that interact with nanoparticles (Stebe and Lin 2001; Langevin 1998). Therefore, this observation might have occurred due to the breakdown of aggregated nanoparticles. Comparatively, the viscosity of Al_2O_3/H_2O nanofluid with SDS, ARB and SDBS was independent of shear rate.

Compared to other surfactants, SDBS appeared to have the least deformation against shear rate for water-based nanofluids; hence confirming Newtonian behaviour as illustrated in Fig. 4.3.

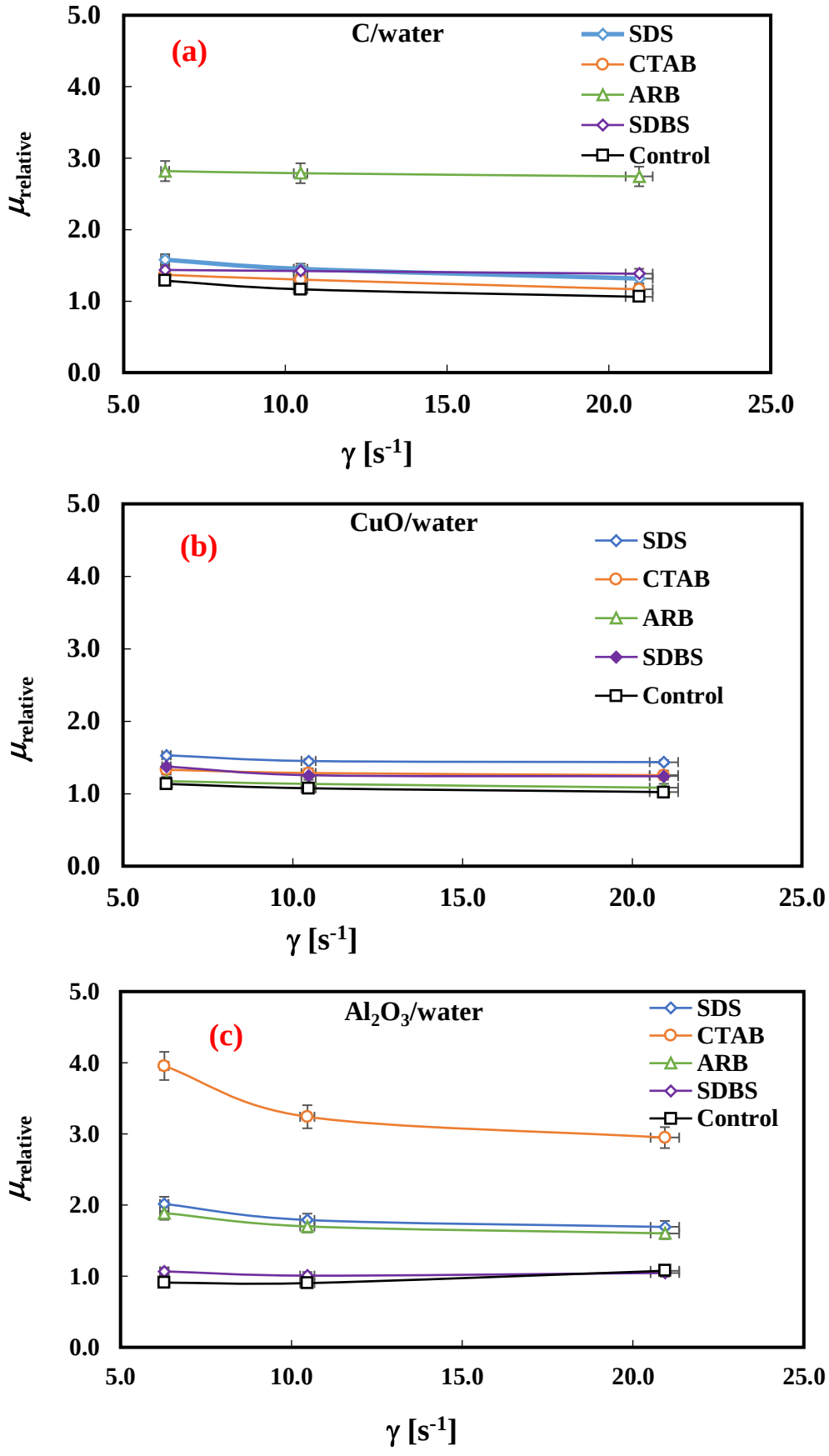

Figure 4.3 Viscosity measurements as a function of shear rate for nanofluids with water as base fluid at *T* = 25 ÁC.

Can the viscosity measurements of nanofluids be replicated after seven weeks? This was one of the questions posed in the beginning of this chapter. Having observed the stability of various combinations of nanofluids in Chapter 3 for over 30 days, in order to determine whether there is consistency or variation in the viscosity of nanofluids over time repeated measurements on immediately prepared fresh samples and those kept after a period of seven weeks were performed with the assistance of undergraduate student (Luka Ellery).

The results across all of the nanofluids showed that relative viscosity had increased to a certain degree for the samples tested after seven weeks (Table 4.2). This was, on average, by a factor of 1.2 for C/H_2O, 1.25 for CuO/H_2O and 1.55 for Al_2O_3/H_2O. It is likely that the increase in viscosity after the seven-week period was due to the nanoparticles agglomerating and increasing shear resistance. It is also believed that thixotropic behaviour was taking place because the viscosity increased with time, possibly due to nanoparticles networks that have formed over time.

Table 4.3 Average relative viscosity of nanofluids without surfactant immediately after preparation and seven-week later.

Nanofluid	$\mu_{relative}$	
	Fresh	**7 weeks**
C/H_2O	1.20	1.45
CuO/H_2O	1.07	1.35
Al_2O_3/H_2O	1.11	1.70

In Fig. 4.4, results show a larger error for the seven-week nanofluids compared to freshly prepare. While this is still a relative uncertainty, it illustrates how the behaviour of nanofluids becomes difficult to predict over time due to large uncertainties in results. However, it appears that freshly prepared nanofluids can be repeatable consistently with low uncertainty.

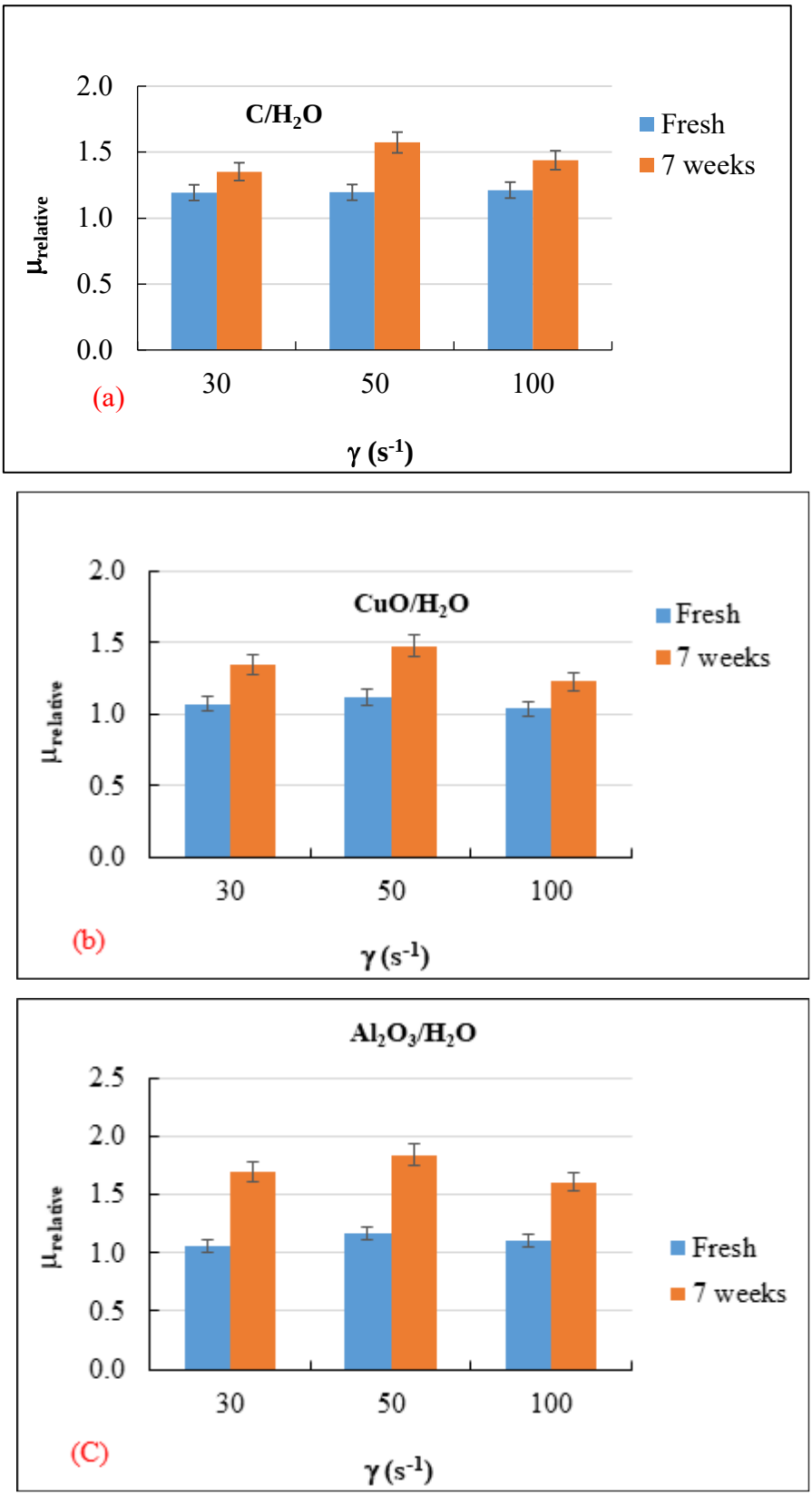

Figure 4.4 A comparison of viscosity measurements on the day of preparation and seven weeks later for: (a) C/H_2O, (b) CuO/H_2O and (C) Al_2O_3/H_2O nanofluids.

In summary, viscosity being a transport property that defines the internal resistance of a fluid to flow is directly related to pressured drop hence determining the capacity and energy consumption of the pumps (Kaggwa and Wang 2016). Therefore, based on the results presented in this section it can be concluded that some surfactants have increased the viscosity of nanofluids. Also, in fluid mechanical applications such as heat transfer, Newtonian nanofluids would be a priority for convective heat transfer accountability. However, the results indicate that some surfactants created shear thinning or thickening behaviour. The results produced in this investigation appear to be relatively consistent and repeatable, particularly in the case of the freshly prepared nanofluids results. The viscosity measurement shear rates in the present study were limited by the measurement viscometer that was available, and may not necessarily match those encountered in practice.

4.3. Thermal conductivity

Nanofluids yield significant magnitudes of thermal conductivity as a result of suspended nanoparticles. For that, a large number of models have been proposed. However, Section 2.6 of Chapter 2 demonstrated significant differences in model predictions; which makes it difficult to know from a wide range of proposed models which model to use to determine effective thermal conductivity of nanofluids.

Various techniques that have been used to measure thermal conductivity include; coaxial cylinders (Pongsawatmanit, Miyawaki, and Yano 1993), temperature oscillation (Bhattacharya et al. 2006; Czarnetzki and Roetzel 1995), parallel-plate (X. Wang, Xu, and Choi 1999), transient analysis (transient hot-wire (Guo et al. 2018) and transient interfacial heat reflectance surface (Thermtest Instruments 2004)). The transient analysis method is the most commonly used approach by many devices across various manufacturers to measure thermal conductivity because transient methods are not affected by contact resistance (Komini Babu et al. 2013; Thermtest Instruments 2004).

Previous studies have reported inconsistent and contradictory thermal conductivity findings of similar nanofluid combinations (see Figs. 4.5 and 4.6); and there is no widely accepted explanation for the wide variability in thermal conductivity data.

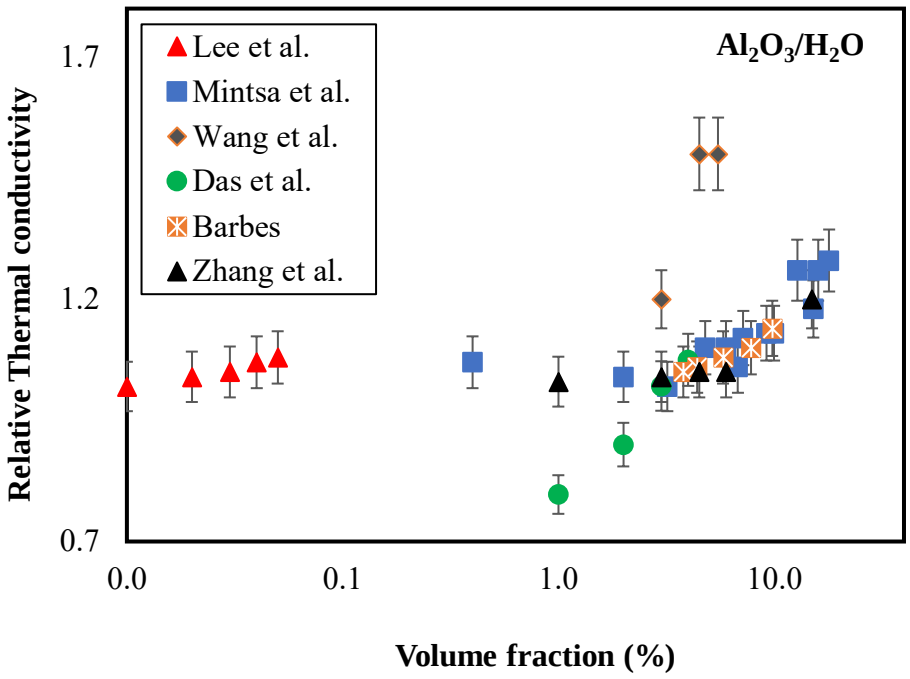

Figure 4.5 A comparison of measured thermal conductivity of Al_2O_3/H_2O nanofluid (S. Lee et al. 1999b; Mintsa et al. 2009; X. Wang, Xu, and Choi 1999; Sarit Kumar Das et al. 2003; Barbés et al. 2013; Zhang et al. 2006)

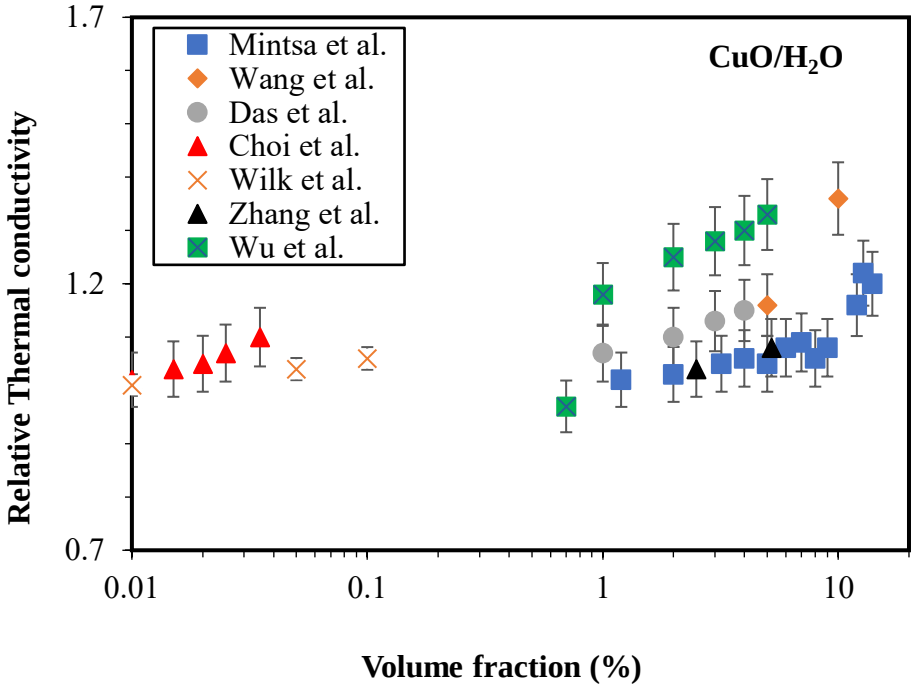

Figure 4.6 A comparison of measured thermal conductivity of CuO/H_2O nanofluid (Mintsa et al. 2009; X. Wang, Xu, and Choi 1999; Sarit Kumar Das et al. 2003; S. Lee et al. 1999b; Wilk, Smusz, and Grosicki 2017; Zhang et al. 2006; Wu et al. 2009; Maxwell 1892)

Initially, the thermal conductivity of C/H_2O, Al_2O_3/H_2O, CuO/H_2O, CuO/H_2O/ARB and C/H_2O/CTAB nanofluids was measured using the transient hot-wire probe, since this device was available at the University of Waikato.

The transient hot-wire method is based on the principle of calculating the transient temperature field around a thin wire, which can be treated as a line heat source. The wire is immersed in the sample in which thermal conductivity is to be measured. The wire serves as both the heat source and the temperature sensor. The heat generated in the wire increases the temperature of both the wire and the sample fluid. The increasing temperature of the wire is proportional to the thermal conductivity of the sample fluid in which the wire is immersed (Thermal Sensors 2019).

4.2.3 Measurement procedure of nanofluid using a probe.

A Hukseflux™ model TP08 Small Size Non-Steady-State (Thermal Sensors 2019) (Fig. 4.7) was used to evaluate thermal conductivity of nanofluids.

Figure 4.7 Thermal conductivity probe.

This probe consists of a needle 70 mm long, with a thermocouple junction (Type K) located at about 15 mm from the tip and a heating wire. In the base, a temperature sensor (Pt 1000, Class B) is mounted (Fig. 4.8). The probe measures thermal conductivity within the range of 0.1 to 6 W m^{-1} K^{-1}. The probe needle can withstand temperatures ranging from −55 to +250 °C. The expected accuracy and repeatability of this equipment is ± 3 % and ± 1 % respectively for homogeneous media with good contact to the needle (Thermal Sensors 2019).

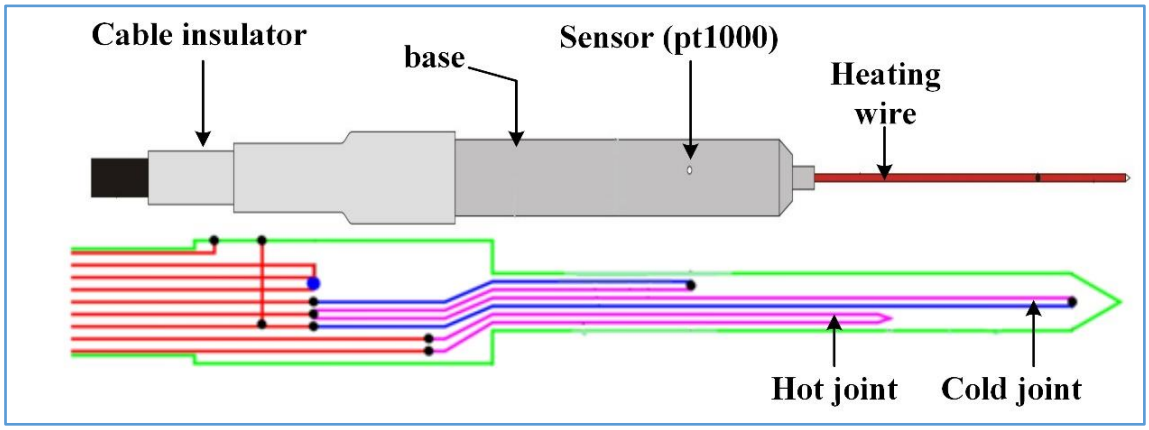

Figure 4.8 Schematic diagram of the thermal sensor probe [17].

Nanofluid samples whose thermal conductivity was to be measured were prepared using similar procedures in Chapter 3. Later on, the container with the nanofluid sample was placed inside a temperature-controlled bath that was set at 25 °C. Once the sample had equilibrated thermally, the TP08 probe was introduced into the container holding nanofluid samples. Based on the user manual of the probe (Thermal Sensors 2019), the expected accuracy and repeatability of this equipment is ± 3 % and ± 1 % respectively for homogeneous media with good contact to the needle. For each sample a minimum of four replicate measurements were performed.

A shunt resistor was connected in the circuit (blue-box Fig. (4.9) to measure current. Thereafter, a multi-meter was connected to the terminals of the box to display and read off the measured current (i).

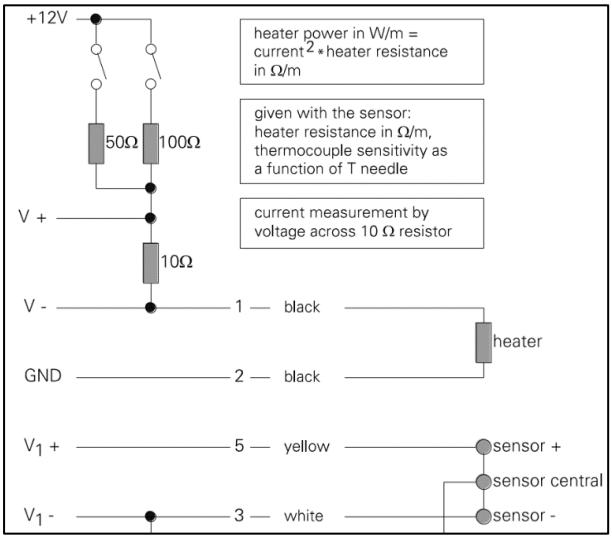

Figure 4.9 An electric circuit diagram of TP08 thermal sensor housed in the box.

The total heat 'Q_{net}' supplied to the measured fluid by the probe is evaluated from

$$Q_{net} = i^2 R_{probe} \tag{4-6}$$

Where the resistance of the probe 'R_{probe}' was specified by the manufacturer to be 83.94 Ω/m. The probe was connected to a channel of a Pico USB TC-08 data-logger (Fig. 4.10).

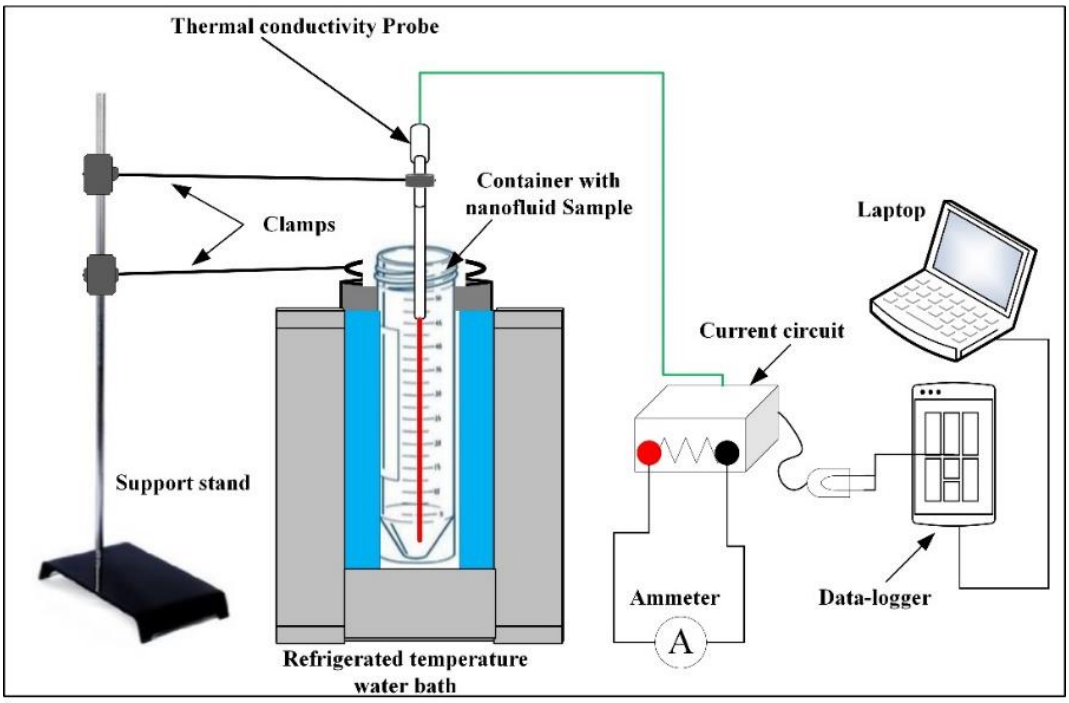

Figure 4.10 Schematic diagram of thermal conductivity measurement.

The data was exported as spreadsheet, containing time and temperature measured from the sample by the probe. Thereafter, the difference between the heating and the baseline temperature ($\Delta T = T_{heating} - T_{baseline}$) against heating time ($\ln(t)$) was plotted and the equation for the linear portion of the curve was displayed from which the slope was obtained.

Finally, the thermal conductivity 'k'is calculated from

$$k = \frac{Q_{net}\, ln\, (t_2/t_1)}{4\pi(T_{t1} - T_{t2})} \tag{4-7}$$

Where $(T_{t1} - T_{t2})/\ln\,(t_2/t_1)$ is the slope obtained by considering over 90 % of the variance of the regression (R^2) as illustrated in Fig. 4.11c.

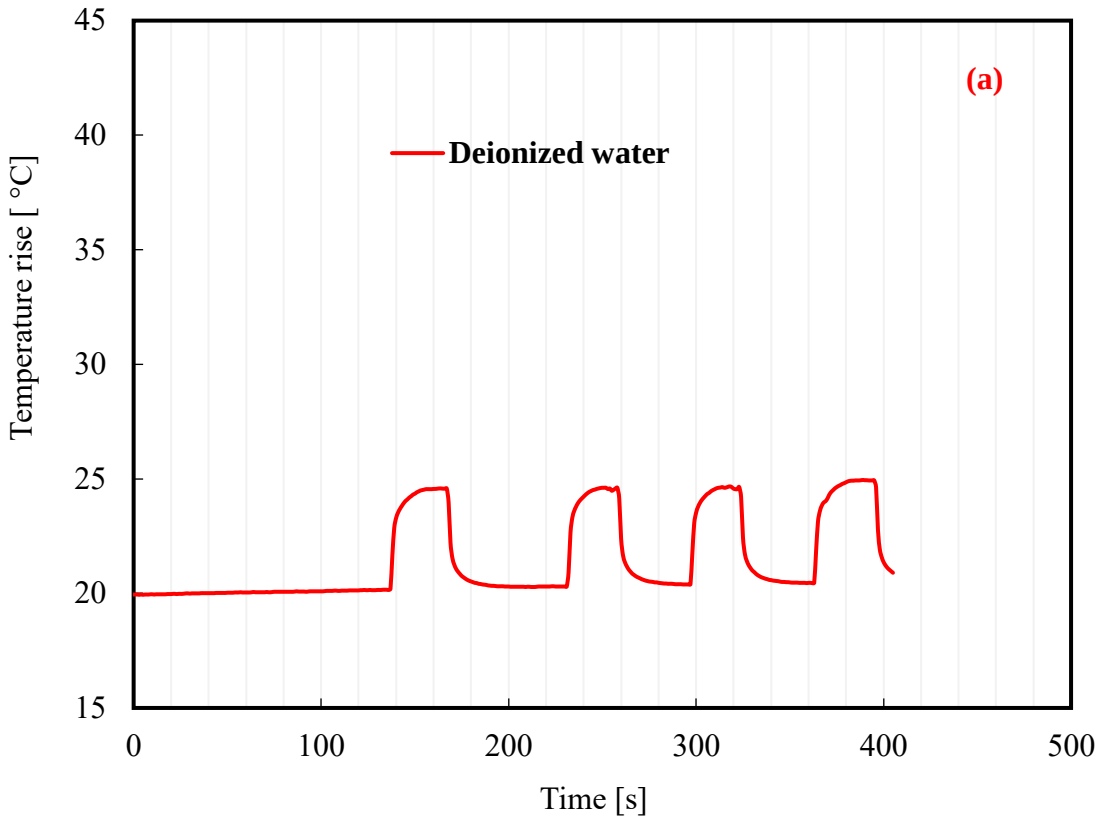

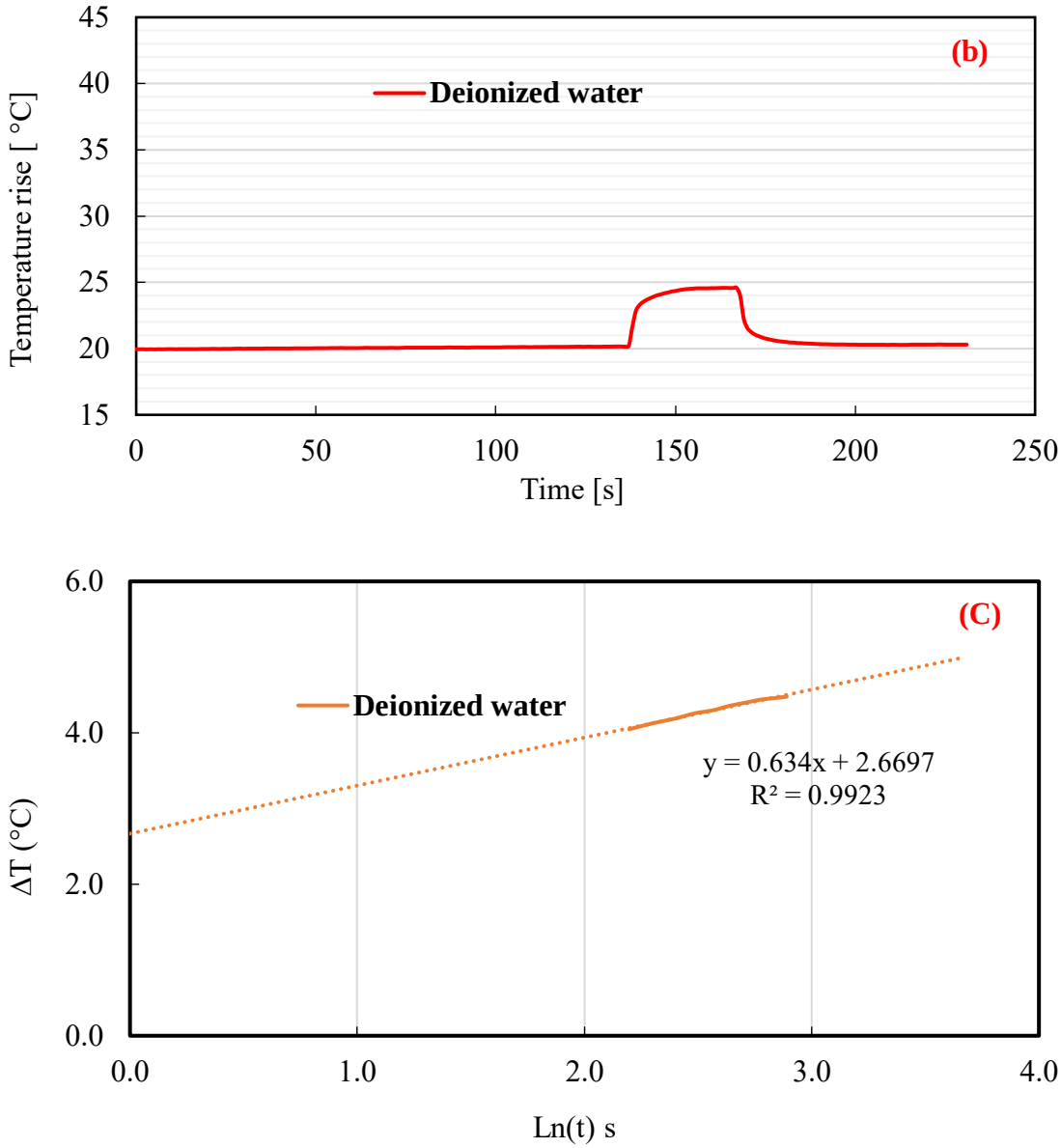

Figure 4.11 full set of 4 replicates in one measurement, (b) the first test out of 4, (C) selected data range based on the variance to determine final thermal conductivity

4.2.2. Calibration analysis

To calibrate the TP08, experiments were conducted for both deionized water and ethylene glycol at temperatures between 20 and 25 degrees Celsius. Three data sets were averaged to obtain one data point as presented in Fig. 4.12. It can be clearly seen that there was a good agreement between literature values of deionized water and ethylene glycol to that of the averaged measured data.

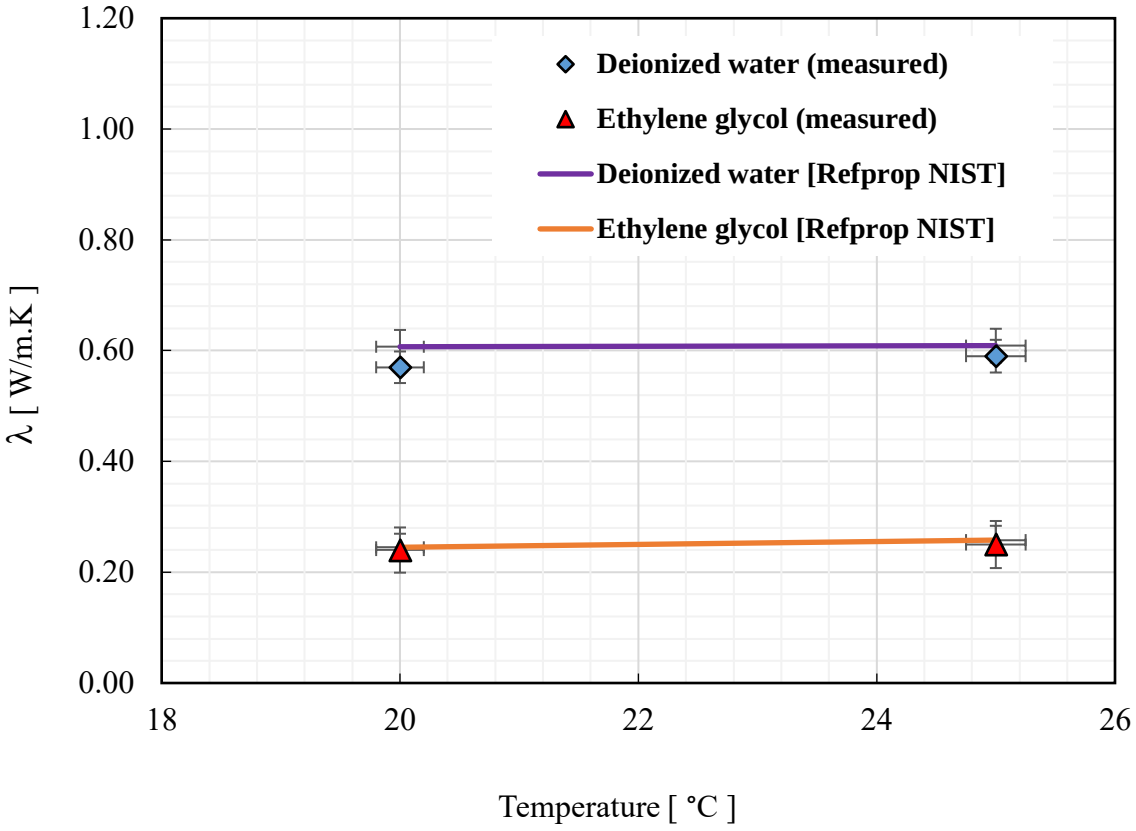

Figure 4.12 A comparison between measured thermal conductivity and literature (Refprop NIST 9.0) (Lemmon, Huber, and McLinden 2013) **values of deionized water and ethylene glycol using transient hot-wire technique.**

Having measured and obtained thermal conductivity results of nanofluids using Hukseflux™ TP08 probe, the standard deviation among 4 replicates for pure water was 5.7 %. This was relatively lower compared to large deviations over 10 % among replicates of nanofluid combinations. The large uncertainties revealed from Hukseflux™ TP08 probe measurements prompted to seek a different device.

For that, measurements of thermal conductivity of similar combinations of nanofluids were carried out at Auckland University using a TC-30™ device manufactured by Mathis Instruments Ltd/Thermtest Inc. Later, thermal conductivity results from both devices were compared.

The Hukseflux™ TP08 probe and TC-30™ device working principle is based on the transient analysis technique. However, several differences including measurement procedures exist between these two devices. For example, Fig. 4.13 show that, heat moves vertically or unidirectional and multidirectional (planar heat flow) for TC-30™ device and TP08 probe respectively.

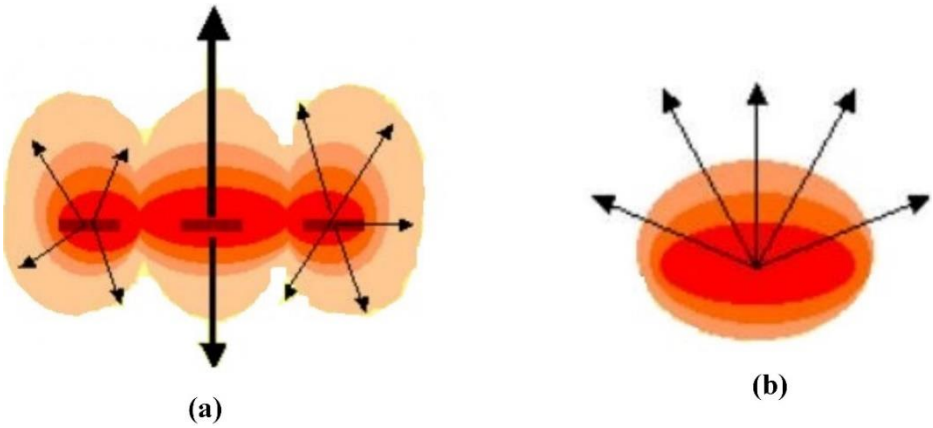

Figure 4.13 Unidirectional (a) and (b) planar directional heat transfer (Thermtest Instruments 2004)

Furthermore, the TC-30™ is less laborious; allows rapid sample testing (test time of 2 seconds and cooling time of 5 min). The TC-30™ device is expensive compared to TP08 probe. According to the user's manual (Thermtest Instruments 2004) , the precision and accuracy of the TC-30™ is said to be ± 1 % and ± 5 % respectively within sample testing.

With TP08 probe, large sample volumes of nanofluids can be measured whereas the testing chamber of TC-30™ device is limited to a specific surface area thus enabling only small quantities tested.

4.2.4 Measurement procedure of nanofluids using TC-30Ê device

Unlike the TP08 probe where containers are used to hold nanofluids, Zip bags were used instead (see Fig. 4.14) for TC-30™ device. Thereafter, the bag was placed in the sensor test chamber and was calibrated with water as reference.

Figure 4.14 Thermal conductivity measurements procedures using TC-30Ê device.

4.2.5 Results and Discussion

The results in Table 4.4 show that standard deviation for pure water was 5.7 %. However, standard deviation for CuO/H_2O/ARB, C/H_2O/CTAB, CuO/H_2O, C/H_2O, Al_2O_3/H_2O, nanofluid was significantly high with 10.5 %, 9.3 %, 9 %, 9.3 % and 8.3 % respectively. These results created a sense of doubt regarding the sensitivity of the probe. Also, using a probe was time consuming because of several steps involved to complete a set of measurements for one combination of nanofluid.

Table 4.4 Measured thermal conductivity using the Hukseflux™ TP08 needle Probe at 25 ÁC.

Replicate	***Deionized water*** (W/m.K)	***C/H₂O*** (W/m.K)	***Al₂O₃/H₂O*** (W/m.K)	***CuO/H₂O*** (W/m.K)	***CuO/H₂O/ARB*** (W/m.K)	***C/H₂O/CTAB*** (W/m.K)
1	0.581	0.730	0.688	0.788	0.917	1.179
2	0.545	0.833	0.794	0.852	1.006	1.284
3	0.543	0.895	0.837	0.942	1.130	1.419
4	0.611	0.904	0.749	0.960	-	-
5	-	0.928	-	0.979	-	-
Average	0.570	0.858	0.767	0.904	1.018	1.294
Stdev	0.03	0.08	0.06	0.08	0.11	0.12
%Stdev	5.7%	9.3%	8.3%	9.0%	10.5%	9.3%

The results in Table 4.5 show standard deviations lower that 5 % for all measured combinations of nanofluid except for C/H_2O/CTAB nanofluid. It was difficult to replicate thermal conductivity of C/H_2O/CTAB nanofluid with the TC-30™ device.

Table 4.5 Measured thermal conductivity using the Thermtest TC-30™ device at 25 ÁC

Replicate	***Deionized water*** (W/m.K)	***C/H₂O*** (W/m.K)	***Al₂O₃/H₂O*** (W/m.K)	***CuO/H₂O*** (W/m.K)	***CuO/H₂O/ARB*** (W/m.K)	***C/H₂O/CTAB*** (W/m.K)
1	0.631	0.725	0.715	0.761	0.900	-
2	0.637	0.726	0.734	0.764	0.898	-
3	0.640	0.737	0.749	0.787	0.908	-
4	-	0.749	0.764	0.785	0.917	-
5	-	0.742	0.772	0.795	0.937	-
Average	0.636	0.736	0.747	0.778	0.912	-
Stdev	0.00	0.01	0.02	0.02	0.02	-
%Stdev	0.7%	1.4%	3.1%	1.9%	1.7%	-

One of the questions posed in the beginning of this chapter was "Why is there so much variability in the reported thermal conductivity measurements?". The results from both devices explains the wide variability in reported data (see Figs. 4.15 and 4.16); some believed to have resulted from the sensitivity of devices employed during thermal conductivity measurements. Most of the reported data in published articles tend either to ignore or not to elaborate critical information such as standard deviation or calibration of devices. Others simply just use established models of which some are outdated and don't account for surfactants added to nanofluids as stabilizers.

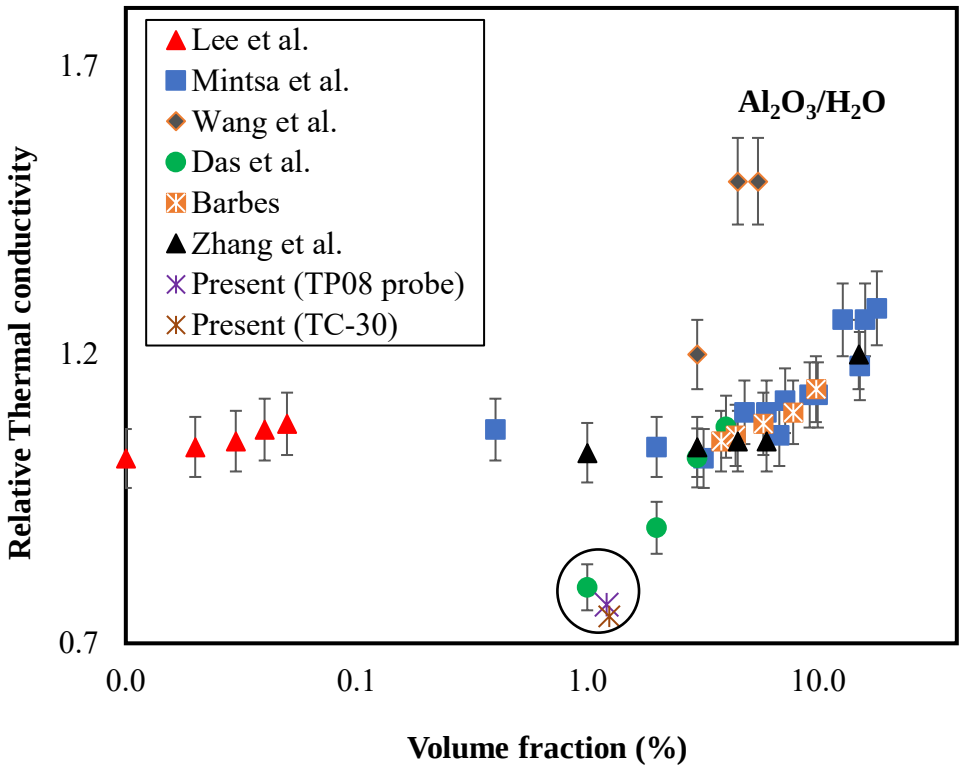

Figure 4.15 A comparison of measured thermal conductivity of Al_2O_3/H_2O nanofluid (S. Lee et al. 1999b; Mintsa et al. 2009; X. Wang, Xu, and Choi 1999; Sarit Kumar Das et al. 2003; Barbés et al. 2013; Zhang et al. 2006)

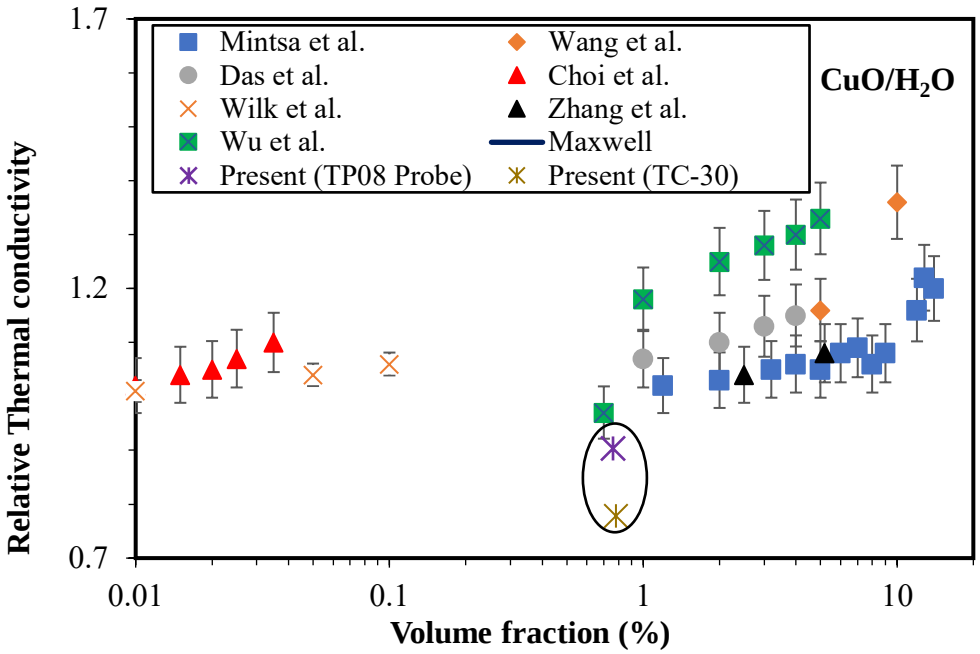

Figure 4.16 A comparison of measured thermal conductivity of CuO/H_2O nanofluid
(Mintsa et al. 2009; X. Wang, Xu, and Choi 1999; Sarit Kumar Das et al. 2003; S. Lee et al. 1999b; Wilk, Smusz, and Grosicki 2017; Zhang et al. 2006; Wu et al. 2009; Maxwell 1892)

Although generally speaking, the addition of surfactants improves stability of nanofluids, their impact on thermal conductivity as presented in this section is an element that should be put in considerations, specifically for heat transfer enhancement applications were consistency in thermophysical property values at specified conditions is necessary.

4.3 Selection of nanofluids tested for heat transfer in the rig.

The selected combinations of nanofluids whose heat transfer performance was later evaluated in a test rig are: C/H_2O/CTAB, Al_2O_3/H_2O and CuO/H_2O/ARB nanofluids. The selection of these nanofluids combinations was based on stability (Chapter 3) and viscosity findings. C/H_2O with CTAB as a surfactant had low viscosity and relatively stable. The pairing of ARB and CuO/H_2O presented better stability and relatively low viscosity compared to other surfactants. For Al_2O_3/H_2O nanofluid, it was found that adding surfactants increased viscosity even though SDBS surfactant showed better stability when added to Al_2O_3/H_2O nanofluid in Chapter 3. Therefore, Al_2O_3/H_2O nanofluid with no surfactant was selected and tested in the rig. The measurements of density and specific heat capacity of the selected nanofluids is detailed in the following sections.

4.4 Density

4.4.1 True density of nanoparticles

The true density of the Al_2O_3, CuO and carbon nanoparticles was determined using Archimedes principle (Archimedes and Heath 1897) since they are insoluble in water. A known mass of the nanoparticles (Table 4.6) was placed in a 500 ml E-MIL' Boro (Grade A, specified accuracy up to ± 0.25 cm^3) volumetric flask and the flask was then filled with distilled water up to the level mark of the volu metric flask. All masses were measured using a Mettler Toledo AG204 balance. Table 4.6 summarises the true density measurement data and provides a comparison between the measured densities and the manufacturers' true density data.

Table 4.6 Density measurements of nanoparticles

Nanomaterial	Nanoparticle mass (kg)	Water mass (kg)	Mixture density (kg/m^3)	True density of nanoparticle (kg/m^3)	Supplier density (kg/m^3)	Difference between measurement and supplier
Al_2O_3	0.0246	0.492	1002.4	3949	3950	0.03%
CuO	0.0247	0.494	1034.4	6311	6315	0.06%
C	0.0239	0.479	1007.4	1273	450	-182.9%

The measured densities of the Al_2O_3, CuO agreed closely with the manufacturers data, however the density of the carbon nanoparticles was very different (with -182.9 % difference between measured and supplier densities). As the carbon nanoparticles sediment over time (Chapter 3) they must have a density greater than that of water so the manufacturer's numbers must be wrong, and so the measured true density of carbon was used throughout this thesis.

4.4.2 Density of water/surfactant mixtures

Because the surfactants dissolve in water it was necessary to determine the density of the water/surfactant mixtures as a function of the amount of surfactant. The quantity of surfactant added to the 500 ml volumetric-flask ranged from 0.002 to 0.1 kg, with the remainder of the flask volume filled with distilled water. Figure.

4.17 shows the density of the ARB/distilled water mixture for a range of concentrations of ARB and Fig. 4.18 shows the density of the CTAB/distilled water mixture for a range of concentrations of CTAB.

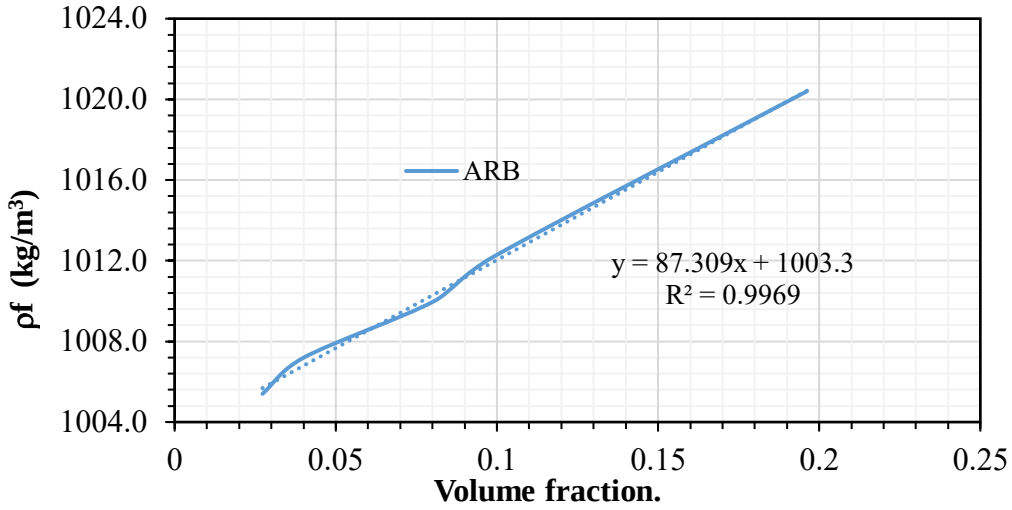

Figure 4.17 Density measurements of ARB surfactants.

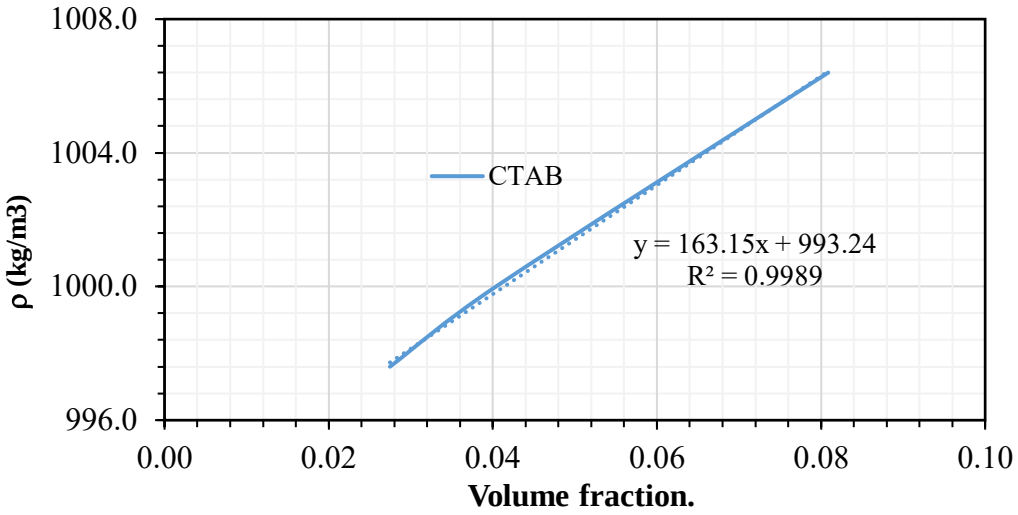

Figure 4.18 Density measurements of CTAB surfactants.

Having measured the true densities of nanoparticles and surfactants water mixture, Eq. (4.8) (Pak and Cho 1998) can be used to obtain the density of Al_2O_3/H_2O, C/H_2O/CTAB and CuO/H_2O/ARB nanofluids as

$$\rho_{nf} = (1 - \emptyset_p)\rho_f + \emptyset_p\rho_P \tag{4-8}$$

Where 'ϕ' is the volume of nanoparticle concentration, subscripts 'p' symbolises nanoparticles, 'nf', and 'f' denote for nanofluid and base fluid/surfactant respectively.

4.5 Specific heat capacity

Specific heat capacity of nanoparticles and surfactants was measured by a differential scanning calorimeter (Perkin Elmer DSC - 8500). Prior to starting the DSC operations, empty aluminium pans were prepared as a reference for the sample measurements. The samples that ranged from 11.5 to 23.7 mg in mass were spread evenly along the base of the aluminium pans (see Fig. 4.19). The weight of the pan and sample was measured using an electronic balance (Mettler Toledo AG204) with a precision and maximum range of ± 0.003 % mg and 210.0 mg respectively. The sample holder cell initial and maximum temperature were set at 30 °C and 80 °C respectively. These temperatures were selected with respect to water which was used as a reference.

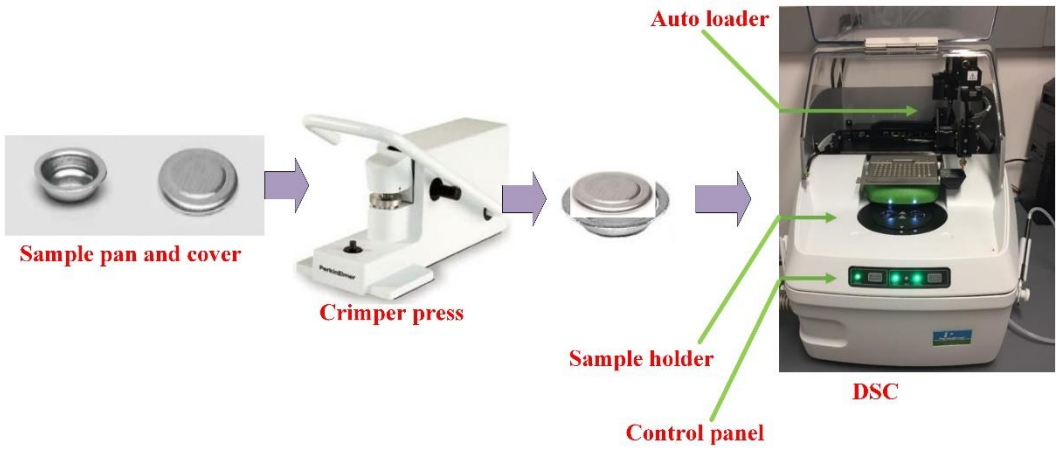

Figure 4.19 Sample preparation process to measure specific heat capacity in DSC

In order to achieve the DSC signal stability, the sample was maintained at the initial temperature for 60 seconds. The average heat flow was 27.8 mW and ± 0.2. The measured specific heat capacities are shown in Table 4.2 along with the measured heat capacity of water for comparison. Since the heat capacity measured for water was 4.3 % higher than the IAPWS value (Wagner and Pruß 2002; Wagner et al. 1997), the heat capacities of the nanoparticles and surfactants were reduced by this amount (shown as the corrected heat capacities in Table 4.7).

Table 4.7 Measured specific heat capacity of nanoparticles and surfactants.

Substance	***Measured specific heat capacity* (J/kg. K)**	***Corrected specific heat capacities* (J/kg. K)**
Deionized water	4358.0	4170.6
Alumina	573.9	549.2
Copper oxide	613.2	586.8
Activated carbon	799.7	765.3
CTAB	1371.9	1312.9
ARB	1569.6	1502.1

Ideally the specific heat capacities of the nanofluids would also have been measured (rather than nanoparticles, surfactants and water individually only); however, this was not practical with the apparatus available. Instead, the specific heat capacity of the nanofluids was calculated as a mass-weighted average of the components' specific heat capacities (assuming negligible heat of solution for the surfactants in water):

$$C_{p,nf} = x_p Cp_p + x_{bf} Cp_f + x_s Cp_s \tag{4-9}$$

Where 'x_i' is the mass fraction (mass of component *i* divided by total mass), and subscripts '*bf*'' and '*s*' denotes for base fluid and surfactant respectively.

4.6 Conclusion

With suspensions of solid nanoparticles in base fluids, physical properties like viscosity, thermal conductivity, density and specific heat capacity not only influence heat transfer coefficients, but also the design of the system and the applicability in general. This chapter has discussed mainly viscosity and thermal conductivity measurement of nanofluids; focusing on the impact of surfactants on selected combinations of nanofluids. The main points drawn from this study are as follows:

- Viscosity testing showed that consistent results were able to be produced for the fresh samples, however slightly less consistent results were seen after seven weeks. It was also noticeable that viscosity appeared to somewhat increase after seven weeks in all types of nanofluids.

- There was no consistency in the thermal conductivity measured by both Hukseflux™ TP08 probe and TC-30™ device. Large deviations among replicates were revealed
- Al_2O_3/H_2O, C/H_2O/CTAB and CuO/H_2O/ARB combinations of nanofluids were selected to be tested in a closed flow-loop because they were relatively stable with lower viscosity.

In the next chapter, what follows is the description of the devices and instruments used to set-up an experimental test rig; that was used to evaluate heat transfer, enhancements of Al_2O_3/H_2O, C/H_2O/CTAB and CuO/H_2O/ARB nanofluids. Also, measurement procedures and uncertainties will be detailed.

Chapter 5
Instrumentation, Experimental set-up and Heat transfer Measurements

5.1 Introduction

Chapter 2 of this thesis reviewed the literature that has reported increases in heat transfer of nanofluids compared to traditional working fluids and identified that there is wide variation both in reported physical properties of nanofluids and in reported heat transfer rate enhancement. It was also identified that very few studies considered the impact of the surfactant on both physical properties and thermal performance. The effect of surfactants on the stability of nanofluids was investigated in Chapter 3, and Chapter 4 described the measurement of viscosity, thermal conductivity, density and specific heat capacity of selected nanofluids, some with surfactants and some without. In this chapter, a test rig is described that was built and used to evaluate the thermal performance of selected nanofluids (Al_2O_3/H_2O, C/H_2O/CTAB and CuO/H_2O/ARB) compared to water.

A number of different apparatus (Mansoury et al. 2020; Zamzamian et al. 2011; Albadr, Tayal, and Alasadi 2013) have been used to measure heat transfer rates in nanofluids; however, the most common seems to be the double-pipe heat exchanger (Han, He, and Asif 2017; Sonawane, Khedkar, and Wasewar 2013; Chandra Sekhara Reddy and Vasudeva Rao 2014; El-Maghlany et al. 2016; Darzi, Farhadi, and Sedighi 2013). The attraction of this device is that it is relatively simple and cost-effective to fabricate, and so a double-pipe heat exchanger test rig was used in this study.

The efficiency of most thermal systems is assessed by comparing overall heat transfer rates against pressure drop because increased pressure drop in thermal systems leads to high pumping costs. Therefore, the performance evaluation approach proposed by Webb and Kim (Webb and Kim 2006) was adopted to quantify the increase in heat transfer coefficient relative to the increase in friction factor for nanofluids compared to water in a double pipe heat exchanger.

5.2 Experimental setup

An experimental testing rig was designed and built (Fig. 5.1). The rig contained a closed test loop consisting of two identical double-pipe heat exchangers (DPHEX) (Fig. 5.2) that contained the working fluid (tube-side) and were connected to a centrifugal pump and an electromagnetic flow meter. Prior to running experimental trials, the system was charged with water and monitored for 3 days to make sure that there was no leakage.

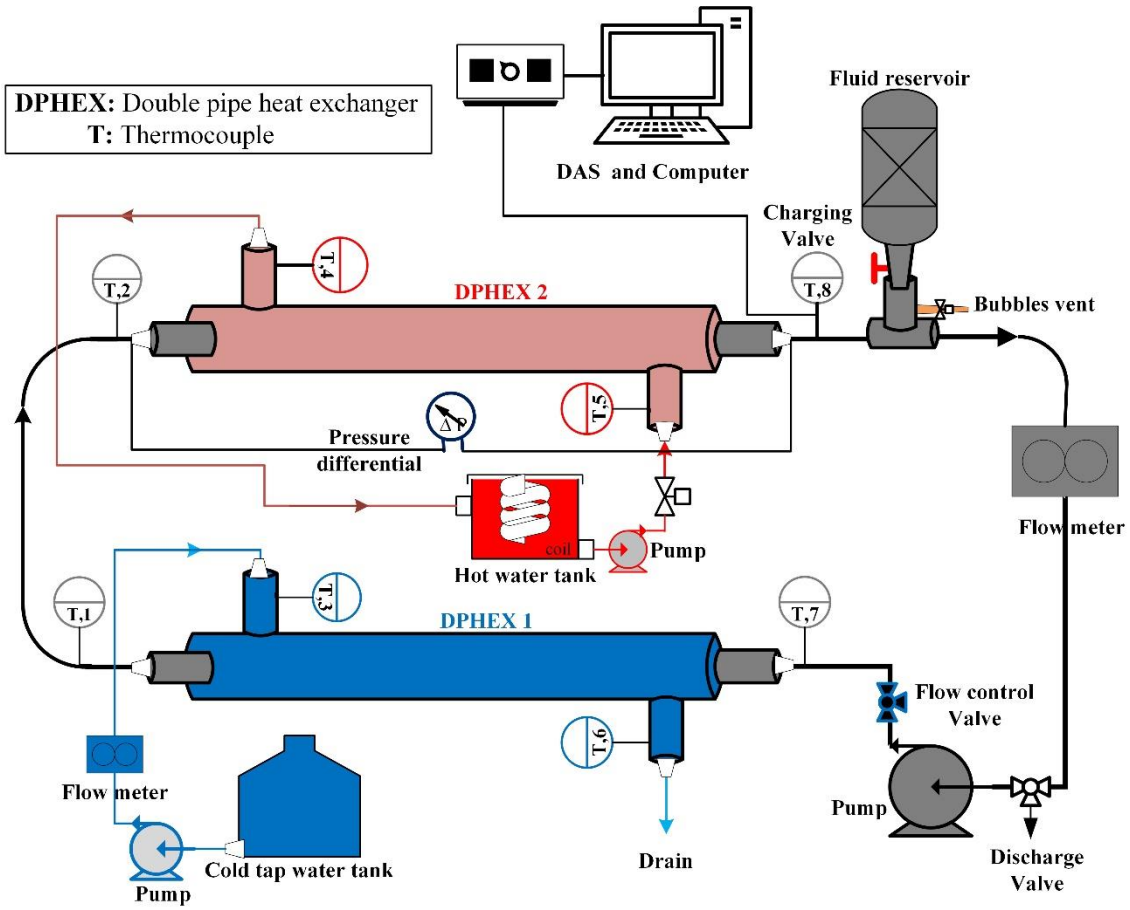

Figure 5.1 Schematic diagram of the closed flow loop

Both heat exchangers (DPHEX 1 and DPHEX 2) and the whole test loop were insulated using rubber foam (R-value 0.7 m^2 K W^{-1} of 20 mm thickness) to minimise heat loss. For each test run, tube-side flow rates were varied between 1.9 to 71 litres per minute (l/m). The shell-side flow rates were held constant at 55.0 litres per minute because it was the maximum steady flow rate that could be achieved. All measurement signals on the test rig were recorded by a data acquisition system and sent to a logging computer for further processing and analysis.

5.3 Instruments and devices.

5.3.1 Double pipe heat exchangers.

A heat exchanger with a large surface area is desirable for experimental purposes to maximise heat transfer rates. However, the larger the surface the larger the volume of nanofluids required to achieve a given concentration, which in turn means higher cost. It was decided that the size of the heat exchangers should be similar to those used in previous studies (e.g. Han et al. (Han, He, and Asif 2017) and Sonawane et al. (Sonawane, Khedkar, and Wasewar 2013)), with a 1 m length and approximately 1 inch diameter. The dimensions of the heat exchangers that were fabricated from stainless-steel grade 316 (corrosion resistance of 0.2 x 10^{-5} m (The international nickel company 1963; Nickel Development institute 1965)) for this work are shown in Table 5.1. The heat exchangers were both installed in the counter-flow configuration.

Table 5.1 Heat exchanger dimensions

Pipe	D_o (mm)	D_i (mm)	l (mm)	δ (mm)	A (m^2)
Inner	25.7	23	1500	1.3	0.072
Outer	77	74	1000	1.5	0.081

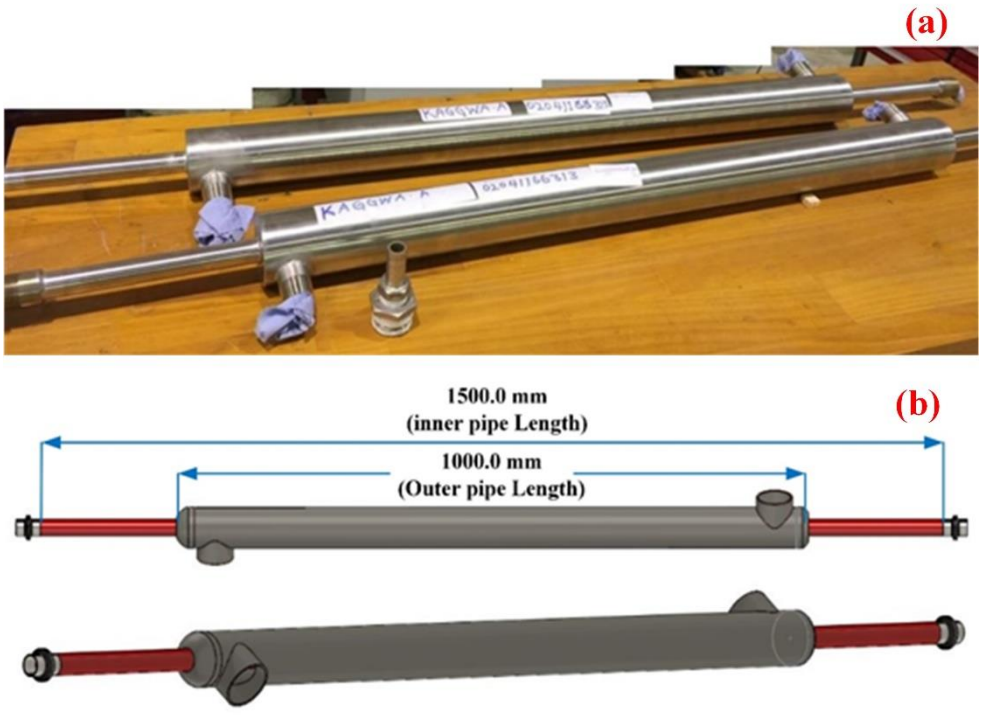

Figure 5.2 Schematic diagram (a) and (b) real double pipe heat exchangers.

5.3.2 Rig support Stand

A frame 1.7 m high, 2.0 m length and 0.8 m wide was constructed using rolled hollow section steel. A plywood board was screwed on the frame to provide a platform for the installation of all the instruments and devices on the rig (Fig. 5.3). Four swivel wheel casters were fixed to the base to allow easy mobility of the rig.

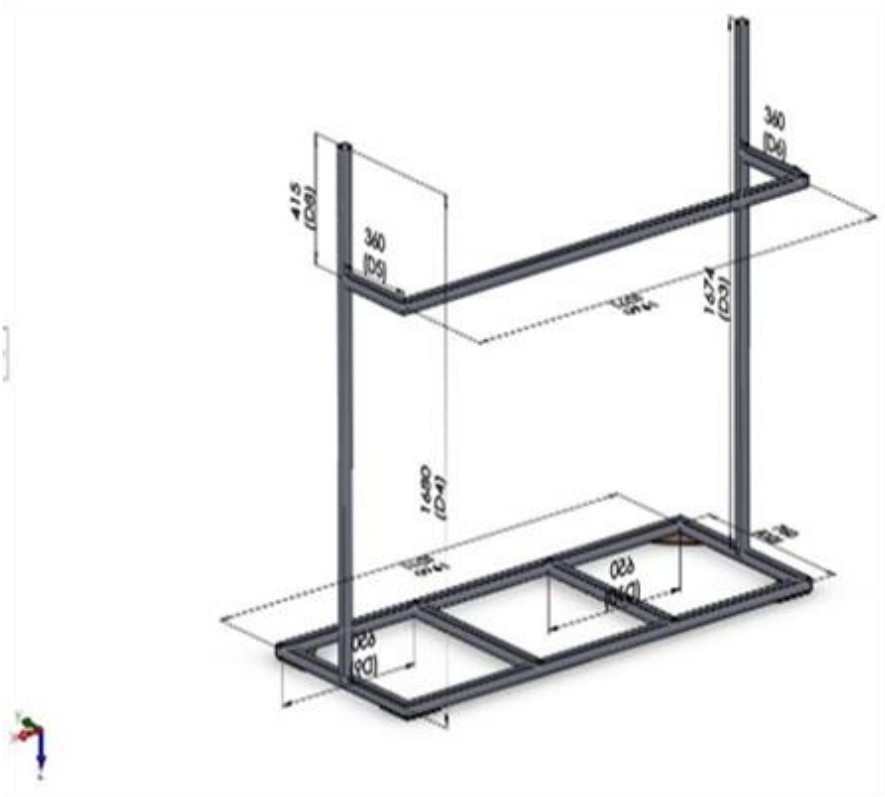

Figure 5.3 Rig support stand and its dimensions.

5.3.3 Cooling Source

Initially, cold water straight from the tap was connected directly to DPHEX 1; however, fluctuations in supply pressure made steady flow rates difficult to achieve. Therefore, a tank was employed to even out the cold-water supply flow-rate (Fig. 5.4). The cold water was driven through the shell-side of DPHEX 1 by a pump and a magnetic flow meter was used to measure the flow rates in the shell-side. Once through the shell-side of DPHEX 1 the cold water was sent to the drain.

Figure 5.4 Cold water tank

5.3.4 Heating Source

Steam coming out at 5.2 bar was passed through a heating coil that was installed in a tank. Water in the tank heated by the steam was used to provide the heating load to the shell-side of DPHEX 2; however, unlike the cooling load the water leaving DPHEX 2 was returned to the hot water tank. The tank (Fig. 5.5) had a volume of approximately 1000 litres and was covered to minimise heat losses to the environment.

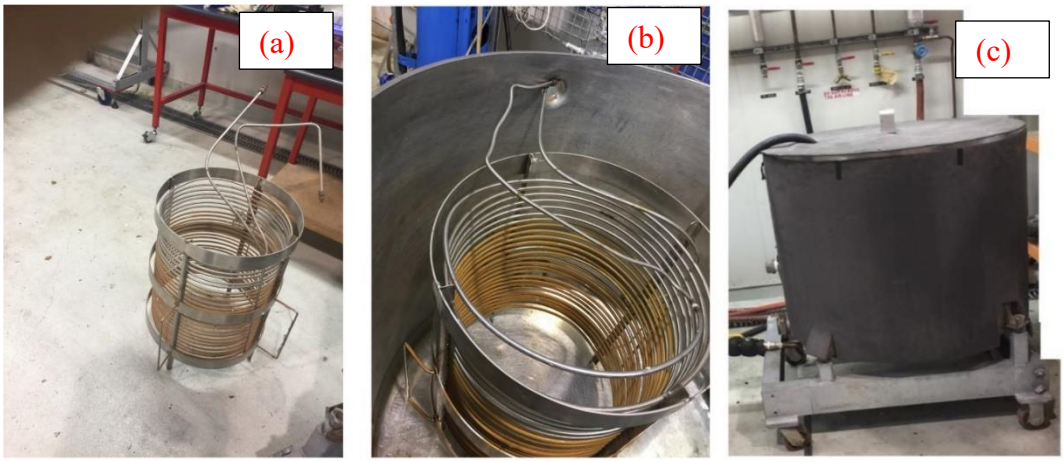

Figure 5.5 Composition of the thermal tank including: (a) heating coil (b) installed coil inside the tank (c) insulated tank

5.3.5 Temperature measurement

T-type thermocouples were selected to record temperatures (Fig. 5.6). These thermocouples can measure temperature in the range between –270 to +370 °C, with an accuracy of ± 1.0 °C (Holman 2012). In this study, two calibration techniques were employed; an ice point test was performed to provide an absolute calibration, and a water bath test was performed for relative calibration over a range temperatures (Burns and Scroger 1989). Calibration graphs are presented in Appendix C.

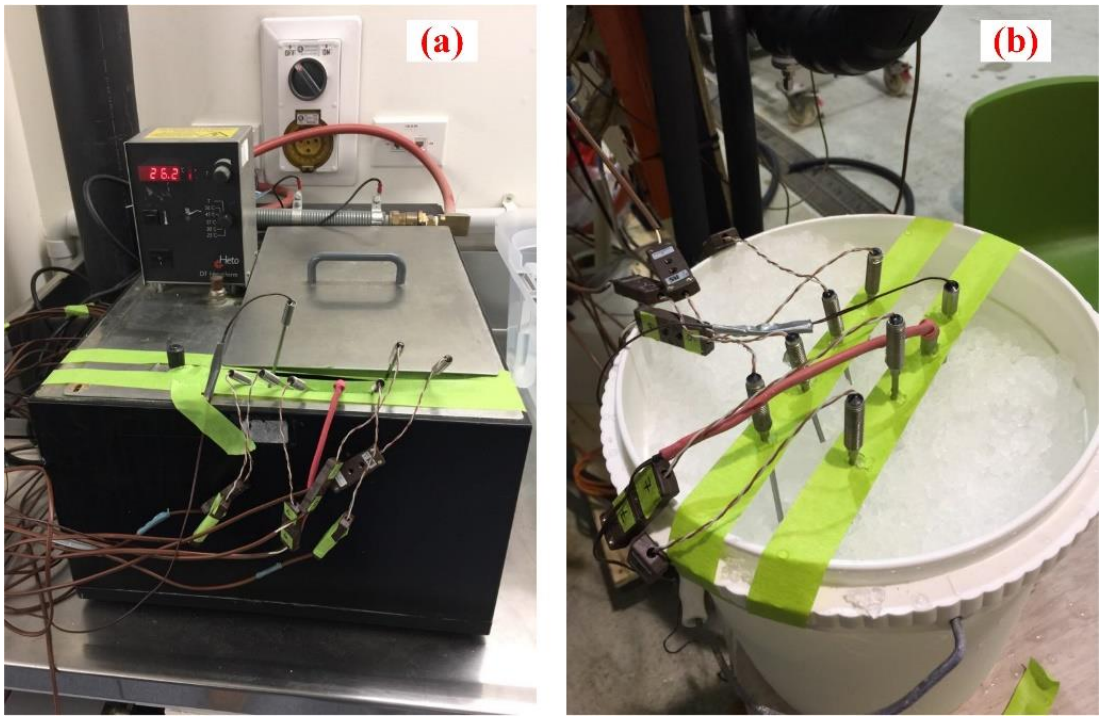

Figure 5.6 Thermocouple calibration (a) water bath method and (b) ice point method.

5.3.6 Pumps

Three centrifugal pumps were installed as illustrated in Fig. 5.1; one for the nanofluids in the tube-side of the heat exchangers, and one each for the heating and cooling loads on the shell-side of the heat exchangers. The pumps had similar flow ranges from 60 to 160.0 litres per minute and operating temperature range –10 to +85 °C.

5.3.7 Flow measurement

Two electromagnetic flowmeters, Promag 50P from Endress Hauser, were installed; one to measure the flow rates in the test closed loop (i.e., tube-side of the heat exchangers), and the other to measure the flow rates of the cooling load. The flow rates from the heating load were regulated by a valve on the pump. According to the manufacturer (Endress+hauser n.d.), the flow meters' measurement range was from 0.0 to 160 litres per minute, the maximum measured volume flow error is ± 0.5 % and the temperature range is from –20 to +150 °C. The selected output signal during this investigation was from 4 - 20 mA. The flow rates from these flow meters were confirmed using a bucket and stopwatch (see Appendix C).

5.3.8 Differential pressure measurement

The pressure drop across the test loop was measured using a differential pressure meter made by Yokogawa, model (EJA110A). The measurement range was from 0.0 to 145 kPa. The selected output signal during this investigation was from 1 - 5 V. The high range value port of the differential pressure transmitter was connected to a hand pump to supply pressure while the lower range value port was left open to the atmosphere. The transmitter was spanned from 0 % to 100 % so that 1~ 5 V corresponded to 0 ~145 kPa respectively. Measured pressure was then compared with the gauge readings. Finally, graphs showing output signal against measured pressure and gauge readings was presented in Appendix C.

5.3.9 Data logger

All measured data was processed using a DAQ 34970A data acquisition system made by Agilent technologies Inc. (Fig. 5.7a) which was connected to the logging computer through the RS-232 interface connector. A plug-in armature multiplexer module was used (Fig. 5.7b) that contained 20 channels of 300 V switching, 2 channels for DC or AC current measurements (100 nA to 1 A), built-in thermocouple reference junction and switching speed of up to 60 channels per second. The first 8 channels were specifically assigned to T-type thermocouples. Since this DAQ was limited to only two

direct-current channels, the two flow meters were assigned to those, and a shunt resistor was employed to convert an extra channel to allow the reading of direct voltage from the pressure transmitter. All measured analogue signals from devices were processed as either current or voltage or temperature, and later converted manually to desired parameters using a spreadsheet (see Appendix D).

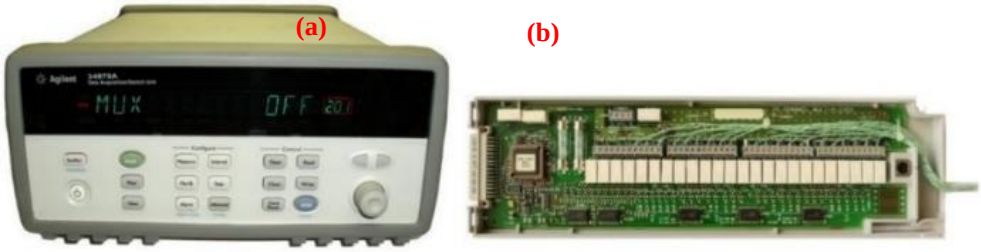

Figure 5.7 (a) DAQ 34970A **and (b) 20 channel armature multiplexer module.**

Finally, the test rig was assembled and installed in the Large-Scale Laboratory (LSL) at the University of Waikato, as shown in Fig. 5.8.

Figure 5.8 Front and back view of the real experimental rig.

5.4 Experimental procedure

An experimental run was started by charging the test loop of the rig with the working fluid being tested. Whenever a fluid was charged into the test loop, the bubble vent (see Figs. 5.1 and 5.8) was partly opened to allow bubbles out of the test loop. The bubble vent was monitored for approximately 30 minutes until fluid drops started coming out; an indicator that prove the test loop was bubble free and the bubble vent was then closed. Once charged, the pump in the test loop was turned on to circulate working fluid. The shell-side flow rates were fixed at maximum of 55.0 litres per minute because it was the maximum steady flow rate that could be achieved whereas flow rates on the tube-side were varied between 1.9 litres per minute and 71.0 litres per minute. After a tube-side flow rate was selected, the system was allowed to reach steady state (which was typically one hour) after which time the flow rates, temperatures and pressure drop were recorded for 30 minutes before changing the tube-side flow rate. A typical run of the experiment took 6 to 7 hours.

After obtaining all the data from the rig, the steam and cold-water valves were closed. All pumps, flow meters and other devices were turned off. Finally, cold tap water was connected to the test loop to hose and drain the tested fluid out of the test loop. The test loop pump was turned on to provide extra pressure to wash all nanoparticles out until clear wash-water was observed. The pump and cold water were later turned off and closed respectively. A full standard operation procedure has been provided in Appendix D.

5.4.1 Raw data processing

Three to four experimental runs for each fluid were carried out. The same procudure was done on each one of the runs; this was to have multiple data points at the same flow rates. The flow rates were matched manually using a valve (see Fig. 5.1). Then, at the end of the experimental run, recorded raw data for each data set was produced on a graph as illustrated in Fig. 5.9. The temperatures were logged by the DAQ in degrees Celsius thanks to the internal theroucouple conversion; however, pressures and flow rates had to be converted manually from electric signals to kPa and litres per minute respectively. The data from an experimental run were subsequently divided into subsets according to the tube-side flow rate as presented in Fig. 5.10. Further data processing procedures including graphs and figures have been presented in Appendix D.

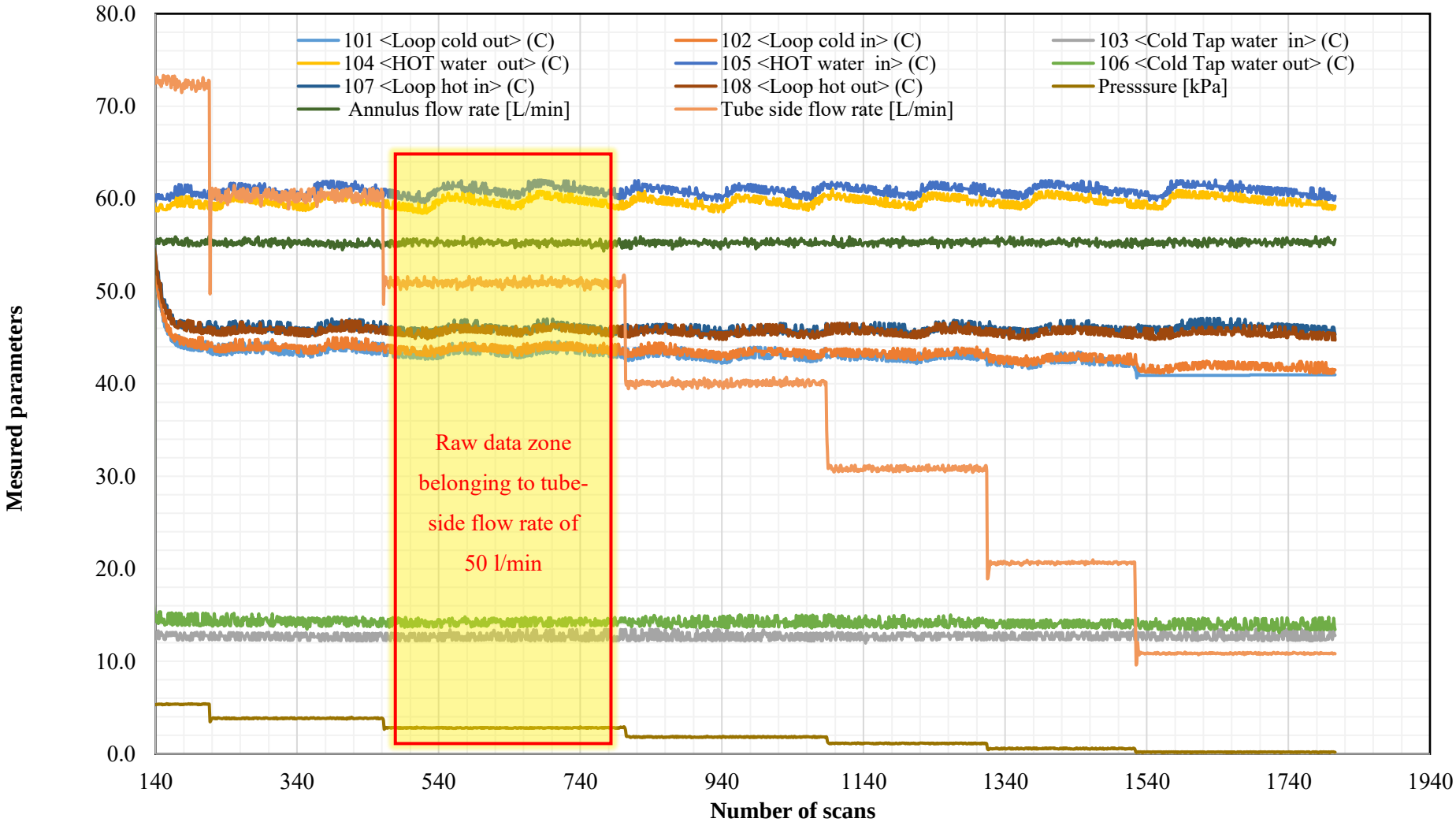

Figure 5.9 Recorded raw data from the logger

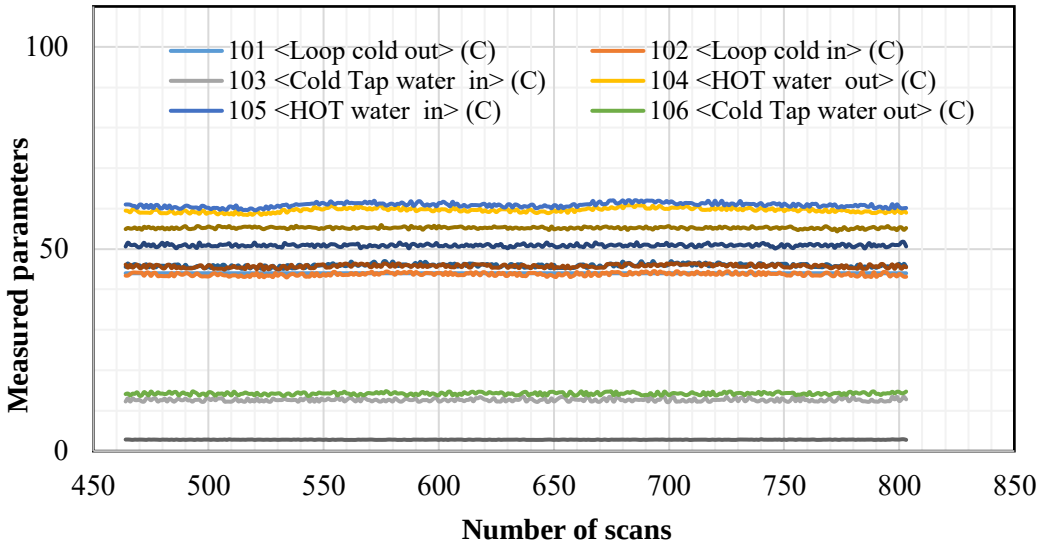

Figure 5.10 Processed data belonging to similar tube-side flow rate (50.0 l/min) (yellow highlighted zone in Figure 5.9)

5.5 Calculations for heat transfer analysis

Temperature-dependent properties of water used in the calculation of heat transfer rates were calculated from the International Association for the Properties of Water and Steam (IAPWS) functions (Wagner and Pruß 2002; Wagner et al. 1997). The density and specific heat capacity of the nanofluids were obtained using Eqs. 5.1 and 5.2:

$$\rho_{nf} = (1 - \emptyset_p)\rho_f + \emptyset_p \rho_P \tag{5-1}$$

$$C_{p,nf} = x_p Cp_p + x_{bf} Cp_f + x_s Cp_s \tag{5-2}$$

where the true particle densities (ρ_p) and specific heat capacities of the nanoparticles (Cp_p) and surfactants (Cp_s) were measured directly as described in Chapter 4. The viscosity of nanofluids that was used to obtain experimental Reynolds number was calculated using Eq. 5.3 as:

$$\mu_{nf} = [1 + \emptyset]\mu_{bf} \tag{5-3}$$

Reynolds number were obtained from:

$$Re = \left(\frac{\rho_{nf} v D_i}{\mu_{nf}}\right) \tag{5-4}$$

where 'v' is the flow velocity, and 'D_i' is the inside diameter of the heat exchanger tube.

The Prandtl number was calculated as:

$$Pr = \frac{\mu_{nf} Cp_{nf}}{k_{nf}} \tag{5-5}$$

The average heat transfer rate was obtained from:

$$\dot{Q}_{avg} = \frac{\left(\dot{m} Cp_{nf} \Delta T\right)_i + (\dot{m} Cp \Delta T)_o}{2} \tag{5-6}$$

where '$\dot{m}$' is the mass flow rate, ΔT is the temperature difference between the inlet and the outlet, subscripts *i* and *o* denote tube-side and the annulus side respectively.

The average overall heat transfer coefficient 'U' was evaluated as:

$$U = \frac{\dot{Q}_{avg}}{A \Delta T_{LM}} \tag{5-7}$$

where A is the heat transfer surface area and ΔT_{LM} is the log mean temperature difference:

$$\Delta T_{LM} = \frac{\Delta T_A - \Delta T_B}{ln(\Delta T_A / \Delta T_B)} \tag{5-8}$$

where ΔT_A is the difference between fluid (tube-side) inlet and cold tap water (annulus) outlet temperatures. ΔT_B is the difference between fluid (tube-side) outlet and cold tap water (annulus) inlet temperatures.

Friction factor 'f' for the test closed loop was obtained from the Fanning friction factor (Rouse 1978) equation as:

$$f = \frac{D_i}{l}\left(\frac{\Delta P}{\frac{1}{2}\rho v^2}\right) \tag{5-9}$$

where 'ΔP' is the measured pressure drop and 'l' is the length of the tube heat exchanger.

5.5.1 Uncertainty analysis

In this thesis a root-sum-square approach Eq. 5.12 proposed by Kline and McClintock (McClintock 1953) was used to calculate the uncertainties in measured quantities. Detailed information on the presented uncertainties in Tables 5.2 and 5.3 is accessible in Appendix D.

$$\partial R = \left[\sqrt{\left(\frac{\partial a}{a}\right)^2 + \left(\frac{\partial b}{b}\right)^2 + \cdots + \left(\frac{\partial z}{z}\right)^2}\right] R \tag{5-10}$$

Where 'R' is given as any defined function of independent variables (a, b and z). The uncertainty of each independent variable (e.g., ∂a) is obtained as

$$\partial a = \frac{\sigma}{\sqrt{N}} \tag{5-11}$$

Where 'σ' is the standard deviation and 'N' is the number of measurements.

Table 5.2 Summary of apparatus accuracy

Apparatus		**Accuracy**	**Calibration range**
Flow meter	Tube-side	± 0.03 *l*/min	0 - 80 *l*/min
	Annulus	± 0.44 *l*/min	
Pressure differential		± 0.18 kPa	0 – 100 kPa
T-type thermocouple		± 1.3 °C	0 – 80 °C

Table 5.3 Estimated uncertainties from primary measurements and derived quantities

Primary measurements		**Derived quantities**		
Parameter	uncertainty	Parameter		uncertainty
Tube-side flow rate (m_i)	± 2 %	Friction factor (f)		± 0.5 %
Annulus flow rate(m_o)	± 0.15 %	Heat transfer rate (Q)	Tube-side	± 6 %
			annulus	± 0.2 %
Pressure difference (ΔP)	± 4 %	Overall heat transfer coefficients (U)		± 17 %
Temperature difference (ΔT_i)	± 0.6 °C			
Temperature difference (ΔT_o)	± 0.2 °C			

5.6 Performance evaluation of nanofluids

One of the objectives of this thesis was to evaluate and compare the performance of tested nanofluids. Therefore, a quantitative method is required to evaluate the performance improvement provided by a given enhancement with respect to its associated increased pressure drop.

Webb and Kim (Webb and Kim 2006) presented a generalised quantitative approach to evaluating heat transfer performance. They started by pointing out that every heat exchanger is a potential candidate for enhanced heat transfer. Each potential application must be tested to see if the heat transfer enhancement method is effective based on either performance objective or operating conditions or the constraints.

Therefore, they identified performance evaluation criteria (PEC) that are applicable to single-phase laminar or turbulent flows in tubes or normal to tube banks based on four possible performance objectives:

1) Reduced heat transfer surface material for fixed heat duty and pressure drop.

2) Reduced log-mean temperature difference for fixed heat duty and surface area.

3) Reduced pumping power for fixed heat duty and surface area.

4) Increased heat duty for fixed surface area.

Among the four possible performance objectives listed previously, this present study falls under Objective 4 (increased heat duty for fixed surface area).

Calculation of the performance enhancement involves algebraic relations that quantify the objective function and constraints. The major operational variables include

the heat transfer rate, pumping power (or pressure drop), heat exchanger flow rate, and the fluid velocity (or the flow frontal area). When Webb and Kim (Webb and Kim 2006) considered single-phase heat exchange system with a constant diameter and cross-sectional flow area, they chose the Chilton-Colburn factor (j) to represent the heat transfer rate:

$$j = \left[\frac{h}{\rho v c_p}\right]\left[\frac{c_p \mu}{k}\right]^{2/3} = \mathrm{St}\mathrm{Pr}^{2/3} \tag{5-12}$$

Where 'h' is the convective heat transfer coefficient, 'ρ' 'c_p' 'μ'and 'v' is the density, specific heat capacity, viscosity and the velocity of the fluid respectively. Because the tube inside diameter was held constant, heat transfer coefficient could be written as:

$$h = C_p Pr^{2/3} jG \tag{5-13}$$

where G is the tube-side mass flow velocity (ρv). The main interest was to obtain convective heat transfer coefficient and surface area (hA) value of the enhanced surface, relative to that of the smooth surface. By writing Eq. 5.13 as the ratio, relative to a smooth surface (subscript 's') resulted into Eq. 5.14 as:

$$\frac{hA}{h_s A_s} = \frac{jAG}{j_s A_s G_s} \tag{5-14}$$

The pumping power 'λ' was calculated as:

$$\lambda = \left(\frac{fA}{A_c}\frac{G^2}{2\rho}\right)\left(\frac{GA_c}{\rho}\right) \tag{5-15}$$

Writing Eq. 5.15 as a ratio relative to the smooth surface, gave them Eq. 5.16 as:

$$\frac{\lambda}{\lambda_s} = \left(\frac{f}{f_s}\frac{A}{A_s}\right)\left(\frac{G}{G_s}\right)^3 \tag{5-16}$$

Elimination of mass velocities (G/G_s) from Eqs. 5.14 and 5.16 gives

$$\frac{hA/h_s A_s}{(\lambda/\lambda_s)^{1/3}\ (A/A_s)^{2/3}} = \frac{j/j_s}{(f/f_s)^{1/3}} \tag{5-17}$$

The variables on the left side of Eq. 5.17 are hA/h_sA_s, λ/λ_s, and A/A_s. As the heat transfer area was held constant in this study the ration A/A_s was 1.0 and hence all area terms could be removed from Eq. 5.17.

To maximise heat transfer coefficients, nanofluids are used to increase the heat exchange capacity of the two double pipe heat exchangers with fixed surface area. The pumping power will vary with varying mass flow rate. Therefore, efficiency index 'η' can be defined as:

$$\eta = \frac{h/h_s}{(\lambda/\lambda_s)^{1/3}} = \frac{j/j_s}{(f/f_s)^{1/3}} \tag{5-18}$$

Since Webb and Kim formulated Eq. 5.18, it seems that most researchers (R Ranjbarzadeh, Isfahani, and Hojaji 2018; Hashemian et al. 2017; Hazbehian et al. 2016; S Eiamsa-ard, Ketrain, and Chuwattanakul 2018; Ghahdarijani, Hormozi, and Asl 2017; Kumar et al. 2018; L. Zheng, Xie, and Zhang 2017; Omidi, Farhadi, and Jafari 2017) prefer using the Nusselt number rather than the Chilton-Colburn heat transfer factor to calculate 'η', hence:

$$\eta = \frac{\left(\frac{Nu_{nf}}{Nu_{bf}}\right)}{\left(\frac{f_{nf}}{f_{bf}}\right)^{1/3}} \tag{5-19}$$

Where 'Nu_{nf}' and 'Nu_{bf}' are the Nusselt number for nanofluid and base fluid (water) respectively. 'f_{nf}' and 'f_{bf}' are nanofluid and base fluid friction factor respectively.

Although Eq. 5.19 has received widespread use, Sahit et al. [27,28] argued that although these dimensionless parameters are suitable for scaling purposes among geometrically similar heat exchangers, their direct comparison does not offer the answer of which type of heat exchanger surface or enhancement element (such as nanofluids) will meet the performance objectives within the design constraints. They pointed out that methods of comparison used in the past are in many respects approximate and hence fail to predict accurately the relative performance of conventional heat exchanger surfaces operated with different heat exchanger elements. Owing to the direct use of the Chilton-Colburn factor for performance assessment, these methods over-predict the relative performance of heat exchangers. They suggested that the selection of elements for heat

transfer enhancement in heat exchangers requires a methodology to make a direct comparison of the performances of heat exchanger surfaces with different elements.

In this thesis, a method that allows for direct comparison of measured heat transfer coefficients and friction factors without the need to calculate Nusselt numbers that incorporate the large uncertainties from thermal conductivity measurements (Chapter 4) was employed. The ratio of directly measured heat transfer coefficients 'E_u' (Eq. 5.20) was divided by the ratio of friction factor 'E_f' (Eq. 5.21), and the thermal performance factor 'φ' of tested combinations of nanofluids in a closed test loop was produced from Eqs. 5.20 to 5.22 as:

$$E_U = \frac{U_{nf}}{U_{water}} \tag{5-20}$$

$$E_f = \frac{f_{nf}}{f_{water}} \tag{5-21}$$

$$\varphi = \frac{E_U}{E_f} \tag{5-22}$$

5.5. Conclusion

This chapter has discussed the development and instrumentation of the experimental rig that was used to produce the experimental data presented and analysed in Chapters 6 and 7.

Chapter 6

Experimental evaluation of the performance of Al_2O_3/H_2O, $C/H_2O/CTAB$ and $CuO/H_2O/ARB$ nanofluids.

6.1 Introduction

It was noted in Section 2.3 that nanofluids have demonstrated their potential to replace conventional working fluids in heat transfer systems because of their significantly higher thermal conductivities compared to conventional fluids. For that reason, there has been a significant amount of interest in nanofluids and much theoretical and experimental information has been published across various disciplines of science.

However, the quantity of work undertaken to bridge the gap between characterisation of physical properties and real application of nanofluids is relatively small. Currently it appears that material scientists and chemists perform most investigations on physical characteristics of nanoparticles, whereas engineering researchers carry out the experiments on the heat transfer applications of nanofluids, and there is not always close collaboration or communication between the two groups, which may contribute to the lack of agreements between results of different studies.

Previous works have assessed the performance of alumina/water (Al_2O_3/H_2O) as a nanofluid. Darzi et al. (Darzi, Farhadi, and Sedighi 2013) observed an enhancement of 20 % in Nusselt numbers of Al_2O_3/H_2O nanofluid with increased pressure drop in a double pipe heat exchanger of 2.2 m long and heat transfer area of 0.056 m^2; their volume of nanoparticle concentration varied up to 1 %. They created an empirical correlation for Nusselt number as a function of the Reynolds number and nanoparticle concentration**.**

Han et al. (Han, He, and Asif 2017; M. Zheng et al. 2020a) experimentally investigated the effect of Al_2O_3/H_2O nanofluids on heat transfer enhancement in a double pipe heat exchanger 1.0 m long with heat transfer area of 0.251 m^2. They concluded that 0.25 % and 0.5 % nanoparticle concentration significantly increased Nusselt number up to 24.5 %. Similarly, Sonawane et al. (Sonawane, Khedkar, and Wasewar 2013) studied Al_2O_3/H_2O nanofluids in a 1.0 m long double pipe heat exchanger with heat transfer area of 0.025 m^2; They observed 16 % overall heat transfer enhancement with 3 % volume concentration of nanoparticles.

Pak and Cho (Pak and Cho 1998) studied the hydrodynamic, turbulent friction and heat transfer behaviours of Al_2O_3/H_2O nanofluid in a stainless-steel tube of 4.8 m long with heat transfer area of 0.016 m^2. They found out that an additional pumping penalty of approximately 30 % at a volume concentration of 3% was observed. Figure 6.1 shows the results of Darzi et al. (Darzi, Farhadi, and Sedighi 2013), Han et al. (Han, He, and Asif 2017; M. Zheng et al. 2020a), Sonowane et al. (Sonawane, Khedkar, and Wasewar 2013) and Pak and Cho's (Pak and Cho 1998) studies presented as Nusselt number against Reynolds number.

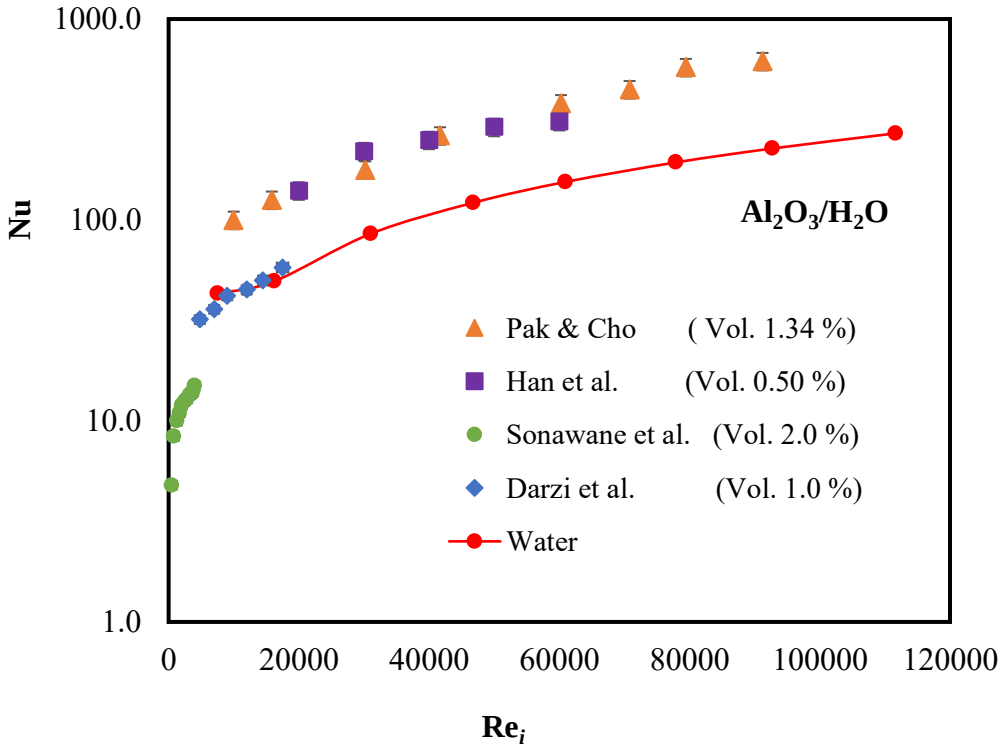

Figure 6.1 A comparison of experimental Nusselt number against Reynolds number for Al_2O_3/H_2O nanofluid (Pak and Cho 1998; Han, He, and Asif 2017; Sonawane, Khedkar, and Wasewar 2013; Darzi, Farhadi, and Sedighi 2013; M. Zheng et al. 2020a; V. Gnielinski 2013)

Darzi et al. (Darzi, Farhadi, and Sedighi 2013) used almost the same volume concentration of nanoparticles as Pak and Cho and their heat transfer areas were similar but, Pak and Cho's Nusselt number was 64 times higher than that of Darzi et al.'s at Re ~ 10000. In turn, Darzi et al.'s Nusselt number was 18 times greater than Sonowane's Nusselt number at Re ~ 5000 even though Sonowane's volume concentration of nanoparticles was double that of Darzi et al. A possible reason why there are such wide variations in results is perhaps due to the thermal conductivity data used to calculate Nusselt numbers. None of these studies used thermal conductivity data that came from

direct measurements of the thermal conductivity of the nanoparticles they used in their experiments. Pak and Cho used Masuda et al. (Masuda et al. 1993) thermal conductivity values as a reference to perform Nusselt numbers presented in Fig 6.1 whereas Darzi et al. (Darzi, Farhadi, and Sedighi 2013) and Sonowane et al. (Sonawane, Khedkar, and Wasewar 2013) used Maxwell's model (Maxwell 1892). Han et al. (Han, He, and Asif 2017; M. Zheng et al. 2020a) used Hamilton's model (Hamilton and Crosser 1962); however, they did not state where their nanoparticles thermal conductivity data came from. Chapter 2 showed the high variation in reported thermal conductivity data for nanofluids and Chapter 4 described the difficulties of getting repeatable data for thermal conductivity of nanofluids using commonly employed transient techniques such as the conductivity probe, which is likely to have contributed significantly to the large variation in the literature.

In addition, Han et al. (Han, He, and Asif 2017; M. Zheng et al. 2020a) and Sonawane et al. (Sonawane, Khedkar, and Wasewar 2013) failed to evaluate the resulting pressure drop in order to give a better picture about the overall performance since increased pressure drop means increased pumping costs which will offset cost-savings of increased heat transfer rates.

In this chapter, experimental results of heat transfer, pressure drop and performance evaluation of nanofluids compared to water as a base are presented and discussed. All the physical properties used in the calculations came from direct measurements (as described in Chapter 4), and performance was characterised using heat transfer coefficients rather than Nusselt numbers (as described in Chapter 5) to avoid the use of thermal conductivity data where possible. In this way the uncertainty in performance enhancement calculations is greatly reduced compared to most previous studies. Practical challenges encountered while testing nanofluids are also addressed.

6.2 Water as a base case.

It is a common practise by researchers (M. Zheng et al. 2020b; Abdelmagied 2020; Jassim and Ahmed 2020; Mukesh Kumar and Chandrasekar 2020; Syam Sundar et al. 2019) to establish a base case or control experiment by comparing experimental data with established correlations or datasets. In this study, deionised water was charged into the test closed loop and several runs were carried out.

6.2.1 Heat transfer

The results in Fig. 6.2 shows directly measured overall heat transfer coefficients from both the tube-side (U_i) and shell-side (U_o) versus tube-side Reynolds number. The shell-side Reynolds number was maintained at Re ~ 9900.

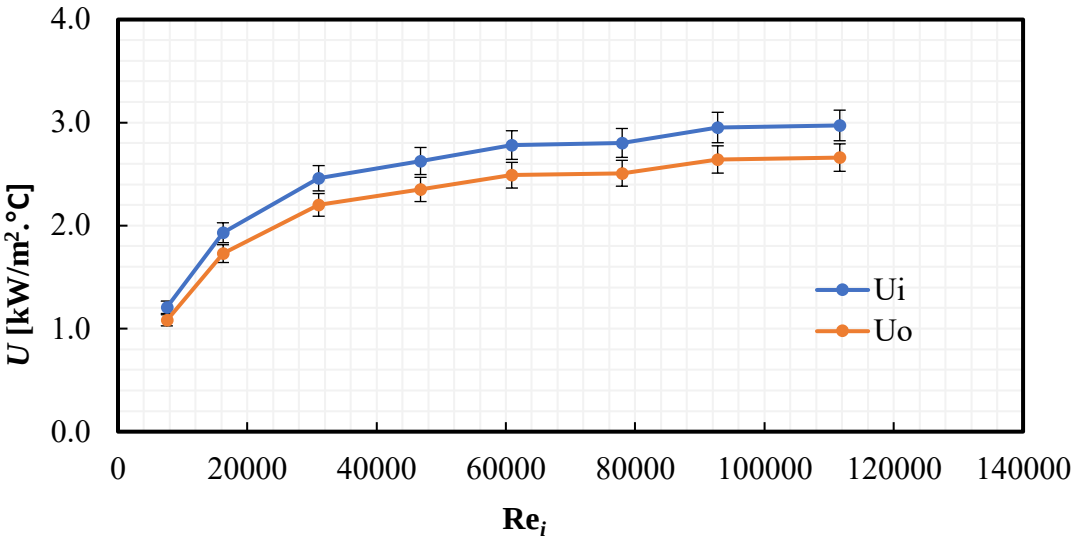

Figure 6.2 Measured tube and shell-side overall heat transfer coefficients for water

The overall heat transfer coefficient (U) is made up of two film heat transfer coefficients (h_i and h_o) and a wall resistance (Cengel and Boles 2006):

$$\frac{1}{U_i A_i} = \frac{1}{h_i A_i} + \frac{ln\left({}^{D_o}/_{D_i}\right)}{2\pi kL} + \frac{1}{h_o A_o} \tag{6-1}$$

When evaluating the effectiveness of nanofluids, it would be preferable to compare measured h_i against the h_i measured from literature for similar fluids. So, the question is how do we get measured h_i? In principle h_i, may be determined from U provided a suitable correlation for h_o is available, i.e.:

$$h_i = \frac{1}{\frac{1}{U_i} - \left(\frac{ln\left({}^{D_o}/_{D_i}\right)}{2\pi kL} - \frac{1}{h_o A_o}\right) A_i} \tag{6-2}$$

Dirker (Dirker, Van Der Vyver, and Meyer 2004) performed a study of heat transfer coefficients in double pipe heat exchangers that considered a range of ratios of outer to inner diameter of the annulus (a). They used the Wilson-Plot method (Wilson 1915) to create a correlation from experimental data for the shell-side heat transfer coefficients presented in Eq. (6.3)

$$h_o = C_o \frac{k_o}{D_o} Re_o^P Pr_o^{0.33} \left(\frac{\mu}{\mu_w}\right)_o^{0.14} \tag{6-3}$$

The shell-side constants C_o and exponent P account for heat exchanger geometry influences, and were defined by Eqs. (6.4) and (6.5) respectively. The Euler's number e in Eq. (6.4) was taken to be (e = 2.8).

$$P = \ 1.013e^{-0.067a} \tag{6-4}$$

$$C_o = \frac{0.003a^{1.86}}{0.063a^3 - 0.674a^2 + 2.225a - 1.157} \tag{6-5}$$

The inner diameter in the study was not varied. However, the shell-side coefficient C_o and the exponent P depend on annular diameter ratio (a) which is obtained by dividing the diameter of inner wall of outer tube (D_2) by diameter of outer wall of inner tube (D_1). Dirker's study covered a values between 1.7 and 5.1, which covers the a value from the apparatus used in this thesis (2.87). Inserting a = 2.87 into Eqs. 6.4 and 6.5 produces P = 0.835 and C_o = 0.018 respectively. Therefore, Eq. 6.3 (Dirker correlation) with P = 0.835 and C_o = 0.018 could be used to calculate h_o, and subsequently h_i can be determined from the measured U_i and from h_o from the Dirker correlation using Eq. 6.2, and the results are shown in Fig. 6.3 as the 'Measured' data.

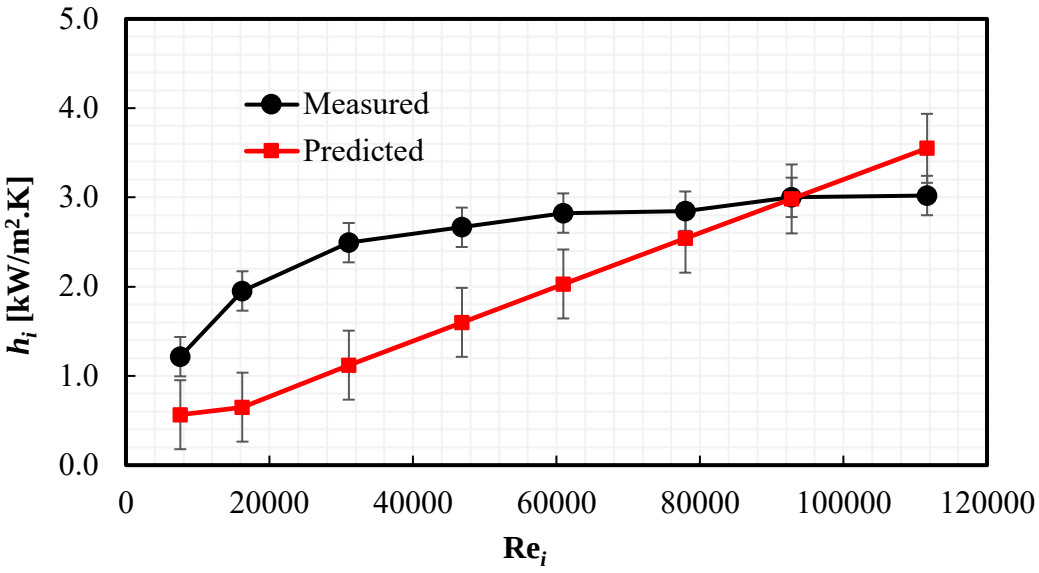

Figure 6.3 Comparison between h_i measured and predicted.

The Gnielinski correlation (Volker Gnielinski 1975) (Eq. 6.6) which is widely recommended by many studies (Kays and Crawford 1993; Bhatti and Shah 1987; Volker Gnielinski 1975) to be more accurate for modelling heat transfer coefficients in straight tubes than the Dittus-Boelter correlation (Dittus, F.W. and Boelter 1930) was used for h_i and is shown in Fig 6.3 as 'predicted' data. The results in Fig. 6.3 show that measured h_i does not match the predicted correlation h_i and yet, this is for a straight tube circular cross-section. The large deviation between h_i measured and predicted suggests Dirker's (h_o) correlation may not be suitable for this study.

$$Nu_i = \frac{\left(\frac{f}{8}\right)(Re - 1000)Pr}{1.07 + 12.7\left(\frac{f}{8}\right)^{0.5}\left(Pr^{2/3} - 1\right)}\left[1 + \left(\frac{D}{L}\right)^{2/3}\right]\left(\frac{Pr}{Pr_w}\right)^{0.11} \qquad (6\text{-}6)$$

If h_i could be determined independently then h_o itself can be calculated from the measured U_i data. Figure 6.4 shows h_o calculated from the measured U_i data using Eq. 6.6 to calculate h_i. and for low Reynolds, numbers negative values of h_i were obtained, before a sharp crossover to positive values.

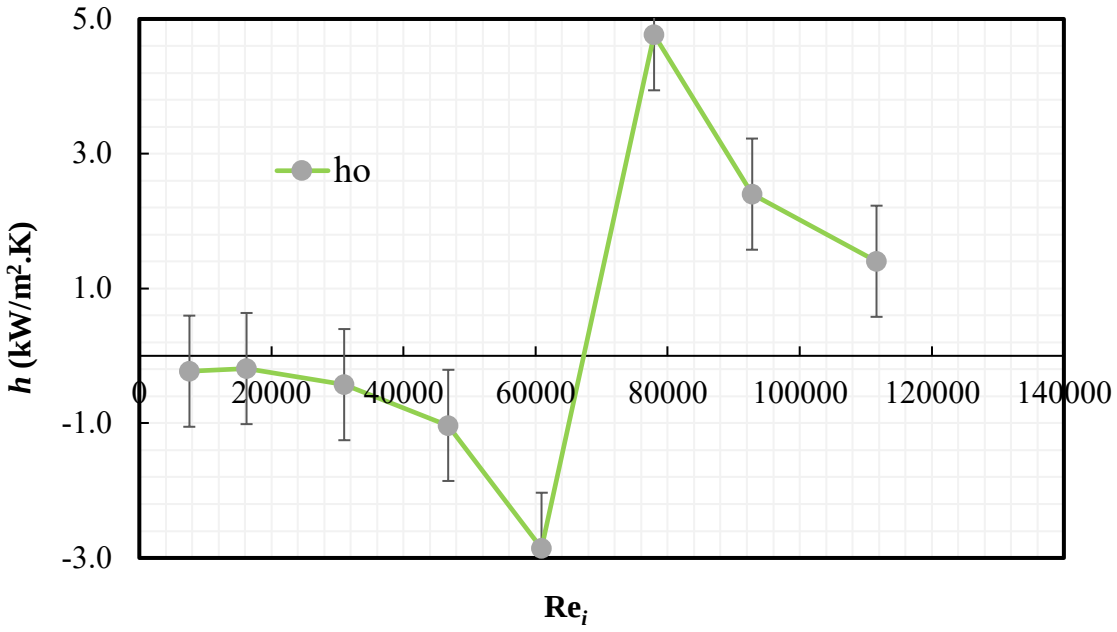

Figure 6.4 Shows h_o calculated from U_i when Gnielinski correlation (Volker Gnielinski 1975) **is used for h_i**

Figure 6.5 shows a comparison of predicted U_i (with h_o from Dirker and h_i from Gnielinski) against measured U_i (see Fig. 6.2). The predicted values were much lower than the measured U_i.

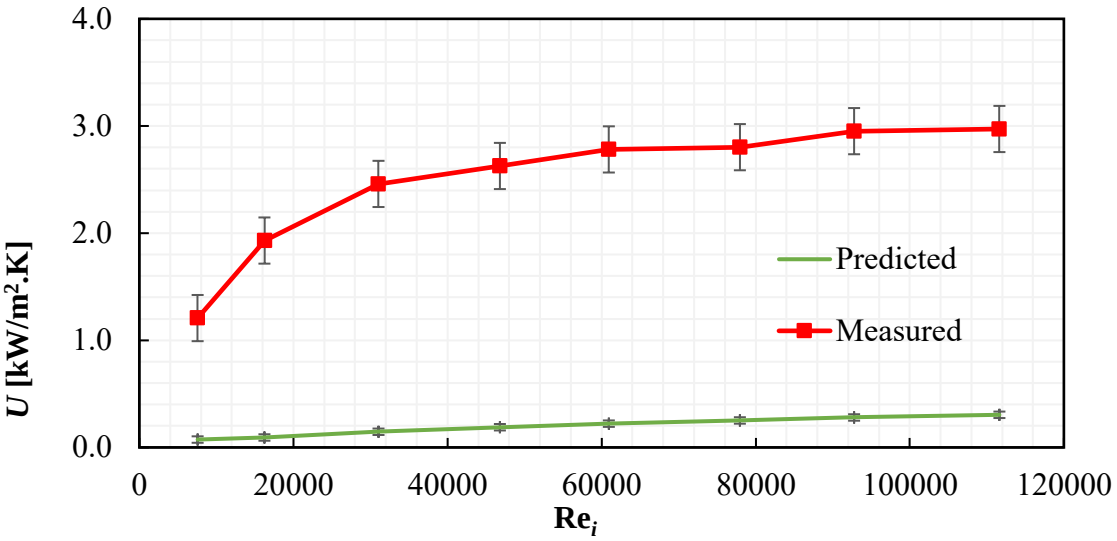

Figure 6.5 Comparison between U_i Measured and that predicted using h_o from Dirker et al. (Dirker, Van Der Vyver, and Meyer 2004) **proposed correlation and h_i from Gnielinski correlation** (Volker Gnielinski 1975)**.**

Figures 6.3 to 6.5 illustrate the difficulty of trying to extract reliable data for h_i or h_o from the measured U_i data, since neither h_i or h_o were measured directly. A possible explanation for these results might be that, while the fluid flow was likely to have been

fully developed with a 250.0 mm length of straight pipe (corresponding to at least ten diameters) prior to the heat exchanger (see Chapter 5, Fig. 5.2) (Incropera et al. 2017), on the shell-side, the fluid encounters a sharp expansion followed by an abrupt 90 °C turn when entering the annulus. Also the hydrodynamic entry length on the shell-side of the heat exchanger would be longer for the shell-side due to its larger diameters, so it is unlikely that the velocity profile was fully developed (Cengel and Cimbala 2013; S. Perry et al. 1997). Therefore, the problem is likely to be with obtaining a suitable correlation for h_o. In Dirker's study the double-pipe heat exchangers where 6 m long, compared to 1 m in this study, which would have ensured fully developed flow through most of the heat exchanger, and hence the correlation for the annular flow heat transfer correlation be for fully developed flow. Elsewhere, Wang et al. (C. C. Wang, Chiou, and Lu 1996) investigated single-phase heat transfer and flow friction correlations. They found that there was a detectable deviation between the experimental data and the Dittus-Boelter correlation. Similarly, Bhatti et al. (Bhatti and Shah 1987) and Kays and Crawford (Kays and Crawford 1993) in their books about single-phase convective heat transfer, and convective heat and mass transfer respectively illustrated that most correlations overpredict data and appears to be outdated, and this as well cannot be ruled out as one of the possible reasons for unmatched results between measured and predictions from correlations.

Since h_o could not be calculated independently, it was not possible to extract h_i from the measured U_i data. Therefore, the heat transfer analysis has to be based on U_i. However, because water was always used in the shell-side, and the shell-side flow rate was always constant in all the experiments with nanofluids, comparisons of performance of nanofluids with respect to water and between nanofluid will be nevertheless be meaningful.

6.2.2 Pressure Drop

As pumping cost should be taken into consideration when evaluating heat transfer fluids, the pressure drop on the tube side was measured at different flow-rates and friction factors were calculated using Eq. 5.9. Figure 6.6 shows the measured Fanning friction factor as a function of Reynolds number compared with predictions from the Petukhov (Petukhov 1970), Blasius (Blasius H. 1913) and Swamee (Swamee and Jain 1976)

correlations. The experimental data in Fig. 6.6 showed that friction factor was slightly higher but the trend is similar to the correlations from the literature.

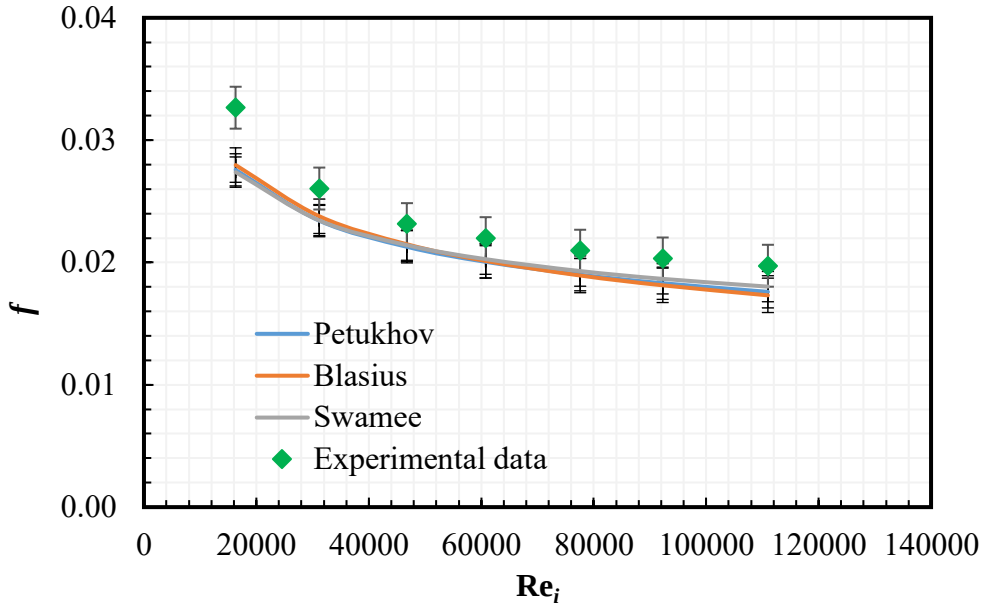

Figure 6.6 Test results for measured and predicted data of friction factor.

6.3 Nanofluids

It was mentioned in Chapter 4 that Al_2O_3/H_2O, C/H_2O/CTAB and CuO/H_2O/ARB nanofluids were selected to be tested in the rig because they had comparatively low viscosity and were relatively stable.

Therefore, following similar preparation procedures as described in Chapter 3 these three selected combinations of nanofluids were prepared. Nanoparticles weighing 0.35 kg were added to 5 litres of deionised water. In terms of heat transfer enhancements, the enhancement effect has a greater dependence on volumetric concentration than mass concentration, since thermal conductivity is a volumetric property. However, the cost of these nanoparticles is per gram not per millilitre, and therefore the same mass of nanoparticles and deionised water was used in all three selected combinations of nanofluids, rather than the same volume.

Equal amounts of CTAB and ARB surfactants (0.1 kg) were later added to C/H_2O and CuO/H_2O nanofluids respectively. These nanofluids with percentage volume of nanoparticle concentrations 1.74, 13.29 and 1.09 for Al_2O_3/H_2O, C/H_2O/CTAB and CuO/H_2O/ARB nanofluids respectively were charged in the closed flow loop and tested.

6.3.1 Al_2O_3/H_2O nanofluid

Figure 6.7 shows overall heat transfer coefficients of Al_2O_3/H_2O nanofluid along with the results of deionised water versus tube-side Reynolds numbers. The average heat transfer coefficients are found to increase with the increase of Reynolds number as expected. Also, the heat transfer coefficients of the Al_2O_3/H_2O nanofluids are found to be higher than that of water at any Reynolds number.

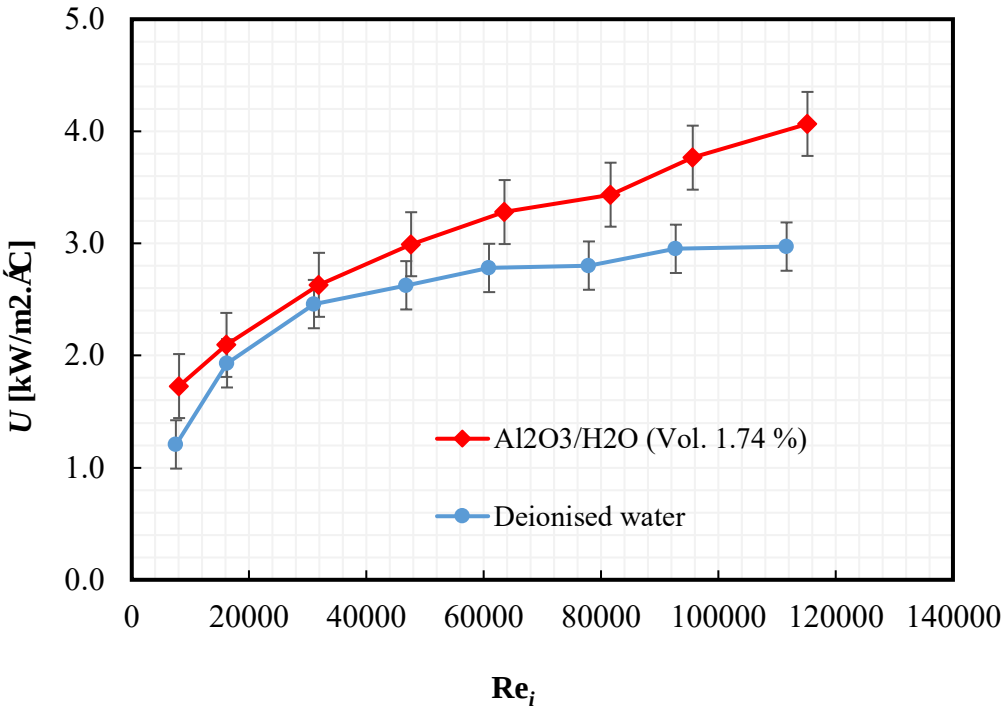

Figure 6.7. Heat transfer of Al_2O_3/H_2O nanofluids compared to water

In the beginning of this Chapter, Fig. 6.1 demonstrated experimental Nusselt number against Reynolds number for Al_2O_3/H_2O nanofluid from literature and the results showed large differences in Nusselt numbers when compared among them.

It was previously mentioned that thermal conductivity is complicated to measure due to large uncertainties. Also, it was not possible to extract tube-side heat transfer coefficient data from the overall heat transfer coefficient measurements (Section 6.2) and therefore only the measured overall heat transfer coefficients could be used in for comparisons with results from the literature. Han et al. (Han, He, and Asif 2017; M. Zheng et al. 2020a) and Pak and Cho (Pak and Cho 1998) only provided data for film heat transfer coefficients which was calculated from Nusselt numbers and calculated thermal conductivity using Hamilton's model (Hamilton and Crosser 1962) and Masuda

et al. (Masuda et al. 1993) thermal conductivity values respectively. However, Sonawane et al. (Sonawane, Khedkar, and Wasewar 2013) provided measured overall heat transfer data that can be compared to the currently measured heat transfer coefficient results, as shown in Fig. 6.8. Although Sonawane et al. (Sonawane, Khedkar, and Wasewar 2013) did not explicitly mention what their shell-side Reynolds number was, the results in Fig. 6.8 still are comparable to this current study. However, the maximum Reynolds numbers from Sonawane et al. (Sonawane, Khedkar, and Wasewar 2013) are way below even for the lowest Reynolds number for the present measured heat transfer.

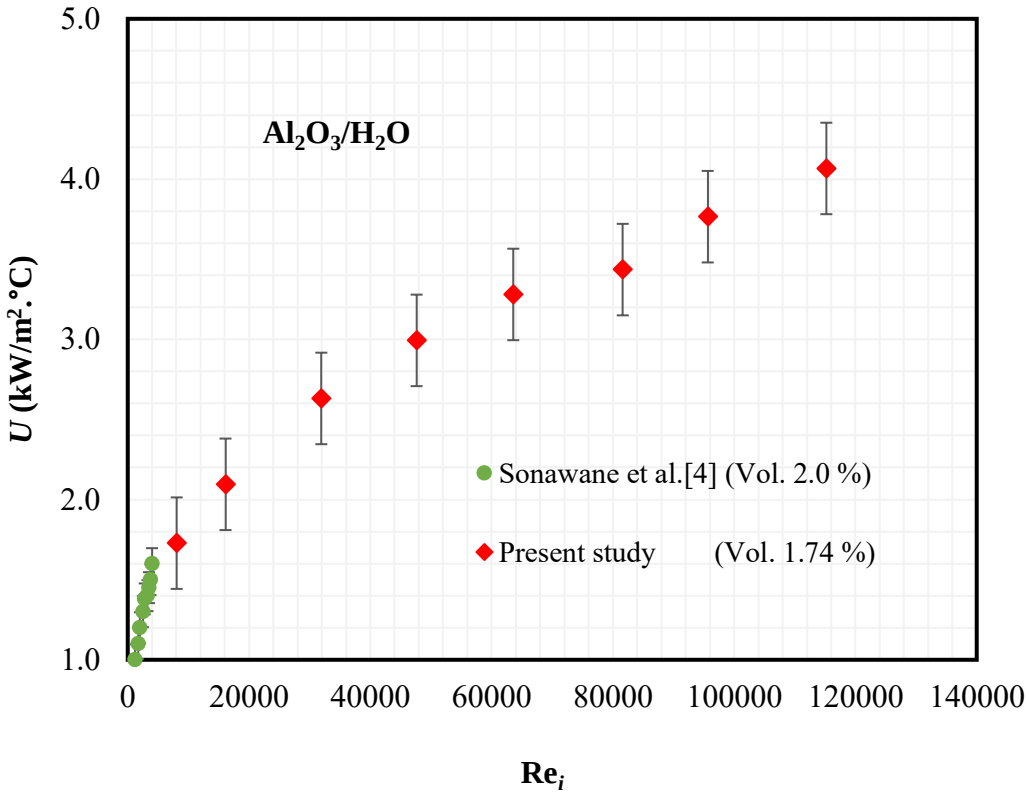

Figure 6.8. A comparison of heat transfer present results for Al_2O_3/H_2O nanofluid with that from Sonowane et al. (Sonawane, Khedkar, and Wasewar 2013)

Figure 6.9 shows pressure drop and friction factor against Reynolds number for Al_2O_3/H_2O nanofluid and water. The results show that the pressure drop and friction factor for Al_2O_3/H_2O nanofluid with 1.7 % nanoparticles concentration was much higher than that of water at every Reynolds number for which measurements were performed.

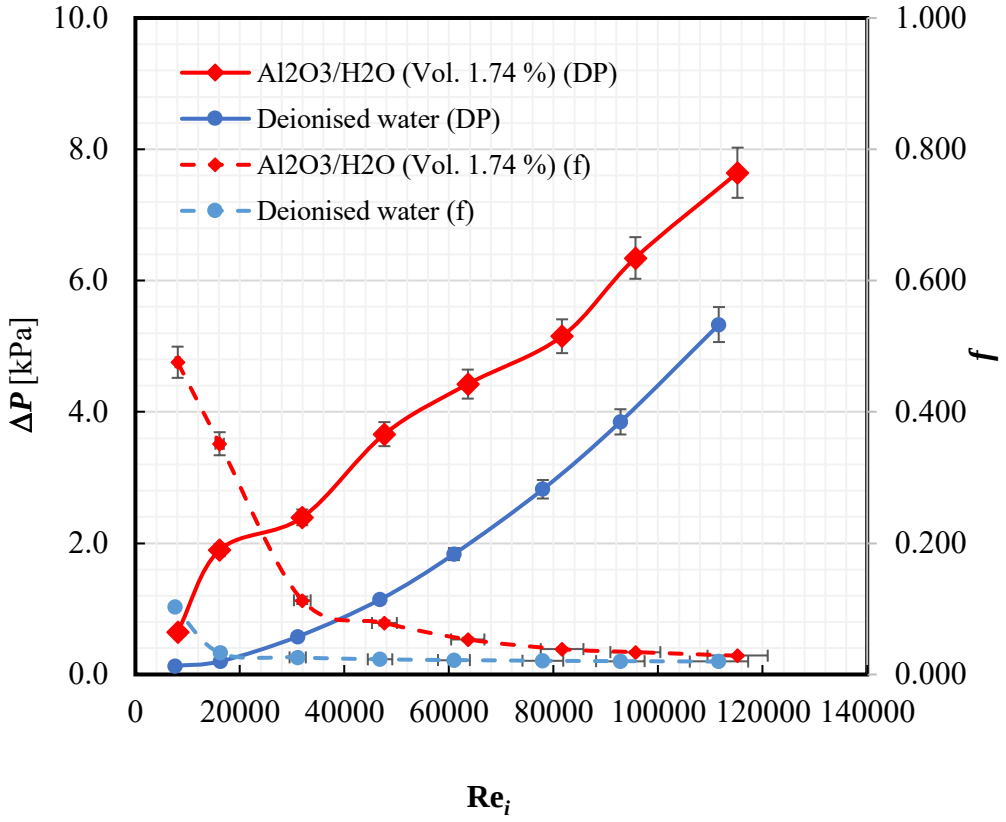

Figure 6.9. Pressure drop and friction factor of Al_2O_3/H_2O compared to deionised water.

6.3.2 CuO/H_2O/ARB Nanofluid

Figure 6.10 shows that overall heat transfer coefficients versus Reynolds number for CuO/H_2O/ARB nanofluid and water. For a volume of 1 % nanoparticles concentration, it is observed that CuO/H_2O/ARB nanofluid gives slightly better heat transfer coefficients than the pure water for all the Reynolds numbers.

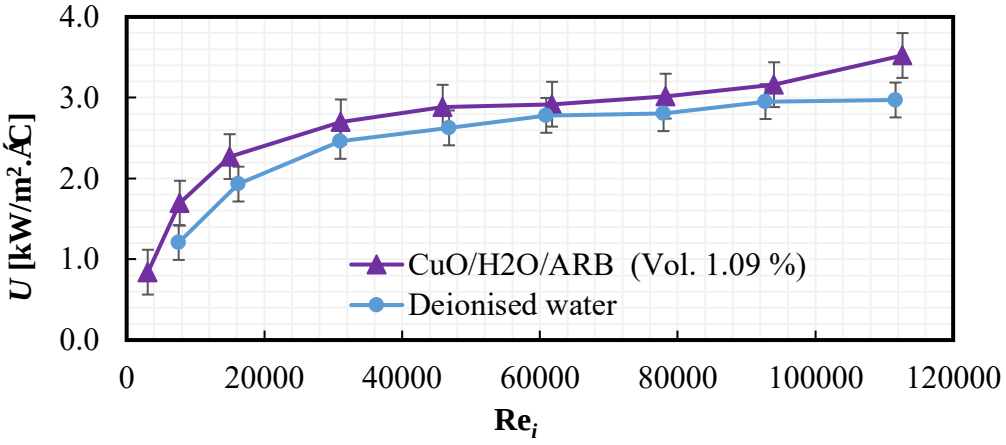

Figure 6.10. Heat transfer of CuO/H_2O/ARB nanofluids compared to water

No comparisons with the literature data were made because there does not appear to be any measured heat transfer coefficient data for this nanofluid (unlike Al_2O_3).

Figure 6.11 presents pressure drop and friction factor against Reynolds number for CuO/H_2O/ARB nanofluid and water. The results show that the pressure drop and friction factor for CuO/H_2O/ARB nanofluid with 1.09 % nanoparticles concentration was higher than that of water at every Reynolds number.

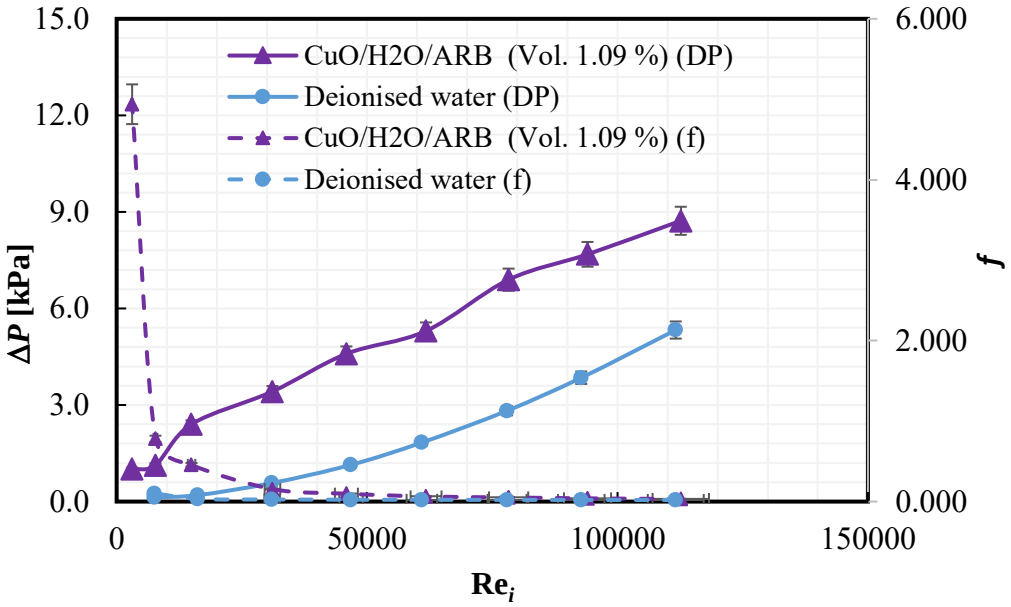

Figure 6.11. Pressure drop and friction factor of CuO/H_2O/ARB compared to water.

6.3.3 C/H_2O/CTAB Nanofluid

Figure 6.12 shows heat transfer coefficients increase against Reynolds number for C/H_2O/CTAB nanofluid and water. For a volume of 13 % nanoparticles concentration, the heat transfer of C/H_2O/CTAB nanofluid was higher at every Reynolds number compared to that of water.

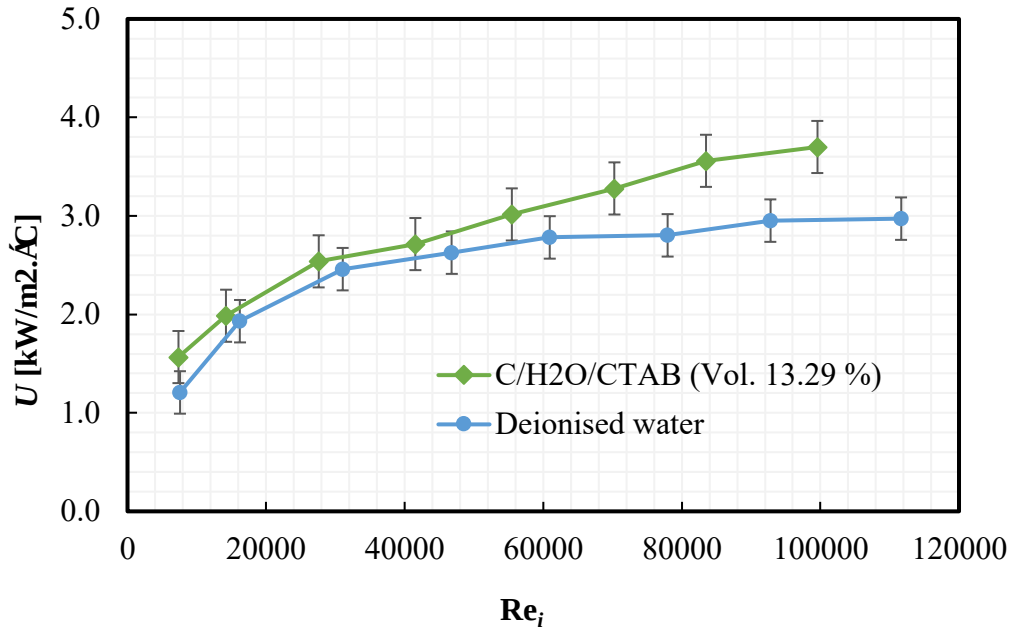

Figure 6.12. Heat transfer of C/H_2O/CTAB nanofluids compared to water

No comparisons with the literature data were made because there does not appear to be any measured heat transfer coefficient data for this nanofluid (unlike Al_2O_3).

Figure 6.13 presents pressure drop and friction factor against Reynolds number for C/H_2O/TAB nanofluid and water. The results show that the pressure drop and friction factor for C/H_2O/TAB nanofluid with 13 % nanoparticles concentration was higher than that of water at every Reynolds number.

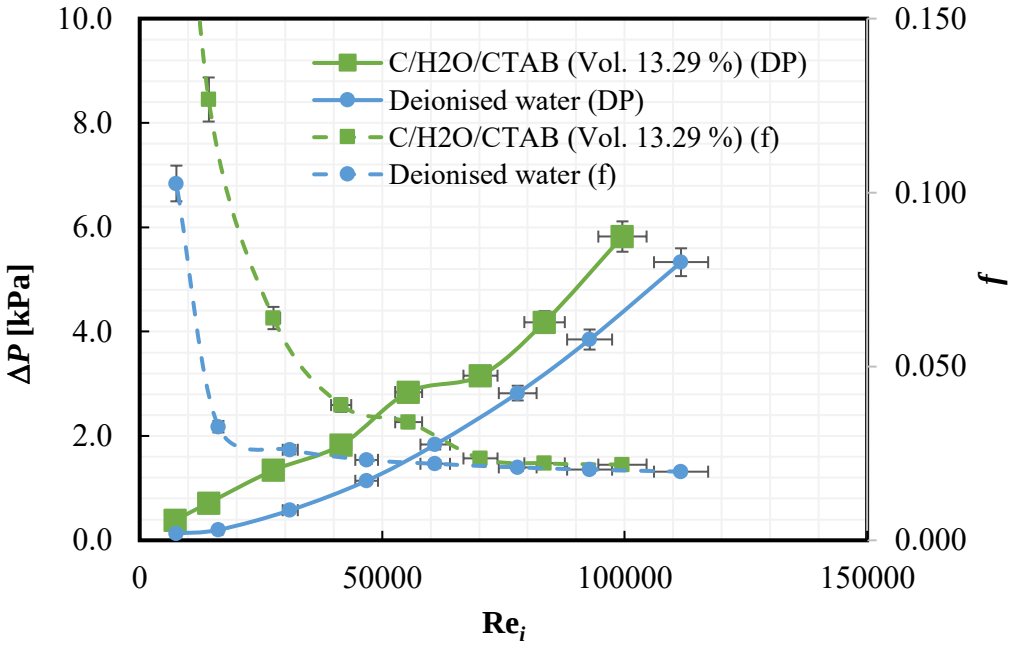

Figure 6.13. Pressure drop and friction factor of C/H_2O/CTAB compared to water.

6.4 Comparison of heat transfer, pressure drop and friction factor of nanofluids to water

6.4.1 Heat transfer of nanofluids compared to water

In Fig. 6.14, a comparison between the results of Al_2O_3/H_2O, C/H_2O/CTAB and CuO/H_2O/ARB nanofluids is shown graphically and compared to water. In the range of Re = 8142.8 to Re = 46151.2 CuO/H_2O/ARB nanofluids heat transfer was slightly higher than the rest of nanofluids; and beyond that point, it was overtaken by Al_2O_3/H_2O, C/H_2O/CTAB nanofluids. On overall, Al_2O_3/H_2O appeared to yield the highest heat transfer rate which increased from 1.7 to 4.0 kW/m^2.K followed by C/H_2O/CTAB which increased from 1.5 to 3.7 kW/m^2.K over the range of Re = 8070.5 to Re = 115202.9.

Compared to pure water, the heat transfer of these three nanofluids at maximum Reynolds numbers improved on average by 36.15 %, 23.88 % and 17.96 % for Al_2O_3/H_2O followed by C/H_2O/CTAB and CuO/H_2O/ARB nanofluids respectively.

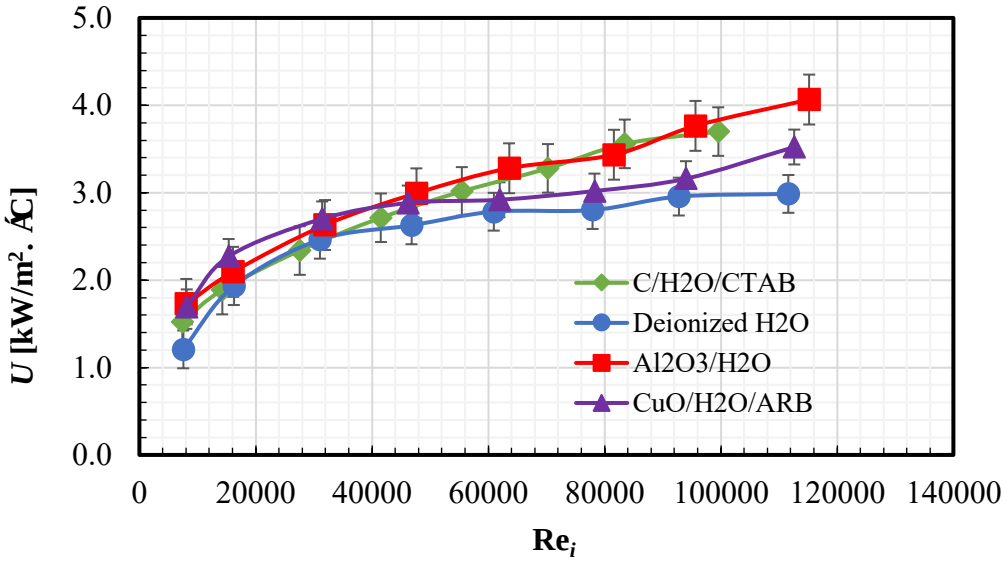

Figure 6.14. Comparison of nanofluid heat transfer enhancement to deionized water

When it comes to experimental heat transfer enhancements, most of the explanation on experimental results are based on reasoning that the increase in heat transfer coefficient is because of intensified turbulence of nanoparticles (Buongiorno 2006), or heat transfer takes place when the metallic oxide particle comes into contact with water to form hydroxyl radical at the surface of the metallic oxide particle (Pak and Cho 1998). Brownian motion and micro-convection effect of nanoparticles that many groups assume

to be one possible reason for heat transfer enhancements have been challenged by the argument that its contribution as a mechanism for nanoparticles ability to enhance thermal conductivity is too small (Nie, Marlow, and Hassan 2008).

The Pak and Cho (Pak and Cho 1998), Xuan and Roetzel (Xuan and Roetzel 2000), and Xuan and Li (Xuan and Li 2003) assumptions that convective heat transfer enhancement is due mainly to dispersion of the suspended nanoparticles were refuted by Buongiorno (Buongiorno 2006) who claimed that his mechanistic description of particle dispersion effect was very small in nanofluids, and thus cannot explain the observed heat transfer enhancement.

From the above explanations, it can be concluded that there is no single theory that can explain heat transfer enhancements of nanofluids. It appears that various factors contribute to heat transfer enhancements of nanofluids.

6.4.2 Friction factor and pressure drop of nanofluids and water

Besides the heat transfer enhancements of nanofluids, it is necessary to analyse and understand flow resistance of nanofluids in order to evaluate these nanofluids to application in practical settings.

Figure 6.15 presents friction factor of nanofluids against Reynolds number. The results show that CuO/H_2O/ARB nanofluids yielded the highest friction factor. It also appeared that friction factor was most significant during lower Reynolds number up to Re ~ 31345.41; and relatively independent at high Reynolds number.

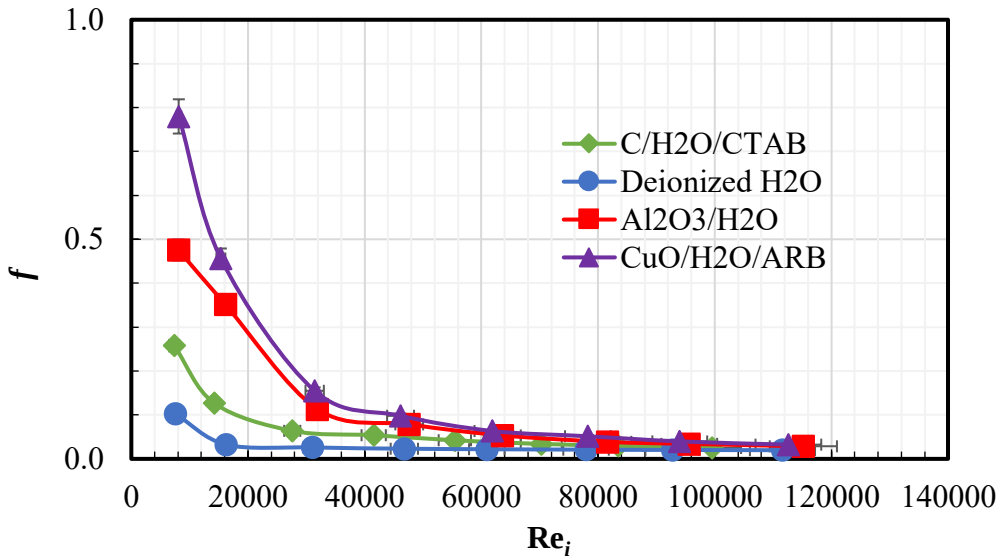

Figure 6.15 Friction against Reynolds number for nanofluids

Although Friction factor data provides information that allows the understanding of the hydraulic resistance of the fluid as a result of momentum transfer to the walls of the heat exchanger specifically at low Reynolds numbers, Friction factor data is more relevant for scaling purposes among geometrically similar heat exchangers.

Unlike Friction factor which is dimensionless, pressure drop was measured in kPa and is directly related to pumping costs. Figure 6.16 show the effect of Al_2O_3/H_2O, CuO/H_2O/ARB and C/H_2O/CTAB nanofluid on pressure drop. In comparison to pure water, there was an increase in pressure drop of 51.6 %, 43.4 % and 24.3 % for CuO/H_2O/ARB, Al_2O_3/H_2O and C/H_2O/CTAB respectively. In Chapter 3 and 4, C/H_2O with CTAB as a surfactant was stable for 17 days and had the lowest viscosity compared to CuO/H_2O/ARB and Al_2O_3/H_2O nanofluids. Increased pressure drops demands increased pumping power and operational costs. These results indicate that C/H_2O/CTAB nanofluid having the lowest pressure drop, would be cost saving compared to the rest of tested nanofluids.

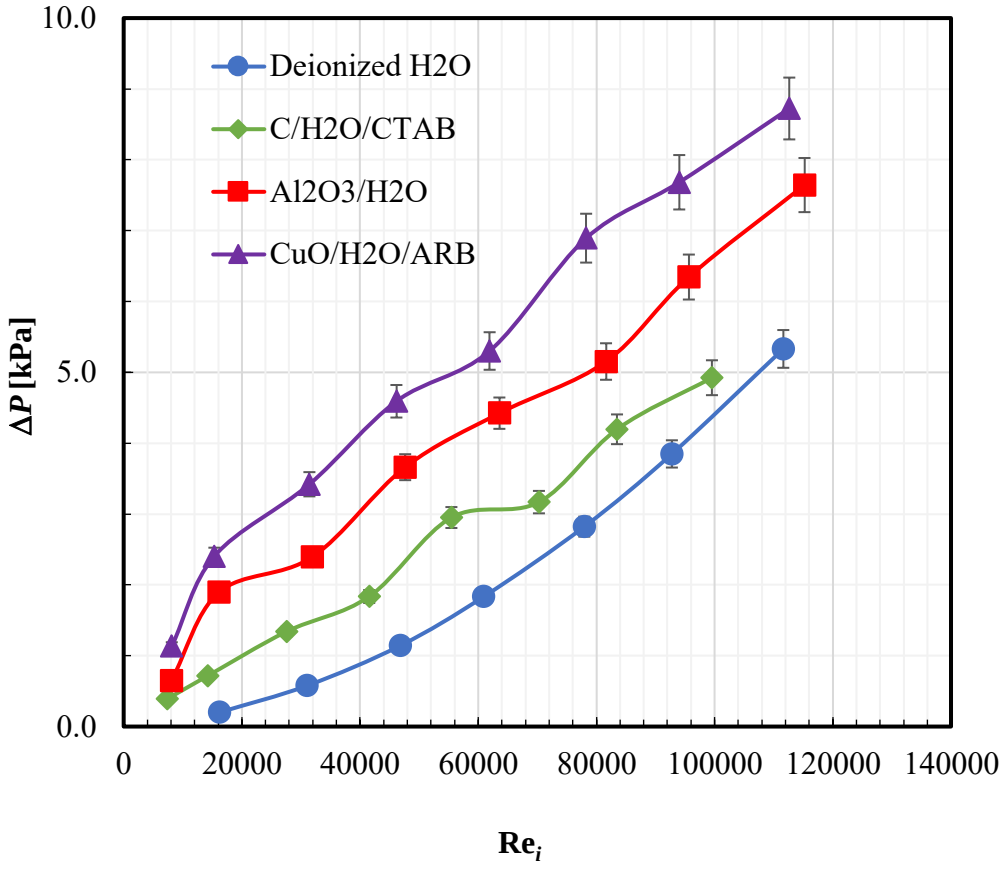

Figure 6.16. Effect of nanofluids on pressure drop compared to water

6.5 Practical Challenges associated with nanofluids

In this study, several practical challenges were encountered while testing nanofluids in a closed flow loop as follows:

- Replacing one nanofluid by another: Each time a new nanofluid was to be tested, it required a lot of water to hose and wash out the previously tested fluid from the closed test loop; which also revealed that large aggregated particles formed for all tested nanofluids but mostly for Al_2O_3/H_2O nanofluid which had no surfactant during operation. The cleaning process was time consuming too because it took a full day to typically wash nanofluid out of all parts in the closed loop.
- The pump that was used to circulate nanofluids in the closed loop could not run smoothly at the beginning of each test run especially for Al_2O_3/H_2O nanofluid that had no surfactant. Therefore, the pump had to be restarted several times whenever it stopped running. It is suspected that nanoparticles may have harboured or clogged the pump. In order to avoid both clogging and accumulation of nanoparticles inside the closed flow loop, El-Maghlany et al. (El-Maghlany et al. 2016) used a rotational double pipe heat exchanger of 1.2 m long at rotational speed from 0 to 500, and 1% to 3.0 % nanoparticle concentration to study the performance of CuO/H_2O nanofluid. However, this technique increased pressure penalty up to 136 %.
- At times during testing of nanofluid, it was noticeable that nanoparticles blocked pressure taps. This was revealed whenever the pressure differential displayed error signal. Therefore, it required extra hours to carefully clean the taps and retest the fluid.
- Reusing nanofluid: It was difficult to reuse the same nanofluid because some aggregated nanoparticles were either stuck in the mechanical parts (Pumps, valves or pressure taps) that make up the closed flow loop especially for Al_2O_3/H_2O nanofluid that had no surfactant compared to CuO/H_2O/ARB and C/H_2O/CTAB nanofluids. Therefore, the fluid in the rig had to be drained and hosed out; and new samples were prepared for every single test run. This was not only laborious, but also increased the operation cost because each time a new sample was to be tested, it required more quantities of nanoparticles; yet nanoparticles and surfactants are not cheap.

Most of the encountered challenges during nanofluid testing were related to instability of suspended nanoparticles. Although it was mentioned in Chapter 3 that there is no permanent stability of suspended nanoparticles, this study's practical tests revealed that it was more challenging to test Al_2O_3/H_2O nanofluid that had no surfactant compared to CuO/H_2O/ARB and C/H_2O/CTAB nanofluids.

6.6 Performance evaluation of Al_2O_3/H_2O, C/H_2O/CTAB and CuO/H_2O/ARB nanofluids

Figures 6.17 and 6.18 shows the thermal performance factors (η and φ) defined in Chapter 5 versus Reynolds number for Al_2O_3/H_2O, CuO/H_2O/ARB and C/H_2O/CTAB nanofluids calculated using Webb and Kim's Eq. 5.19 and directly measured heat transfer and friction factor ratios Eq. 5.22.

The highest thermal performance achieved from using η was up to 120 %, 115 % and 103 % for Al_2O_3/H_2O, C/H_2O/CTAB and CuO/H_2O/ARB nanofluids respectively. Whereas using φ, the highest thermal performance at their maximum Reynolds number achieved was from C/H_2O/CTAB nanofluid with 99 % followed by Al_2O_3/H_2O nanofluid with 94 %. The lowest thermal performance was registered from CuO/H_2O/ARB nanofluids with 73 % compared to pure water.

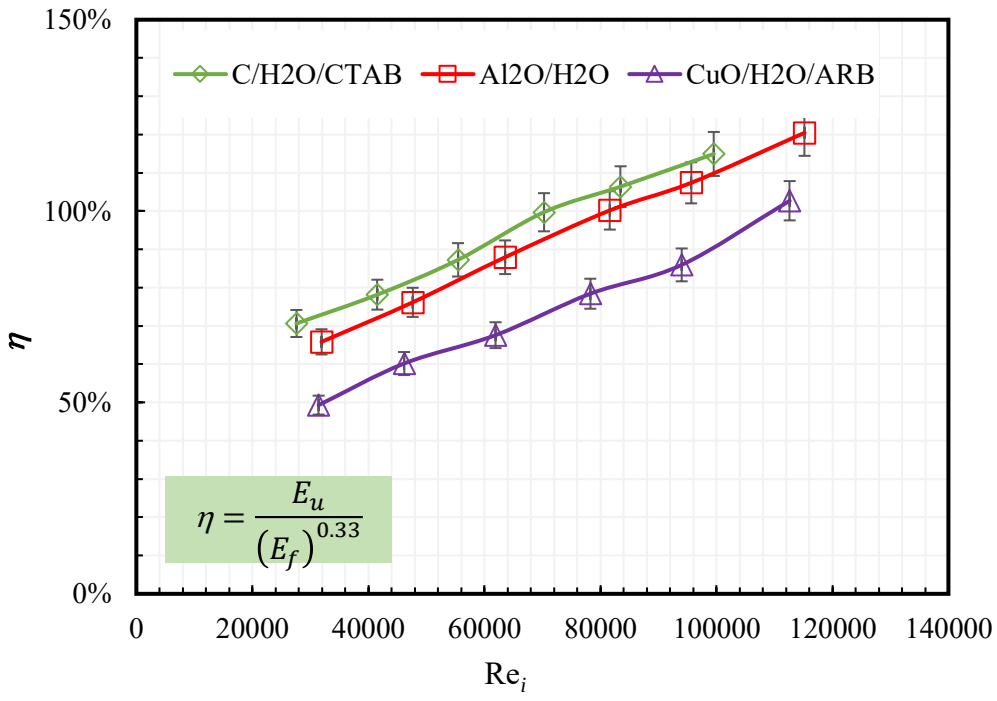

Figure 6.17 Thermal performance of nanofluids calculated using Web and Kimôs method.

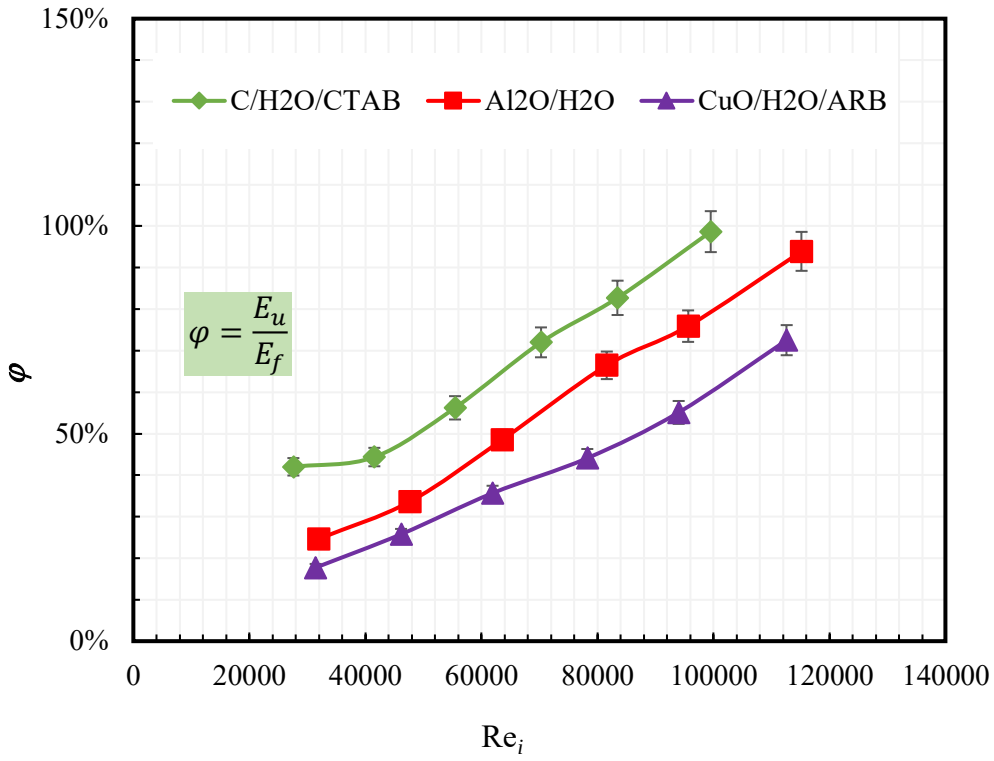

Figure 6.18 Thermal performance of nanofluids calculated directly using measured heat transfer and friction factor ratios.

C/H_2O/CTAB nanofluid appears the best compared to the other two tested nanofluids. Although the results in Fig. 6.14 for C/H_2O/CTAB and Al_2O_3/H_2O nanofluids appear to be close after the increased pressure drops are considered (Figs. 6.17 and 6.18) C/H_2O/CTAB clearly had the best performance evaluated by either η or φ. These results show that adding a surfactant does not necessarily result in increased pressure drop. Even with a surfactant, C/H_2O/CTAB still performed better than Al_2O_3/H_2O nanofluids without a surfactant.

Beside thermal performances, stability results in Chapter 3 showed that C/H_2O/CTAB nanofluid was stable for 17 days compared to 10 days for CuO/H_2O/ARB nanofluids, or 2 hours for Al_2O_3/H_2O nanofluids. The purchase cost (New Zealand dollar) of nanoparticles and surfactants used to create the three combinations of nanofluids and later tested in the rig are presented in Table 6.1. Yes, nanoparticles or even surfactants are not cheap but, still activated carbon nanoparticle's cost is slightly cheaper compared to the rest. Similarly, the cost of CTAB surfactant is even much cheaper compared to ARB. Therefore, based on those reasons it is concluded that C/H_2O/CTAB nanofluid is the best of the nanofluids considered in this thesis.

Table 6.1 purchased cost of nanoparticles and analytical grade surfactants (Nanostructured and amorphous Inc. 2019; Sigma-Aldrich 2021a, 2021b)

Nanoparticles -	**Cost [$/0.1 kg]**	**Surfactant** -	**Cost [$/0.1 kg]**
Alumina	$118.10	-	$0.00
Copper oxide	$173.67	ARB	$1130.00
Activated carbon	$111.15	CTAB	$122.20

It is worth to note that η values below 100 % correspond to worse performance than water and vice versa. From Fig. 6.17, the results show that η is only greater than 100 % for C/H_2O/CTAB and Al_2O_3/H_2O, nanofluids at Reynolds number above Re ~70000 and Re ~81000 respectively. However, η discounts the cost of pumping relative to the cost of heating. For φ values in Fig. 6.18, the results show no values are greater than 100 % when heat transfer and pumping are weighted equally. Therefore, which parameter gives better commercial indication of whether to use nanofluids?

If η is to be selected then, thermal performance will be weighted more highly than compared to φ. For example, there is a large difference in thermal performances between η and φ amounting to 41 %, 40 % and 32 % for Al_2O_3/H_2O, CuO/H_2O/ARB and C/H_2O/CTAB nanofluids respectively. This is because the exponent power (= 0.33) on friction factor ratio in η (Chapter 5, Eq. 5.18). The discounted friction factor ratio in η implies that more heat is transferred with less friction factor which in the end gives higher performance factor of the fluid tested. This does not give the true performance of these nanofluids because friction factor is directly associated with heat transfer and also related to the pumping costs which in the end determines the energy consumption costs for the system. Therefore, thermal performances from φ are considered to be more meaningful compared to η because heat transfer and pumping for φ are weighted equally. φ gives more accurate evaluations from directly measured heat transfer and friction ratios.

To this end, the final question is, should these nanofluids be used in real heat transfer systems? To answer this question, one has to look at the cost of creating nanofluids in Table 6.1 and all the practical challenges (section 6.5) involved during the testing of nanofluids, then you can say there is a merit in using any combination of the tested nanofluids. For example, φ values above 100 % would mean there is a benefit for using nanofluids. Unfortunately, all φ values (see Fig. 6.18) were below 100 %. However, C/H_2O/CTAB nanofluid thermal performance reached 99 % at the maximum Re ~100000. The advantage that C has over CuO and Al_2O_3 is that it is less dense. So, for a given mass

fraction it has a significantly higher volume fraction of 13.29 % compared to 1.74 % and 1.09 % for Al_2O_3/H_2O and CuO/H_2O/ARB respectively. Therefore, it is believed that may be higher concentrations of C/H_2O/CTAB could result in φ values significantly above 100 %, however, due to time and resource constraints equal amounts of surfactants and nanoparticles were used.

6.7 Conclusion

In this chapter, directly measured U_i and friction factor from measured pressure drop were used to evaluate thermal performance of Al_2O_3/H_2O, CuO/H_2O/ARB and C/H_2O/CTAB nanofluids in the test rig described in Chapter 5. The major conclusions from this study are:

- C/H_2O/CTAB nanofluid had the best performance of the three nanofluids considered, and it is believed that may be higher concentrations of C/H_2O/CTAB could result in φ values significantly above 100 %, however, due to time and resource constraints equal amounts of surfactants and nanoparticles were used.
- Many studies rely on Webb and Kim's method to evaluate the performance of nanofluid. However, in this chapter it has been shown that the φ factor gives a more accurate indication of the benefit of the nanofluid than Webb and Kim's η factor.
- Practical challenges encountered show that the application of nanofluids in real devices is still challenging because of the difficulties in reusing, replacing and instability of nanofluids. Replacing and reusing nanofluids was not only time consuming, it was also costly and laborious.

The improvement in the heat transfer of nanofluids offset the associated pumping costs compared to pure water. However, many practical challenges were faced in testing nanofluid. Therefore, is it worth using nanofluids? The answer is nanofluids should not be used at the concentrations in this study, but could be beneficial for systems that do not require pumping such as space heaters. Also, there is the possibility that by using both nanofluids and inserts in double heat exchanger, the heat transfer could be further enhanced. Therefore, the following Chapter (7) shall experimentally investigate and evaluate heat transfer performance of nanofluids combined with hiTRAN® inserts.

Chapter 7
Experimental heat transfer evaluation of nanofluids combined with hiTRANÈ inserts.

7.1 Introduction

In the previous chapter, the thermal performances of Al_2O_3/H_2O, C/H_2O/CTAB and CuO/H_2O/ARB were evaluated and C/H_2O/CTAB nanofluid showed the best performance of the three. In this chapter, hiTRAN® inserts provided by the manufacturer (Calgavin Ltd (Calgavin Limited 2019)) were installed in the test rig and trials were performed with both plain water and the three nanofluids. Similar to nanofluids, inserts are passive heat transfer enhancement techniques (see Table 2.1) that have been shown to be cost effective, particularly in single phase heat exchangers (Omidi, Farhadi, and Jafari 2017; Webb and Kim 2006). Inserts disrupt the laminar boundary layer and create additional fluid shear and swirl flow mixing hence promoting heat transfer (Webb and Kim 2006; Sheikholeslami, Gorji-Bandpy, and Ganji 2015; Keklikcioglu and Ozceyhan 2018). It is thought therefore that a combination of nanofluids and inserts may give better thermal performances than nanofluids alone (Chapter 6).

There have been a few attempts to combine nanofluids with inserts of various geometric designs (Table 2.5 summarised these studies). From those studies, it was noticed that the most commonly used inserts are twisted tapes and wire coils. Although twisted tapes and wire coil inserts enable the fluid to spiral along the tube length and enhance mixing in the downstream boundary layer, the disadvantage of using these types of inserts is they do not have good thermal contact with the tube wall (Thome 2004; Tabatabaeikia et al. 2014). During fluid flow processes, the swirl flow may decay due to the periodic wire coil space or between nodes of twisted tapes hence diminishing their potential performance (Smith Eiamsa-ard, Thianpong, and Promvonge 2006). The hiTRAN® inserts used in this study have been designed with matrix geometrical elements to provide good thermal contact with the surface wall of the heat exchanger tube (Calgavin Limited 2019).

This Chapter presents overall heat transfer coefficients, pressure drop, friction factor and evaluates thermal performance (φ) from Al_2O_3/H_2O, C/H_2O/CTAB and CuO/H_2O/ARB

nanofluids combined with inserts for a range of tube-side flowrates. The results are be compared to the results for nanofluids without inserts from Chapter 6.

7.2 hiTRANÈ inserts

The hiTRAN® inserts are 1.0 m long stainless-steel wire matrix ‘turbulators’ that are manufactured by Calgavin Ltd (Fig. 7.1). According to the manufacturer (Calgavin Limited 2019), these inserts are designed to provide consistent performance along the tube length compared to plain bore tubes where heat transfer rates are reduced as tube length increases. The matrix geometrical elements help to prevent decaying swirl fluid flow along the tube length due to free space between nodes of the commonly used twisted tape inserts (Smith Eiamsa-ard, Thianpong, and Promvonge 2006) or general interruption of the continuous swirl fluid flow by periodic wire coil space.

Figure 7.1. hiTRANÈ inserts.

7.2.1 Installation of hiTRANÈ inserts in heat exchangers

The installation of inserts began with the disassembly of the closed test flow-loop (See Chapter 5, Fig. 5.8) by disconnecting the two heat exchangers (DPHEX 1and 2) from other parts that make up the test closed-loop. The heat exchangers were cleaned by hosing with water to ensure removal of any nanoparticles from previous experiments. Then, following the guidelines from the manufacturer, hiTRAN® inserts were installed in the

direction of fluid flow within the double pipe heat exchangers. This was done by hooking the extreme end of the insert with a long metal rod as demonstrated in Fig. 7.2. Thereafter, the hooked insert was pulled through the first heat exchanger using the rod until the insert was correctly installed in the heat exchanger as illustrated in Fig. 7.3. The hook was detached from the installed insert and the same installation procedure was repeated for the second heat exchanger.

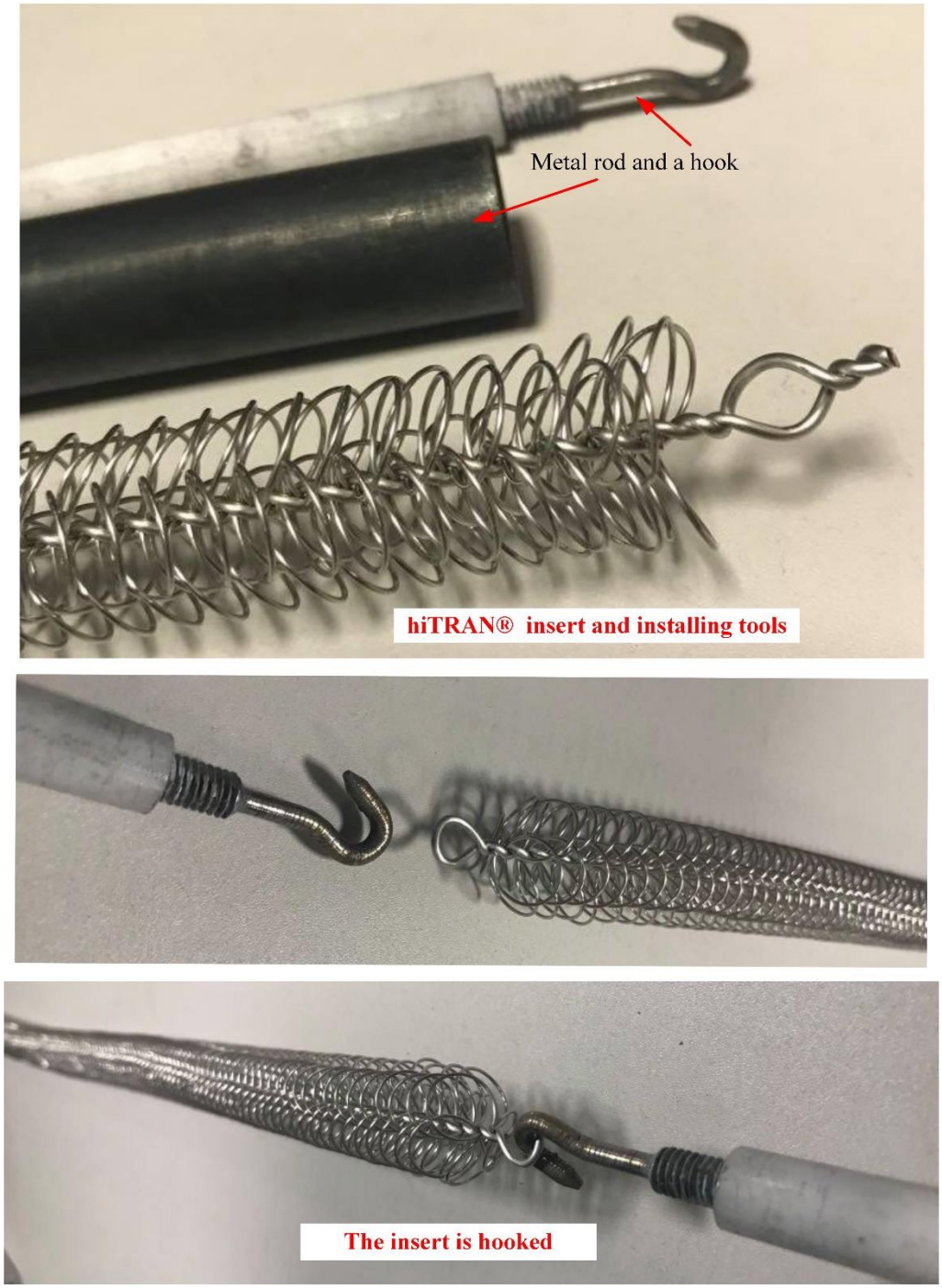

Figure 7.2. hiTRANÈ insert and the tools used during installation process

After the installation of two identical inserts in both heat exchangers, the rig was reassembled. The system was charged with water and was observed for 3 days to make sure that there was no leakage. Within these three days, the rig was operated during the day and rested overnight. Frequent observations and checks were made specifically around the connections or joints between devices that make-up the closed test-loop. Once it was clear there were no leaks, the rig was insulated again using rubber foam (R-value 0.7 m^2 K W^{-1} of 20 mm thickness). Similar procedures in Chapter 5 (Section 5.4) were adopted for the performance assessment trials except that the maximum flow-rates on the tube-side that was achievable from the pump was 42 litres per minute (l/m) rather than 71 litres per minute (l/m) for the experiments described in Chapter 6. But, the shell-side flow rate stayed the same as in Chapter 6 and was maintained at 55 litres per minute.

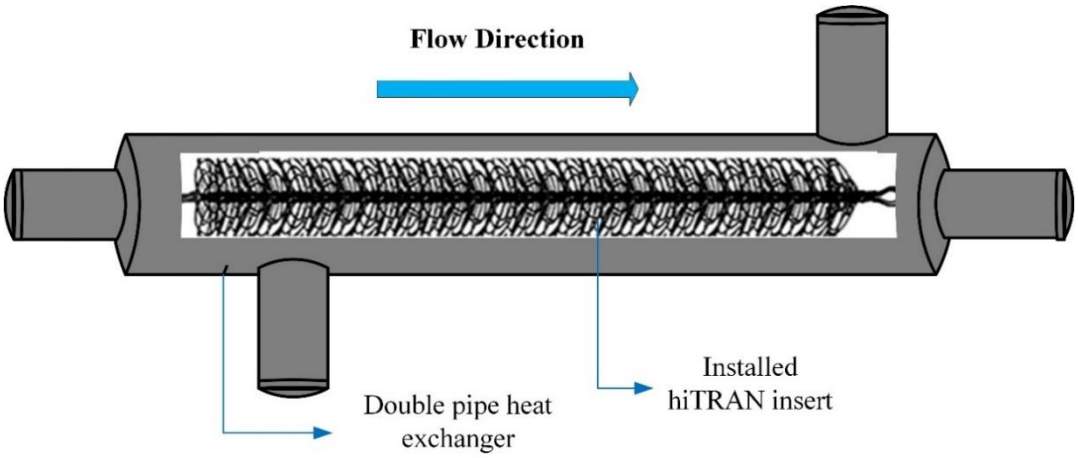

Figure 7.3 Installed insert in a heat exchanger.

7.3 Water combined with inserts

7.3.1 Heat transfer

Figure 7.4 shows U_i of deionised water combined with inserts versus tube-side Reynolds number along with the results for deionised water tested as part of the experimentation described in Chapter 6. The results in Fig. 7.4 indicate that for the range of Reynolds number covered by the trials with inserts (Re ~ 2900 to Re ~ 61777), significantly more heat up to a maximum of 3.1 kW/m^2.°C was transferred compared to 2.8 kW/m^2.°C for water without inserts, confirming that inserts enhance heat transfer as claimed.

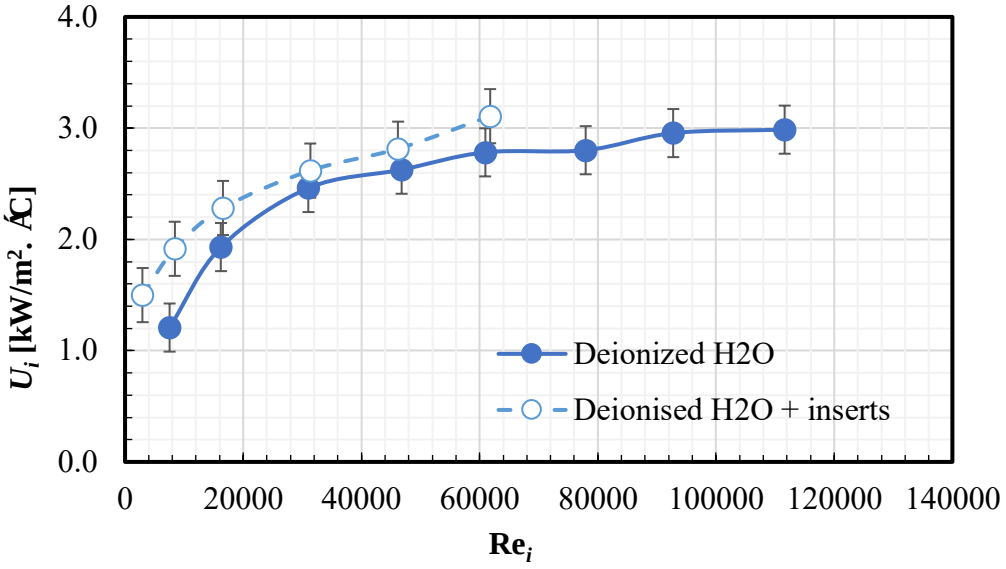

Figure 7.4. A comparison of U_i before and after the installation of inserts

7.3.2 Pressure drop

The major disadvantage of using inserts is the increased pumping cost as a result of higher pressure drop caused by the inserts. Most studies that investigate the efficiency of inserts use water as a base case to calculate the friction factor from measured pressure drop. Figure 7.5 presents pressure drop for water combined with inserts and pressure drop from Chapter 6 for water without inserts against Reynolds number. The results show that at the maximum Reynolds number achieved (61777), the pressure drop with inserts was about 40 times larger than for water alone.

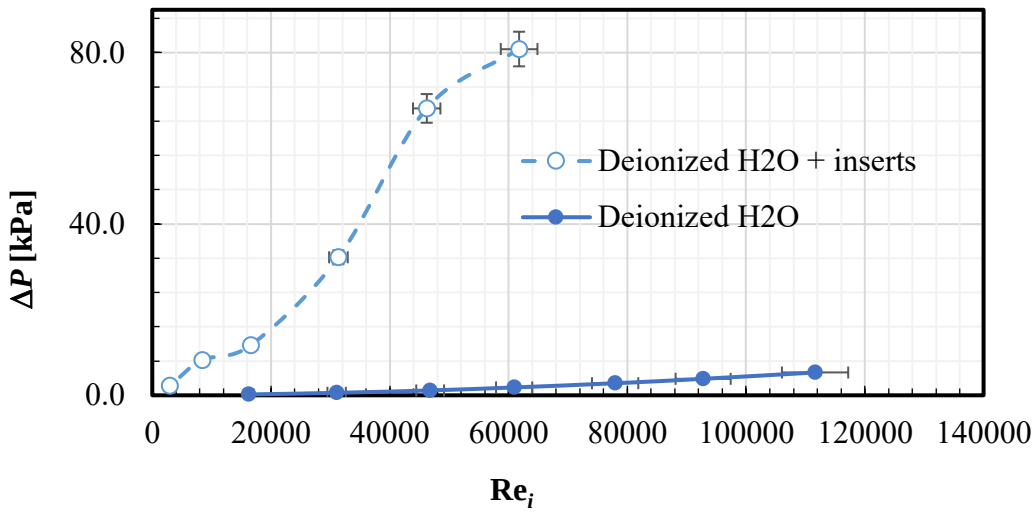

Figure 7.5. Measured pressure drop for water combined with and without inserts

Figure 7.6 presents friction factor for water combined with inserts and friction factor from Chapter 6 for water without inserts against Reynolds number. As expected, friction factor was high during low Reynolds number before it greatly reduced and become relatively independent in the range from Re ~ 16000 and beyond.

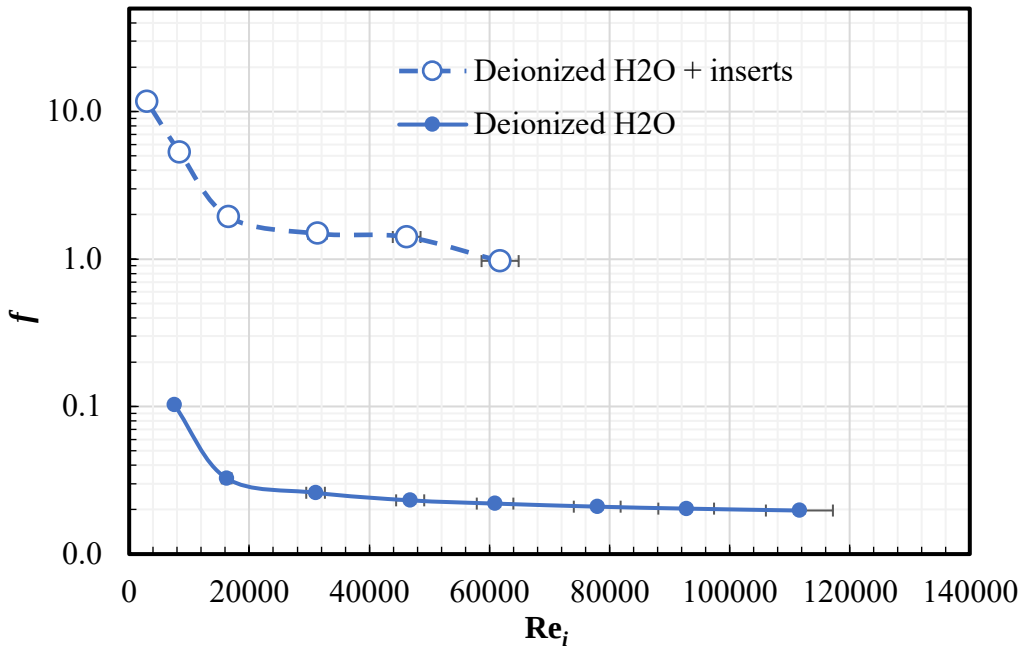

Figure 7.6. A comparison of friction factor for water before and after installation of inserts

7.4 Nanofluids

Al_2O_3/H_2O, C/H_2O/CTAB and CuO/H_2O/ARB nanofluids were prepared following similar procedures as described in Chapter 3 with amounts of nanoparticles and surfactants equal to those in Chapter 6. These were charged in the closed flow loop that contained the inserts and tested.

7.4.1 Al_2O_3/H_2O nanofluid and inserts

Figure 7.7 shows overall heat transfer coefficients of Al_2O_3/H_2O nanofluid with inserts along with the results of deionised water with inserts versus tube-side Reynolds numbers. For a volume concentration of 1.74 % nanoparticles, the average heat transfer coefficients of the Al_2O_3/H_2O nanofluids were found to be higher than that of water with inserts at any Reynolds number.

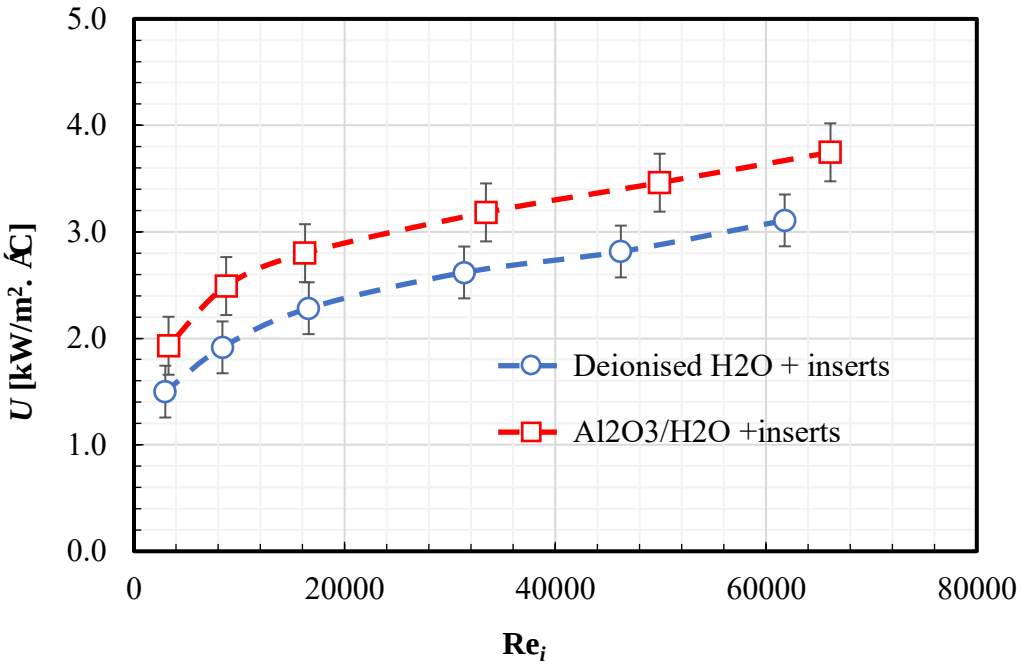

Figure 7.7. Heat transfer of Al_2O_3/H_2O nanofluids with inserts compared to water with inserts

Figure 7.8 shows pressure drop and friction factor against Reynolds number for Al_2O_3/H_2O nanofluid with inserts, and water with inserts. The results show that the pressure drop and friction factor for Al_2O_3/H_2O nanofluid with inserts was much higher than that of water with inserts at every Reynolds number for which measurements were performed.

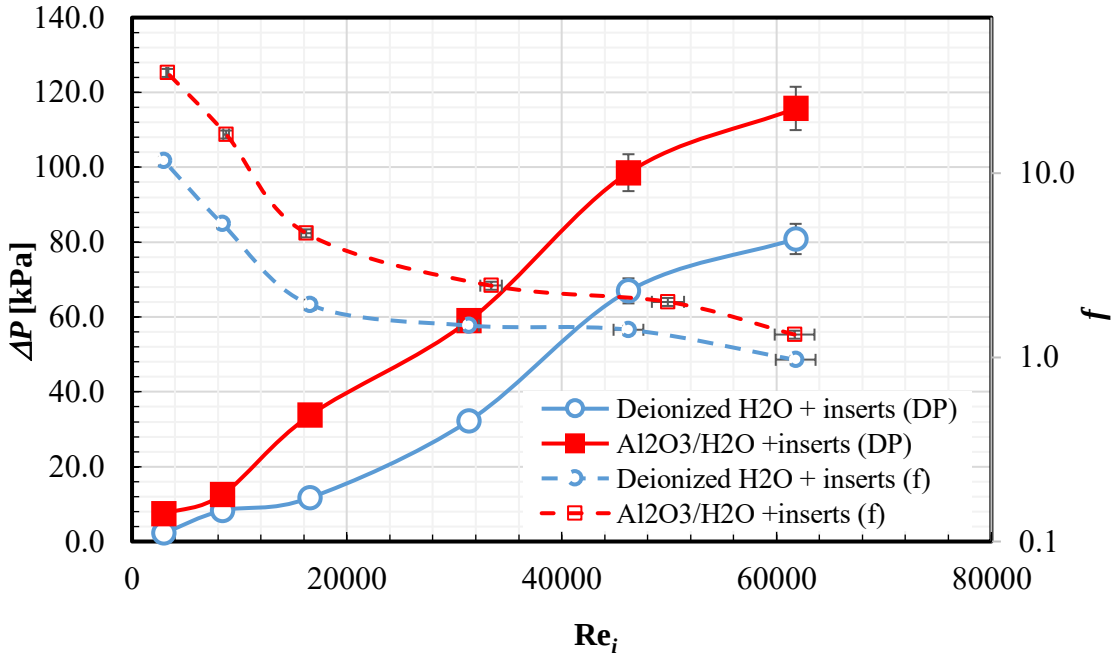

Figure 7.8. Pressure drop and friction factor of Al_2O_3/H_2O with inserts compared to deionised water with inserts.

7.4.2 CuO/H_2O/ARB nanofluids and inserts

Figure 7.9 shows overall heat transfer coefficients versus Reynolds number for CuO/H_2O/ARB nanofluid and water. For a volume concentration of 1 % nanoparticles, it was observed that CuO/H_2O/ARB nanofluid with inserts gives better heat transfer coefficients than the pure water with inserts for all the Reynolds numbers.

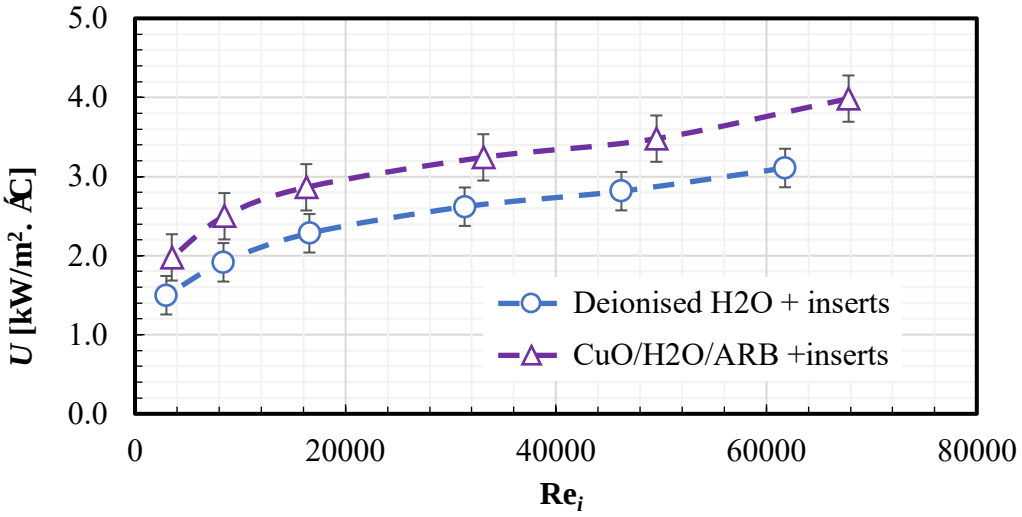

Figure 7.9. Heat transfer of CuO/H_2O/ARB nanofluids with inserts compared to water with inserts

Figure 7.10 presents pressure drop and friction factor against Reynolds number for CuO/H_2O/ARB nanofluid with inserts and water with inserts. The results show that the pressure drop and friction factor for CuO/H_2O/ARB nanofluid with inserts was higher than that of water with inserts at every Reynolds number.

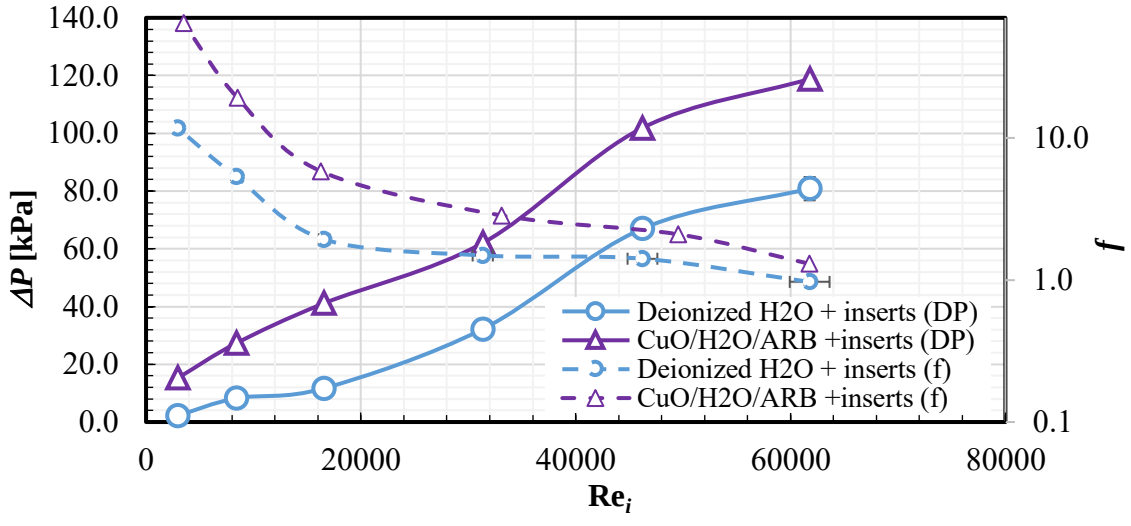

Figure 7.10. Pressure drop and friction factor of CuO/H_2O/ARB with inserts compared to water with inserts.

7.4.3 C/H_2O/CTAB nanofluids and inserts

Figure 7.11 shows heat transfer coefficients increase against Reynolds number for C/H_2O/CTAB nanofluid with inserts and water with inserts. For a volume concentration of 13 % nanoparticles, the heat transfer of C/H_2O/CTAB nanofluid with inserts was higher at every Reynolds number compared to that of water with inserts.

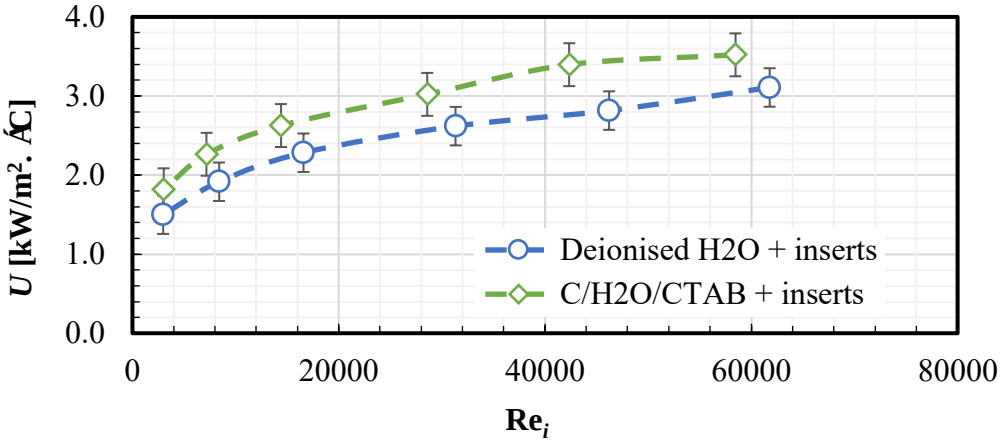

Figure 7.11. Heat transfer of C/H_2O/CTAB nanofluids with inserts compared to water with inserts.

Figure 7.12 presents pressure drop and friction factor against Reynolds number for C/H_2O/TAB nanofluid with inserts and water with inserts. The results show that the pressure drop and friction factor for C/H_2O/TAB nanofluid with inserts was higher than that of water with inserts at every Reynolds number.

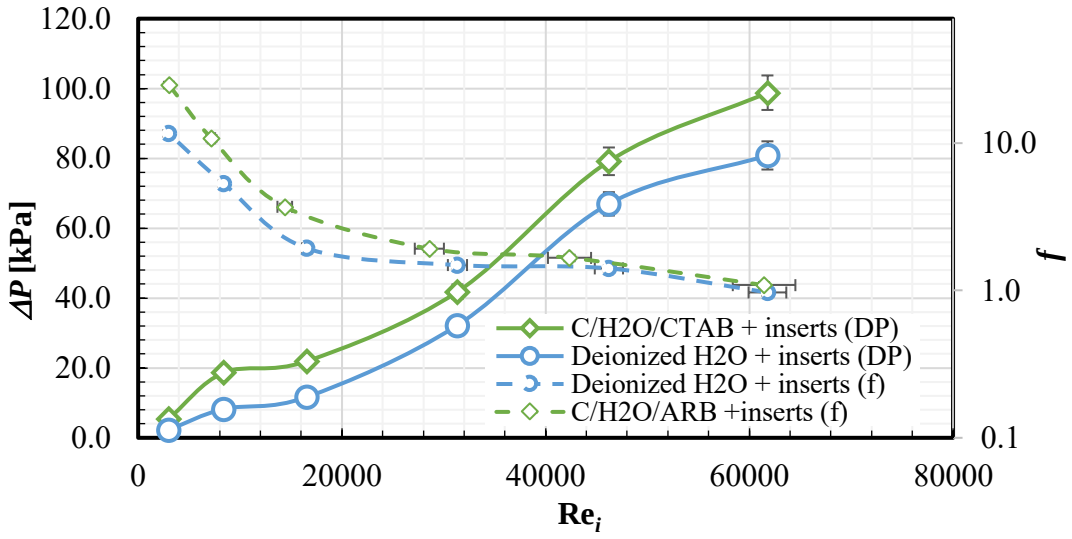

Figure 7.12. Pressure drop and friction factor of C/H_2O/CTAB with inserts compared to water with inserts.

7.5 Comparison of heat transfer, pressure drop and friction factor of nanofluids with inserts to water with inserts

7.5.1 Heat transfer of nanofluids with inserts compared to water with inserts

In Fig. 7.13, a comparison between the results of water, Al_2O_3/H_2O, $C/H_2O/CTAB$ and $CuO/H_2O/ARB$ nanofluids combined with inserts is presented. Compared to pure water combined with inserts, Table 7.1 shows that at Re = 61777, there was no significant differences in the overall heat transfer yielded among nanofluids.

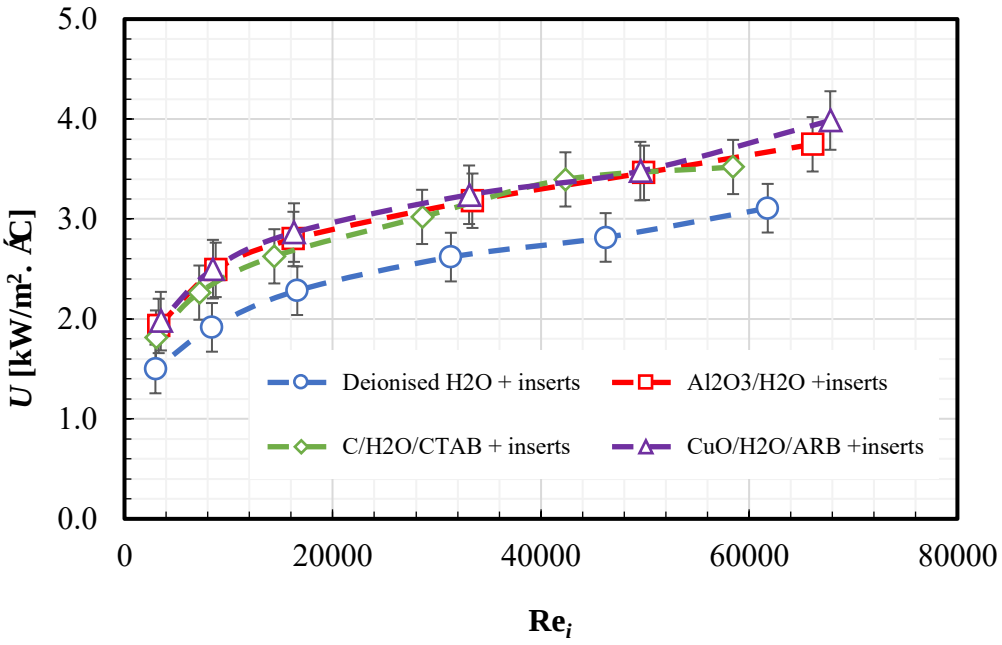

Figure 7.13. Heat transfer results of nanofluids with inserts.

Table 7.1 Heat transfer improvement of nanofluids combined with inserts compared to water with inserts at Re = 61777

Fluid	U_i (kW/m^2.K)	Enhancement (%)
Water +inserts	2.9	-
Al_2O_3/H_2O + inserts	4.0	38.3
$CuO/H_2O/ARB$ + inserts	4.0	38.8
$C/H_2O/CTAB$ + inserts	3.9	33.1

7.5.2 Friction factor and pressure drop of nanofluids with inserts and water with inserts

Figure 7.14 presents friction factor of nanofluids against Reynolds number. The results show that CuO/H_2O/ARB nanofluids with inserts yielded the highest friction factor.

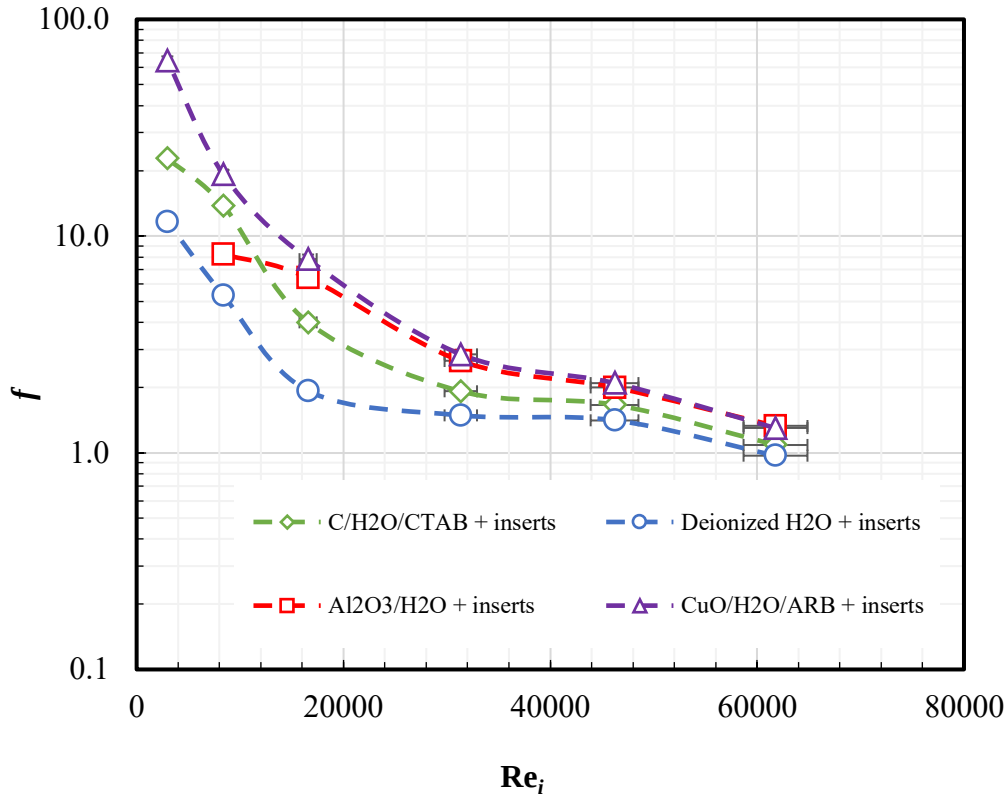

Figure 7.14 Friction factor against Reynolds number for nanofluids combined with inserts.

Figure 7.15 shows the effect of pressure drop on Al_2O_3/H_2O with inserts, CuO/H_2O/ARB with inserts and C/H_2O/CTAB nanofluid with inserts. In comparison to pure water with inserts, there was a maximum increase in pressure drop of 47.0 %, 43.1 % and 22.2 % for CuO/H_2O/ARB with inserts, Al_2O_3/H_2O with inserts and C/H_2O/CTAB with inserts respectively.

A similar explanation to that discussed in Chapter 6 (see Fig. 6.16) about pressure drop applies here. The addition of inserts to the nanofluids significantly increased pressure drop but, the order from the highest to the lowest nanofluid pressured drop remained the same, with C/H_2O/CTAB nanofluid with inserts having the lowest increase in pressure drop compared to the trials without inserts.

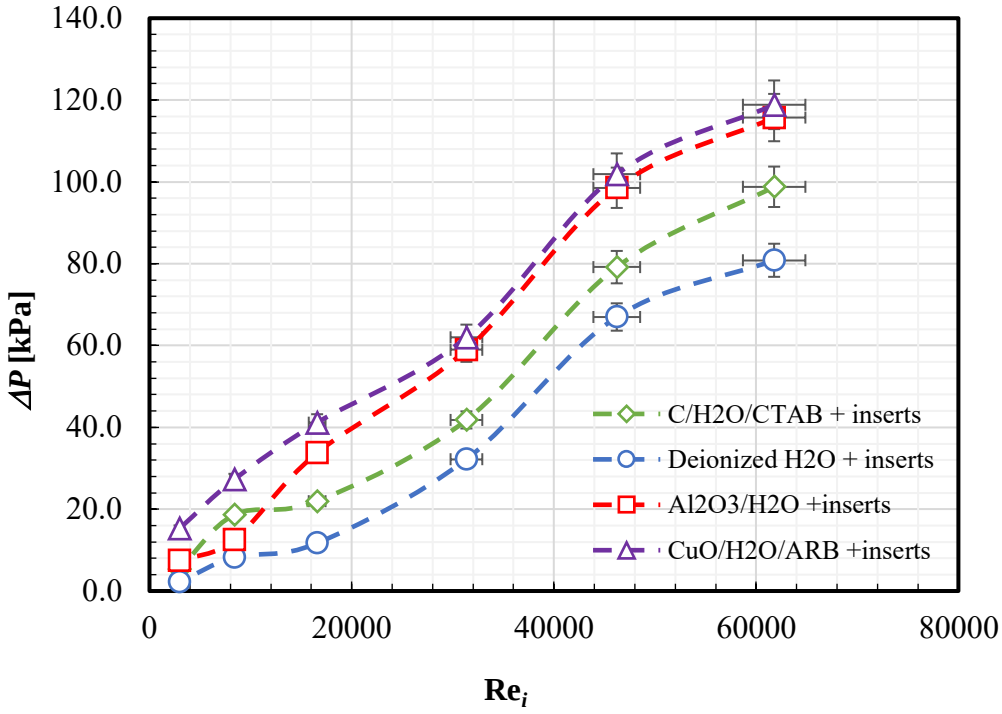

Figure 7.15 Pressure drop versus Reynolds number for nanofluids combined with inserts.

7.6 Comparison of heat transfer, pressure drop and friction factor of nanofluids combined with inserts, and without inserts

7.6.1 Heat transfer of nanofluids with and without inserts

Figure 7.16 presents the overall heat transfer coefficient results of nanofluids combined with inserts and those from Chapter 6 (Fig. 6.14) without inserts against tube-side Reynolds number. The results show that nanofluids tested with inserts yielded more heat transfer compared to those with no inserts. The results in Table 7.1 demonstrate that at the same Reynolds number (Re = 61777), heat transfer for nanofluids with no inserts improved on average by 32.9 % for Al_2O_3/H_2O, followed by 27.8 % for $C/H_2O/CTAB$ and 13.9 % for $CuO/H_2O/ARB$ nanofluids compared to water alone. Whereas for nanofluids with inserts, heat transfer improved by 76.3 % for $CuO/H_2O/ARB$, followed by 75.6 % for Al_2O_3/H_2O and finally 69 % for $C/H_2O/CTAB$ nanofluid compared to water alone.

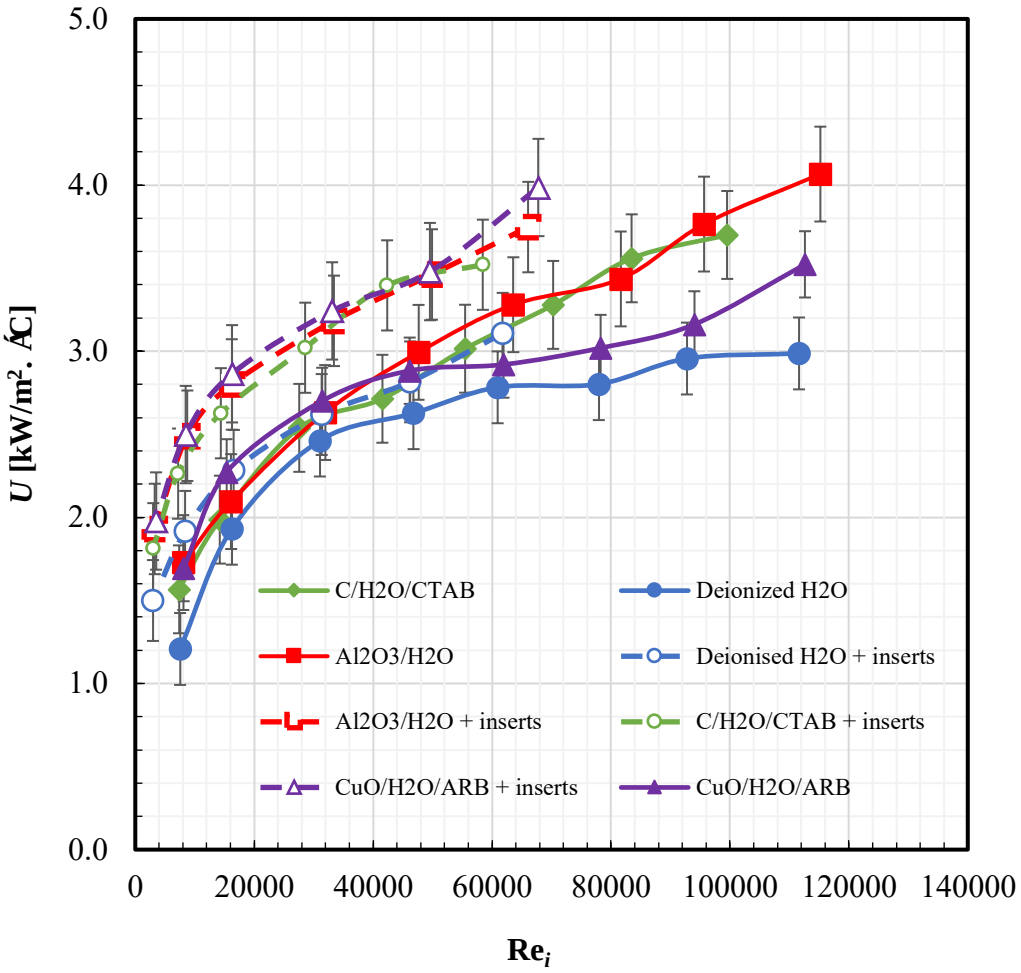

Figure 7.16. Combined heat transfer results for nanofluids with and without inserts.

Table 7.2. Heat transfer improvement of nanofluids compared to water at Re = 61777

Fluid	U_i (kW/m^2.K)	Enhancement (%)
water	2.29	-
water + inserts	2.91	27.0
Al_2O_3/H_2O	3.05	32.9
$CuO/H_2O/ARB$	2.61	13.9
$C/H_2O/CTAB$	2.93	27.8
Al_2O_3/H_2O + inserts	4.03	75.6
$CuO/H_2O/ARB$ + inserts	4.04	76.3
$C/H_2O/CTAB$ + inserts	3.88	69.0

7.6.2 Pressure drop and friction factor of nanofluids with and without inserts

Figure 7.17 shows friction factor results of nanofluids combined with inserts and those without inserts against Reynolds number. The results show that the friction factor for nanofluids tested with inserts was high compared to those with no inserts.

In both cases for nanofluids combined with and without inserts, friction factor was highest during lower ranges of Reynolds number.

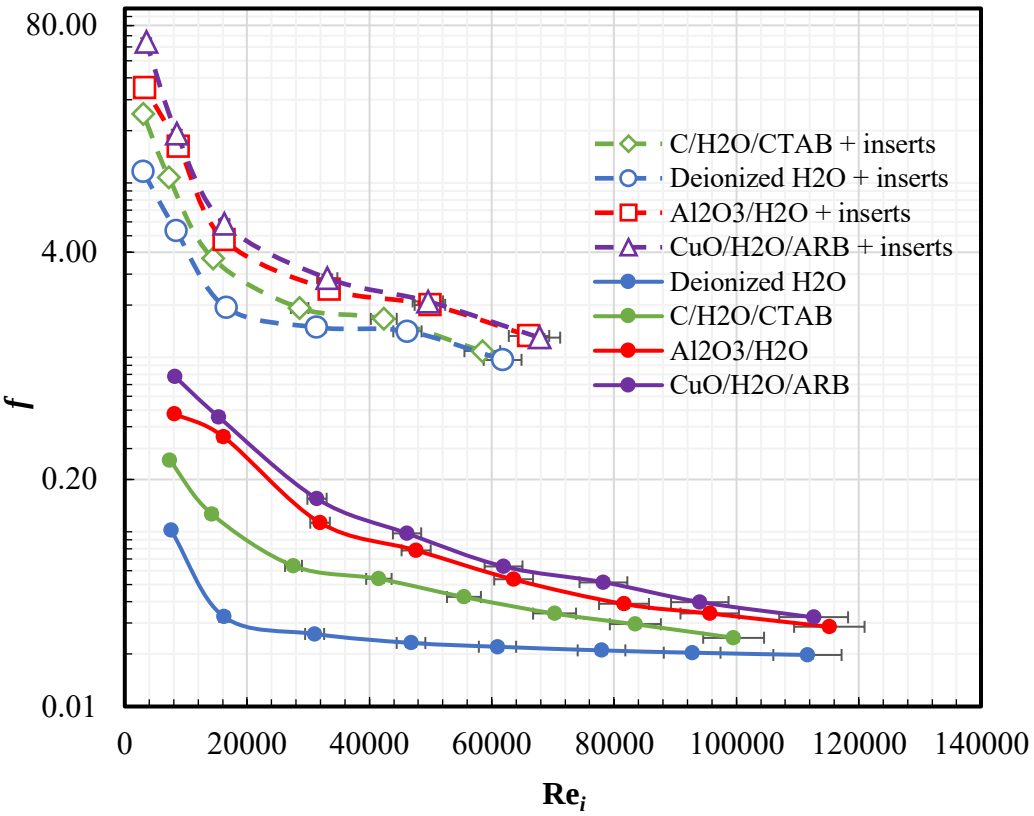

Figure 7.17 Friction factor for nanofluids combined with and without inserts

Figure 7.18 presents pressure drop results of nanofluids combined with inserts and those without inserts against Reynolds number. The results show that nanofluids tested with inserts produced markedly higher pressure drop than those with no inserts.

Table 7.3 shows that at Re = 61777, large pressure drop differences of 78.5 kPa, 119.2 kPa, 116.2 kPa and 96.1 kPa for water with inserts, followed by Al_2O_3/H_2O with inserts, CuO/H_2O/ARB with inserts and C/H_2O/CTAB nanofluids with inserts respectively compared to those results for water and nanofluids with no inserts. Also, it can be noticed from Figs. 7.17 and 7.18 that the order from highest to the lowest remained the same regardless whether inserts are installed or not.

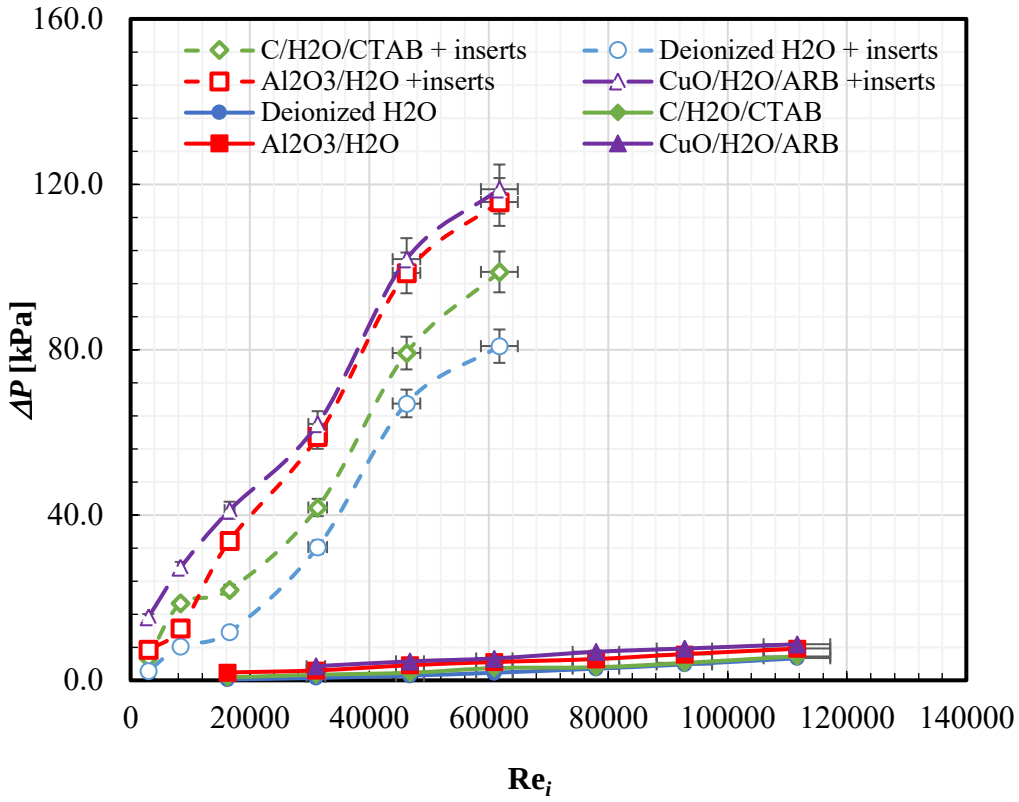

Figure 7.18. Pressure drop for nanofluids combined with and without inserts

Table 7.3. Pressure drop and ratio for similar fluid with and without inserts at Re = 61777

Fluid	ΔP (kPa)	Ratio -
water	1.98	
water + inserts	80.56	40.78
Al_2O_3/H_2O	4.43	
Al_2O_3/H_2O + inserts	123.64	27.92
$CuO/H_2O/ARB$	5.73	
$CuO/H_2O/ARB$ + inserts	121.99	21.31
$C/H_2O/CTAB$	2.42	
$C/H_2O/CTAB$ + inserts	98.53	40.69

These results show that the heat transfer enhancement effects of nanofluids and inserts are comparable in magnitude, and that in combination the heat transfer effects are additive. However, the pressure drop associated with nanofluids is significantly less than that of the inserts.

7.7 Thermal performance of Al_2O_3/H_2O, $C/H_2O/CTAB$ and $CuO/H_2O/ARB$ nanofluids combined with inserts

It was previously concluded in Chapter 6 that using φ formula (Eq. 5.22) to evaluate the thermal performance of nanofluids gives a better indication of whether to use nanofluids because heat transfer and pumping are weighted equally. Therefore, the results in Fig. 7.19 shows the thermal performance factor evaluated using φ formula (Eq. 5.22) against Reynolds number. $C/H_2O/CTAB$ nanofluid with inserts appears to have the best with thermal performance of up to 102 % at Re = 58455.9 compared to Al_2O_3/H_2O with inserts and $CuO/H_2O/ARB$ nanofluid with inserts which are below 100 %.

In the range of Re = 3283.8 to Re = 49547.7 Al_2O_3/H_2O nanofluid with inserts the thermal performance varied from 43 % up to 83 %; and beyond that point, it was overtaken by $CuO/H_2O/ARB$ nanofluids with inserts and reached a maximum of 96 %.

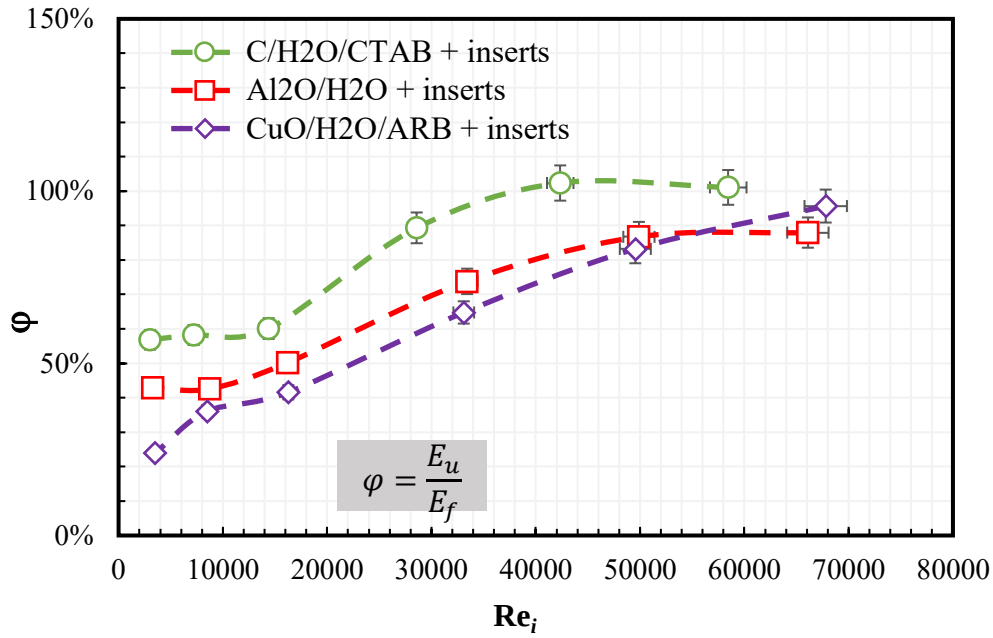

Figure 7.19 Thermal performance of nanofluids combined with inserts.

Fig. 7.20 presents thermal performances of nanofluids combined with and without inserts versus Reynolds number. The results show that the thermal performances for all nanofluids combinations with or without inserts were below 100 % except for $C/H_2O/CTAB$ combined with inserts that was 102 %.

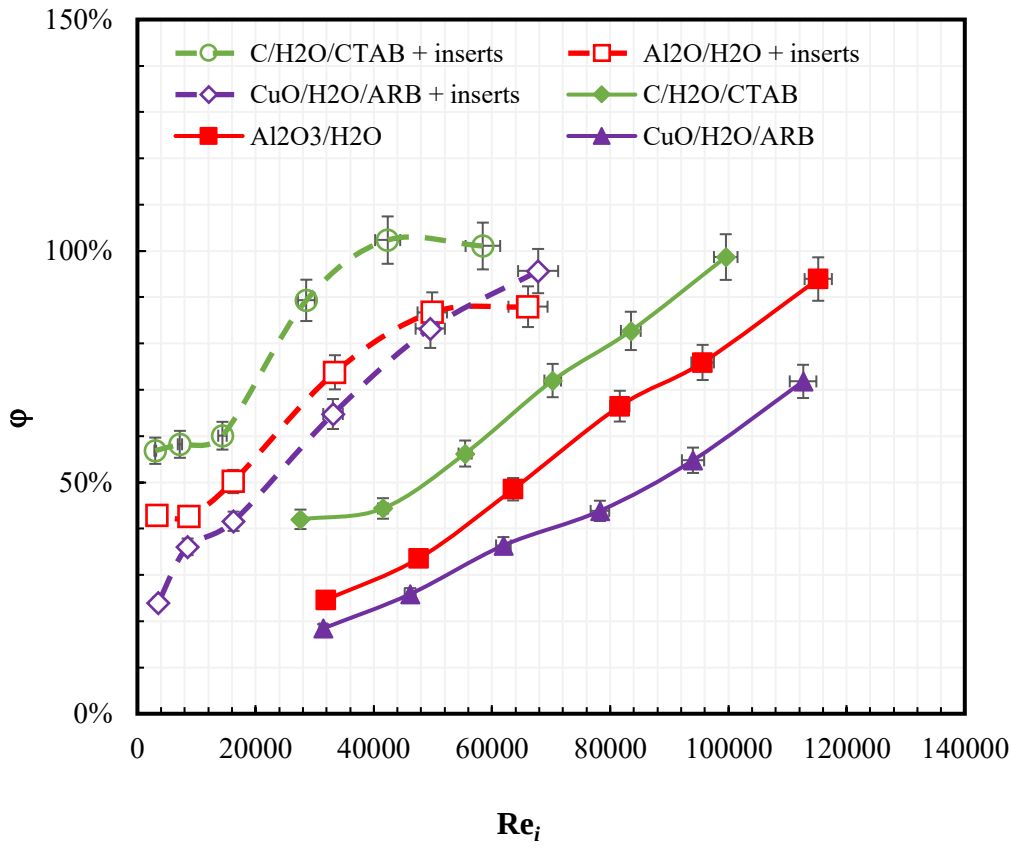

Figure 7.20 A comparison between thermal performance of nanofluids combined with and without inserts.

7.8 Comparison of heat transfer, pressure drop and thermal performance at full pumping speed.

Figure 7.21 shows the maximum overall heat transfer coefficients yielded for each nanofluid with and without inserts at full pumping speed. Interestingly, the maximum overall heat transfer coefficient is about the same both with and without inserts and that is because the inserts increase the heat transfer rates at slower pumping speeds, but the same velocities cannot be reached as for the cases without inserts.

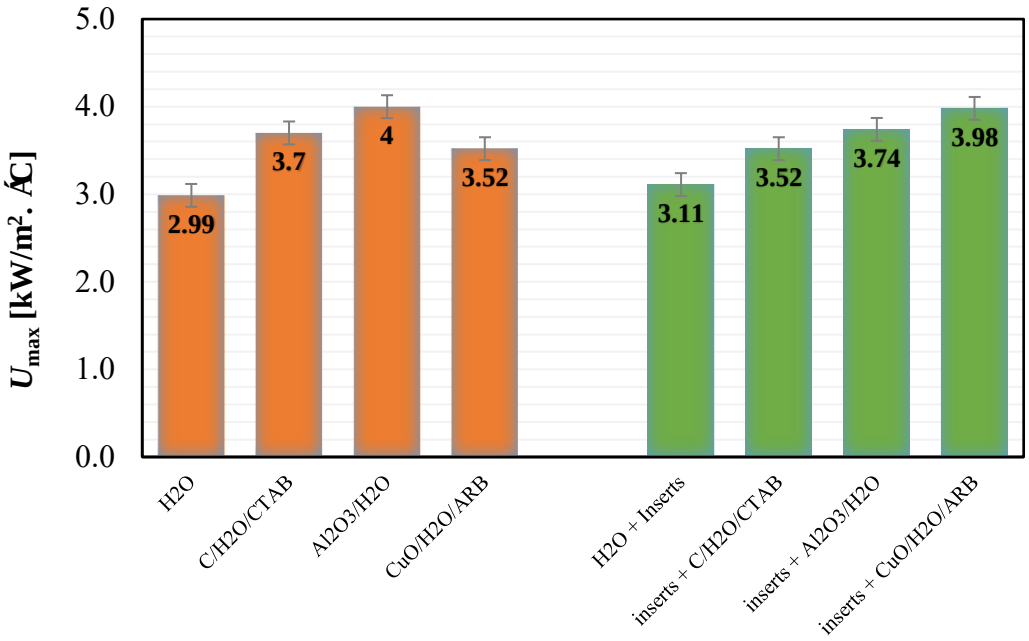

Figure 7.21 Maximum *U* at full pumping speed for nanofluids combined with and without inserts

Figure 7.22 shows the maximum pressure drop for each nanofluid with and without inserts at full pumping speed. These results show that the pressure drop is markedly higher when inserts are added to nanofluids at full pumping speed compared to nanofluids alone.

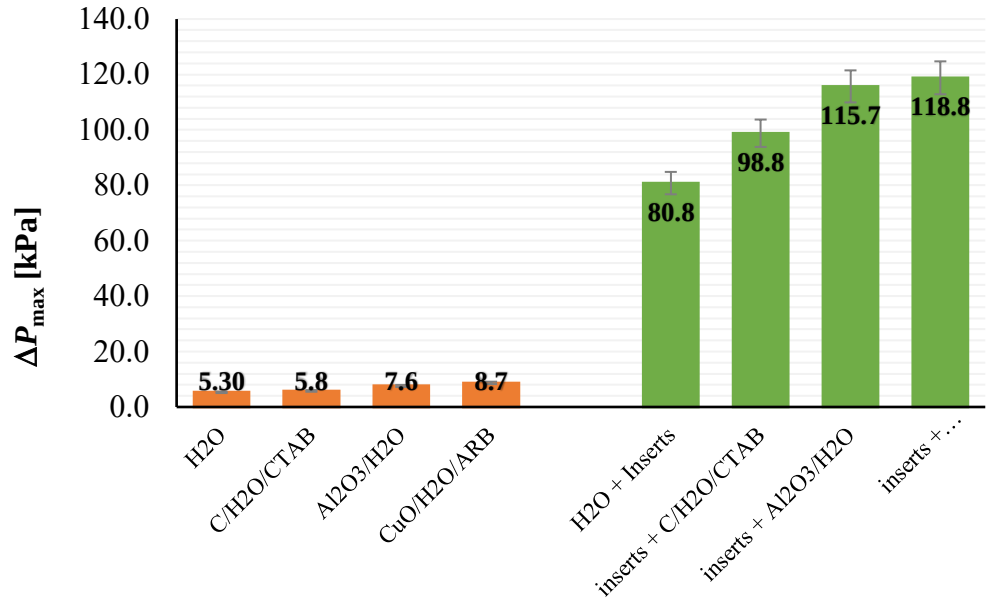

Figure 7.22 Maximum pressure drop at full pumping speed for nanofluids combined with and without inserts

Figure 7.23 shows the maximum thermal performance for each nanofluid with and without inserts at full pumping speed. The results demonstrate that thermal performance is about the same for C/H_2O/CTAB and Al_2O_3/H_2O nanofluids with and without insert at full pumping speed, whereas for CuO/H_2O/ARB nanofluid, there is a 33 % increase in the thermal performance with inserts compared to CuO/H_2O/ARB nanofluid alone at full pumping speed.

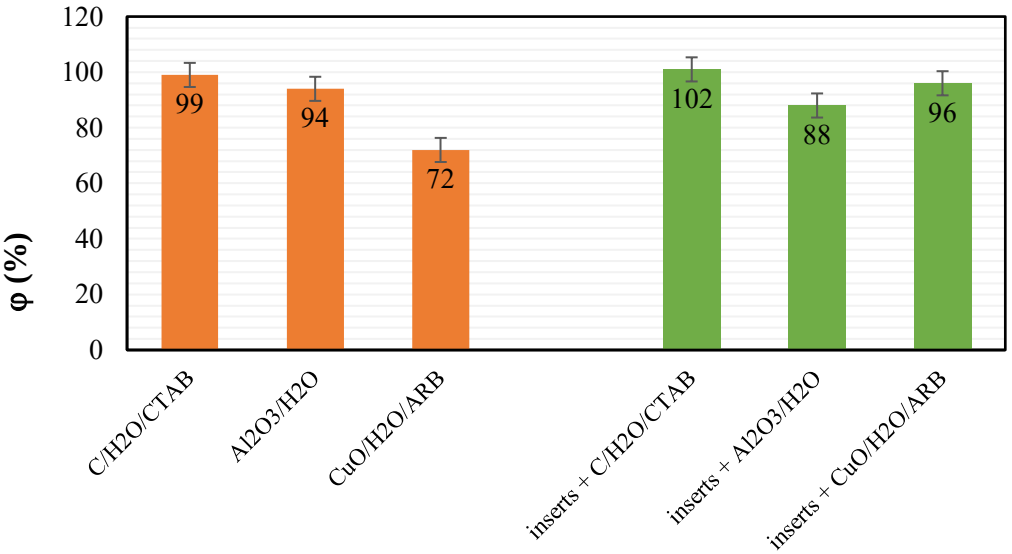

Figure 7.23 Maximum thermal performances achieved at full pumping speed for nanofluids combined with and without inserts

Having demonstrated and compared overall heat transfer, pressure drop, friction factor and thermal performance of nanofluids combinations with and without inserts, should inserts be used in addition to nanofluids? These results show that if you have a limit on pumping speed, you don't need to use inserts because overall heat transfer coefficient without inserts is about the same overall heat transfer coefficient with inserts at maximum pumping speed. In addition, it is possible to increase the concentration of nanofluids in order to increase the thermal conductivity, and while, this will most likely increase the pressure drop marginally it will probably increase overall heat transfer coefficients to a greater extent. However, unlike the nanofluids that presented practical challenges during operation in double pipe heat exchangers, inserts don't have stability/sedimentation issues.

The fact that pressure drop is a trade-off to heat transfer means that the optimum heat transfer enhancement solution will depend on the relative cost of heating versus pumping.

7.9 Conclusion

This chapter has presented directly measured heat transfer coefficient, friction factor and pressure drop data, which were used to evaluate thermal performance of Al_2O_3/H_2O, CuO/H_2O/ARB and C/H_2O/CTAB nanofluids combined with hiTRAN® inserts in the test rig. The major conclusions from this study are:

- C/H_2O/CTAB nanofluid with inserts had the best thermal performance of the three nanofluids considered.
- Nanofluids combined with inserts significantly improve heat transfer. However, they yield high pressure drop.
- At maximum pumping speed, nanofluids with inserts yield about the same amount of heat transfer coefficients compared to nanofluids alone.

Chapter 8
Conclusions and recommendations

8.1 Conclusions

In this thesis, the effect of surfactants on stability and physical properties of various combinations of nanofluids was investigated and consequently three combinations of nanoparticles and surfactants (C/H_2O/CTAB, Al_2O_3/H_2O and CuO/H_2O/ARB) were selected for thermal performance testing in a closed flow rig consisting of two identical double pipe heat exchangers.

In Chapter 2, the literature review showed that nanofluids have a wide range of potential applications for heat transfer enhancement, including single-phase cooling /heating. However, there was inadequate information about the effect of a surfactant on thermal conductivity, viscosity, density and specific heat capacity of nanofluids. There was inconsistent and contradictory thermal conductivity findings of similar nanofluid combinations; and there was no widely accepted explanation for the wide variability in thermal conductivity data. There was limited heat transfer or thermal performance information about nanofluids combined with inserts.

In Chapter 3, nanofluids were with various combinations from two base fluids (water, ethylene glycol), three types of nanoparticles (alumina, copper oxide and activated carbon) and four different surfactants (ARB, CTAB, SDBS, SDS) were prepared using the two-step method to assess how surfactants affected the stability of the nanofluid. The sedimentation approach was adopted to observe the stability of suspended nanoparticles in base fluids for 30 days. The results showed that over time the nanoparticles investigated in this thesis agglomerate and later sediment at the bottom of the vessel to form a thick solution regardless of any combination of either surfactant or base fluid. The most stable nanofluids where achieved with ARB as a surfactant kept, which kept the C/H_2O and CuO/EG nanofluids stable for 29 days. CTAB added to C/H_2O kept the solution stable for 17 days respectively.

In Chapter 4, physical property measurements of nanofluids with various surfactants were conducted. The viscosity results showed that the addition of CTAB

increased the viscosity of Al_2O_3/H_2O nanofluid. Whereas ARB and SDS increased the viscosity of C/H_2O and CuO/H_2O nanofluids respectively. With the use of surfactants, the viscosity of nanofluids after standing for seven weeks was slightly greater than it was originally. Water was found to be the most effective base fluid compared to Ethylene glycol because of its low viscosity when added to nanoparticles and surfactants.

Thermal conductivity of deionised water (H_2O) and combinations of nanofluids including C/H_2O, Al_2O_3/H_2O, CuO/H_2O, CuO/H_2O/ARB and C/H_2O/CTAB was initially measured using the transient hot-wire Hukseflux™ model TP08 probe. The thermal conductivity measurement of water alone was consistently repeatable (±10 %); however, there was significant variations in the measurements of nanofluids (greater than 60 % in some cases). Therefore, a second method for measuring thermal conductivity (TC-30™ device) was also used to measure and compare thermal conductivity of the same combinations of nanofluids. While there was on average less variability with the TC-30™ there were significant differences between the average measurements from the two devices. Therefore, it was decided to use overall heat transfer coefficients for comparison rather than Nusselt number because of the uncertainty in thermal conductivity.

From the stability analyses and physical properties measurement results, three combinations of nanofluid and surfactants were chosen, which included C/H_2O/CTAB, $Al_2O_3/H_2O$and CuO/H_2O/ARB. The pairing of ARB and CuO/H_2O presented good stability and relatively low viscosity. C/H_2O with CTAB as a surfactant had low viscosity and was relatively stable. For Al_2O_3/H_2O nanofluid, it was found that adding surfactants caused a significant increase in viscosity, so no surfactant was used. The thermal performance of these three nanofluids was assessed in a purpose-built test rig, described in Chapter 5.

In Chapter 6, the results showed that the overall heat transfer of the three selected nanofluids improved on average by 36.15 %, 23.88 % and 17.96 % for Al_2O_3/H_2O, C/H_2O/CTAB and CuO/H_2O/ARB nanofluids respectively compared to pure water. The associated pressure drop increased on average by 51.6%, 43.4% and 24.3% for CuO/H_2O/ARB, Al_2O_3/H_2O and C/H_2O/CTAB respectively. CuO/H_2O/ARB had the best performance of the three nanofluids considered, and it is believed that if higher concentrations of C/H_2O/CTAB were employed φ values significantly above 100 % could result. Due to resource constraints and the significant cost of nanoparticles and surfactants nanofluids with higher concentrations of nanoparticles were not investigated during this study.

While testing nanofluids in the test rig, practical challenges were encountered. These included; replacing one nanofluid by a new one, reusing the same nanofluid was impossible, failure of the pump at the beginning of each test run, at times pressure taps were blocked by aggregated nanoparticles. These challenges were mostly encountered while testing Al_2O_3/H_2O nanofluid which had no surfactant. Therefore, it is recommended that surfactants are used in nanofluids.

In chapter 7, Al_2O_3/H_2O, CuO/H_2O/ARB and C/H_2O/CTAB nanofluids were combined with hiTRAN® inserts and tested in the double pipe heat exchangers of the closed flow test rig. The heat transfer results revealed improvements of 38.7%, 38.1% and 32.9% for CuO/H_2O/ARB, Al_2O_3/H_2O and C/H_2O/CTAB respectively compared to water and inserts alone. A comparison between nanofluids combined with inserts and without installation of inserts (Chapter 6) over the same range of Reynolds number showed that heat transfer improved on average by 74.6% for Al_2O_3/H_2O, 75.3% for CuO/H_2O/ARB, and 68.0% for C/H_2O/CTAB respectively. The pressure drop for combinations of nanofluids with inserts compared to water and inserts alone increased on average by 43.1%, 22.2% and 47.0% for Al_2O_3/H_2O, C/H_2O/CTAB and CuO/H_2O/ARB nanofluids respectively.

The results for thermal performance while using φ method showed that C/H_2O/CTAB nanofluid with inserts had the best thermal performance of the three nanofluids considered. At maximum pumping speed, nanofluids with inserts yield almost the same amount of heat transfer coefficients compared to nanofluids alone.

While the addition of inserts to nanofluids will increase the rate of heat transfer, it may be counteracted by the increase of pressure drop depending on the amount of nanoparticles concentration of the nanofluid.

8.2 Contributions

The contributions of this thesis are summarised as:

- Out of the 20 combinations of nanofluids created and observed, ARB and CTAB as surfactants are identified to keep C/H_2O nanofluids stable (Chapter 3).

- Surfactants have a significant effect on viscosity and thermal conductivity measurements of nanofluids. (Chapter 4).

- New C/H_2O/CTAB combination of nanofluid has been identified (Chapter 4) and its data (Chapters 6 and 7)

- New data for nanofluids combined with hiTRAN® inserts has been created (Chapter 7).

8.3 Recommendations for future work

In Chapter 3 the results indicated that even with the addition of surfactants there is no permanent stability of nanofluids although surfactants definitely kept nanoparticles in suspension for more days than nanofluids without surfactants. Most challenges encountered during nanofluid testing in the rig were related to instability of nanoparticles which is related to aggregation of nanoparticles around mechanical parts that constitute the closed flow loop. It may be possible to improve stability of nanofluids while using the 'one-step method' technology of creating nanofluids compared to the two-step method that was used in this thesis. However, the 'one-step method' technology is expensive and cannot synthesize nanofluids in large quantities.

In Chapter 4 there were difficulties in measuring the thermal conductivity of nanofluids because of the variability of measured thermal conductivity from Hukseflux™ model TP08 probe and TC-30™ device. It may be possible to deploy an advanced device that uses laser flash technique to determine thermal conductivity because it is based on a vertical application of energy to the bottom side of the sample.

In Chapter 6 it was not possible to extract h_i from the measured U_i data because the problem was likely to be with obtaining a suitable correlation for h_o. I recommend double-pipe heat exchangers with larger length than presently used in this thesis; this would ensure fully developed flow throughout the heat exchanger, and hence the correlation for the annular flow would be used to extract h_i. While testing nanofluids with inserts, the pumping speed was limited to a maximum Reynolds number of approximately Re ~ 61777. It is recommended that using a pump with greater capacity would allow coverage of a wide range of Reynolds beyond Re ~ 61777 that is currently presented in this thesis for nanofluids with inserts.

References

Abdelmagied, Mahmoud. 2020. “Thermal Performance Characteristics of a Triple Spiral Tube Heat Exchanger.” *Chemical Engineering and Processing - Process Intensification* 149 (March): 107707. https://doi.org/10.1016/j.cep.2019.107707.

Abdul, Kaggwa, James K Carson, Martin Atkin, and Michael Walmsley. 2018. “Physical Properties and Rheological Characteristics of Activated Carbon Nanofluids with Varying Filler Fractions and Surfactants.” *Applied Mechanics and Materials* 884 (August): 58–65. https://doi.org/10.4028/www.scientific.net/AMM.884.58.

Afrand, Masoud, Davood Toghraie, and Behrooz Ruhani. 2016. “Effects of Temperature and Nanoparticles Concentration on Rheological Behavior of Fe3O4-Ag/EG Hybrid Nanofluid: An Experimental Study.” *Experimental Thermal and Fluid Science* 77: 38–44. https://doi.org/10.1016/j.expthermflusci.2016.04.007.

Akpinar, Ebru Kavak, and Yasar Bicer. 2005. “Investigation of Heat Transfer and Exergy Loss in a Concentric Double Pipe Exchanger Equipped with Swirl Generators.” *International Journal of Thermal Sciences* 44 (6): 598–607. https://doi.org/10.1016/j.ijthermalsci.2004.11.001.

Al-Waeli, Ali H.A., K. Sopian, Miqdam T. Chaichan, Hussein A. Kazem, Husam Abdulrasool Hasan, and Ali Najah Al-Shamani. 2017. “An Experimental Investigation of SiC Nanofluid as a Base-Fluid for a Photovoltaic Thermal PV/T System.” *Energy Conversion and Management* 142: 547–58. https://doi.org/10.1016/j.enconman.2017.03.076.

Alawi, Omer A., Nor Azwadi Che Sidik, and A.Sh. Kherbeet. 2015. “Nanorefrigerant Effects in Heat Transfer Performance and Energy Consumption Reduction: A Review.” *International Communications in Heat and Mass Transfer* 69: 76–83. https://doi.org/10.1016/j.icheatmasstransfer.2015.10.009.

Albadr, Jaafar, Satinder Tayal, and Mushtaq Alasadi. 2013. “Heat Transfer through Heat Exchanger Using Al2O3 Nanofluid at Different Concentrations.” *Case Studies in Thermal Engineering* 1 (1): 38–44. https://doi.org/10.1016/j.csite.2013.08.004.

Ali, Muazzam, Ahmad Adnan Shoukat, Hussain Ahmed Tariq, Muhammad Anwar, and Hassan Ali. 2019. “Header Design Optimization of Mini-Channel Heat Sinks Using CuO–H2O and Al2O3–H2O Nanofluids for Thermal Management.” *Arabian Journal for Science and Engineering* 44 (12): 10327–38. https://doi.org/10.1007/s13369-019-04022-2.

Alim, M. A., Z. Abdin, R. Saidur, A. Hepbasli, M. A. Khairul, and N. A. Rahim. 2013. "Analyses of Entropy Generation and Pressure Drop for a Conventional Flat Plate Solar Collector Using Different Types of Metal Oxide Nanofluids." *Energy and Buildings* 66: 289–96. https://doi.org/10.1016/j.enbuild.2013.07.027.

Archimedes, and Thomas Little Heath. 1897. *"On Floating Bodies I" The Works of Archimedes*. London: Cambridge, University Press.

Aref, Amir Hossein, Ali Akbar Entezami, Hamid Erfan-Niya, and Esmaeil Zaminpayma. 2017. "Thermophysical Properties of Paraffin-Based Electrically Insulating Nanofluids Containing Modified Graphene Oxide." *Journal of Materials Science* 52 (5): 2642–60. https://doi.org/10.1007/s10853-016-0556-6.

Arslan, Kamil. 2017. "Three-Dimensional Computational Fluid Dynamics Modeling of TiO2/R134a Nanorefrigerant." *Thermal Science* 21 (1 Part A): 175–86. https://doi.org/10.2298/TSCI140425002A.

Babita, S.K. Sharma, and Shipra Mital Gupta. 2016. "Preparation and Evaluation of Stable Nanofluids for Heat Transfer Application: A Review." *Experimental Thermal and Fluid Science* 79: 202–12. https://doi.org/10.1016/j.expthermflusci.2016.06.029.

Barbés, Benigno, Ricardo Páramo, Eduardo Blanco, María José Pastoriza-Gallego, Manuel M. Piñeiro, José Luis Legido, and Carlos Casanova. 2013. "Thermal Conductivity and Specific Heat Capacity Measurements of Al2O3 Nanofluids." *Journal of Thermal Analysis and Calorimetry* 111 (2): 1615–25. https://doi.org/10.1007/s10973-012-2534-9.

Batchelor, G. K. 1977. "The Effect of Brownian Motion on the Bulk Stress in a Suspension of Spherical Particles." *Journal of Fluid Mechanics* 83 (01): 97. https://doi.org/10.1017/S0022112077001062.

Bécaye Maïga, Sidi El, Samy Joseph Palm, Cong Tam Nguyen, Gilles Roy, and Nicolas Galanis. 2005. "Heat Transfer Enhancement by Using Nanofluids in Forced Convection Flows." *International Journal of Heat and Fluid Flow* 26 (4 SPEC. ISS.): 530–46. https://doi.org/10.1016/j.ijheatfluidflow.2005.02.004.

Bengtson, Harlan. n.d. "Double Pipe Heat Exchanger Design with Counterflow or Parallel Flow." Accessed October 25, 2019. https://www.brighthubengineering.com/hvac/64548-double-pipe-heat-exchanger-design/.

Bhardwaj, Vinay, and Ajeet Kaushik. 2017. "Biomedical Applications of Nanotechnology and Nanomaterials." *Micromachines* 8 (10): 298. https://doi.org/10.3390/mi8100298.

Bhattacharya, P., S. Nara, P. Vijayan, T. Tang, W. Lai, P. E. Phelan, R. S. Prasher, D. W. Song, and J. Wang. 2006. "Characterization of the Temperature Oscillation Technique to Measure the Thermal Conductivity of Fluids." *International Journal of Heat and Mass Transfer* 49 (17–18): 2950–56. https://doi.org/10.1016/j.ijheatmasstransfer.2006.02.023.

Bhatti, M.S, and R K Shah. 1987. "In Handbook of Single-Phase Convective Heat Transfer." In *Turbulent and Transition Flow Convective Heat Transfer in Ducts*, 900. New York- USA: John Wiley and Sons Inc.

Blasius H. 1913. "Das Aehnlichkeitsgesetz Bei Reibungsvorgängen in Flüssigkeiten." *Mitteilungen Über Forschungsarbeiten Auf Dem Gebiete Des Ingenieurwesens* 131: 1–41. https://doi.org/10.1007/978-3-662-02239-9.

BP. 2020a. "Global Energy Outlook." 2020. https://www.bp.com/en/global/corporate/energy-economics/energy-outlook/global-backdrop.html.

———. 2020b. "Statistical Review of World Energy | Energy Economics | Home." London. https://www.bp.com/en/global/corporate/energy-economics/statistical-review-of-world-energy.html.

Brinkman, H. C. 1952. "The Viscosity of Concentrated Suspensions and Solutions." *The Journal of Chemical Physics* 20 (4): 571–571. https://doi.org/10.1063/1.1700493.

Buongiorno, J. 2006. "Convective Transport in Nanofluids." *Journal of Heat Transfer* 128 (3): 240. https://doi.org/10.1115/1.2150834.

Burns, G W, and M G Scroger. 1989. "NIST Measurement Services: The Calibration of Thermocouples and Thermocouple Materials." *NIST Special Publication 250-35 Temperature and Pressure Division*, 208.

Calgavin Limited. 2019. "HITRAN THERMAL SYSTEMS." 2019. https://www.calgavin.com/products-and-software/hitran-thermal-systems.

Carson, James K., Simon J. Lovatt, David J. Tanner, and Andrew C. Cleland. 2005. "Thermal Conductivity Bounds for Isotropic, Porous Materials." *International Journal of Heat and Mass Transfer* 48 (11): 2150–58. https://doi.org/10.1016/J.IJHEATMASSTRANSFER.2004.12.032.

Celine. 2012. "Difference Between TEM and SEM." *DifferenceBetween.Net*. http://www.differencebetween.net/science/difference-between-tem-and-sem/.

Cengel, Yunus, and Michael Boles. 2006. *Thermodynamics: An Engineering Approach*. 6th ed. New York- USA: McGraw-Hill.

Cengel, Yunus, and John Cimbala. 2013. *Fluid Mechanics Fundamentals and*

Applications. 3rd editio. New York: McGraw-Hill Education.

Chandra Sekhara Reddy, M., and Veeredhi Vasudeva Rao. 2014. "Experimental Investigation of Heat Transfer Coefficient and Friction Factor of Ethylene Glycol Water Based TiO2 Nanofluid in Double Pipe Heat Exchanger with and without Helical Coil Inserts." *International Communications in Heat and Mass Transfer* 50 (January): 68–76. https://doi.org/10.1016/j.icheatmasstransfer.2013.11.002.

Chen, Haisheng, Sanjeeva Witharana, Yi Jin, Chongyoup Kim, and Yulong Ding. 2009. "Predicting Thermal Conductivity of Liquid Suspensions of Nanoparticles (Nanofluids) Based on Rheology." *Particuology* 7 (2): 151–57. https://doi.org/10.1016/j.partic.2009.01.005.

Chen, Lifei, Huaqing Xie, Yang Li, and Wei Yu. 2008. "Nanofluids Containing Carbon Nanotubes Treated by Mechanochemical Reaction." *Thermochimica Acta* 477 (1–2): 21–24. https://doi.org/10.1016/j.tca.2008.08.001.

Chen, Wenjing, Changjun Zou, Xiaoke Li, and Lu Li. 2017. "Experimental Investigation of SiC Nanofluids for Solar Distillation System: Stability, Optical Properties and Thermal Conductivity with Saline Water-Based Fluid." *International Journal of Heat and Mass Transfer* 107: 264–70. https://doi.org/10.1016/j.ijheatmasstransfer.2016.11.048.

Choi Argonne, IL (United States). Energy Technology Division], Stephen U.-S. [Argonne National Lab. (ANL). 1998. "Nanofluid Technology: Current Status and Future Research." In . United States. https://www.osti.gov/servlets/purl/11048.

Choi, S.U.S., and J.A. Eastman. 1995a. "Enhancing Thermal Conductivity of Fluids with Nanoparticles." *ASME International Mechanical Engineering Congress and Exposition* 66 (March): 99–105. https://doi.org/10.1115/1.1532008.

———. 1995b. "Enhancing Thermal Conductivity of Fluids with Nanoparticles." *ASME International Mechanical Engineering Congress and Exposition* 66 (march): 99–105.

Choi, Tae Jong, Bimal Subedi, Hyun Jun Ham, Myeong Soo Park, and Seok Pil Jang. 2018. "A Review of the Internal Forced Convective Heat Transfer Characteristics of Nanofluids: Experimental Features, Mechanisms and Thermal Performance Criteria." *Journal of Mechanical Science and Technology* 32 (8): 3491–3505. https://doi.org/10.1007/s12206-018-0701-z.

Choudhari, Prof Shashank S, and Prof Taji S G. 2013. "Experimental Studies on Effect of Coil Wire Insert On Heat Transfer Enhancement and Friction Factor of Double Pipe Heat Exchanger." *International Journal of Computational Engineering*

Research 3 (5): 32–39.

Colangelo, Gianpiero, Ernani Favale, Arturo De Risi, and Domenico Laforgia. 2013. "A New Solution for Reduced Sedimentation Flat Panel Solar Thermal Collector Using Nanofluids." *Applied Energy* 111: 80–93. https://doi.org/10.1016/j.apenergy.2013.04.069.

Czarnetzki, W., and W. Roetzel. 1995. "Temperature Oscillation Techniques for Simultaneous Measurement of Thermal Diffusivity and Conductivity." *International Journal of Thermophysics* 16 (2): 413–22. https://doi.org/10.1007/BF01441907.

D'Adamo, P. 1996. "Larch Arabinogalactan Is a Novel Immune Modulator," no. 4: 32–39.

Darzi, A. A.Rabienataj, Mousa Farhadi, and Kurosh Sedighi. 2013. "Heat Transfer and Flow Characteristics of AL2O3-Water Nanofluid in a Double Tube Heat Exchanger." *International Communications in Heat and Mass Transfer* 47 (October): 105–12. https://doi.org/10.1016/j.icheatmasstransfer.2013.06.003.

Das, Pritam Kumar, Arnab Kumar Mallik, Ranjan Ganguly, and Apurba Kumar Santra. 2018. "Stability and Thermophysical Measurements of TiO2(Anatase) Nanofluids with Different Surfactants." *Journal of Molecular Liquids* 254: 98–107. https://doi.org/10.1016/j.molliq.2018.01.075.

Das, S K, S U Choi, W Yu, and T Pradeep. 2007. *Nanofluids: Science and Technology*. Wiley. https://books.google.co.nz/books?id=QpbOpMSpXpYC.

Das, Sarit K., Stephen U. S. Choi, Wenhua Yu, and T. Pradeep. 2007. *NANOFLUIDS Science and Technology*. John Wiley & Sons. https://books.google.co.nz/books?id=QpbOpMSpXpYC.

Das, Sarit Kumar, Nandy Putra, Peter Thiesen, and Wilfried Roetzel. 2003. "Temperature Dependence of Thermal Conductivity Enhancement for Nanofluids." *Journal of Heat Transfer* 125 (4): 567–74. https://doi.org/10.1115/1.1571080.

Deepak Selvakumar, R., and S. Dhinakaran. 2016. "A Multi-Level Homogenization Model for Thermal Conductivity of Nanofluids Based on Particle Size Distribution (PSD) Analysis." *Powder Technology* 301: 310–17. https://doi.org/10.1016/j.powtec.2016.05.049.

Devendiran, Dhinesh Kumar, and Valan Arasu Amirtham. 2016. "A Review on Preparation, Characterization, Properties and Applications of Nanofluids." *Renewable and Sustainable Energy Reviews* 60: 21–40. https://doi.org/10.1016/j.rser.2016.01.055.

Dirker, J., H. Van Der Vyver, and J. P. Meyer. 2004. “Convection Heat Transfer in Concentric Annuli.” *Experimental Heat Transfer* 17 (1): 19–29. https://doi.org/10.1080/08916150490246528.

Dittus, F.W. and Boelter, L.M.K. 1930. “Publications on Engineering 2.” University of Califonia Publications on Engineering 2.

Duangthongsuk, Weerapun, and Somchai Wongwises. 2009. “Measurement of Temperature-Dependent Thermal Conductivity and Viscosity of TiO2-Water Nanofluids.” *Experimental Thermal and Fluid Science* 33 (4): 706–14. https://doi.org/10.1016/j.expthermflusci.2009.01.005.

Eastman, J. A., S. U S Choi, S. Li, W. Yu, and L. J. Thompson. 2001. “Anomalously Increased Effective Thermal Conductivities of Ethylene Glycol-Based Nanofluids Containing Copper Nanoparticles.” *Applied Physics Letters* 78 (6): 718–20. https://doi.org/10.1063/1.1341218.

Ebrahimnia-Bajestan, Ehsan, Mohammad Charjouei Moghadam, Hamid Niazmand, Weerapun Daungthongsuk, and Somchai Wongwises. 2016. “Experimental and Numerical Investigation of Nanofluids Heat Transfer Characteristics for Application in Solar Heat Exchangers.” *International Journal of Heat and Mass Transfer* 92 (January): 1041–52. https://doi.org/10.1016/j.ijheatmasstransfer.2015.08.107.

Eiamsa-ard, S., K. Kiatkittipong, and W. Jedsadaratanachai. 2015. “Heat Transfer Enhancement of TiO2/Water Nanofluid in a Heat Exchanger Tube Equipped with Overlapped Dual Twisted-Tapes.” *Engineering Science and Technology, an International Journal* 18 (3): 336–50. https://doi.org/10.1016/j.jestch.2015.01.008.

Eiamsa-ard, S, R Ketrain, and V Chuwattanakul. 2018. “TiO $_2$ /Water Nanofluid Heat Transfer in Heat Exchanger Equipped with Double Twisted-Tape Inserts.” *IOP Conference Series: Materials Science and Engineering* 350: 012015. https://doi.org/10.1088/1757-899X/350/1/012015.

Eiamsa-ard, Smith, Chinaruk Thianpong, and Pongjet Promvonge. 2006. “Experimental Investigation of Heat Transfer and Flow Friction in a Circular Tube Fitted with Regularly Spaced Twisted Tape Elements.” *International Communications in Heat and Mass Transfer* 33 (10): 1225–33. https://doi.org/10.1016/j.icheatmasstransfer.2006.08.002.

Einstein, A. 1906. “Eine Neue Bestimmung Der Moleküldimensionen.” *Annalen Der Physik* 324 (2): 289–306. https://doi.org/10.1002/andp.19063240204.

El-Maghlany, Wael M., Ahmed A. Hanafy, Amr A. Hassan, and Mohamed A. El-Magid. 2016. “Experimental Study of Cu-Water Nanofluid Heat Transfer and Pressure Drop

in a Horizontal Double-Tube Heat Exchanger." *Experimental Thermal and Fluid Science* 78 (November): 100–111. https://doi.org/10.1016/j.expthermflusci.2016.05.015.

Endress+hauser. n.d. "Electromagnetic Flowmeter Proline Promag 50 HART." Accessed October 22, 2019. https://www.manualslib.com/products/EndressPlushauser-Proline-Promag-50-5903758.html.

Engineering ToolBox. n.d. "Thermal Conductivity of Common Materials and Gases." Accessed November 7, 2017. https://www.engineeringtoolbox.com/thermal-conductivity-d_429.html.

Fadhilah, S A, R S Marhamah, and A H M Izzat. 2014. "Copper Oxide Nanoparticles for Advanced Refrigerant Thermophysical Properties: Mathematical Modeling." *Journal of Nanoparticles* 2014: 1–5. https://doi.org/10.1155/2014/890751.

Farzaneh, H., A. Behzadmehr, M. Yaghoubi, A. Samimi, and S. M H Sarvari. 2016. "Stability of Nanofluids: Molecular Dynamic Approach and Experimental Study." *Energy Conversion and Management* 111: 1–14. https://doi.org/10.1016/j.enconman.2015.12.044.

Feynman, Richard P. 1960. *There's Plenty of Room at the Bottom*. *Engineering and Science*. Vol. 23. https://resolver.caltech.edu/CaltechES:23.5.1960Bottom.

Fuskele, Veeresh, and R. M. Sarviya. 2017. "Recent Developments in Nanoparticles Synthesis, Preparation and Stability of Nanofluids." *Materials Today: Proceedings* 4 (2): 4049–60. https://doi.org/10.1016/j.matpr.2017.02.307.

Ghadimi, A., R. Saidur, and H. S.C. Metselaar. 2011. "A Review of Nanofluid Stability Properties and Characterization in Stationary Conditions." *International Journal of Heat and Mass Transfer* 54 (17–18): 4051–68. https://doi.org/10.1016/j.ijheatmasstransfer.2011.04.014.

Ghahdarijani, Alireza Mohammadi, Faramarz Hormozi, and Ali Haghighi Asl. 2017. "Convective Heat Transfer and Pressure Drop Study on Nanofluids in Double-Walled Reactor by Developing an Optimal Multilayer Perceptron Artificial Neural Network." *International Communications in Heat and Mass Transfer* 84: 11–19. https://doi.org/10.1016/j.icheatmasstransfer.2017.03.014.

Ghazvini, M., M. A. Akhavan-Behabadi, E. Rasouli, and M. Raisee. 2012. "Heat Transfer Properties of Nanodiamond-Engine Oil Nanofluid in Laminar Flow." *Heat Transfer Engineering* 33 (6): 525–32. https://doi.org/10.1080/01457632.2012.624858.

Gnielinski, V. 2013. "On Heat Transfer in Tubes." *International Journal of Heat and Mass Transfer* 63 (August): 134–40.

https://doi.org/10.1016/j.ijheatmasstransfer.2013.04.015.

Gnielinski, Volker. 1975. “Neue Gleichungen Für Den Wärme- Und Den Stoffübergang in Turbulent Durchströmten Rohren Und Kanälen.” *Forschung Im Ingenieurwesen* 41 (1): 8–16. https://doi.org/10.1007/BF02559682.

Gorji, Tahereh B., and A. A. Ranjbar. 2017. “A Review on Optical Properties and Application of Nanofluids in Direct Absorption Solar Collectors (DASCs).” *Renewable and Sustainable Energy Reviews* 72 (July 2016): 10–32. https://doi.org/10.1016/j.rser.2017.01.015.

Grassi, Walter, and Daniele Testi. 2006. “Heat Transfer Enhancement by Electric Fields in Several Heat Exchange Regimes.” *Annals of the New York Academy of Sciences* 1077: 527–69. https://doi.org/10.1196/annals.1362.062.

Guo, Wenwen, Guoneng Li, Youqu Zheng, and Cong Dong. 2018. “Measurement of the Thermal Conductivity of SiO 2 Nanofluids with an Optimized Transient Hot Wire Method.” *Thermochimica Acta* 661 (March): 84–97. https://doi.org/10.1016/j.tca.2018.01.008.

Haddad, Zoubida, Chérifa Abid, Hakan F. Oztop, and Amina Mataoui. 2014. “A Review on How the Researchers Prepare Their Nanofluids.” *International Journal of Thermal Sciences* 76 (February): 168–89. https://doi.org/10.1016/j.ijthermalsci.2013.08.010.

Hakiki, Farizal, Dara Ayuda Maharsi, and Taufan Marhaendrajana. 2015. “Surfactant-Polymer Coreflood Simulation and Uncertainty Analysis Derived from Laboratory Study.” *Journal of Engineering and Technological Sciences* 47 (6): 706–25. https://doi.org/10.5614/j.eng.technol.sci.2015.47.6.9.

Hamilton, R. L., and O. K. Crosser. 1962. “Thermal Conductivity of Heterogeneous Two-Component Systems.” *Industrial & Engineering Chemistry Fundamentals* 1 (3): 187–91. https://doi.org/10.1021/i160003a005.

Han, D., W. F. He, and F. Z. Asif. 2017. “Experimental Study of Heat Transfer Enhancement Using Nanofluid in Double Tube Heat Exchanger.” *Energy Procedia* 142: 2547–53. https://doi.org/10.1016/j.egypro.2017.12.090.

Harikrishnan, A. R., Sarit K. Das, Prabhat K. Agnihotri, and Purbarun Dhar. 2017. “Particle and Surfactant Interactions Effected Polar and Dispersive Components of Interfacial Energy in Nanocolloids.” *Journal of Applied Physics* 122 (5). https://doi.org/10.1063/1.4997123.

Hashemian, Mehran, Samad Jafarmadar, Javid Nasiri, and Hamed Sadighi Dizaji. 2017. “Enhancement of Heat Transfer Rate with Structural Modification of Double Pipe

Heat Exchanger by Changing Cylindrical Form of Tubes into Conical Form." *Applied Thermal Engineering* 118: 408–17. https://doi.org/10.1016/j.applthermaleng.2017.02.095.

Hazbehian, Mohammad, Heydar Maddah, Hamid Mohammadiun, and Mostafa Alizadeh. 2016. "Experimental Investigation of Heat Transfer Augmentation inside Double Pipe Heat Exchanger Equipped with Reduced Width Twisted Tapes Inserts Using Polymeric Nanofluid." *Heat and Mass Transfer/Waerme- Und Stoffuebertragung* 52 (11): 2515–29. https://doi.org/10.1007/s00231-016-1764-y.

Hemmat Esfe, Mohammad, and Seyfolah Saedodin. 2014. "An Experimental Investigation and New Correlation of Viscosity of ZnO-EG Nanofluid at Various Temperatures and Different Solid Volume Fractions." *Experimental Thermal and Fluid Science* 55: 1–5. https://doi.org/10.1016/j.expthermflusci.2014.02.011.

Hemmat Esfe, Mohammad, Seyfolah Saedodin, Omid Mahian, and Somchai Wongwises. 2014. "Efficiency of Ferromagnetic Nanoparticles Suspended in Ethylene Glycol for Applications in Energy Devices: Effects of Particle Size, Temperature, and Concentration." *International Communications in Heat and Mass Transfer* 58: 138–46. https://doi.org/10.1016/j.icheatmasstransfer.2014.08.035.

Heris, S Zeinali, M Shokrgozar, S Poorpharhang, M Shanbedi, and S H Noie. 2014. "Experimental Study of Heat Transfer of a Car Radiator with CuO/Ethylene Glycol-Water as a Coolant." *Journal of Dispersion Science and Technology* 35 (5): 677–84. https://doi.org/10.1080/01932691.2013.805301.

Ho, C Y, R W Powell, and P E Liley. 1968. "Thermal Conductivity of Selected Materials, Part 2." *Nsrds-Nbs 16*. Washington, D.C. https://nvlpubs.nist.gov/nistpubs/Legacy/NSRDS/nbsnsrds8.pdf.

Holman, Jack Philip. 2012. *Experimental Methods for Engineers*. 8th ed. New York: McGraw-Hill.

Hooman Yarmand, Azim Ataollahi, Oshkour Samira, Gharehkhani Seyed Farid, Seyed Shirazi, Siamak Pilban, Jahromi Mehran, Sookhakian, Saeid, Baradaran, and Basirun Salim Newaz Kazi, Wan Jefrey. 2015. "Spongy Nitrogen-Doped Activated Carbonaceous Hybrid Derived from Biomass Material/Graphene Oxide for Supercapacitor Electrodes." *RSC Advances* 5 (51): 40505–13. https://doi.org/10.1039/C5RA01525A.

Hu, Yanwei, Yurong He, Zhenduo Zhang, and Dongsheng Wen. 2017. "Effect of Al2O3 Nanoparticle Dispersion on the Specific Heat Capacity of a Eutectic Binary Nitrate Salt for Solar Power Applications." *Energy Conversion and Management* 142: 366–

73. https://doi.org/10.1016/j.enconman.2017.03.062.

Hussein, A.M., K. Kadirgama, and M.M. Noor. 2016. “Nanoparticles Suspended in Ethylene Glycol Thermal Properties and Applications: An Overview.” *Renewable and Sustainable Energy Reviews* 69 (December 2016): 1324–30. https://doi.org/10.1016/j.rser.2016.12.047.

Hussein, Adnan M, R A Bakar, and K Kadirgama. 2014. “Study of Forced Convection Nanofluid Heat Transfer in the Automotive Cooling System.” *Case Studies in Thermal Engineering* 2: 50–61. https://doi.org/https://doi.org/10.1016/j.csite.2013.12.001.

IMF. 2019. “World Economic Outlook Update.” https://www.imf.org/en/Publications/WEO/Issues/2019/07/18/WEOupdateJuly2019.

Incropera, Frank P., David P. DeWitt, Theodore L. Bergman, and Adrienne S Lavine. 2017. *Fundamentals of Heat and Mass Transfer*. Edited by 8. Wiley.

Jassim, Esam I., and Faizan Ahmed. 2020. “Experimental Assessment of Al2O3 and Cu Nanofluids on the Performance and Heat Leak of Double Pipe Heat Exchanger.” *Heat and Mass Transfer/Waerme- Und Stoffuebertragung* 56 (6): 1845–58. https://doi.org/10.1007/s00231-020-02826-9.

Jiang, Weiting, Guoliang Ding, and Hao Peng. 2009. “Measurement and Model on Thermal Conductivities of Carbon Nanotube Nanorefrigerants.” *International Journal of Thermal Sciences* 48 (6): 1108–15. https://doi.org/10.1016/j.ijthermalsci.2008.11.012.

Jiang, Weixue, Kai Du, Yanjun Li, and Liu Yang. 2017. “Experimental Investigation on Influence of High Temperature on Viscosity, Thermal Conductivity and Absorbance of Ammonia-Water Nanofluids.” *International Journal of Refrigeration* 82: 189–98. https://doi.org/10.1016/j.ijrefrig.2017.05.030.

Kabeel, A.E., Emad M.S. El-Said, and Mohamed Abdulaziz. 2015. “Thermal Solar Water Heater with H 2 O-Al 2 O 3 Nano-Fluid in Forced Convection: Experimental Investigation.” *International Journal of Ambient Energy* 0750 (August 2015): 1–9. https://doi.org/10.1080/01430750.2015.1041653.

Kaggwa, Abdul, and Chi-chuan Wang. 2016. “Investigation of Thermal-Hydrodynamic Heat Transfer Performance of R-1234ze and R-134a Refrigerants in a Microfin and Smooth Tube.” *Journal of Enhanced Heat Transfer* 23 (3): 221–39. https://doi.org/10.1615/JEnhHeatTransf.2017019585.

Kamel, Mohammed Saad, Ferenc Lezsovits, Adnan M Hussein, Omid Mahian, and

Somchai Wongwises. 2018. “Latest Developments in Boiling Critical Heat Flux Using Nanofluids: A Concise Review.” *International Communications in Heat and Mass Transfer* 98: 59–66. https://doi.org/https://doi.org/10.1016/j.icheatmasstransfer.2018.08.009.

Kang, Zhanxiao, and Liqiu Wang. 2017. “Effect of Thermal-Electric Cross Coupling on Heat Transport in Nanofluids.” *Energies* 10 (1): 123. https://doi.org/10.3390/en10010123.

Kannaiyan, Sathishkumar, Chitra Boobalan, Avinash Umasankaran, Abhaiguru Ravirajan, Sneha Sathyan, and Tiju Thomas. 2017. “Comparison of Experimental and Calculated Thermophysical Properties of Alumina/Cupric Oxide Hybrid Nanofluids.” *Journal of Molecular Liquids* 244: 469–77. https://doi.org/10.1016/j.molliq.2017.09.035.

Kasaeian, Alibakhsh, Amin Toghi Eshghi, and Mohammad Sameti. 2015. “A Review on the Applications of Nanofluids in Solar Energy Systems.” *Renewable and Sustainable Energy Reviews* 43: 584–98. https://doi.org/10.1016/j.rser.2014.11.020.

Kays, William M., and Michael E. Crawford. 1993. *Convective Heat and Mass Transfer*. Edited by Jack Philip Holman and R John Lloyd. 3rd ed. New York- USA: McGraw-Hill.

Keklikcioglu, Orhan, and Veysel Ozceyhan. 2018. “A Review of Heat Transfer Enhancement Methods Using Coiled Wire and Twisted Tape Inserts.” In *Heat Transfer - Models, Methods and Applications*, 38. InTech. https://doi.org/10.5772/intechopen.74516.

Khaled, A. R.A., M. Siddique, N. I. Abdulhafiz, and A. Y. Boukhary. 2010. “Recent Advances in Heat Transfer Enhancements: A Review Report.” *International Journal of Chemical Engineering* 2010 (1). https://doi.org/10.1155/2010/106461.

Kim, Hyun Jin, Seung Hyun Lee, Ji Hwan Lee, and Seok Pil Jang. 2015. “Effect of Particle Shape on Suspension Stability and Thermal Conductivities of Water-Based Bohemite Alumina Nanofluids.” *Energy* 90: 1290–97. https://doi.org/10.1016/j.energy.2015.06.084.

Komini Babu, Siddharth, K. S. Praveen, B. Raja, and P. Damodharan. 2013. “Measurement of Thermal Conductivity of Fluid Using Single and Dual Wire Transient Techniques.” *Measurement: Journal of the International Measurement Confederation* 46 (8): 2746–52. https://doi.org/10.1016/j.measurement.2013.05.017.

Kouloulias, K., A. Sergis, and Y. Hardalupas. 2016. “Sedimentation in Nanofluids during a Natural Convection Experiment.” *International Journal of Heat and Mass*

Transfer 101: 1193–1203. https://doi.org/10.1016/j.ijheatmasstransfer.2016.05.113.

Krieger, Irvin M., and Thomas J. Dougherty. 1959. "A Mechanism for Non-Newtonian Flow in Suspensions of Rigid Spheres." *Transactions of the Society of Rheology* 3 (1): 137–52. https://doi.org/10.1122/1.548848.

Kulkarni, Devdatta P., Ravikanth S. Vajjha, Debendra K. Das, and Daniel Oliva. 2008. "Application of Aluminum Oxide Nanofluids in Diesel Electric Generator as Jacket Water Coolant." *Applied Thermal Engineering* 28 (14–15): 1774–81. https://doi.org/10.1016/j.applthermaleng.2007.11.017.

Kumar, Bipin, Gaurav Prakash Srivastava, Manoj Kumar, and Anil Kumar Patil. 2018. "A Review of Heat Transfer and Fluid Flow Mechanism in Heat Exchanger Tube with Inserts." *Chemical Engineering and Processing: Process Intensification*. Elsevier B.V. https://doi.org/10.1016/j.cep.2017.11.007.

Langevin, Dominique. 1998. "Structure and Dynamic Properties of Surfactant Systems." In *Mesoporous Molecular Sieves 1998*, edited by L Bonneviot, F Béland, C Danumah, S Giasson, and S B T - Studies in Surface Science and Catalysis Kaliaguine, 117:129–34. Elsevier. https://doi.org/https://doi.org/10.1016/S0167-2991(98)80986-5.

Léal, L., M. Miscevic, P. Lavieille, M. Amokrane, F. Pigache, F. Topin, B. Nogarède, and L. Tadrist. 2013. "An Overview of Heat Transfer Enhancement Methods and New Perspectives: Focus on Active Methods Using Electroactive Materials." *International Journal of Heat and Mass Transfer* 61 (1): 505–24. https://doi.org/10.1016/j.ijheatmasstransfer.2013.01.083.

Lee, Jaeseon, and Issam Mudawar. 2007a. "Assessment of the Effectiveness of Nanofluids for Single-Phase and Two-Phase Heat Transfer in Micro-Channels." *International Journal of Heat and Mass Transfer* 50 (3–4): 452–63. https://doi.org/10.1016/j.ijheatmasstransfer.2006.08.001.

———. 2007b. "Assessment of the Effectiveness of Nanofluids for Single-Phase and Two-Phase Heat Transfer in Micro-Channels." *International Journal of Heat and Mass Transfer* 50 (3–4): 452–63. https://doi.org/10.1016/j.ijheatmasstransfer.2006.08.001.

Lee, S., S. U.-S. Choi, S. Li, and J. A. Eastman. 1999a. "Measuring Thermal Conductivity of Fluids Containing Oxide Nanoparticles." *Journal of Heat Transfer* 121 (2): 280. https://doi.org/10.1115/1.2825978.

Lee, S. L., R. Saidur, M. F. M. Sabri, and T. K. Min. 2016. "Effects of the Particle Size and Temperature on the Efficiency of Nanofluids Using Molecular Dynamic

Simulation." *Numerical Heat Transfer, Part A: Applications* 69 (9): 996–1013. https://doi.org/10.1080/10407782.2015.1109369.

Lee, S, S. U.-S. Choi, S. Li, and J. A. Eastman. 1999b. "Measuring Thermal Conductivity of Fluids Containing Oxide Nanoparticles." *Journal of Heat Transfer* 121 (2): 280–89. https://doi.org/10.1115/1.2825978.

Lemmon, Eric W., Marcia L. Huber, and Mark O. McLinden. 2013. "NIST Standard Reference Database 23: Reference Fluid Thermodynamic and Transport Properties-REFPROP, Version 9.1 | NIST." *Natl Std. Ref. Data Series (NIST NSRDS)* -, May. https://www.nist.gov/publications/nist-standard-reference-database-23-reference-fluid-thermodynamic-and-transport.

Lenin, Ramanujam, and Pattayil Alias Joy. 2017. "Studies on the Role of Unsaturation in the Fatty Acid Surfactant Molecule on the Thermal Conductivity of Magnetite Nanofluids." *Journal of Colloid and Interface Science* 506: 162–68. https://doi.org/10.1016/j.jcis.2017.07.038.

Leong, Kin Yuen, Idayu Razali, K. Z. Ku Ahmad, Hwai Chyuan Ong, M. J. Ghazali, and Mohd Rosdzimin Abdul Rahman. 2018. "Thermal Conductivity of an Ethylene Glycol/Water-Based Nanofluid with Copper-Titanium Dioxide Nanoparticles: An Experimental Approach." *International Communications in Heat and Mass Transfer* 90 (November 2017): 23–28. https://doi.org/10.1016/j.icheatmasstransfer.2017.10.005.

Lewis, Nathan S., George Crabtree, Arthur J Nozik, Michael R Wasielewski, and Paul Alivisatos. 2005. "Basic Research Needs for Solar Energy Utilization." *Basic Energy Sciences Workshop on Solar Energy Utilization*, 276. https://doi.org/10.2172/899136.

Li, Yanjiao, Jing'en Zhou, Simon Tung, Eric Schneider, and Shengqi Xi. 2009. "A Review on Development of Nanofluid Preparation and Characterization." *Powder Technology* 196 (2): 89–101. https://doi.org/10.1016/j.powtec.2009.07.025.

Lim, S. K., W. H. Azmi, and A. R. Yusoff. 2016. "Investigation of Thermal Conductivity and Viscosity of Al2O3/Water???Ethylene Glycol Mixture Nanocoolant for Cooling Channel of Hot-Press Forming Die Application." *International Communications in Heat and Mass Transfer* 78: 182–89. https://doi.org/10.1016/j.icheatmasstransfer.2016.09.018.

Lin, Lingnan, Hao Peng, Zheng Chang, and Guoliang Ding. 2017a. "Experimental Investigation on TiO 2 Nanoparticle Migration from Refrigerant–Oil Mixture to Lubricating Oil during Refrigerant Dryout." *International Journal of Refrigeration*

77: 75–86. https://doi.org/10.1016/j.ijrefrig.2017.02.026.

———. 2017b. “Experimental Research on Degradation of Nanolubricant–Refrigerant Mixture during Continuous Alternation Processes of Condensation and Evaporation.” *International Journal of Refrigeration* 76: 97–108. https://doi.org/10.1016/j.ijrefrig.2016.12.021.

Lin, Lingnan, Hao Peng, and Guoliang Ding. 2015. “Dispersion Stability of Multi-Walled Carbon Nanotubes in Refrigerant with Addition of Surfactant.” *Applied Thermal Engineering* 91: 163–71. https://doi.org/10.1016/j.applthermaleng.2015.08.011.

Luo, Yan, Xiaoze Du, Afrah Awad, and Dongsheng Wen. 2017. “Thermal Energy Storage Enhancement of a Binary Molten Salt via In-Situ Produced Nanoparticles.” *International Journal of Heat and Mass Transfer* 104: 658–64. https://doi.org/10.1016/j.ijheatmasstransfer.2016.09.004.

Machrafi, H., and G. Lebon. 2016. “The Role of Several Heat Transfer Mechanisms on the Enhancement of Thermal Conductivity in Nanofluids.” *Continuum Mechanics and Thermodynamics* 28 (5): 1461–75. https://doi.org/10.1007/s00161-015-0488-4.

Mahbubul, I.M. 2019. “Preparation of Nanofluid.” In *Preparation, Characterization, Properties and Application of Nanofluid*, 15–45. Elsevier. https://doi.org/10.1016/B978-0-12-813245-6.00002-2.

Mahendran, V., and John Philip. 2013. “Naked Eye Visualization of Naked Eye Visualization of Defects in Ferromagnetic Materials and Components.” *NDT and E International* 60: 100–109. https://doi.org/10.1016/j.ndteint.2013.07.011.

Mahian, Omid, Ali Kianifar, Soteris A. Kalogirou, Ioan Pop, and Somchai Wongwises. 2013. “A Review of the Applications of Nanofluids in Solar Energy.” *International Journal of Heat and Mass Transfer* 57 (2): 582–94. https://doi.org/10.1016/j.ijheatmasstransfer.2012.10.037.

Maïga, Sidi El Bécaye, Cong Tam Nguyen, Nicolas Galanis, and Gilles Roy. 2004. “Heat Transfer Behaviours of Nanofluids in a Uniformly Heated Tube.” *Superlattices and Microstructures* 35 (3–6): 543–57. https://doi.org/10.1016/j.spmi.2003.09.012.

Manilo, M., K. Bohacs, N. Lebovka, and S. Barany. 2018. “Impact of Surfactant and Clay Platelets on Electrokinetic Potential and Size Distribution in Carbon Nanotubes Aqueous Suspensions.” *Colloids and Surfaces A: Physicochemical and Engineering Aspects* 544 (February): 205–12. https://doi.org/10.1016/j.colsurfa.2018.02.030.

Mansoury, Dariush, Faramarz Ilami Doshmanziari, Abolfazl Kiani, Ali J Chamkha, and Mohsen Sharifpur. 2020. “Heat Transfer and Flow Characteristics of Al2O3/Water Nanofluid in Various Heat Exchangers: Experiments on Counter Flow.” *Heat*

Transfer Engineering 41 (3): 220–34. https://doi.org/10.1080/01457632.2018.1528051.

Mariano, Alejandra, María José Pastoriza-Gallego, Luis Lugo, Lelia Mussari, and Manuel M. Piñeiro. 2015. "Co3O4 Ethylene Glycol-Based Nanofluids: Thermal Conductivity, Viscosity and High Pressure Density." *International Journal of Heat and Mass Transfer* 85: 54–60. https://doi.org/10.1016/j.ijheatmasstransfer.2015.01.061.

Masuda H., Ebata A., Teramae K. and Hishinuma N. 1993. "Alteration of Thermal Conductivity and Viscosity of Liquid (Dispersion of Al2O3, SiO2 and TiO2 Ultra-Fine Particles)." *Netsu Bus-Sei (Japan)* 7 (4): 227–33.

Masuda, Hidetoshi, Akira Ebata, Kazunari Teramae, and Nobuo Hishinuma. 1993. "Alteration of Thermal Conductivity and Viscosity of Liquid by Dispersing Ultra-Fine Particles. Dispersion of Al2O3, SiO2 and TiO2 Ultra-Fine Particles." *Netsu Bussei* 7 (4): 227–33. https://doi.org/10.2963/jjtp.7.227.

Maxwell. 1892. *A Treatise on Electricity and Magnetism*. Vol. 1. Cambridge U. K. Oxford University Press.

McClintock, S. J. Kline and F. A. 1953. "Describing Uncertainties in Single-Sample Experiments." *Mechanical Engineering* 75 (1): 3–8.

Mendoza-Miranda, J. M., A. Mota-Babiloni, J. J. Ram??rez-Minguela, V. D. Mu??oz-Carpio, M. Carrera-Rodr??guez, J. Navarro-Esbr??, and C. Salazar-Hern??ndez. 2016. "Comparative Evaluation of R1234yf, R1234ze(E) and R450A as Alternatives to R134a in a Variable Speed Reciprocating Compressor." *Energy* 114: 753–66. https://doi.org/10.1016/j.energy.2016.08.050.

Michaelides, Efstathios E. 2013. "Transport Properties of Nanofluids. A Critical Review." *Journal of Non-Equilibrium Thermodynamics* 38 (1): 1–79. https://doi.org/10.1515/jnetdy-2012-0023.

Michonski, Katherine, and Michael A. Levi. 2010. "Harnessing International Institutions to Address Climate Change." *Council on Foreign Relations*. New York. https://www.cfr.org/energy-and-environment/climate-change.

Mintsa, Honorine Angue, Gilles Roy, Cong Tam Nguyen, and Dominique Doucet. 2009. "New Temperature Dependent Thermal Conductivity Data for Water-Based Nanofluids." *International Journal of Thermal Sciences* 48 (2): 363–71. https://doi.org/10.1016/j.ijthermalsci.2008.03.009.

Mooney, M. 1951. "The Viscosity of a Concentrated Suspension of Spherical Particles." *Journal of Colloid Science* 6 (2): 162–70. https://doi.org/10.1016/0095-

8522(51)90036-0.

Mucalo, M. R., C. R. Bullen, Merilyn Manley-Harris, and Theresa M. McIntire. 2002. "Arabinogalactan from the Western Larch Tree: A New, Purified and Highly Water-Soluble Polysaccharide-Based Protecting Agent for Maintaining Precious Metal Nanoparticles in Colloidal Suspension." *Journal of Materials Science* 37 (3): 493–504. https://doi.org/10.1023/A:1013757221776.

Mukesh Kumar, P. C., and M. Chandrasekar. 2020. "Heat Transfer and Friction Factor Analysis of MWCNT Nanofluids in Double Helically Coiled Tube Heat Exchanger." *Journal of Thermal Analysis and Calorimetry*, February, 1–13. https://doi.org/10.1007/s10973-020-09444-x.

Munyalo, Jotham Muthoka, and Xuelai Zhang. 2018. "Particle Size Effect on Thermophysical Properties of Nanofluid and Nanofluid Based Phase Change Materials: A Review." *Journal of Molecular Liquids* 265: 77–87. https://doi.org/10.1016/j.molliq.2018.05.129.

Nair, Vipin, P. R. Tailor, and A. D. Parekh. 2016. "Nanorefrigerants: A Comprehensive Review on Its Past, Present and Future." *International Journal of Refrigeration* 67: 290–307. https://doi.org/10.1016/j.ijrefrig.2016.01.011.

Namburu, Praveen K., Devdatta P. Kulkarni, Debasmita Misra, and Debendra K. Das. 2007. "Viscosity of Copper Oxide Nanoparticles Dispersed in Ethylene Glycol and Water Mixture." *Experimental Thermal and Fluid Science* 32 (2): 397–402. https://doi.org/10.1016/j.expthermflusci.2007.05.001.

Nanocomposix. 2012. "Zeta Potential Analysis of Nanoparticles." *Nanocomposix Publications*, 1–6.

Nanostructured and amorphous Inc. 2019. "Carbon Nanopowder." 2019. https://www.nanoamor.com/inc/sdetail/20185.

Nanostructured and amorphous Materials Inc. 2019. "Aluminum Oxide Powder." 2019. https://www.nanoamor.com/inc/sdetail/50582.

Nickel Development institute. 1965. *Design Guidelines for the Selection and Use of Stainless Steels*. https://www.nickelinstitute.org/media/1667/designguidelinesfortheselectionanduseofstainlesssteels_9014_.pdf.

Nie, Chu, W. H. Marlow, and Y. A. Hassan. 2008. "Discussion of Proposed Mechanisms of Thermal Conductivity Enhancement in Nanofluids." *International Journal of Heat and Mass Transfer* 51 (5–6): 1342–48. https://doi.org/10.1016/j.ijheatmasstransfer.2007.11.034.

Nieh, Hwa-Ming, Tun-Ping Teng, and Chao-Chieh Yu. 2014. “Enhanced Heat Dissipation of a Radiator Using Oxide Nano-Coolant.” *International Journal of Thermal Sciences* 77: 252–61. https://doi.org/https://doi.org/10.1016/j.ijthermalsci.2013.11.008.

Omidi, Mohamad, Mousa Farhadi, and Mohamad Jafari. 2017. “A Comprehensive Review on Double Pipe Heat Exchangers.” *Applied Thermal Engineering* 110: 1075–90. https://doi.org/10.1016/j.applthermaleng.2016.09.027.

Paar, Anton, and Digital Viscometers. 2006. “DV-1 P New Series of Digital Viscometers Introducing” B64is64-j. https://www.anton-paar.com/nz-en/products/group/viscometer/.

Pak, Bock Choon, and Young I. Cho. 1998. “Hydrodynamic and Heat Transfer Study of Dispersed Fluids with Submicron Metallic Oxide Particles.” *Experimental Heat Transfer* 11 (2): 151–70. https://doi.org/10.1080/08916159808946559.

Pal, Rajinder. 2014. “A Novel Method to Determine the Thermal Conductivity of Interfacial Layers Surrounding the Nanoparticles of a Nanofluid.” *Nanomaterials* 4 (4): 844–55. https://doi.org/10.3390/nano4040844.

Pandey, Shive Dayal, and V. K. Nema. 2012. “Experimental Analysis of Heat Transfer and Friction Factor of Nanofluid as a Coolant in a Corrugated Plate Heat Exchanger.” *Experimental Thermal and Fluid Science* 38 (April): 248–56. https://doi.org/10.1016/j.expthermflusci.2011.12.013.

Perry, Robert H., Don W. Green., and James O. Maloney. 1998. *Perry’s Chemical Engineers’ Handbook*. Edited by Don W. Green., James O’Hara, and Maloney. Seventh Ed. New York: McGraw-Hill. https://chembugs.files.wordpress.com/2015/12/perrys-chemical-engineering-handbook1.pdf.

Perry, S, Robert H Perry, Don W Green, and James O Maloney. 1997. *Perry’s Chemical Engineers’ Handbook*. Edited by Don W. Green. and James O. Maloney. *Choice Reviews Online*. Seventh. New York: McGraw-Hill.

Petukhov, B.S. 1970. “Heat Transfer and Friction in Turbulent Pipe Flow with Variable Physical Properties.” *Advances in Heat Transfer* 6 (January): 503–64. https://doi.org/10.1016/S0065-2717(08)70153-9.

Pinto, Rodrigo Vidonscky, and Flávio Augusto Sanzovo Fiorelli. 2016. “Review of the Mechanisms Responsible for Heat Transfer Enhancement Using Nanofluids.” *Applied Thermal Engineering* 108: 720–39. https://doi.org/10.1016/j.applthermaleng.2016.07.147.

Pongsawatmanit, R, O Miyawaki, and T Yano. 1993. “Measurement of the Thermal Conductivity of Unfrozen and Frozen Food Materials by a Steady State Method with Coaxial Dual-Cylinder Apparatus.” *Bioscience, Biotechnology, and Biochemistry* 57 (7): 1072–76. https://doi.org/10.1271/bbb.57.1072.

Promvonge, P. 2008. “Heat Transfer Behaviors in Round Tube with Conical Ring Inserts.” *Energy Conversion and Management* 49 (1): 8–15. https://doi.org/10.1016/j.enconman.2007.06.009.

Ranjbarzadeh, R, A H Meghdadi Isfahani, and M Hojaji. 2018. “Experimental Investigation of Heat Transfer and Friction Coefficient of the Water / Graphene Oxide Nanofluid in a Pipe Containing Twisted Tape Inserts under Air Cross-Flow.” *Experimental Heat Transfer* 00 (00): 1–18. https://doi.org/10.1080/08916152.2018.1431736.

Ranjbarzadeh, Ramin, Alireza Akhgar, Sogand Musivand, and Masoud Afrand. 2018. “Effects of Graphene Oxide-silicon Oxide Hybrid Nanomaterials on Rheological Behavior of Water at Various Time Durations and Temperatures: Synthesis, Preparation and Stability.” *Powder Technology* 335: 375–87. https://doi.org/10.1016/j.powtec.2018.05.036.

Redhwan, A.A.M., W.H. Azmi, M.Z. Sharif, and N.N.M. Zawawi. 2017. “Thermal Conductivity Enhancement of Al2O3 and SiO2 Nanolubricants for Application in Automotive Air Conditioning (AAC) System A.A.M.” *MATEC Web of Conferences* 90: 01051. https://doi.org/10.1016/j.ijrefrig.2016.06.025.

Ritchie, Hannah. 2014. “Energy.” *Our World in Data*. https://ourworldindata.org/energy.

Ritchie, Hannah, and Max Roser. 2020. “CO_2 and Greenhouse Gas Emissions.” *Our World in Data*. https://ourworldindata.org/co2-and-other-greenhouse-gas-emission.

Rouse, Hunter. 1978. *Elementary Mechanics of Fluids*. New York: Dover Publications, INC. https://discovery.upc.edu/iii/encore/record/C__Rb1105468__SElementary Mechanics of Fluids__Orightresult__U__X7?lang=cat.

Saha, Goutam, and Manosh C. Paul. 2014. “Numerical Analysis of the Heat Transfer Behaviour of Water Based Al2O3 and TiO2 Nanofluids in a Circular Pipe under the Turbulent Flow Condition.” *International Communications in Heat and Mass Transfer* 56 (August): 96–108. https://doi.org/10.1016/j.icheatmasstransfer.2014.06.008.

Sahiti, N., F. Durst, and A. Dewan. 2006. “Strategy for Selection of Elements for Heat Transfer Enhancement.” *International Journal of Heat and Mass Transfer* 49 (19–20): 3392–3400. https://doi.org/10.1016/j.ijheatmasstransfer.2006.03.011.

Sánchez-Coronilla, Antonio, Javier Navas, Teresa Aguilar, Elisa I. Martín, Juan Jesús Gallardo, Mr Roberto Gómez-Villarejo, Mr Iván Carrillo-Berdugo, Rodrigo Alcántara, Concha Fernández-Lorenzo, and Joaquín Martín-Calleja. 2017. "The Role of Surfactants in the Stability of NiO Nanofluids: An Experimental and DFT Study." *ChemPhysChem* 18 (4): 346–56. https://doi.org/10.1002/cphc.201601161.

Sanukrishna, A. S. Vishnu, and M. Jose Prakash. 2017. "Nanorefrigerants for Energy Efficient Refrigeration Systems." *Journal of Mechanical Science and Technology* 31 (8): 3993–4001. https://doi.org/10.1007/s12206-017-0746-4.

Sezer, Nurettin, Muataz A. Atieh, and Muammer Koç. 2019. "A Comprehensive Review on Synthesis, Stability, Thermophysical Properties, and Characterization of Nanofluids." *Powder Technology*. Elsevier B.V. https://doi.org/10.1016/j.powtec.2018.12.016.

Shao, Xuefeng, Ying Chen, Songping Mo, Zhengdong Cheng, and Tao Yin. 2015. "Dispersion Stability of TiO2-H2O Nanofluids Containing Mixed Nanotubes and Nanosheets." *Energy Procedia* 75: 2049–54. https://doi.org/10.1016/j.egypro.2015.07.282.

Sharif, M.Z., W.H. Azmi, A.A.M. Redhwan, R. Mamat, and T.M. Yusof. 2017. "Performance Analysis of SiO2/PAG Nanolubricant in Automotive Air Conditioning System." *International Journal of Refrigeration* 75: 204–16. https://doi.org/10.1016/j.ijrefrig.2017.01.004.

Sheikholeslami, Mohsen, Mofid Gorji-Bandpy, and Davood Domiri Ganji. 2015. "Review of Heat Transfer Enhancement Methods: Focus on Passive Methods Using Swirl Flow Devices." *Renewable and Sustainable Energy Reviews* 49: 444–69. https://doi.org/10.1016/j.rser.2015.04.113.

Shekarian, E, A H Tarighaleslami, and F Khodaverdi. 2014. "Review of Effective Parameters on the Nanofluid Thermal Conductivity." *Journal of Middle East Applied Science and Technology* 4 (15): 776–80.

Shin, Ji Yong, Thathan Premkumar, and Kurt E. Geckeler. 2008. "Dispersion of Single-Walled Carbon Nanotubes by Using Surfactants: Are the Type and Concentration Important?" *Chemistry - A European Journal* 14 (20): 6044–48. https://doi.org/10.1002/chem.200800357.

Sidik, Nor Azwadi Che, H.A. Mohammed, Omer A. Alawi, and S. Samion. 2014. "A Review on Preparation Methods and Challenges of Nanofluids." *International Communications in Heat and Mass Transfer* 54 (May): 115–25. https://doi.org/10.1016/j.icheatmasstransfer.2014.03.002.

Sigma-Aldrich. 2021a. “Arabinogalactan.” 2021. https://www.sigmaaldrich.com/NZ/en/search/9036-66-2?focus=products&page=1&perPage=30&sort=relevance&term=9036-66-2&type=cas_number.

———. 2021b. “CTAB | Hexadecyltrimethylammonium Bromide.” 2021. https://www.sigmaaldrich.com/NZ/en/search/ctab?focus=products&page=1&perPage=30&sort=relevance&term=ctab&type=product_name.

Sizochenko, Natalia, Michael Syzochenko, Agnieszka Gajewicz, Jerzy Leszczynski, and Tomasz Puzyn. 2017. “Predicting Physical Properties of Nanofluids by Computational Modeling.” *The Journal of Physical Chemistry C* 121 (3): 1910–17. https://doi.org/10.1021/acs.jpcc.6b08850.

Sohel Murshed, S M, and C A Nieto de Castro. 2017. “A Critical Review of Traditional and Emerging Techniques and Fluids for Electronics Cooling.” *Renewable and Sustainable Energy Reviews* 78: 821–33. https://doi.org/https://doi.org/10.1016/j.rser.2017.04.112.

Sonawane, Shriram S., Rohit S. Khedkar, and Kailas L. Wasewar. 2013. “Study on Concentric Tube Heat Exchanger Heat Transfer Performance Using Al2O3 - Water Based Nanofluids.” *International Communications in Heat and Mass Transfer* 49 (December): 60–68. https://doi.org/10.1016/j.icheatmasstransfer.2013.10.001.

Stebe, Kathleen J, and Shi-Yow Lin. 2001. “Chapter 2 - DYNAMIC SURFACE TENSION AND SURFACTANT MASS TRANSFER KINETICS: MEASUREMENT TECHNIQUES AND ANALYSIS.” In , edited by Hari Singh B T - Handbook of Surfaces and Interfaces of Materials Nalwa, 55–106. Burlington: Academic Press. https://doi.org/https://doi.org/10.1016/B978-012513910-6/50021-9.

Stewart, Maurice. 2016a. “6 - Fluid Flow and Pressure Drop.” In *Surface Production Operations*, edited by Maurice Stewart, 343–470. Boston: Gulf Professional Publishing. https://doi.org/https://doi.org/10.1016/B978-1-85617-808-2.00006-7.

———. 2016b. *Fluid Flow and Pressure Drop*. *Surface Production Operations*. https://doi.org/10.1016/b978-1-85617-808-2.00006-7.

Suganthi, K. S., and K. S. Rajan. 2017. “Metal Oxide Nanofluids: Review of Formulation, Thermo-Physical Properties, Mechanisms, and Heat Transfer Performance.” *Renewable and Sustainable Energy Reviews* 76 (October 2015): 226–55. https://doi.org/10.1016/j.rser.2017.03.043.

Swamee, Prabhata K., and Akalank K. Jain. 1976. “Explicit Equations for Pipe-Flow

Problems.” *Journal of the Hydraulics Division*.

Syam Sundar, L., P. Bhramara, N. T. Ravi Kumar, Manoj K. Singh, and Antonio C.M. Sousa. 2017. “Experimental Heat Transfer, Friction Factor and Effectiveness Analysis of Fe3O4 Nanofluid Flow in a Horizontal Plain Tube with Return Bend and Wire Coil Inserts.” *International Journal of Heat and Mass Transfer* 109: 440–53. https://doi.org/10.1016/j.ijheatmasstransfer.2017.02.022.

Syam Sundar, L., N. T. Ravi Kumar, Birhanu Mulat Addis, P. Bhramara, Manoj K. Singh, and Antonio C.M. Sousa. 2019. “Heat Transfer and Effectiveness Experimentally-Based Analysis of Wire Coil with Core-Rod Inserted in Fe3O4/Water Nanofluid Flow in a Double Pipe U-Bend Heat Exchanger.” *International Journal of Heat and Mass Transfer* 134 (May): 405–19. https://doi.org/10.1016/j.ijheatmasstransfer.2019.01.041.

Tabatabaeikia, S., H. A. Mohammed, N. Nik-Ghazali, and B. Shahizare. 2014. “Heat Transfer Enhancement by Using Different Types of Inserts.” *Advances in Mechanical Engineering*. Hindawi Publishing Corporation. https://doi.org/10.1155/2014/250354.

Tanuguchi, Norio. 1974. “On the Basic Concept of ’Nano-Technology.” In *Proceedings of the International Conference on Production Engineering*, 18–23. Tokyo.

Tazarv, S., M. Saffar-Avval, F. Khalvati, E. Mirzaee, and Z. Mansoori. 2016. “Experimental Investigation of Saturated Flow Boiling Heat Transfer to TiO<inf>2</Inf>/R141b Nanorefrigerant.” *Experimental Heat Transfer* 29 (2). https://doi.org/10.1080/08916152.2014.973976.

The international nickel company. 1963. *Corrosion Resistance of the Austenitic Chromium-Nickel Stainless Steel in Chemicla Environments*. New York. https://www.parrinst.com/wp-content/uploads/downloads/2011/07/Parr_Stainless-Steels-Corrosion-Info.pdf.

Thermal Sensors. 2019. “Small Size Non-Steady-State Probe for Thermal Conductivity Measurement TP08 Manual V1611.” http://www.hukseflux.com.

Thermtest Instruments. 2004. “Thermtest TC-30 User Manual.(Thermal Conductivity Measurements).” *Mathis Instruments Ltd/Thermtest Inc*. New Brunswick, Canada. https://thermtest.com/.

Thome, Jr. 2004. “Engineering Data Book III.” *Wolverine Tube Inc*. http://www.wlv.com/wp-content/uploads/2014/06/databook3/DataBookIII.pdf.

Timofeeva, Elena V., Michael R. Moravek, and Dileep Singh. 2011. “Improving the Heat Transfer Efficiency of Synthetic Oil with Silica Nanoparticles.” *Journal of Colloid*

and Interface Science 364 (1): 71–79. https://doi.org/10.1016/j.jcis.2011.08.004.

Tiznobaik, Hani, and Donghyun Shin. 2013. "Enhanced Specific Heat Capacity of High-Temperature Molten Salt-Based Nanofluids." *International Journal of Heat and Mass Transfer* 57 (2): 542–48. https://doi.org/10.1016/j.ijheatmasstransfer.2012.10.062.

U.S. Energy Information Adminstration. n.d. "Rankings about Energy in the World." Independent Statistics & Analysis. Accessed August 14, 2020. https://www.eia.gov/international/overview/world.

Ueki, Yoshitaka, Takashi Aoki, Kenta Ueda, and Masahiko Shibahara. 2017. "Thermophysical Properties of Carbon-Based Material Nanofluid." *International Journal of Heat and Mass Transfer* 113: 1130–34. https://doi.org/10.1016/j.ijheatmasstransfer.2017.06.008.

UNFCCC. Conference of the Parties (COP). 2015. "Adoption of the Paris Agreement. Proposal by the President." *Paris Climate Change Conference - November 2015, COP 21* 21932 (December): 32. https://doi.org/FCCC/CP/2015/L.9/Rev.1.

United Nations. 2020. "World Population Prospects." 2020. https://population.un.org/wpp/Graphs/Probabilistic/POP/TOT/900.

US Research Nanomaterials, Inc. n.d. "The Advanced Nanomaterials Provider." Accessed February 24, 2019. https://us-nano.com/nanoparticle_suppliers.

Wagner, W., and A. Pruß. 2002. "The IAPWS Formulation 1995 for the Thermodynamic Properties of Ordinary Water Substance for General and Scientific Use." *Journal of Physical and Chemical Reference Data* 31 (2): 387–535. https://doi.org/10.1063/1.1461829.

Wagner, W, J R Cooper, A Dittmann, J Kijima, H.-J Kretzschmar, A Kruse, R Mareš, et al. 1997. "For the Thermodynamic Properties of Water and Steam." http://www.asme.org/about-asme/terms-of-use.

Wang, C. C., C. B. Chiou, and D. C. Lu. 1996. "Single-Phase Heat Transfer and Flow Friction Correlations for Microfin Tubes." *International Journal of Heat and Fluid Flow* 17 (5): 500–508. https://doi.org/10.1016/0142-727X(96)00048-3.

Wang, K. J., G. L. Ding, and W. T. Jiang. 2006. "Nano-Scale Thermal Transporting and Its Use in Engineering." *Proceedings of the 4th Symposium on Refrigeration and Air Conditioning*, no. 2006: 66–75.

Wang, Xinwei, Xianfan Xu, and Stephen U. S. Choi. 1999. "Thermal Conductivity of Nanoparticle - Fluid Mixture." *Journal of Thermophysics and Heat Transfer* 13 (4): 474–80. https://doi.org/10.2514/2.6486.

Webb, Ralph L, and Nae-Hyun Kim. 2006. *Principles Enhanced Heat Transfer*. 2nd ed. New York: Taylor & Francis Group. https://www.taylorfrancis.com/books/9781135434793.

Wilk, Joanna, Robert Smusz, and Sebastian Grosicki. 2017. "Thermophysical Properties of Water Based Cu Nanofluid Used in Special Type of Coil Heat Exchanger." *Applied Thermal Engineering* 127 (December): 933–43. https://doi.org/10.1016/j.applthermaleng.2017.08.078.

Wilson, E.E. 1915. "A Basis of Rational Design of Heat Transfer Apparatus." *ASME Journal of Heat Transfer*, no. 37: 47–70.

World Bank. 2020. "Total Population Data." 2020. https://data.worldbank.org/indicator/SP.POP.TOTL.

Wu, Daxiong, Haitao Zhu, Liqiu Wang, and Lumei Liu. 2009. "Critical Issues in Nanofluids Preparation, Characterization and Thermal Conductivity." *Current Nanoscience* 5 (1): 103–12. https://doi.org/10.2174/157341309787314548.

Xie, Huaqing, Jinchang Wang, Tonggeng Xi, Yan Liu, Fei Ai, and Qingren Wu. 2002. "Thermal Conductivity Enhancement of Suspensions Containing Nanosized Alumina Particles." *Journal of Applied Physics* 91 (7): 4568–72. https://doi.org/10.1063/1.1454184.

Xing, Meibo, Jianlin Yu, and Ruixiang Wang. 2016. "Experimental Investigation and Modelling on the Thermal Conductivity of CNTs Based Nanofluids." *International Journal of Thermal Sciences* 104: 404–11. https://doi.org/10.1016/j.ijthermalsci.2016.01.024.

Xuan, Yimin, and Qiang Li. 2003. "Investigation on Convective Heat Transfer and Flow Features of Nanofluids." *Journal of Heat Transfer* 125 (1): 151–55. https://doi.org/10.1115/1.1532008.

Xuan, Yimin, and Wilfried Roetzel. 2000. "Conceptions for Heat Transfer Correlation of Nanofluids." *International Journal of Heat and Mass Transfer* 43 (19): 3701–7. https://doi.org/10.1016/S0017-9310(99)00369-5.

Yadav, Anil Singh. 2009. "Effect of Half Length Twisted-Tape Turbulators on Heat Transfer and Pressure Drop Characteristics inside a Double Pipe U-Bend Heat Exchanger." *Jordan Journal of Mechanical and Industrial Engineering* 3 (1): 17–22.

Yang, Dong, Feng Yang, Jianhua Hu, Jiang Long, Changchun Wang, Deliang Fu, and Quanxing Ni. 2009. "Hydrophilic Multi-Walled Carbon Nanotubes Decorated with Magnetite Nanoparticles as Lymphatic Targeted Drug Delivery Vehicles." *Chemical*

Communications, no. 29: 4447–49. https://doi.org/10.1039/b908012k.

Yang, Liu, Jianyong Xu, Kai Du, and Xiaosong Zhang. 2017. "Recent Developments on Viscosity and Thermal Conductivity of Nanofluids." *Powder Technology* 317: 348–69. https://doi.org/10.1016/j.powtec.2017.04.061.

Yarmand, Hooman, Samira Gharehkhani, Seyed Farid, Seyed Shirazi, Ahmad Amiri, Elham Montazer, Hamed Khajeh Arzani, Rad Sadri, Mahidzal Dahari, and S N Kazi. 2016. "Nano Fl Uid Based on Activated Hybrid of Biomass Carbon / Graphene Oxide : Synthesis , Thermo-Physical and Electrical Properties ☆." *International Communications in Heat and Mass Transfer* 72: 10–15. https://doi.org/10.1016/j.icheatmasstransfer.2016.01.004.

Yu, Fan, Yingying Chen, Xingbo Liang, Jiale Xu, Chiahsun Lee, Qi Liang, Peng Tao, and Tao Deng. 2017. "Dispersion Stability of Thermal Dispersion Stability of Thermal Nanofluids." *Progress in Natural Science: Materials International* 27 (5): 531–42. https://doi.org/10.1016/j.pnsc.2017.08.010.

Yu, Wenhua, David M. France, David S. Smith, Dileep Singh, Elena V. Timofeeva, and Jules L. Routbort. 2009. "Heat Transfer to a Silicon Carbide/Water Nanofluid." *International Journal of Heat and Mass Transfer* 52 (15–16): 3606–12. https://doi.org/10.1016/j.ijheatmasstransfer.2009.02.036.

Zamzamian, Amirhossein, Shahin Nasseri Oskouie, Ahmad Doosthoseini, Aliakbar Joneidi, and Mohammad Pazouki. 2011. "Experimental Investigation of Forced Convective Heat Transfer Coefficient in Nanofluids of Al2O3/EG and CuO/EG in a Double Pipe and Plate Heat Exchangers under Turbulent Flow." *Experimental Thermal and Fluid Science* 35 (3): 495–502. https://doi.org/10.1016/j.expthermflusci.2010.11.013.

Zhang, X, H Gu, M Fujii, 570 Zhang, and Fujii Gu. 2006. "Experimental Study on the Effective Thermal Conductivity and Thermal Diffusivity of Nanofluids." *International Journal of Thermophysics* 27 (2). https://doi.org/10.1007/s10765-006-0054-1.

Zheng, Lu, Yonghui Xie, and Di Zhang. 2017. "Numerical Investigation on Heat Transfer Performance and Flow Characteristics in a Rectangular Air Cooling Channel (AR=2) with Ridged Dimples." *International Journal of Heat and Mass Transfer* 107: 403–17. https://doi.org/10.1016/j.ijheatmasstransfer.2016.11.039.

Zheng, Mingrui, Dong Han, Faizan Asif, and Zetian Si. 2020a. "Effect of Al2O3/Water Nanofluid on Heat Transfer of Turbulent Flow in the Inner Pipe of a Double-Pipe Heat Exchanger." *Heat and Mass Transfer/Waerme- Und Stoffuebertragung* 56 (4):

1127–40. https://doi.org/10.1007/s00231-019-02774-z.

———. 2020b. “Effect of Al2O3/Water Nanofluid on Heat Transfer of Turbulent Flow in the Inner Pipe of a Double-Pipe Heat Exchanger.” *Heat and Mass Transfer/Waerme- Und Stoffuebertragung* 56 (4): 1127–40. https://doi.org/10.1007/s00231-019-02774-z.

Zhu, Bao Jie, Wei Lin Zhao, Jin Kai Li, Yan Xiang Guan, and Dong Dong Li. 2011. “Thermophysical Properties of Al2O3-Water Nanofluids.” In *Nano-Scale and Amorphous Materials*, 688:266–71. Materials Science Forum. Trans Tech Publications. https://doi.org/10.4028/www.scientific.net/MSF.688.266.

Appendix A

Published Articles

International Nano Letters (2019) 9:277–288
https://doi.org/10.1007/s40089-019-00281-x

REVIEW

Developments and future insights of using nanofluids for heat transfer enhancements in thermal systems: a review of recent literature

Abdul Kaggwa[1] · James K. Carson[1]

Received: 3 January 2019 / Accepted: 30 July 2019 / Published online: 9 August 2019

Abstract
The twenty-first century is experiencing a wave of technologies and innovations making use of unique features of nanofluids, in applications such as industrial and process heating, air conditioning and refrigeration systems, heat pipes, solar energy, thermal storage systems, electronic cooling systems and others. Recent literature indicates that suspending solid nanoparticles in traditional working fluids can enhance heat transfer rates by increasing thermal conductivity and heat transfer coefficients. However, there is a wide variation in the extent of heat transfer enhancements reported in the literature. In this review, which mainly focuses on the research published within the last 5 years, experimental investigations from recent developments of nanofluids usage and performance in various heat transfer systems are summarised. In addition, heat transfer mechanisms in nanofluids, the challenges and future direction of nanofluids regarding heat transfer enhancement are discussed. Popular preparation methods of nanofluids and the models of thermophysical properties such as thermal conductivity and viscosity have been reviewed.

Keywords Nanofluids · Heat transfer enhancement · Challenges and heat transfer mechanism · Stability · Review

Introduction

The knowledge and understanding of heat transfer are important for the design of a wide range of industrial, commercial and domestic processes and appliances, including chemical processing, air conditioning and refrigeration, solar energy production and conversion, oil and gas industries and electronics cooling. In thermal engineering, the improvement in the thermal performance of systems is termed 'heat transfer enhancement'. Over the past decade, several techniques have been proposed as ways of enhancing heat transfer [1–3]. These techniques have been classified as passive or active (Table 1).

Figure 1 shows thermal conductivities of different materials. Since the thermal conductivity of solids may be several orders of magnitude higher than the thermal conductivities of conventional heat transfer fluids such as water, oil or ethylene glycol (EG), the addition of highly conducting solid particles to a fluid has the potential to increase the effective thermal conductivity of the fluid.

Choi and Eastman [5] introduced the term "nanofluids" to describe suspensions of copper nanoparticles in water. Their investigations revealed that the thermal conductivity of the fluid was enhanced by a factor of 1.5 and 3.5 compared to water at low volume fractions of 5% and 20%, respectively. Further experiments with copper nanoparticles in acidified ethylene glycol showed apparently anomalous increases in thermal conductivity [6]. However, they also observed that the thermal conductivity of copper/ethylene–glycol nanofluids decreased with time, which was most likely due to agglomeration and/or sedimentation of the nanoparticles.

Similar encouraging results were observed by other researchers and subsequently the use of nanofluids for heat transfer enhancement became a very active area of research [7–11]. However, to date, it does not appear that nanofluids have received widespread usage outside the research environment. In practice, the usage of nanoparticles in heat transfer equipment still faces a number of challenges arising from issues such as (1) lack of stability of the nanofluids, (2) high variation on reported physical properties and heat transfer enhancement effects in the literature, (3) lack of understanding about the mechanisms and forces that act on

✉ Abdul Kaggwa
Kaggwaabu@ymail.com

[1] School of Engineering, Faculty of Science and Engineering, University of Waikato, Private Bag 3105, Hamilton 3240, New Zealand

Table 1 Passive and active heat transfer enhancement techniques [4]

Passive	Active
Treated surfaces	Mechanical aids
Rough surfaces	Surface vibration
Extended surfaces	Fluid vibration
Displaced enhancement devices	Electrostatic fields
Swirl flow devices	Injection
Coiled tubes	Suction
Surface tension devices	Jet impingement
Additives for liquids	
Additives for gases	

the nanoparticles during and after suspension. These issues have slowed the process of standardisation and formulation of nanofluid technology. The aim of this paper is to review the recent developments and the future prospects for nanofluids in heat transfer systems.

Preparation of nanofluids

Nanoparticles used in nanofluids range in size from 1 to 100 nm and different shapes such as nanospheres (spherical), nanoreefs, nanoboxes, nanoclusters and nanotubes. Some studies [12–15] have concluded that the morphology of nanoparticles is defined during synthesis, and the average size of nanoparticles plays a significant role in the enhancement of thermal conductivity a primary factor for heat transfer enhancement.

There are two popular methods used in the preparation of nanofluids: the single-step method and the two-step method [16] as shown in Fig. 2. The single-step method involves the simultaneous production of nanoparticles and suspension of the particles into the base fluid. For example, the nanoparticles may be formed by condensation from the vapour phase directly into the heat transfer liquid. This method has the advantage of producing minimal nanoparticle agglomeration; however, it is characterised by high costs, and is

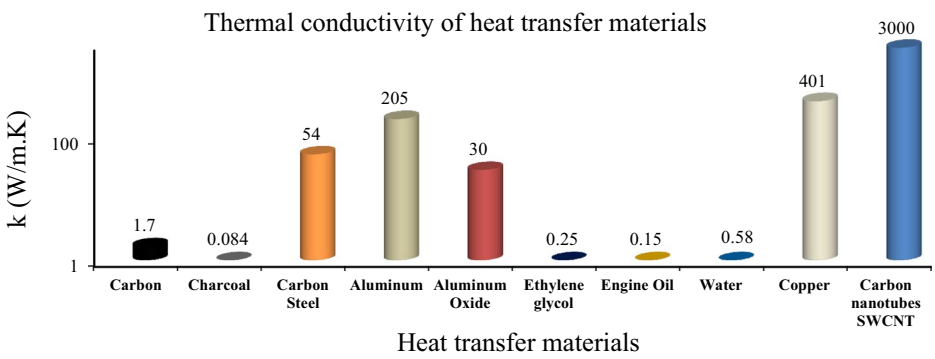

Fig. 1 Thermal conductivity of some heat transfer materials

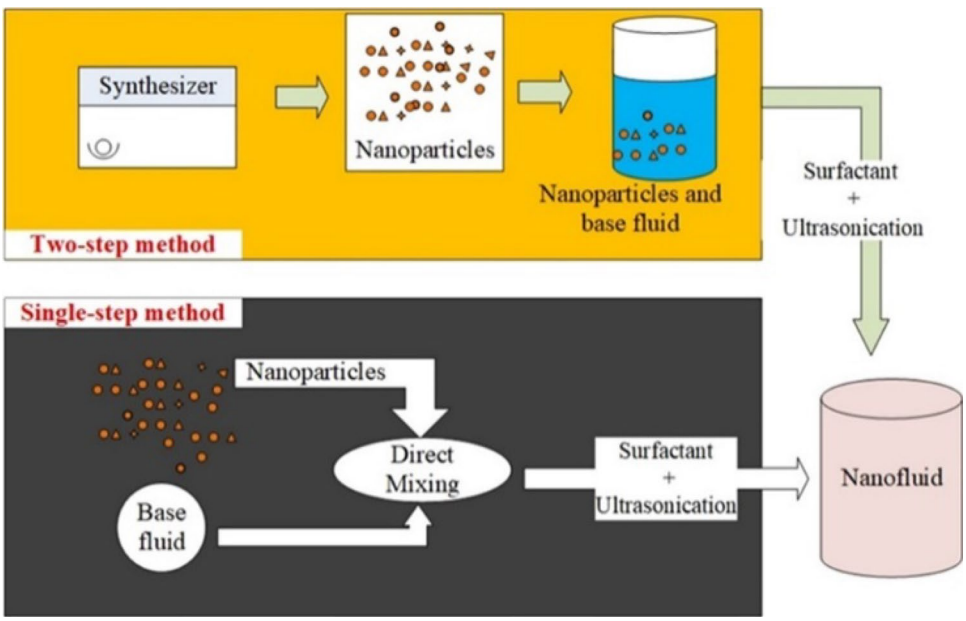

Fig. 2 Methods of nanofluids preparation

therefore likely to be infeasible on an industrial scale. In contrast, in the two-step method, nanoparticles are produced in a separate process before being dispersed into the base fluid [17]. Stabilising agents such as surfactants can be added to reduce the interfacial forces between the nanoparticles and base fluid molecules. Subsequently, the solution may be mixed using mechanical devices such as homogeniser, stirrer and ultrasonicator. The two-step method appears to have received the most widespread use, since it is generally less labour intensive and more cost effective [17–19].

Mechanism of heat transfer enhancement in nanofluids

Maxwell [20] proposed a model for determining the electrical conductivity of a dispersion of spheres in a continuous medium that has subsequently been applied successfully to the prediction of thermal conductivities of heterogeneous materials [21, 22]. Maxwell's model and derivatives may be thought of as 'classic theory' for thermal conductivity modelling [23]. However, the rise in popularity of nanofluids has largely been due to reports of experimentally determined thermal conductivities being many times higher than those predicted by classic theory [24, 25]. In the open literature, there does not appear to be any single theory that can explain the apparently anomalous heat transfer enhancement effects in nanofluids that have been reported by some researchers [6, 26]. However, a variety of mechanisms have been proposed. For instance, in a review of metal-oxide nanoparticles Suganthi et al. [27] concluded that Brownian motion plays a significant role in increasing thermal conductivity of nanofluids. The stochastic movement of nanoparticles in a fluid depends on temperature, diameter of the particles and viscosity of the fluid. Farzaneh et al. [28] suggested that in addition to Brownian motion, nanoparticles once suspended also experience drag, thermophoresis, Van der Waals and electric double layer forces. The study added that a combination of inter-particle Van der Waals and electric double layer forces produces a combined force called "DLVO", which together with other forces play a significant role in the mechanism of heat transfer in nanofluids.

Kang et al. [29] proposed a mechanism based on the cross coupling of thermal and electric transports in nanofluids. They explained that due to the fact that nanoparticles have surface charges, a varying electric field can be generated to accompany the particle thermal motion. Therefore, the base fluid is heated by the nanoparticles through molecular collision such that the nanoparticles may be considered as an internal heat source.

Sanukrishna et al. [30] reported that the mechanism of molecular layer formation inside evaporator tubes during evaporation could be the reason for heat transfer enhancement in two-phase flow boiling.

However, to date, none of these theories have been used to produce models that can accurately predict heat transfer enhancement across a wide range of applications.

Thermophysical properties of nanofluids

The thermal properties that affect conduction and convection include thermal conductivity, specific heat capacity, density and viscosity. Therefore, any heat transfer model requires accurate thermal property data. For specific heat capacity and density, it is often assumed that a weighted arithmetic mean of the components' base fluid and nanoparticle densities or specific heat capacities can provide accurate predictions of the nanofluids density or specific heat capacity. However, determining the thermal conductivity and viscosity of nanofluids is not as straightforward.

Thermal conductivity

Thermal conductivity is the most studied transport property in nanofluids, as it is commonly assumed that the significant increases in heat transfer rates observed with nanofluids are primarily caused by the increased thermal conductivity. For nanofluids, common thermal conductivity measurement methods include the transient hot-wire device [31] or the thermal property analyser [32].

Hemmat Esfe et al. [33] studied the efficiency of ferromagnetic nanoparticles suspended in ethylene glycol. They focussed on the effect of particle size, temperature and concentration to determine the thermal conductivity and viscosity of the nanofluids with volume fraction of up to 3% in the temperature range of 26–55 °C. Their results showed that the efficiency of nanofluids increased with an increase in the temperature and solid volume fraction. They also concluded that the optimum particle size depended on the flow regime (i.e. the laminar vs. turbulent).

Deepak et al. [15] developed a model to predict the thermal conductivity of nanofluids based on particle size distribution and multi-level homogenization. They mainly focused on the effects of Brownian motion, interfacial layer formation and particle clustering. Similarly, Lee et al. [12] reported that the efficiency of nanofluids was improved by increasing particle size and temperature. However, particle size variation was more noticeable than temperature variation for thermal conductivity and viscosity measurements.

Ueki et al. [34] conducted an experiment on thermophysical properties of carbon-based material nanofluid. They concluded that nanoparticle geometry and temperature influenced thermal conductivity. In addition, they found out

that carbon black and carbon nanopowder enhanced thermal conductivity by 7% and 19%, respectively.

Lenin and Roy [35] reported that the critical concentration for thermal conductivity enhancement varies with the surfactant used, possibly due to the difference in the degree of aggregation of the nanoparticles and conformation of the surfactant molecules on the nanoparticle's surface. They added that base fluids with lower thermal conductivity and dielectric constant showed larger enhancement in the thermal conductivity relative to base fluids with higher thermal conductivities.

However, despite the many positive results, Hussein et al. [36] found that the effect of volume fraction, temperature and the size diameter on friction is not clearly elaborated in the literature yet, it is vital for developing correlations of thermal properties of nanoparticles. A large number of thermal conductivity models that have been proposed (examples shown in Tables 2, 3), some of which consider the morphology of nanoparticles, assume that all particles are spherical and introduce a variety of (mostly empirical) constants. Therefore, it is difficult to know which model should be used for particular nanofluids. To demonstrate, Fig. 3 shows predictions from the classical model of Maxwell [20], that are compared to those of Buongiorno et al. [37] and Maiga et al. [38] showing significant differences. Yang et al. [39] explained that factors such as particle parameters (particle

Table 2 Summary of models for thermal conductivity of nanofluids

Author	Empirical model	Remarks
Maxwell [20]	$K_{nf} = \left[\frac{K_p + K_{bf} + 2\phi(K_p - K_{bf})}{K_p + K_{bf} + \phi(K_p - K_{bf})}\right] K_{bf}$	Volume fraction of solid spherical particles
Pak and Cho [81]	$K_{nf} = (1 + 7.74\phi)K_{bf}$	Depends on spherical and non-spherical particles
Maiga et al. [38]	$K_{nf} = (1 + 4.97\phi^2 + 2.72\phi)K_{bf}$	Considered spherical particles
Boungiorno [37]	$K_{nf} = (1 + 2.92\phi - 11.99\phi^2)K_{bf}$	Titania spherical and non-spherical particles
Mintsa et al. [82]	$K_{nf} = (1 + 1.7\phi)K_{bf}$	–

Table 3 Summary of measured thermal conductivity data of nanofluids

Author	Nanofluid	Temperature (°C)	Enhancement (%)
Ueki et al. [35]	Carbon nanopowder–water	20	19
	Carbon black–water		7
Jiang et al. [25]	Ammonia–water	120	3–12
Murshed et al. [83]	TiO_2–water	–	30–33
Parametthanuwat et al. [84]	Ag–water	20–80	80
Hafiz et al. [85]	TiO_2_water	29.4	15.87
Karimi et al. [86]	$NiFe_2O_4$_water	25–55	17.2
Mehrail et al. [87]	Nitrogen-doped graphene–water	5–40	22.15–36.78
Kole et al. [88]	Graphene–EG/water	10–70	15
Branson et al. [89]	NanoDiamond–EG	10–80	11–12

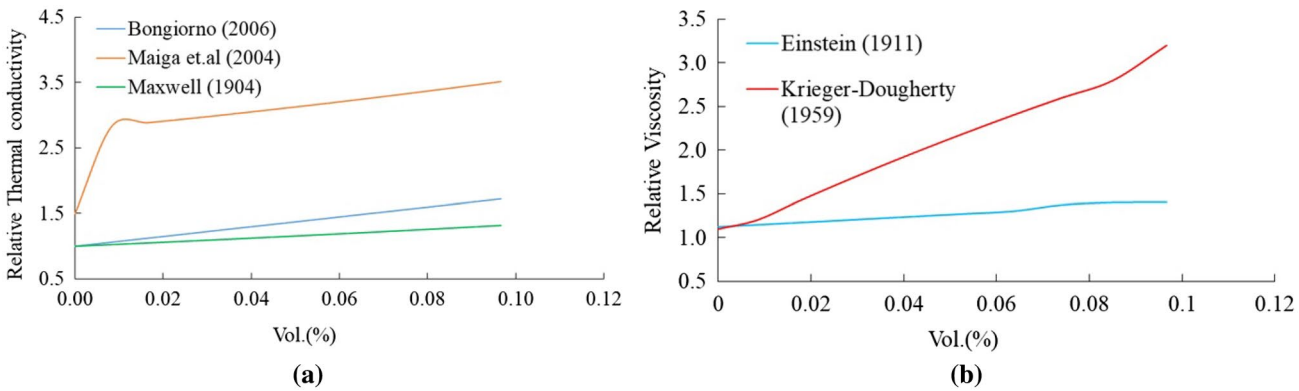

Fig. 3 The effect of nanoparticle concentration on thermal conductivity (**a**) and viscosity (**b**) using different models for carbon–water nanofluid

type, loading, size and shape) and environmental parameters (base fluid, pH value, temperature and the standing time) influence thermal conductivity. These aforementioned factors as well as preparation methods could be significant causes of the discrepancy in thermal conductivity enhancement reported in the literature.

Viscosity

In their landmark paper, Choi and Eastman [5] assumed that the addition of nanoparticles would not significantly affect the viscosity of the nanofluids; however, this is not necessarily the case. For example, Namburu et al. [40] measured the viscosity of copper oxide nanoparticles dispersed in a mixture of ethylene glycol and water and found that the viscosity of 6.12% volume concentration of the nanofluids was four times the value of the base fluid. In addition, they concluded that the viscosity of nanofluids increases with increasing amounts of nanoparticles. Similarly, Hemmat et al. [41] found that the viscosity of zinc-oxide/ethylene glycol nanofluids increased considerably with particle volume concentration significantly, as did Mariano et al. [42] and Yu et al. [43], who also made the point that heat transfer enhancement effects of the nanofluid were offset by the increased pumping power requirements.

It is also possible that the addition of nanoparticles and/or surfactants may cause the nanofluids to behave in a non-Newtonian manner, even though the base fluid may be Newtonian. While, Mariano et al. [42] reported that the viscosity of the nanofluids is 'nearly independent' of the shear rate, Kaggwa et al. [44] observed that the viscosity of carbon–water nanofluids decreased with an increase in shear rate and the viscosity of carbon–hexane nanofluids increased with the increase in shear rate. They concluded that base fluids, nanoparticle concentration as well as surfactants have a significant effect on viscosity measurements.

It can be difficult to model the viscosity of nanofluids. To illustrate, Fig. 3b shows two different viscosity models, the popular Einstein [45] model for mixture viscosity and the Krieger–Dougherty [46] model for nanofluids that produce widely differing predictions. The discrepancy between predictions is due to a number of factors. For example, Einstein [45] assumed the particles to be rigid, uncharged and devoid of any attractive forces and in low concentration, whereas Krieger–Dougherty [46] considered the full range of particle volume fractions, the influence of aggregation and the formation of interfacial layers.

As with thermal conductivity, the viscosity of nanofluids remains to be an area requiring further investigation, particularly as the effect of the surfactant on viscosity is not always taken into consideration or reported in viscosity studies (Tables 4, 5).

Potential applications of nanofluids

Solar applications

As society makes attempts to combat climate change and provide sustainable energy access for all, solar energy stands out as a primary means of reducing global carbon emissions to the Earth's atmosphere. In fact, Lewis et al. [47] pointed out that more energy from sunlight strikes the Earth in 1 h (4.3×1020 J) than all the energy consumed on the planet in

Table 5 Summary of measured viscosities of nanofluids

Author	Nanofluid	Temperature (°C)	Viscosity ratio
Namburu et al. [40]	CuO–EG	− 30 to 50	6.12
Mariano et al. [42]	Co_3O_4–EG	10–50	40
Hemmat et al. [41]	ZnO–EG	50	30
Yu et al. [43]	SiC–water Al_2O_3–water	25–70	8 6
Jiang et al. [25]	Ammonia–water	120	2–7
He et al. [93]	TiO_2–water	22	11
Ding et al. [94]	CNT–water	25–40	–
Das et al. [95]	Al_2O_3–water	20–60	45

Table 4 Summary of empirical models for viscosity of nanofluids

Author	Empirical model	Remarks
Einstein [45]	$\mu_{nf} = (1 + 2.5\varnothing)\mu_{bf}$	Infinite dilution of spherical, and rigid nanoparticles devoid of any attractive forces
Mooney [90]	$\mu_{nf} = \exp\left[\frac{2.5\phi}{1-(\phi/\phi_m)}\right]\mu_{bf}$	Einstein's model extended to apply to a suspension of finite concentration
Brinkman [91]	$\mu_{nf} = \exp\left[\frac{1}{(1-\phi)^{2.5}}\right]\mu_{bf}$	Modified Einstein model of spherical particles extended up to 4% volume concentration
Batchelor [92]	$\mu_{nf} = (1 + 2.5\phi + 6.2)\mu_{bf}$	Considered large nanoparticle concentration up to 10%
Krieger and Dougherty [46]	$\mu_{nf} = \left(1 - \frac{\phi}{\phi_m}\right)^{-\eta\phi_m}\mu_{bf}$	Considered the full range of particle volume fraction

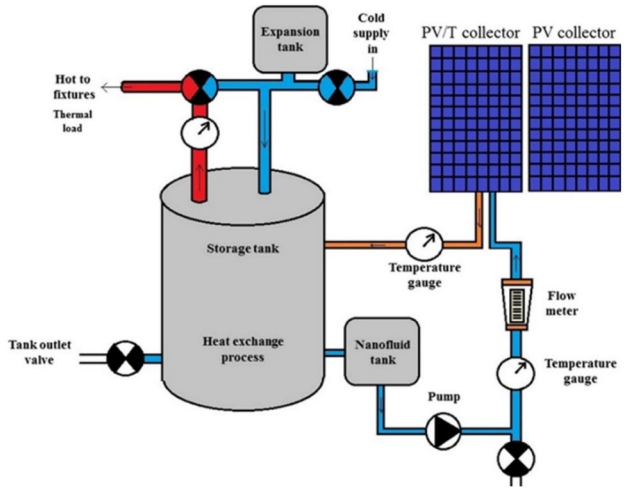

Fig. 4 A schematic diagram of the experimental rig [52]. Reproduced with permission from Elsevier

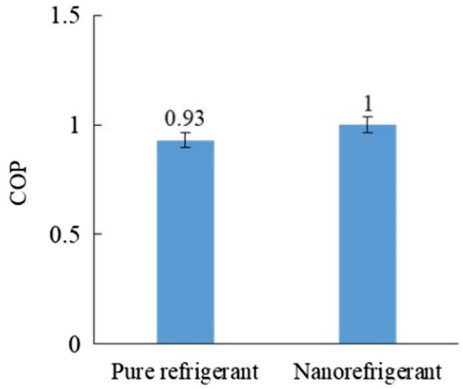

Fig. 6 Comparison of the coefficient of performance, Sanukrishna et al. [30]. Reproduced with permission from Springer

a year (4.1 × 1020 J). They added that 120,000 TW of radiation arrives at the surface of the Earth, far exceeding human needs even in the most aggressive energy demand scenarios. However, many solar capture devices suffer from relatively low collection efficiencies. Recent studies [48, 49] indicate that nanofluids can be used specifically in low optical and thermal performance solar energy conversion systems to boost their performance.

Kabeel et al. [50] investigated thermal solar water heater with Al_2O_3/H_2O nanofluid in forced convection, and their results showed an increased solar collector efficiency of 11% for 3% nanoparticle concentration. An enhancement of 21% in average heat transfer coefficient was reported by Ebrahimnia et al. [51] after conducting laminar flow convective heat transfer experiments of water-based TiO_2 nanofluid flowing through a uniformly heated tube.

Al-Waeli et al. [52] conducted an experimental investigation of SiC/water nanofluid as a working fluid for a photovoltaic/thermal (PV/T) system (Fig. 4). They concluded that the thermal conductivity was enhanced by up to 8.2% for the temperature range of 25–60 °C, and the thermal efficiency of the collector was increased by up to 100.19% compared to the efficiency when water was used as the working fluid.

Luo et al. [53] investigated thermal energy storage enhancement of a binary molten salt nanoparticles. They observed 4.71% enhancement of the total storage capacity at temperature range of 160–300 °C. Their results also indicated an improvement in specific heat of the nanosalt by 11.48%.

With these promising results, it seems likely that solar energy capture devices may be one of the first applications to have the wide spread uptake of nanofluids technology, although the stability of nanofluids remains a significant barrier.

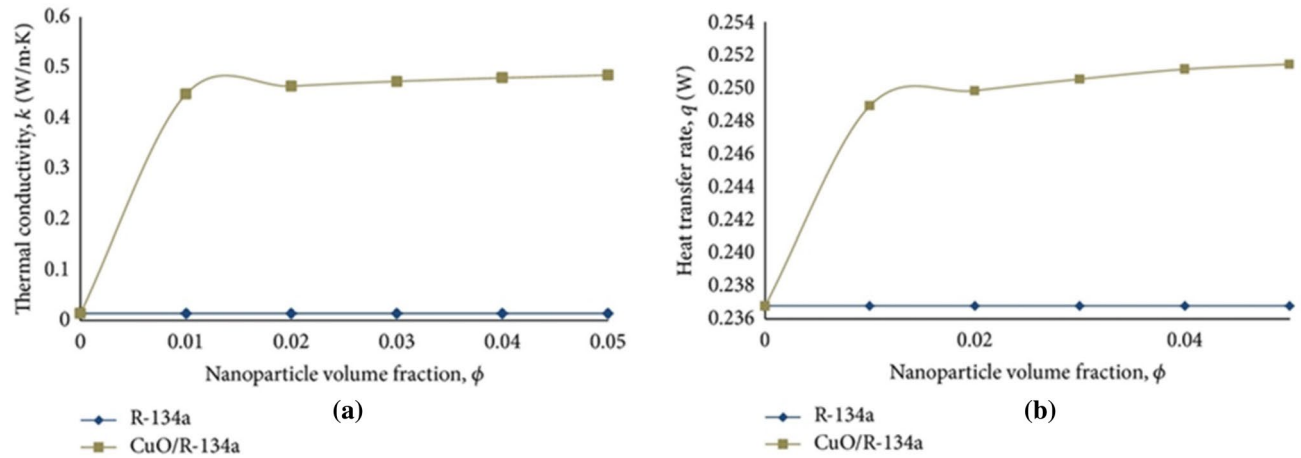

Fig. 5 Thermal conductivity (**a**) and heat transfer rate (**b**) as function of nanoparticle volume fraction, Fadhilah et al. [60]

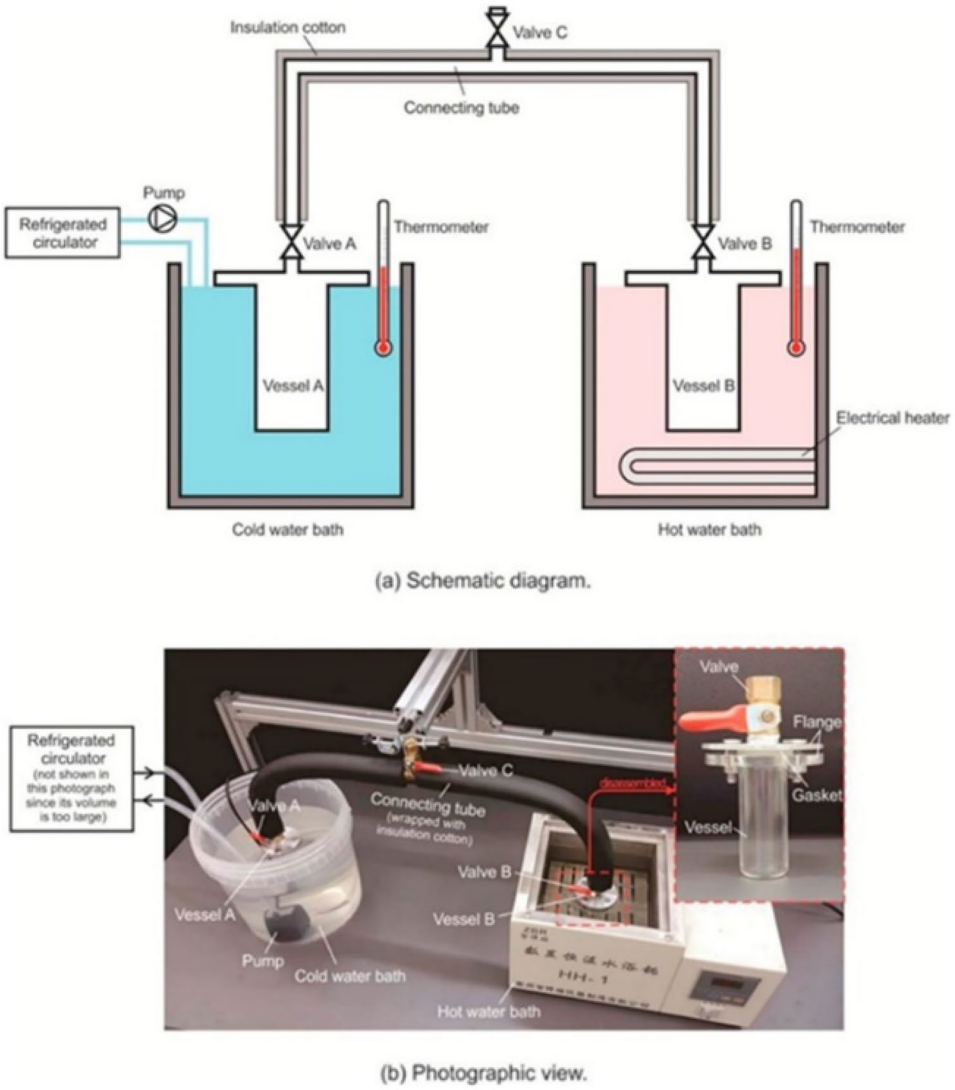

Fig. 7 Experimental setup for condensation–evaporation alternation, Lin et al. [61]. Reproduced with permission from Elsevier

Nanorefrigerants

The refrigeration industry is progressively making efforts to replace traditional refrigerants with ones that have less impact on the environment. However, studies on potential replacements such as R1234ze or R1234yf or R450A have indicated that they yield lower heat transfer performance than the refrigerants they are intended to replace [54, 55]. Therefore, the suspension of solid nanoparticles in low performing heat transfer refrigerants produces a solution termed

Table 6 A summary of additional research on nanorefrigerants

Author	Nanorefrigerant	Results
Lim et al. [58]	Al_2O_3/water–EG	Convective heat transfer coefficient enhanced by 25.4%
Redhwan et al. [96]	Al_2O_3/PAG SiO_2/PAG	Enhancement was 1.04 times higher than the base lubricant
Wang et al. [97]	Al_2O_3/R-22	Nanoparticles can enhance the heat transfer characteristic of the refrigerant, and the bubble size diminishes and moves quickly near the heat transfer surface
Jiang et al. [98]	CNT-R-113	Measured thermal conductivities of four kinds of 1.0 vol. % CNT– R113 nanorefrigerant increase to 82%, 104%, 43% and 50%, respectively
Tazarv et al. [99]	TiO_2/R-141B	Enhancement of convective heat transfer coefficient and higher vapour qualities

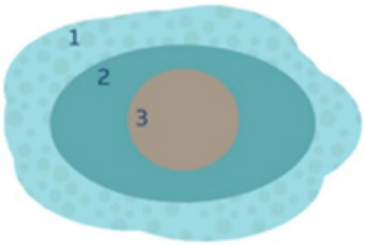

Fig. 8 Structure of nanoparticle in the base fluid. Molecules of the liquid (1) can form a specific, highly ordered layer (2) near the nanoparticle surface (3) [66]. Reproduced with permission from ACS publications

'nanorefrigerant' that can enhance refrigeration system performance. Several experimental and numerical investigations [56–59] have concluded that nanorefrigerants improve thermophysical properties, energy efficiency and the overall system performance. For instance, Fig. 5 indicates that the thermal conductivity and heat transfer of nanorefrigerant (CuO/R-134a) are higher than R-134a alone [60].

Sanukrishna et al. [30] dispersed copper oxide nanoparticles in R-134a and polyalkylene glycol. Their results revealed 12.67% increase in thermal conductivity and a flow boiling heat transfer enhancement of 37%. The coefficient of performance (COP) of nanorefrigerant was 7.5% higher than pure refrigerant as shown in Fig. 6.

However, Lin et al. [61] carried out an experiment (Fig. 7) to evaluate the degradation of a nanolubricant–refrigerant mixture during continuously alternating condensation and evaporation processes. They discovered that the mixture degrades by 28–77% after 20 cycles for nanoparticle concentrations of 0.2–1.0%, heating and temperature of 50–80 °C and 5–15 °C, respectively. They concluded that degradation would be reduced by low heating and cooling temperatures, and low nanoparticle concentrations.

Lin et al. [62] conducted an experiment using TiO_2 nanoparticles and concluded that only a small fraction of the total number of nanoparticles circulate by migration from the mixture to vapour with refrigerant dry-out process. Lee et al. [63]. concluded that nanoparticles should not be used in two-phase micro-channel heat sinks due to the clustering phenomenon that propagates upstream to fill the entire channel, thus preventing coolant from entering the heat sink and causing catastrophic failure of the cooling system.

It appears, therefore, that the use of nanofluids in two-phase flow has more technological hurdles to overcome than for single-phase applications (Table 6).

Current challenges and the future of nanofluids

Despite the promising heat transfer enhancement potential observed by many researchers, there are several barriers to widespread implementation in industrial settings. Most studies on nanofluids largely rely on commercially available nanoparticles. Nanoparticles are not cheap and there is no standard price for these particles as at present (for example, at the time of writing, 100 g of the commonly studied alumina or copper oxide nanoparticles cost $492.00 and $80.00 US dollars, respectively [64]). In addition, it seems that the properties of nanoparticles differ according to the manufacturer, which adds to the uncertainty of physical property data. Equally important, some nanomaterials are toxic and therefore extra measures taken in preparation increase production cost. Mahian et al. [65] explained that challenges such as the high cost of nanoparticles, instability and agglomeration, pumping power and pressure drop, erosion and corrosion of components make nanofluid usage commercially unattractive. However, they concluded that the general application of nanofluids is still in its infant stages and, therefore, future investigations will increase the potential applications of nanofluids.

Nanofluids experience a number of effective forces during and after suspension such as drag, thermophoresis, Brownian, Van der Waals and electric double layer forces. Interfacial layers (Fig. 8) can build bridges between nanoparticles within the base fluid molecules, reducing their effectiveness [66]. This is a major challenge with no solution cited in the

Fig. 9 Suspension and stability of nanoparticles

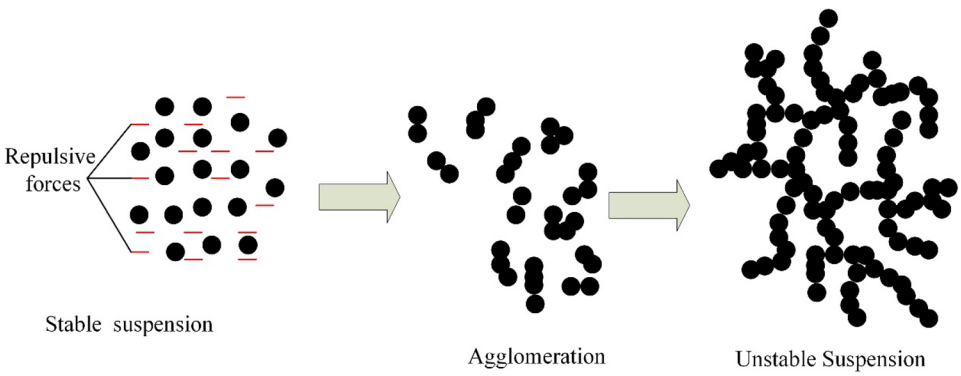

current literature, yet is one of the primary factors that many researchers think it contributes to aggregation and subsequent sedimentation [67–69].

The sedimentation of nanoparticles over time (Fig. 9) is still a major challenge [70–73] that needs to be overcome before there can be widespread uptake of nanofluids [48]. Simple methods have been proposed such as adding stabilising agents (surfactants) to the base fluid before the suspension of nanoparticles to lower the interfacial forces between the fluid molecules and the nanoparticles. However, even with the addition of surfactants there is no guarantee of permanent stability.

In short, the use of nanofluids in a wide range of applications appears to be growing steadily. However, currently it appears that material scientists and chemists perform most investigations of nanofluids characterisation, whereas thermal and mechanical engineering researchers carry the experiments on the application of nanofluids, and there is not always close collaboration or communication between the two groups, which may contribute to the agreements of results. Yu et al. [74] suggested that a systematic summary of dispersing strategies of nanofluids in thermal applications is needed to provide general guideline on the preparation and characterization of stably dispersed thermal nanofluids, and also to help bridge the gap between researchers in different disciplines.

Despite the fact that the field of nanofluids is still in the infancy, the future of nanofluids seems promising. Apart from solar and refrigeration applications, industrial and research institutions have progressively gained interest in the usage of nanofluids in other applications [75] including drug delivery for cancer treatment [76] and surface and subsurface defect sensors [77]. It is clear based on the review of the recent literature that significant efforts continue to be devoted to theoretical and experimental studies to improve the general performance and potential applications of nanofluids. In addition, efforts are being made to reduce the production costs of nanofluids by developing large-scale production methods [17, 78], and to improve the stability of nanofluids [79, 80].

Conclusion

This paper has reviewed experimental and theoretical developments of nanofluids in different applications. The challenges and the future insights about the potential usage of nanofluids have been discussed. The following major conclusions are drawn from this review study:

- There are wide ranges in heat transfer enhancements data reported by different studies.
- There is no universal formulation of nanofluids which may contribute to the wide range of physical property data reported, as well as wide ranges in price.
- Stability tests reveal there is currently no solution to the sedimentation of nanoparticles over time; however, stabilising agents, such as surfactants, have been shown to improve stability significantly.
- Nanofluids have a wide range of potential applications for heat transfer enhancement, with solar thermal, and refrigeration applications in particular currently being the focus of many studies.

Compliance with ethical standards

Conflict of interest The authors declare that they have no conflict of interest.

References

1. Khaled, A.R.A., Siddique, M., Abdulhafiz, N.I., Boukhary, A.Y.: Recent advances in heat transfer enhancements: a review report. Int. J. Chem. Eng. (2010). https://doi.org/10.1155/2010/106461
2. Léal, L., Miscevic, M., Lavieille, P., Amokrane, M., Pigache, F., Topin, F., Nogarède, B., Tadrist, L.: An overview of heat transfer enhancement methods and new perspectives: focus on active methods using electroactive materials. Int. J. Heat Mass Transf. **61**, 505–524 (2013). https://doi.org/10.1016/j.ijheatmasstransfer.2013.01.083
3. Sheikholeslami, M., Gorji-Bandpy, M., Ganji, D.D.: Review of heat transfer enhancement methods: focus on passive methods using swirl flow devices. Renew. Sustain. Energy Rev. **49**, 444–469 (2015). https://doi.org/10.1016/j.rser.2015.04.113
4. Grassi, W., Testi, D.: Heat transfer enhancement by electric fields in several heat exchange regimes. Ann. NY Acad. Sci. **1077**, 527–569 (2006). https://doi.org/10.1196/annals.1362.062
5. Choi, S.U.S., Eastman, J.A.: Enhancing thermal conductivity of fluids with nanoparticles. ASME Int. Mech. Eng. Congr. Expo. **66**, 99–105 (1995). https://doi.org/10.1115/1.1532008
6. Eastman, J.A., Choi, S.U.S., Li, S., Yu, W., Thompson, L.J.: Anomalously increased effective thermal conductivities of ethylene glycol-based nanofluids containing copper nanoparticles. Appl. Phys. Lett. **78**, 718–720 (2001). https://doi.org/10.1063/1.1341218
7. Alawi, O.A., Sidik, N.A.C., Kherbeet, A.S.: Nanorefrigerant effects in heat transfer performance and energy consumption reduction: a review. Int. Commun. Heat Mass Transf. **69**, 76–83 (2015). https://doi.org/10.1016/j.icheatmasstransfer.2015.10.009
8. Lefebvre, D., Tezel, F.H.: A review of energy storage technologies with a focus on adsorption thermal energy storage processes for

heating applications. Renew. Sustain. Energy Rev. **67**, 116–125 (2017). https://doi.org/10.1016/j.rser.2016.08.019
9. Gorji, T.B., Ranjbar, A.A.: A review on optical properties and application of nanofluids in direct absorption solar collectors (DASCs). Renew. Sustain. Energy Rev. **72**, 10–32 (2017). https://doi.org/10.1016/j.rser.2017.01.015
10. Kasaeian, A., Eshghi, A.T., Sameti, M.: A review on the applications of nanofluids in solar energy systems. Renew. Sustain. Energy Rev. **43**, 584–598 (2015). https://doi.org/10.1016/j.rser.2014.11.020
11. Khairul, M.A., Alim, M.A., Mahbubul, I.M., Saidur, R., Hepbasli, A., Hossain, A.: Heat transfer performance and exergy analyses of a corrugated plate heat exchanger using metal oxide nanofluids. Int. Commun. Heat Mass Transf. **50**, 8–14 (2014). https://doi.org/10.1016/j.icheatmasstransfer.2013.11.006
12. Lee, S.L., Saidur, R., Sabri, M.F.M., Min, T.K.: Effects of the particle size and temperature on the efficiency of nanofluids using molecular dynamic simulation. Numer. Heat Transf. A Appl. **69**, 996–1013 (2016). https://doi.org/10.1080/10407782.2015.1109369
13. Harikrishnan, A.R., Das, S.K., Agnihotri, P.K., Dhar, P.: Particle and surfactant interactions effected polar and dispersive components of interfacial energy in nanocolloids. J. Appl. Phys. (2017). https://doi.org/10.1063/1.4997123
14. Chen, H., Witharana, S., Jin, Y., Kim, C., Ding, Y.: Predicting thermal conductivity of liquid suspensions of nanoparticles (nanofluids) based on rheology. Particuology. **7**, 151–157 (2009). https://doi.org/10.1016/j.partic.2009.01.005
15. Deepak Selvakumar, R., Dhinakaran, S.: A multi-level homogenization model for thermal conductivity of nanofluids based on particle size distribution (PSD) analysis. Powder Technol. **301**, 310–317 (2016). https://doi.org/10.1016/j.powtec.2016.05.049
16. Sharma, B., Sharma, S.K., Gupta, S.M.: Preparation and evaluation of stable nanofluids for heat transfer application: a review. Exp. Therm. Fluid Sci. **79**, 202–212 (2016). https://doi.org/10.1016/j.expthermflusci.2016.06.029
17. Haddad, Z., Abid, C., Oztop, H.F., Mataoui, A.: A review on how the researchers prepare their nanofluids. Int. J. Therm. Sci. **76**, 168–189 (2014). https://doi.org/10.1016/j.ijthermalsci.2013.08.010
18. Sidik, N.A.C., Mohammed, H.A., Alawi, O.A., Samion, S.: A review on preparation methods and challenges of nanofluids. Int. Commun. Heat Mass Transf. **54**, 115–125 (2014). https://doi.org/10.1016/j.icheatmasstransfer.2014.03.002
19. Li, Y., Zhou, J., Tung, S., Schneider, E., Xi, S.: A review on development of nanofluid preparation and characterization. Powder Technol. **196**, 89–101 (2009). https://doi.org/10.1016/j.powtec.2009.07.025
20. Maxwell, J.C.: A treatise on electricity and magnetism, vol. 1. Oxford University Press, Cambridge (1873) (ISBN 13: 9780198503736)
21. Hamilton, R.L., Crosser, O.K.: Thermal conductivity of heterogeneous two-component systems. Ind. Eng. Chem. Fundam. **1**, 187–191 (1962). https://doi.org/10.1021/i160003a005
22. Carson, J.K., Lovatt, S.J., Tanner, D.J., Cleland, A.C.: Thermal conductivity bounds for isotropic, porous materials. Int. J. Heat Mass Transf. **48**, 2150–2158 (2005). https://doi.org/10.1016/J.IJHEATMASSTRANSFER.2004.12.032
23. Lee, S., Choi, S.U.-S., Li, S., Eastman, J.A.: Measuring thermal conductivity of fluids containing oxide nanoparticles. J. Heat Transf. **121**, 280 (1999). https://doi.org/10.1115/1.2825978
24. Xing, M., Yu, J., Wang, R.: Experimental investigation and modelling on the thermal conductivity of CNTs based nanofluids. Int. J. Therm. Sci. **104**, 404–411 (2016). https://doi.org/10.1016/j.ijthermalsci.2016.01.024
25. Jiang, W., Du, K., Li, Y., Yang, L.: Experimental investigation on influence of high temperature on viscosity, thermal conductivity and absorbance of ammonia-water nanofluids. Int. J. Refrig. **82**, 189–198 (2017). https://doi.org/10.1016/j.ijrefrig.2017.05.030
26. Leong, K.Y., Razali, I., Ku Ahmad, K.Z., Ong, H.C., Ghazali, M.J., Abdul Rahman, M.R.: Thermal conductivity of an ethylene glycol/water-based nanofluid with copper-titanium dioxide nanoparticles: an experimental approach. Int. Commun. Heat Mass Transf. **90**, 23–28 (2018). https://doi.org/10.1016/j.icheatmasstransfer.2017.10.005
27. Suganthi, K.S., Rajan, K.S.: Metal oxide nanofluids: review of formulation, thermo-physical properties, mechanisms, and heat transfer performance. Renew. Sustain. Energy Rev. **76**, 226–255 (2017). https://doi.org/10.1016/j.rser.2017.03.043
28. Farzaneh, H., Behzadmehr, A., Yaghoubi, M., Samimi, A., Sarvari, S.M.H.: Stability of nanofluids: molecular dynamic approach and experimental study. Energy Convers. Manag. **111**, 1–14 (2016). https://doi.org/10.1016/j.enconman.2015.12.044
29. Kang, Z., Wang, L.: Effect of thermal-electric cross coupling on heat transport in nanofluids. Energies. **10**, 123 (2017). https://doi.org/10.3390/en10010123
30. Sanukrishna, S.S., Vishnu, A.S., Jose Prakash, M.: Nanorefrigerants for energy efficient refrigeration systems. J. Mech. Sci. Technol. **31**, 3993–4001 (2017). https://doi.org/10.1007/s12206-017-0746-4
31. Duangthongsuk, W., Wongwises, S.: Measurement of temperature-dependent thermal conductivity and viscosity of TiO2-water nanofluids. Exp. Therm. Fluid Sci. **33**, 706–714 (2009). https://doi.org/10.1016/j.expthermflusci.2009.01.005
32. Kannaiyan, S., Boobalan, C., Umasankaran, A., Ravirajan, A., Sathyan, S., Thomas, T.: Comparison of experimental and calculated thermophysical properties of alumina/cupric oxide hybrid nanofluids. J. Mol. Liq. **244**, 469–477 (2017). https://doi.org/10.1016/j.molliq.2017.09.035
33. Hemmat Esfe, M., Saedodin, S., Mahian, O., Wongwises, S.: Efficiency of ferromagnetic nanoparticles suspended in ethylene glycol for applications in energy devices: effects of particle size, temperature, and concentration. Int. Commun. Heat Mass Transf. **58**, 138–146 (2014). https://doi.org/10.1016/j.icheatmasstransfer.2014.08.035
34. Ueki, Y., Aoki, T., Ueda, K., Shibahara, M.: Thermophysical properties of carbon-based material nanofluid. Int. J. Heat Mass Transf. **113**, 1130–1134 (2017). https://doi.org/10.1016/j.ijheatmasstransfer.2017.06.008
35. Lenin, R., Joy, P.A.: Studies on the role of unsaturation in the fatty acid surfactant molecule on the thermal conductivity of magnetite nanofluids. J. Colloid Interface Sci. **506**, 162–168 (2017). https://doi.org/10.1016/j.jcis.2017.07.038
36. Hussein, A.M., Kadirgama, K., Noor, M.M.: Nanoparticles suspended in ethylene glycol thermal properties and applications: an overview. Renew. Sustain. Energy Rev. **69**, 1324–1330 (2016). https://doi.org/10.1016/j.rser.2016.12.047
37. Buongiorno, J.: convective transport in nanofluids. J. Heat Transf. **128**, 240 (2006). https://doi.org/10.1115/1.2150834
38. Maïga, S.E.B., Nguyen, C.T., Galanis, N., Roy, G.: Heat transfer behaviours of nanofluids in a uniformly heated tube. Superlattices Microstruct. **35**, 543–557 (2004). https://doi.org/10.1016/j.spmi.2003.09.012
39. Yang, L., Xu, J., Du, K., Zhang, X.: Recent developments on viscosity and thermal conductivity of nanofluids. Powder Technol. **317**, 348–369 (2017). https://doi.org/10.1016/j.powtec.2017.04.061
40. Namburu, P.K., Kulkarni, D.P., Misra, D., Das, D.K.: Viscosity of copper oxide nanoparticles dispersed in ethylene glycol and water mixture. Exp. Therm. Fluid Sci. **32**, 397–402 (2007). https://doi.org/10.1016/j.expthermflusci.2007.05.001

41. Hemmat Esfe, M., Saedodin, S.: An experimental investigation and new correlation of viscosity of ZnO–EG nanofluid at various temperatures and different solid volume fractions. Exp. Therm. Fluid Sci. **55**, 1–5 (2014). https://doi.org/10.1016/j.expthermflusci.2014.02.011
42. Mariano, A., Pastoriza-Gallego, M.J., Lugo, L., Mussari, L., Piñeiro, M.M.: Co3O4 ethylene glycol-based nanofluids: thermal conductivity, viscosity and high pressure density. Int. J. Heat Mass Transf. **85**, 54–60 (2015). https://doi.org/10.1016/j.ijheatmasstransfer.2015.01.061
43. Yu, W., France, D.M., Smith, D.S., Singh, D., Timofeeva, E.V., Routbort, J.L.: Heat transfer to a silicon carbide/water nanofluid. Int. J. Heat Mass Transf. **52**, 3606–3612 (2009). https://doi.org/10.1016/j.ijheatmasstransfer.2009.02.036
44. Abdul, K., Carson, J.K., Atkin, M., Walmsley, M.: Physical properties and rheological characteristics of activated carbon nanofluids with varying filler fractions and surfactants. Appl. Mech. Mater. **884**, 58–65 (2018). https://doi.org/10.4028/www.scientific.net/AMM.884.58
45. Einstein, A.: Eine neue Bestimmung der Moleküldimensionen. Ann. Phys. **324**, 289–306 (1906). https://doi.org/10.1002/andp.19063240204
46. Krieger, I.M., Dougherty, T.J.: A mechanism for non-newtonian flow in suspensions of rigid spheres. Trans. Soc. Rheol. **3**, 137–152 (1959). https://doi.org/10.1122/1.548848
47. Lewis, N.S., Crabtree, G., Nozik, A.J., Wasielewski, M.R., Alivisatos, P.: Basic research needs for solar energy utilization. Basic Energy Sci. Work. Sol. Energy Util. (2005). https://doi.org/10.2172/899136
48. Colangelo, G., Favale, E., De Risi, A., Laforgia, D.: A new solution for reduced sedimentation flat panel solar thermal collector using nanofluids. Appl. Energy **111**, 80–93 (2013). https://doi.org/10.1016/j.apenergy.2013.04.069
49. Alim, M.A., Abdin, Z., Saidur, R., Hepbasli, A., Khairul, M.A., Rahim, N.A.: Analyses of entropy generation and pressure drop for a conventional flat plate solar collector using different types of metal oxide nanofluids. Energy Build. **66**, 289–296 (2013). https://doi.org/10.1016/j.enbuild.2013.07.027
50. Kabeel, A.E., El-Said, E.M.S., Abdulaziz, M.: Thermal solar water heater with H 2 O-Al 2 O 3 nano-fluid in forced convection: experimental investigation. Int. J. Ambient Energy **0750**, 1–9 (2015). https://doi.org/10.1080/01430750.2015.1041653
51. Ebrahimnia-Bajestan, E., Charjouei Moghadam, M., Niazmand, H., Daungthongsuk, W., Wongwises, S.: Experimental and numerical investigation of nanofluids heat transfer characteristics for application in solar heat exchangers. Int. J. Heat Mass Transf. **92**, 1041–1052 (2016). https://doi.org/10.1016/j.ijheatmasstransfer.2015.08.107
52. Al-Waeli, A.H.A., Sopian, K., Chaichan, M.T., Kazem, H.A., Hasan, H.A., Al-Shamani, A.N.: An experimental investigation of SiC nanofluid as a base-fluid for a photovoltaic thermal PV/T system. Energy Convers. Manag. **142**, 547–558 (2017). https://doi.org/10.1016/j.enconman.2017.03.076
53. Luo, Y., Du, X., Awad, A., Wen, D.: Thermal energy storage enhancement of a binary molten salt via in situ produced nanoparticles. Int. J. Heat Mass Transf. **104**, 658–664 (2017). https://doi.org/10.1016/j.ijheatmasstransfer.2016.09.004
54. Kaggwa, A., Wang, C.: Investigation of thermal-hydrodynamic heat transfer performance of R-1234ze and R-134a refrigerants in a microfin and smooth tube. J. Enhanc. Heat Transf. **23**, 221–239 (2016). https://doi.org/10.1615/JEnhHeatTransf.2017019585
55. Mendoza-Miranda, J.M., Mota-Babiloni, A., Ramírez-Minguela, J.J., Muñoz-Carpio, V.D., Carrera-Rodríguez, M., Navarro-Esbrí, J., Salazar-Hernández, C.: Comparative evaluation of R1234yf, R1234ze(E) and R450A as alternatives to R134a in a variable speed reciprocating compressor. Energy. **114**, 753–766 (2016). https://doi.org/10.1016/j.energy.2016.08.050
56. Arslan, K.: Three-dimensional computational fluid dynamics modeling of TiO2/R134a nanorefrigerant. Therm. Sci. **21**, 175–186 (2017). https://doi.org/10.2298/TSCI140425002A
57. Sharif, M.Z., Azmi, W.H., Redhwan, A.A.M., Mamat, R., Yusof, T.M.: Performance analysis of SiO2/PAG nanolubricant in automotive air conditioning system. Int. J. Refrig. **75**, 204–216 (2017). https://doi.org/10.1016/j.ijrefrig.2017.01.004
58. Lim, S.K., Azmi, W.H., Yusoff, A.R.: Investigation of thermal conductivity and viscosity of Al2O3/water–ethylene glycol mixture nanocoolant for cooling channel of hot-press forming die application. Int. Commun. Heat Mass Transf. **78**, 182–189 (2016). https://doi.org/10.1016/j.icheatmasstransfer.2016.09.018
59. Nair, V., Tailor, P.R., Parekh, A.D.: Nanorefrigerants: a comprehensive review on its past, present and future. Int. J. Refrig. **67**, 290–307 (2016). https://doi.org/10.1016/j.ijrefrig.2016.01.011
60. Fadhilah, S.A., Marhamah, R.S., Izzat, A.H.M.: Copper oxide nanoparticles for advanced refrigerant thermophysical properties: mathematical modeling. J. Nanopart. **2014**, 1–5 (2014). https://doi.org/10.1155/2014/890751
61. Lin, L., Peng, H., Chang, Z., Ding, G.: Experimental research on degradation of nanolubricant–refrigerant mixture during continuous alternation processes of condensation and evaporation. Int. J. Refrig. **76**, 97–108 (2017). https://doi.org/10.1016/j.ijrefrig.2016.12.021
62. Lin, L., Peng, H., Chang, Z., Ding, G.: Experimental investigation on TiO2 nanoparticle migration from refrigerant–oil mixture to lubricating oil during refrigerant dryout. Int. J. Refrig. **77**, 75–86 (2017). https://doi.org/10.1016/j.ijrefrig.2017.02.026
63. Lee, J., Mudawar, I.: Assessment of the effectiveness of nanofluids for single-phase and two-phase heat transfer in micro-channels. Int. J. Heat Mass Transf. **50**, 452–463 (2007). https://doi.org/10.1016/j.ijheatmasstransfer.2006.08.001
64. Amorphous Products | Nanoscale Products | Nanopowder | Nanoparticles—Aluminum Oxide Powder (gamma, 99.5%(metal basis), ~ 80 nm). https://www.nanoamor.com/inc/sdetail/50582. Accessed Dec 2017
65. Mahian, O., Kianifar, A., Kalogirou, S.A., Pop, I., Wongwises, S.: A review of the applications of nanofluids in solar energy. Int. J. Heat Mass Transf. **57**, 582–594 (2013). https://doi.org/10.1016/j.ijheatmasstransfer.2012.10.037
66. Sizochenko, N., Syzochenko, M., Gajewicz, A., Leszczynski, J., Puzyn, T.: Predicting physical properties of nanofluids by computational modeling. J. Phys. Chem. C **121**, 1910–1917 (2017). https://doi.org/10.1021/acs.jpcc.6b08850
67. Pal, R.: A novel method to determine the thermal conductivity of interfacial layers surrounding the nanoparticles of a nanofluid. Nanomaterials. **4**, 844–855 (2014). https://doi.org/10.3390/nano4040844
68. Machrafi, H., Lebon, G.: The role of several heat transfer mechanisms on the enhancement of thermal conductivity in nanofluids. Contin. Mech. Thermodyn. **28**, 1461–1475 (2016). https://doi.org/10.1007/s00161-015-0488-4
69. Pinto, R.V., Fiorelli, F.A.S.: Review of the mechanisms responsible for heat transfer enhancement using nanofluids. Appl. Therm. Eng. **108**, 720–739 (2016). https://doi.org/10.1016/j.applthermaleng.2016.07.147
70. Aref, A.H., Entezami, A.A., Erfan-Niya, H., Zaminpayma, E.: Thermophysical properties of paraffin-based electrically insulating nanofluids containing modified graphene oxide. J. Mater. Sci. **52**, 2642–2660 (2017). https://doi.org/10.1007/s10853-016-0556-6
71. Chen, W., Zou, C., Li, X., Li, L.: Experimental investigation of SiC nanofluids for solar distillation system: stability, optical properties and thermal conductivity with saline water-based

fluid. Int. J. Heat Mass Transf. **107**, 264–270 (2017). https://doi.org/10.1016/j.ijheatmasstransfer.2016.11.048
72. Chen, L., Xie, H., Li, Y., Yu, W.: Nanofluids containing carbon nanotubes treated by mechanochemical reaction. Thermochim. Acta **477**, 21–24 (2008). https://doi.org/10.1016/j.tca.2008.08.001
73. Timofeeva, E.V., Moravek, M.R., Singh, D.: Improving the heat transfer efficiency of synthetic oil with silica nanoparticles. J. Colloid Interface Sci. **364**, 71–79 (2011). https://doi.org/10.1016/j.jcis.2011.08.004
74. Yu, F., Chen, Y., Liang, X., Xu, J., Lee, C., Liang, Q., Tao, P., Deng, T.: Dispersion stability of thermal dispersion stability of thermal nanofluids. Prog. Nat. Sci. Mater. Int. **27**, 531–542 (2017). https://doi.org/10.1016/j.pnsc.2017.08.010
75. Bhardwaj, V., Kaushik, A.: Biomedical applications of nanotechnology and nanomaterials. Micromachines. **8**, 298 (2017). https://doi.org/10.3390/mi8100298
76. Yang, D., Yang, F., Hu, J., Long, J., Wang, C., Fu, D., Ni, Q.: Hydrophilic multi-walled carbon nanotubes decorated with magnetite nanoparticles as lymphatic targeted drug delivery vehicles. Chem. Commun. (2009). https://doi.org/10.1039/b908012k
77. Mahendran, V., Philip, J.: Naked eye visualization of naked eye visualization of defects in ferromagnetic materials and components. NDT E Int. **60**, 100–109 (2013). https://doi.org/10.1016/j.ndteint.2013.07.011
78. Gharehkhani, S., Shirazi, S.F.S., Jahromi, S.P., Sookhakian, M., Baradaran, S., Yarmand, H., Oshkour, A.A., Kazi, S.N., Basirun, W.J.: Spongy nitrogen-doped activated carbonaceous hybrid derived from biomass material/graphene oxide for supercapacitor electrodes. RSC Adv. **5**, 40505–40513 (2015). https://doi.org/10.1039/c5ra01525a
79. Devendiran, D.K., Amirtham, V.A.: A review on preparation, characterization, properties and applications of nanofluids. Renew. Sustain. Energy Rev. **60**, 21–40 (2016). https://doi.org/10.1016/j.rser.2016.01.055
80. Fuskele, V., Sarviya, R.M.: Recent developments in nanoparticles synthesis, preparation and stability of nanofluids. Mater. Today Proc. **4**, 4049–4060 (2017). https://doi.org/10.1016/j.matpr.2017.02.307
81. Pak, B.C., Cho, Y.I.: Hydrodynamic and heat transfer study of dispersed fluids with submicron metallic oxide particles. Exp. Heat Transf. **11**, 151–170 (1998). https://doi.org/10.1080/08916159808946559
82. Mintsa, H.A., Roy, G., Nguyen, C.T., Doucet, D.: New temperature dependent thermal conductivity data for water-based nanofluids. Int. J. Therm. Sci. **48**, 363–371 (2009). https://doi.org/10.1016/j.ijthermalsci.2008.03.009
83. Murshed, S.M.S., Leong, K.C., Yang, C.: Enhanced thermal conductivity of TiO2—water based nanofluids. Int. J. Therm. Sci. **44**, 367–373 (2005). https://doi.org/10.1016/j.ijthermalsci.2004.12.005
84. Parametthanuwat, T., Bhuwakietkumjohn, N., Rittidech, S., Ding, Y.: Experimental investigation on thermal properties of silver nanofluids. Int. J. Heat Fluid Flow **56**, 80–90 (2015). https://doi.org/10.1016/j.ijheatfluidflow.2015.07.005
85. Ali, H.M., Arshad, W.: Thermal performance investigation of staggered and inline pin fin heat sinks using water based rutile and anatase TiO2 nanofluids. Energy Convers. Manag. **106**, 793–803 (2015). https://doi.org/10.1016/j.enconman.2015.10.015
86. Karimi, A., Sadatlu, M.A.A., Saberi, B., Shariatmadar, H., Ashjaee, M.: Experimental investigation on thermal conductivity of water based nickel ferrite nanofluids. Adv. Powder Technol. **26**, 1529–1536 (2015). https://doi.org/10.1016/j.apt.2015.08.015
87. Mehrali, M., Sadeghinezhad, E., Latibari, S.T., Mehrali, M., Togun, H., Zubir, M.N.M., Kazi, S.N., Metselaar, H.S.C.: Preparation, characterization, viscosity, and thermal conductivity of nitrogen-doped graphene aqueous nanofluids. J. Mater. Sci. **49**, 7156–7171 (2014). https://doi.org/10.1007/s10853-014-8424-8
88. Kole, M., Dey, T.K.: Investigation of thermal conductivity, viscosity, and electrical conductivity of graphene based nanofluids. J. Appl. Phys. (2013). https://doi.org/10.1063/1.4793581
89. Branson, B.T., Beauchamp, P.S., Beam, J.C., Lukehart, C.M., Davidson, J.L.: Nanodiamond nanofluids for enhanced thermal conductivity. ACS Nano **7**, 3183–3189 (2013). https://doi.org/10.1021/nn305664x
90. Mooney, M.: The viscosity of a concentrated suspension of spherical particles. J. Colloid Sci. **6**, 162–170 (1951). https://doi.org/10.1016/0095-8522(51)90036-0
91. Brinkman, H.C.: The viscosity of concentrated suspensions and solutions. J. Chem. Phys. **20**, 571–571 (1952). https://doi.org/10.1063/1.1700493
92. Batchelor, G.K.: The effect of Brownian motion on the bulk stress in a suspension of spherical particles. J. Fluid Mech. **83**, 97 (1977). https://doi.org/10.1017/S0022112077001062
93. He, Y., Jin, Y., Chen, H., Ding, Y., Cang, D., Lu, H.: Heat transfer and flow behaviour of aqueous suspensions of TiO2 nanoparticles (nanofluids) flowing upward through a vertical pipe. Int. J. Heat Mass Transf. **50**, 2272–2281 (2007). https://doi.org/10.1016/j.ijheatmasstransfer.2006.10.024
94. Ding, Y., Alias, H., Wen, D., Williams, R.A.: Heat transfer of aqueous suspensions of carbon nanotubes (CNT nanofluids). Int. J. Heat Mass Transf. **49**, 240–250 (2006). https://doi.org/10.1016/j.ijheatmasstransfer.2005.07.009
95. Das, S.K., Putra, N., Roetzel, W.: Pool boiling characteristics of nano-fluids. Int. J. Heat Mass Transf. **46**, 851–862 (2003). https://doi.org/10.1016/S0017-9310(02)00348-4
96. Redhwan, A.A.M., Azmi, W.H., Sharif, M.Z., Zawawi, N.N.M.: Thermal conductivity enhancement of Al2O3 and SiO2 nanolubricants for application in automotive air conditioning (AAC) system A.A.M. MATEC Web Conf. **90**, 01051 (2017). https://doi.org/10.1016/j.ijrefrig.2016.06.025
97. Wang, K.J., Ding, G.L., Jiang, W.T.: Nano-scale thermal transporting and its use in engineering. In: Proceedings of the 4th Symposium on Refrigeration and Air Condition, pp. 66–75 (2006)
98. Jiang, W., Ding, G., Peng, H.: Measurement and model on thermal conductivities of carbon nanotube nanorefrigerants. Int. J. Therm. Sci. **48**, 1108–1115 (2009). https://doi.org/10.1016/j.ijthermalsci.2008.11.012
99. Tazarv, S., Saffar-Avval, M., Khalvati, F., Mirzaee, E., Mansoori, Z.: Experimental investigation of saturated flow boiling heat transfer to TiO_2/R141b nanorefrigerant. Exp. Heat Transf. (2016). https://doi.org/10.1080/08916152.2014.973976

Available online at www.sciencedirect.com

ScienceDirect

Materials Today: Proceedings 18 (2019) 510–519

materialstoday: PROCEEDINGS

www.materialstoday.com/proceedings

AEM 2018

The effect of surfactants on viscosity and stability of activated carbon, alumina and copper oxide nanofluids.

Abdul Kaggwa[a*], James K. Carson[b], Martin Atkins[c] and Michael Walmsley[d]

School of Engineering, Faculty of Science and Engineering, University of Waikato, Private Bag 3105, Hamilton 3240, New Zealand

Abstract

In the present study, the effect of using various surfactants on viscosity measurements and stability of nanofluids that can be used in heat transfer systems as working fluid have been investigated. Measurements were conducted on nanofluids containing activated carbon (C), alumina (Al_2O_3) and copper oxide (CuO) in water (H_2O) and ethylene glycol (EG) as base fluids. The results revealed that Cetyltrimethyl ammonium bromide (CTAB) increased the viscosity of C/EG and Al_2O_3/H_2O nanofluids with an enhancement percentage of 67.5% and 261.3% respectively. Arabinogalactan (ARB) increased the viscosity of C/H_2O nanofluids with an enhancement percentage of 81%. CTAB and ARB created a shear thickening behaviour for CuO/H_2O nanofluids whereas sodium lauryl sulphate (SDS) and sodium dodecyl benzene sulfonate (SDBS) were independent of shear rate. The addition of ARB to C/H_2O and CuO/H_2O nanofluids presented the best stability that kept nanoparticles in suspension for more than 20 days compared to other surfactants used.

Selection and peer-review under responsibility of the scientific committee of the Third International Conference on Advanced Energy Materials.

Keywords: Nanofluids; Surfactant ; Viscosity; Stability

1. Introduction

The suspension of nanoparticles into base fluids is increasingly becoming a common practice in various fields of science including medical and heat transfer applications [1]. One use of nanoparticles is to enhance the thermal conductivity of conventional heat transfer fluids such as water, ethylene glycol and oil. However, the addition of nanoparticles to the base fluid also tend to increase the viscosity, which is often undesirable [2-5]. In addition, it is difficult to maintain the stability of the nanofluids due to sedimentation of the nanoparticles that arise because of the difference in densities between solid particles and liquid molecules [6]. For this reason, a number of studies have investigated the use of surfactants to improve nanofluid stability. Das et al. [7] reported that sodium dodecyl benzene sulfonate (SDBS) offered the best stability compared to cetyltrimethyl ammonium bromide (CTAB) and sodium

Selection and peer-review under responsibility of the scientific committee of the Third International Conference on Advanced Energy Materials.

lauryl sulphate (SDS) in Al_2O_3/H_2O nanofluids based on the dynamic light scattering technique that showed reduced particle clustering and polydispersity index of the suspension. Choi et al. [8] also concluded that SDBS provided better stability compared to CTAB and SDS for water-multi walled carbon nanotubes nanofluids when used in solar thermal receivers. Manilo et al. [9] claimed that the addition of CTAB above critical micelle concentrations (CMC) created a mixture of primary and weak secondary aggregates that significantly affected the stability of hybrid carbon nanotubes and water nanofluid. Similarly, an article argued that CTAB provided better stability than SDS for relatively high volume of particle concentration [10].

It has been concluded from previous studies [5, 4] that the suspension of nanoparticles leads to increased viscosity. Although this may be true, there is insufficient information about the effect of surfactant on viscosity measurements. Recently published articles only address the impact of surfactants on nanofluids stability [8, 10, 11] with no or very little information on viscosity measurements. Therefore, this study focuses mainly on the effect of using arabinogalactan (ARB), sodium lauryl sulphate (SDS), Cetyltrimethyl ammonium bromide (CTAB) and Sodium dodecyl benzene sulfonate (SDBS) as surfactants on viscosity measurements. In addition, stability of nanofluids using varying surfactants has been studied.

2. Experimental measurements

2.1. Surfactant selection

Beside the fact that nanoparticles have high densities than most base fluids, suspended nanoparticles experience a number of effective forces during and after suspension such as drag, thermophoresis, Brownian, Van der Waals and electric double layer forces [12]. According to Yu et al. [13] repulsive forces exists between nanoparticles with the same positive or negative surface charges. As a result, suspended nanoparticles undergo processes from being stable to unstable as shown in Fig. 1 that as time elapse, repulsive potential between charged surfaces of nanoparticles are weakened which later creates agglomerates and sedimentation in the end. Nanofluid instability is a limiting reason why they have not received widespread use in heat transfer applications [14].

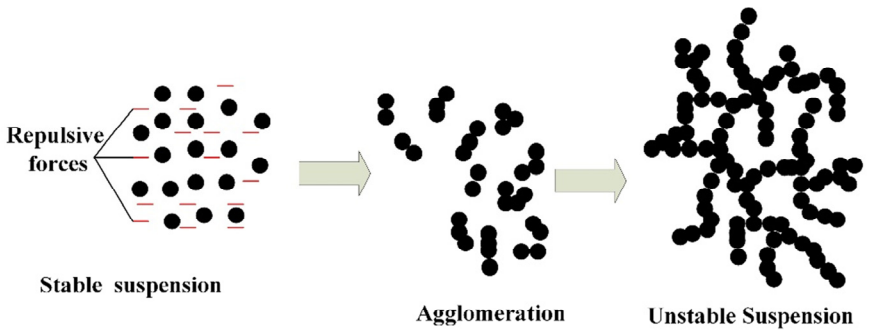

Fig. 1 Instability processes of suspended nanoparticles

Surfactants are capable of improving the stability of nanofluids because they reduce the interfacial tension between the base fluid molecules and the suspended nanoparticles [9]. Therefore, efficient solubilizers, lower toxicity and cost effective surfactants including SDS, CTAB, SDBS and ARB [15, 10] were investigated as stabilizing agents and their physiochemical properties are summarized in Table 1.

Table 1. Physiochemical properties of surfactants

Surfactant	*Class*	*Formula*	*appearance*	*Molar weight (kg/mol)*	*Melting point (°C)*
ARB	-	$C_{20}H_{36}O_{14}$	Creamy- granular	0.500	200 - 204
SDBS	anionic	$CH_3(CH_2)_{11}C_6H_4SO_3Na$	Off white-light yellow flakes	0.348	204 - 207
CTAB	cationic	$C_{19}H_{42}BrN$	White powder	0.364	237 - 243
SDS	anionic	$NaC_{12}H_{25}SO_4$	Cream-coloured solid	0.288	206

2.2. Nanofluids preparations

In this research, activated carbon nano-powder, Copper oxide and alumina were used and their physical characteristics are summarised in Table 2. The two-step method of nanofluids preparation was employed [16]. The base fluids were ethylene glycol or water.

Table 2. Physical characteristics of nanoparticles.

Nanomaterial	*Average particle size (nm)*	*Bulky density ($kg.m^{-3}$)*	*Specific surface area ($m^2.kg^{-1}$)*	*Purity (%)*
Activated carbon	50	3020 - 3300	500000	99.5
Copper Oxide	30 - 50	790	18000	99.0
Alumina	20 - 30	3890	180000	99.97

Prior to suspension, the mass of base fluid and nanoparticles was measured to obtain volume concentration of the nanoparticles as illustrated in Table 3. Subsequently, 2 g of surfactant was added followed by stirring and ultrasonication with Qsonica (Q500) Sonicator. Ultrasonication causes mechanical vibration that creates microscopic bubbles. The bubbles cycle into the solution, collapse and breaks apart the cells thus forming homogenous and stable solutions. Nanofluids were kept under ultra-sonication for 1 hour with the micro-tip probe amplitude and the pulse set to 20% and 10 seconds respectively, based on recommendations of Lin et al. [17].

Table 3. Concentration of nanoparticles in nanofluids

Nanofluid	*Nanoparticles (kg)*	*Volume of concentration (vol. %)*
C/H_2O	0.002	1.45
C/EG	0.002	1.59
CuO/H_2O	0.002	0.75
CuO/EG	0.002	0.82
Al_2O_3/H_2O	0.002	1.23
Al_2O_3/EG	0.002	1.35

2.3. Viscosity measurements

Viscosity measurements were conducted using Anton Paar digital viscometer (DV - 1P) Fig. 2. This viscometer measured the torque created by the rotation of a spindle at constant speed from which dynamic viscosity is obtained as a value proportional to the measured torque [18].

Prior to starting measurements, the flow jacket that housed the sample chamber was connected to the water bath flow loop to maintain steady temperatures of the nanofluids in question. The low viscosity adapter 'LCP spindle' was selected throughout the entire investigation because it allows accurate measurements and most importantly where small quantities are considered as suggested from the user's manual [18]. The spindle was lowered into the sample chamber and the viscometer was perpendicularly levelled for accurate measurements.

The water bath was set at 25 °C, the viscometer spindle was set to rotational speeds that ranged from 30 to 100 revolutions per minute (rpm). The maximum viscosity that can be measured by this viscometer with the LCP spindle settings is 20, 12 and 6 mPa.s for 30, 50 and 100 rpm respectively. The viscometer accuracy and repeatability of the full-scale range of the measurements values was ± 1% and ± 0.2% respectively [user manual]. For each viscosity

measurement three viscosity readings were recorded with a minute time interval between each reading. The viscosity measurements were compared to the viscosity of distilled water, as measured by the viscometer. The final viscosity '$\mu_{relative}$' was reduced using Eqs.1 from which water was used as a point of reference.

$$\mu_{relative} = \frac{\mu_{measured}}{\mu_{water}} \tag{1}$$

Shear rate 'γ'was calculated using Eqs. 2 and 3. Where 'ω' and 'r' are the angular velocity and the radius of the container and spindle denoted with subscripts 'c' and 's' respectively.

$$\omega = 2\pi n \tag{2}$$

$$\dot{\gamma} = \frac{\omega r_s}{r_c - r_s} \tag{3}$$

The enhancement percentage '$E_{\%}$' was calculated using Eqs. 4. Where 'μ_a' is the average relative viscosity of nanofluid with surfactant divided by 'μ_b' relative viscosity of nanofluid with no surfactant.

$$\mathrm{E}_{\%} = 100\left(\frac{\mu_a}{\mu_b} - 1\right) \tag{4}$$

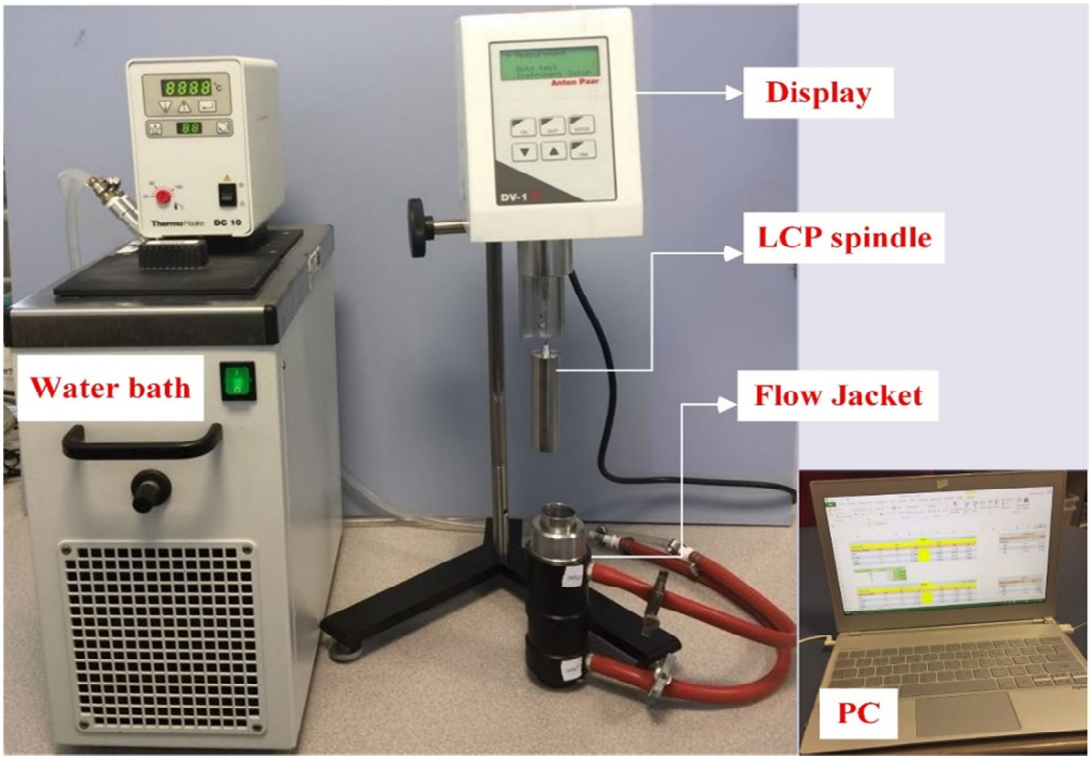

Fig. 2 Viscometer and water bath.

3. Results and discussion

3.1. Viscosity

The viscosity of nanofluids with EG as a base fluid exceeded the range that the viscometer can measure specifically at speeds above 30 rpm. Figure 3 shows the viscosities of nanofluids with the combinations of three nanoparticles and four surfactants, along with control samples that did not have surfactant, measured at 30 rpm. The most significant increase in viscosity due to the presence of surfactants was for SDS and CTAB surfactants in C/EG nanofluid with an enhancement percentage of 63% and 67.5% respectively. ARB yielded the least enhancement percentage of 11.6% and 16.8% for C/EG and Al_2O_3/EG nanofluids respectively. SDS registered the least enhancement percentage of 6.5% for CuO/EG nanofluid.

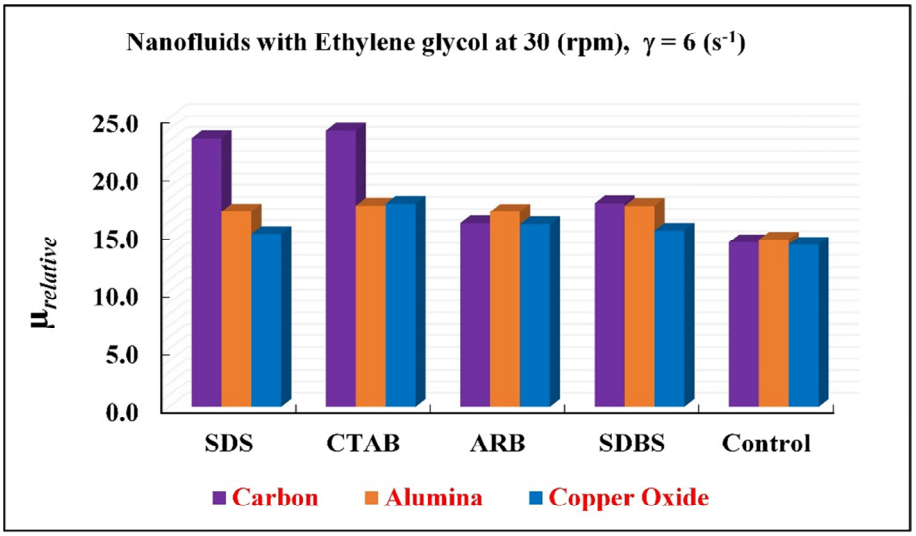

Fig. 3 The effect of surfactants on viscosity measurements of nanofluids with EG as base fluid at T=25°C.

Figure 4a demonstrates that the viscosity of C/H_2O nanofluid was independent of shear rate regardless of any surfactant used. However, ARB showed a remarkable increase in viscosity with an enhancement percentage of 81.5% compared to nanofluid with no surfactant (control). Moreover, Fig. 4b illustrates that the addition of CTAB and ARB created a shear thickening behaviour for CuO/H_2O nanofluids where as SDS and SDBS seemed to be independent of shear rate. Equally important, a slight increase of 15% in viscosity of CuO/H_2O nanofluid with SDS compared to control sample was noticed.

CTAB increased the viscosity of Al_2O_3/H_2O nanofluid with a percentage enhancement of 251.3% (Fig. 4c). In the same line of thought, a shear thinning behaviour can be clearly noticed specifically at low values of shear rate between 5 to 10 s^{-1}. It is known that cationic surfactants like CTAB possess positive charges on their hydrophilic end that interact with nanoparticles. Therefore, this observation might have occurred due to the breakdown of aggregated nanoparticles. Comparatively, the viscosity of Al_2O_3/H_2O nanofluid with SDS, ARB and SDBS was independent of shear rate.

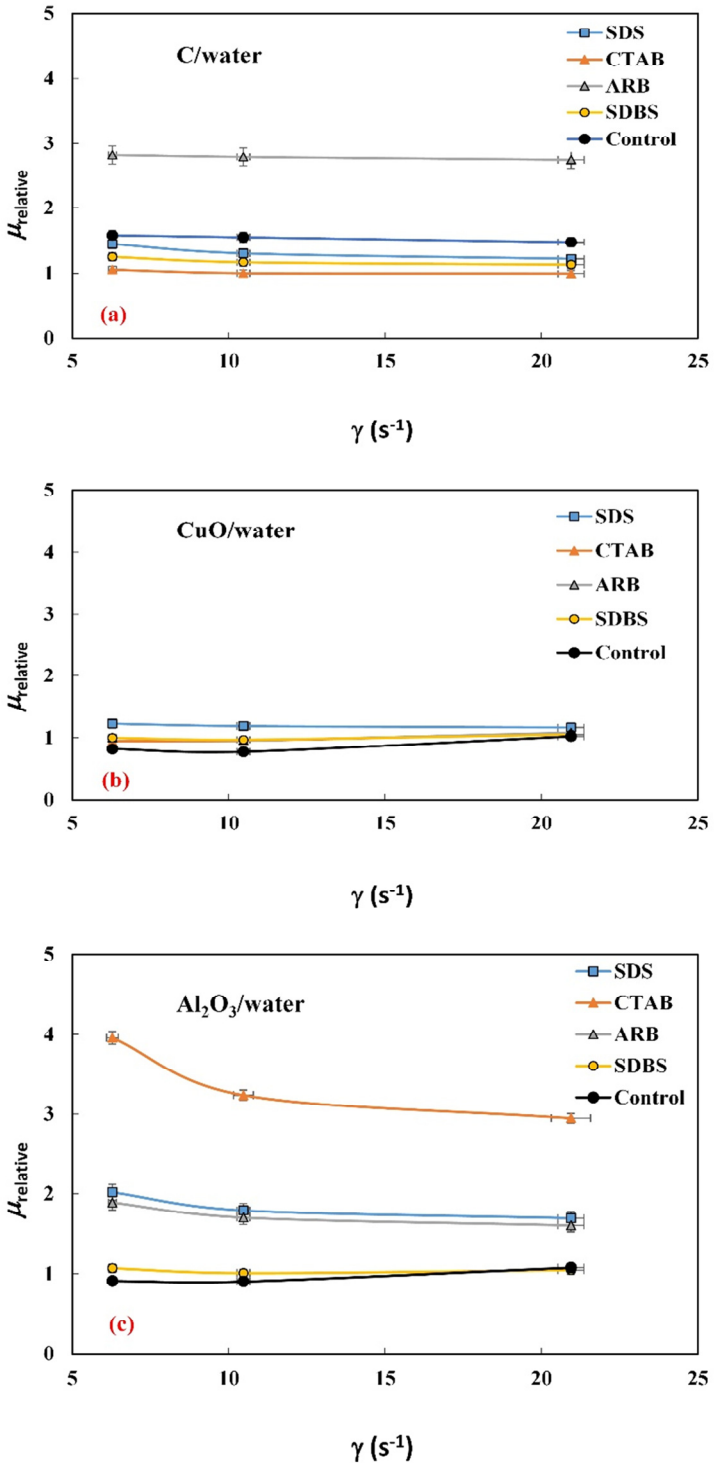

Fig. 4 Viscosity measurements as a function of shear rate for nanofluids with water as base fluid at T=25 °C.

SDBS presented the best results for C/H_2O, Al_2O_3/H_2O and CuO/H_2O nanofluids because the results in Fig. 4 indicate that the shear rate deformation characteristics are linear and confirms a Newtonian behaviour of nanofluids. Comparatively, Fig. 4c illustrates that CTAB created a non-Newtonian behaviour for Al_2O_3/H_2O nanofluid. ARB and SDS in Fig. 4 showed that nanofluids were Newtonian in nature. Therefore, based on the results presented in this study it can be concluded that various surfactants have an impact on rheological behaviour of nanofluids. For instance, in fluid mechanical applications such as heat transfer, Newtonian nanofluids would be a priority for convective heat transfer accountability.

3.2. Stability of nanofluids

Several approaches have been used to evaluate the stability of nanofluids. However, these methods differ from one another based on the nature of the nanofluids. For instance, the Zeta-potential method determines stability by measuring how fast suspended nanoparticles move in an applied electric field. However, nanocomposix [19] points out that this technique cannot apply to highly conductive nanofluids, because the conductive ions movement leads to electrode polarization and degradation.

Other methods include UV-vis spectroscopy and Electron microscopy. However, Ghadimi et al.[20] highlighted that UV-vis spectroscopy method is unsuitable for highly concentrated or dark coloured nanofluids because high concentrated nanofluids leads to high absorbance of incident light and diminish the intensity of scattered light which reduces the quality of data. Celine [21] pointed out that Electron microscopy approach provides relevant data on morphology of nanoparticle, particle size and insufficient information on stability. In addition, accurate measurements depend on the contrast of the sample relative to the background.

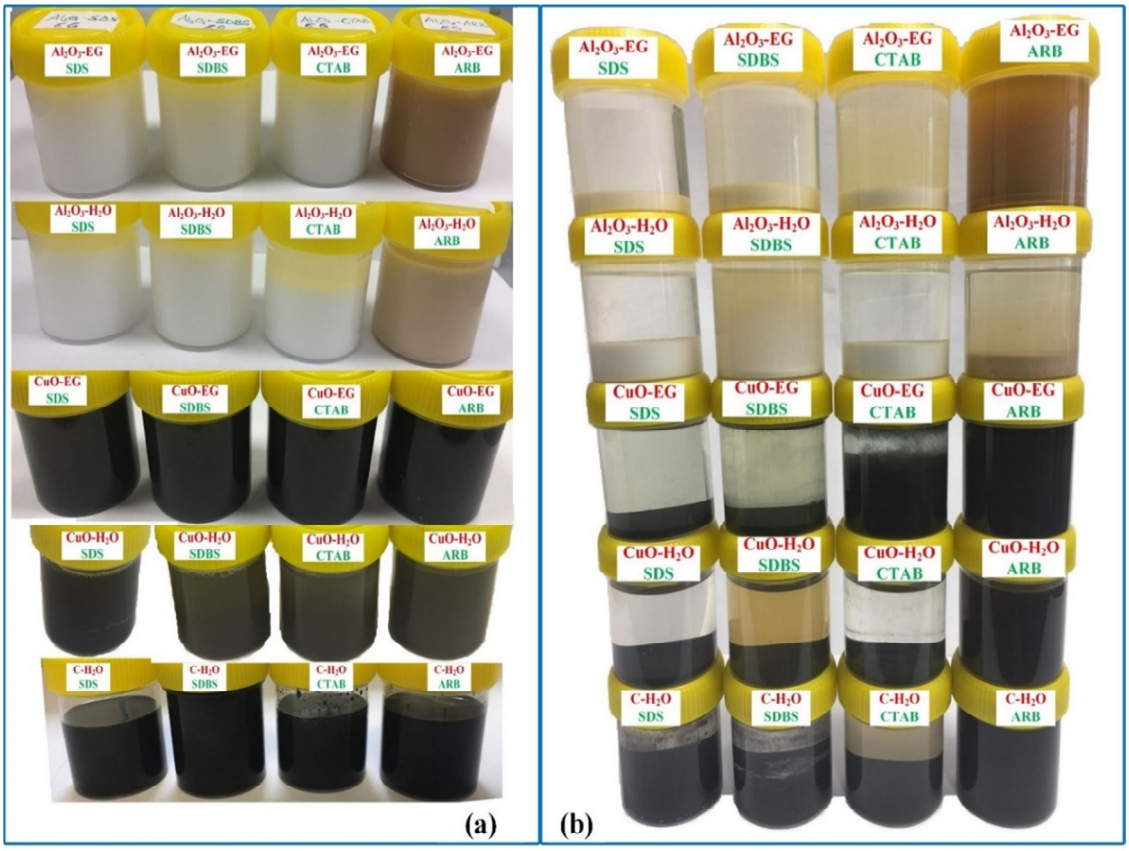

Fig. 5 samples of nanofluid with varying surfactants immediately after preparation (a) and (b) after 30 days.

Many experts [22-24] now believe that the sedimentation approach is more useful because it is simple, inexpensive and provides accurate visual results using photographs compared to other techniques. Stability is determined by measuring the height of a supernatant as a function of settling time. For this reason, nanofluid stability was determined qualitatively by monitoring and observing sedimentation of nanoparticles of sample bottles containing nanofluids for 28 days. Photographs were taken at regular intervals to compare the height of a supernatant as a function of settling time.

Regardless of any surfactant added to nanofluids, there is no guarantee for permanent stability of nanofluids. However, some surfactants can sustain stability of nanofluids for a few days. For instance, Fig. 6a and 6b illustrates that ARB as a surfactant maintained stability of C/H_2O and CuO/EG nanofluids for more than 20 days compared to other surfactants. This might have happened because the structural nature of ARB allows complete solubility, excellent dispersant and stability over a wide range of concentrations [25, 26]. Equally important, Shin et al. [27] pointed out that neutral surfactants exhibits much stronger principal orbital interactions with the surfaces of nanoparticles which may enhance the binding and surface coverage of nanoparticles to molecules. On that ground, we believe that the interaction of anionic (SDBS and SDS) and cationic (CTAB) structural nature of SDBS and SDS surfactant with surfaces of C/H_2O and CuO/EG nanofluids might have been weakened thus leading to short stability of nanofluids.

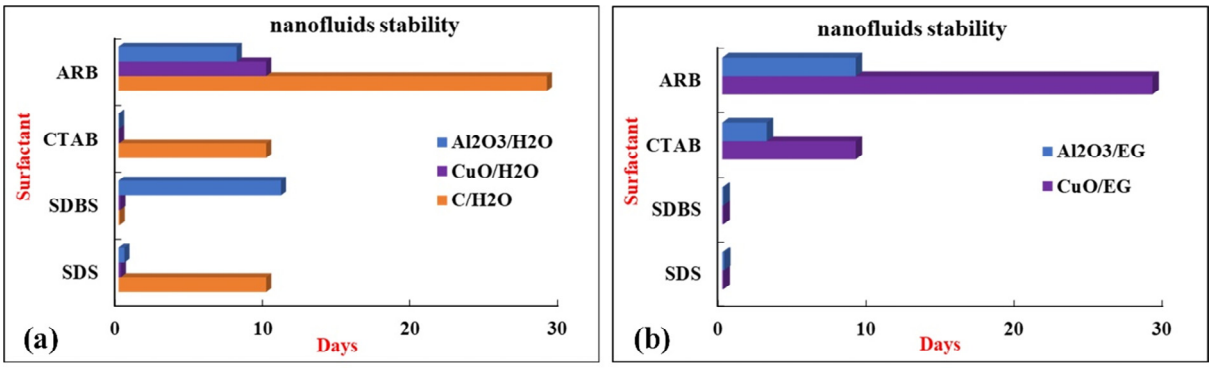

Fig. 6 stability timeline of nanofluids with water (a) and ethylene glycol (b) as base fluid

In Fig. 6a, CTAB and SDS sustained stability of C/H_2O nanofluid for 9 days better than SDBS that lasted for only 2 hours. Hakiki et al. [28] puts it that when the surface coverage by the surfactants increases, the surface free energy decreases and the surfactants start aggregating into micelles. Based on this argument, we can conclude that the SDBS hydrophobic contact area with liquid molecules decreased within 2 hours, which later reduced the free energy of the nanofluid. Surprisingly, SDBS maintained stability of Al_2O_3/H_2O nanofluid for 11 days compared to CuO/H_2O and C/H_2O nanofluids stability that lasted for 3 and 2 hours respectively. It has been suggested that surface tension increase as nanoparticle size increase [29, 30]. For this reason, the time that nanoparticles stayed in suspension might have been reduced because of the difference in the average particle size of Cuo and C compared to Al_2O_3 as demonstrated in Table 2. The adsorbed surfactant is degraded by the increased attractive charges between particles, thereby reducing the time nanoparticles stay in suspension.

4. Conclusion

This paper has investigated the impact of surfactants on viscosity and stability measurements of activated carbon, alumina and copper oxide nanofluids. The main conclusion is that SDBS presented the best results for C/H_2O, Al_2O_3/H_2O and CuO/H_2O nanofluids toward viscosity measurement particularly behaving as Newtonian fluids. ARB

as a surfactant presented the best stability that kept nanoparticles in suspension for more than 20 days. However, it significantly increased the viscosity of C/H_2O nanofluid. This work also is a starting point to the understanding of the effect of surfactants on viscosity measurements of nanofluids. Future studies should target the point of micelle forming of various surfactants with nanofluids. More experimental work is needed to identify optimal pairings of surfactants, nanoparticles and base fluids. Further research is needed to analyse the effect of nanoparticle size towards viscosity measurements and stability as it is important for heat transfer applications.

5. References

[1] D.K. Devendiran, V.A. Amirtham, A review on preparation, characterization, properties and applications of nanofluids, Renew. Sustain. Energy Rev. 60 (2016) 21–40. doi:10.1016/j.rser.2016.01.055.

[2] L. Yang, J. Xu, K. Du, X. Zhang, Recent developments on viscosity and thermal conductivity of nanofluids, Powder Technol. 317 (2017) 348–369. doi:10.1016/j.powtec.2017.04.061.

[3] M. Ghazvini, M.A. Akhavan-Behabadi, E. Rasouli, M. Raisee, Heat transfer properties of nanodiamond-engine oil nanofluid in laminar flow, Heat Transf. Eng. 33 (2012) 525–532. doi:10.1080/01457632.2012.624858.

[4] S. Akilu, A.T. Baheta, K. V. Sharma, Experimental measurements of thermal conductivity and viscosity of ethylene glycol-based hybrid nanofluid with TiO2-CuO/C inclusions, J. Mol. Liq. 246 (2017) 396–405. doi:10.1016/j.molliq.2017.09.017.

[5] L.S. Sundar, M.K. Singh, A.C.M. Sousa, Turbulent heat transfer and friction factor of nanodiamond-nickel hybrid nanofluids flow in a tube: An experimental study, Int. J. Heat Mass Transf. 117 (2018) 223–234. doi:10.1016/j.ijheatmasstransfer.2017.09.109.

[6] K. Abdul, J.K. Carson, M. Atkin, M. Walmsley, Physical Properties and Rheological Characteristics of Activated Carbon Nanofluids with Varying Filler Fractions and Surfactants, Appl. Mech. Mater. 884 (2018) 58–65. doi:10.4028/www.scientific.net/AMM.884.58.

[7] P.K. Das, N. Islam, A.K. Santra, R. Ganguly, Experimental investigation of thermophysical properties of Al2O3–water nanofluid: Role of surfactants, J. Mol. Liq. 237 (2017) 304–312. doi:10.1016/j.molliq.2017.04.099.

[8] T.J. Choi, S.P. Jang, M.A. Kedzierski, Effect of surfactants on the stability and solar thermal absorption characteristics of water-based nanofluids with multi-walled carbon nanotubes, Int. J. Heat Mass Transf. 122 (2018) 483–490. doi:10.1016/j.ijheatmasstransfer.2018.01.141.

[9] M. Manilo, K. Bohacs, N. Lebovka, S. Barany, Impact of surfactant and clay platelets on electrokinetic potential and size distribution in carbon nanotubes aqueous suspensions, Colloids Surfaces A Physicochem. Eng. Asp. 544 (2018) 205–212. doi:10.1016/j.colsurfa.2018.02.030.

[10] P.K. Das, A.K. Mallik, R. Ganguly, A.K. Santra, Stability and thermophysical measurements of TiO2(anatase) nanofluids with different surfactants, J. Mol. Liq. 254 (2018) 98–107. doi:10.1016/j.molliq.2018.01.075.

[11] A. Akhgar, D. Toghraie, An experimental study on the stability and thermal conductivity of water-ethylene glycol/TiO2-MWCNTs hybrid nanofluid: Developing a new correlation, Powder Technol. 338 (2018) 806–818. doi:10.1016/j.powtec.2018.07.086.

[12] N. Sizochenko, M. Syzochenko, A. Gajewicz, J. Leszczynski, T. Puzyn, Predicting Physical Properties of Nanofluids by Computational Modeling, J. Phys. Chem. C. 121 (2017) 1910–1917. doi:10.1021/acs.jpcc.6b08850.

[13] F. Yu, Y. Chen, X. Liang, J. Xu, C. Lee, Q. Liang, P. Tao, T. Deng, Dispersion stability of thermal Dispersion stability of thermal nanofluids, Prog. Nat. Sci. Mater. Int. 27 (2017) 531–542. doi:10.1016/j.pnsc.2017.08.010.

[14] A.A. Minea, Challenges in hybrid nanofluids behavior in turbulent flow: Recent research and numerical comparison, Renew. Sustain. Energy Rev. 71 (2017) 426–434. doi:10.1016/j.rser.2016.12.072.

[15] M. Le Maire, P. Champeil, J. V. Møller, Interaction of membrane proteins and lipids with solubilizing detergents, Biochim. Biophys. Acta - Biomembr. 1508 (2000) 86–111. doi:10.1016/S0304-4157(00)00010-1.

[16] Z. Haddad, C. Abid, H.F. Oztop, A. Mataoui, A review on how the researchers prepare their nanofluids, Int. J. Therm. Sci. 76 (2014) 168–189. doi:10.1016/j.ijthermalsci.2013.08.010.
[17] L. Lin, H. Peng, G. Ding, Dispersion stability of multi-walled carbon nanotubes in refrigerant with addition of surfactant, Appl. Therm. Eng. 91 (2015) 163–171. doi:10.1016/j.applthermaleng.2015.08.011.
[18] A. Paar, D. Viscometers, DV-1 P new series of digital viscometers Introducing, B64is64-j (2006). https://www.anton-paar.com/nz-en/products/group/viscometer/.
[19] Nanocomposix, Zeta Potential Analysis of Nanoparticles, Nanocomposix Publ. (2012) 1–6.
[20] A. Ghadimi, R. Saidur, H.S.C. Metselaar, A review of nanofluid stability properties and characterization in stationary conditions, Int. J. Heat Mass Transf. 54 (2011) 4051–4068. doi:10.1016/j.ijheatmasstransfer.2011.04.014.
[21] Celine, Difference Between TEM and SEM, DifferenceBetween.net. (2012). http://www.differencebetween.net/science/difference-between-tem-and-sem/.
[22] K. Kouloulias, A. Sergis, Y. Hardalupas, Sedimentation in nanofluids during a natural convection experiment, Int. J. Heat Mass Transf. 101 (2016) 1193–1203. doi:10.1016/j.ijheatmasstransfer.2016.05.113.
[23] R. Ranjbarzadeh, A. Akhgar, S. Musivand, M. Afrand, Effects of graphene oxide□silicon oxide hybrid nanomaterials on rheological behavior of water at various time durations and temperatures: Synthesis, preparation and stability, Powder Technol. 335 (2018) 375–387. doi:10.1016/j.powtec.2018.05.036.
[24] X. Shao, Y. Chen, S. Mo, Z. Cheng, T. Yin, Dispersion Stability of TiO2-H2O Nanofluids Containing Mixed Nanotubes and Nanosheets, Energy Procedia. 75 (2015) 2049–2054. doi:10.1016/j.egypro.2015.07.282.
[25] P. D'Adamo, Larch Arabinogalactan Is a Novel Immune Modulator, (1996) 32–39.
[26] M.R. Mucalo, C.R. Bullen, M. Manley-Harris, T.M. McIntire, Arabinogalactan from the Western larch tree: A new, purified and highly water-soluble polysaccharide-based protecting agent for maintaining precious metal nanoparticles in colloidal suspension, J. Mater. Sci. 37 (2002) 493–504. doi:10.1023/A:1013757221776.
[27] J.Y. Shin, T. Premkumar, K.E. Geckeler, Dispersion of single-walled carbon nanotubes by using surfactants: Are the type and concentration important?, Chem. - A Eur. J. 14 (2008) 6044–6048. doi:10.1002/chem.200800357.
[28] F. Hakiki, D.A. Maharsi, T. Marhaendrajana, Surfactant-Polymer Coreflood Simulation and Uncertainty Analysis Derived from Laboratory Study, J. Eng. Technol. Sci. 47 (2015) 706–725. doi:10.5614/j.eng.technol.sci.2015.47.6.9.
[29] B.J. Zhu, W.L. Zhao, J.K. Li, Y.X. Guan, D.D. Li, Thermophysical Properties of Al2O3-Water Nanofluids, in: Nano-Scale Amorph. Mater., Trans Tech Publications, 2011: pp. 266–271. doi:10.4028/www.scientific.net/MSF.688.266.
[30] J.M. Munyalo, X. Zhang, Particle size effect on thermophysical properties of nanofluid and nanofluid based phase change materials: A review, J. Mol. Liq. 265 (2018) 77–87. doi:10.1016/j.molliq.2018.05.129.

Applied Mechanics and Materials
ISSN: 1662-7482, Vol. 884, pp 58-65
doi:10.4028/www.scientific.net/AMM.884.58

Submitted: 2018-02-25
Revised: 2018-06-01
Accepted: 2018-06-08
Online: 2018-08-28

Physical Properties and Rheological Characteristics of Activated Carbon Nanofluids with Varying Filler Fractions and Surfactants

Kaggwa Abdul*, James K. Carson, Martin Atkin, Michael Walmsley

School of Engineering, Faculty of Science and Engineering, University of Waikato, Private Bag 3105, Hamilton 3240, New Zealand

*kaggwaabu@ymail.com

Keywords: Nanofluids; Viscosity; Specific heat capacity; Surfactant; Stability.

Abstract. For the past fifteen years, there has been considerable interest in the use of nanofluids in various fields mainly in heat transfer applications. This paper investigated thermophysical properties of activated carbon nanofluids using hexane, water and ethylene glycol (EG) as base fluids. Experimental and qualitative observational tests were conducted to study the viscosity, specific heat capacity and stability of the nanofluids using arabinogalactan (ARB), sodium lauryl sulphate (SDS) and TritonX-114 as stabilising agents. The results revealed that the addition of ARB to activated carbon-water (C/H_2O) nanofluids yielded nanofluid stability for up to 39 days. However, ARB decreased the heat capacity of C/H_2O nanofluid. C/H_2O nanofluid viscosity decreased with an increase in shear rate. On the other hand, results revealed that C/C_6H_{14} viscosity increased with the increase in shear rate specifically for high shear rate values. C/H_2O heat capacity was enhanced by 6.1% compared to C/EG that decreased by 6.3%.

Introduction

Activated carbon is a porous form of carbon that holds and attracts organic chemicals. The internal pore network that creates large surface area and its cost effectiveness [1], makes it a potential material of interest for use in nanofluids for heat transfer applications.

In the past decade, nanofluids have received much attention and have been widely considered for use in various applications such as automobile radiators, electronic cooling systems, nuclear, heat pipes, solar energy systems, drug delivery [2], cosmetics industries, air-conditioning and refrigeration.

A number of studies [3-5] have claimed that suspension of nano-sized materials significantly enhances the thermal performance of traditional fluids. To illustrate, Choi et al. [6] suspended copper nanoparticles in water and their results revealed that the thermal conductivity of water was enhanced by a factors of 1.5 and 3.5 at relatively low volume fractions of 5% and 20% respectively.

Recent developments suggest that thermal conductivity and viscosity depends on volume fraction, stabilising agents (surfactants), nanoparticle size, morphology, temperature, nature of base fluid and nanoparticle material. For instance, Alawi et al. [7] studied thermophysical properties of metal oxide (Al_2O_3, CuO, SiO_2 and ZnO) nanofluids and found that effective viscosity and viscosity ratio showed a considerable increase with the increase of nanoparticles concentration. Moreover, experimental work by Colangelo et al. [8] revealed that the presence of surfactants creates some bonds with nanoparticles, which improve nanofluid stability. They concluded that besides the increase in viscosity with an increase in volume concentration, nanofluids with and without surfactants show non-Newtonian behaviour.

Tiznobaik et al. [9] investigated silicon-dioxide nanoparticles with molten salt eutectic and their results showed that the specific heat capacity of nanomaterials was enhanced by 25% regardless of the size of embedded nanoparticles. They added that the enhancement in specific heat capacity was due to the high specific surface energies that are associated with the high surface areas of the embedded nanoparticles. In the same line of thought, Seo et al. [10] investigated the effect of nanoparticles on the specific heat of ternary nitrate salt eutectic doped with SiO_2 nanoparticles. They used a modulated differential scanning calorimeter to measure the specific heat and their

results revealed that the specific heat was enhanced by 13-16%. They added that specific heat was independent of the size of the nanoparticles.

However, while nanofluids have been shown to enhance heat transfer rates, there are disadvantages associated with their use. Besides instability and increased viscosity, several other issues limit their popularity and global acceptance. For instance, inconsistency and divergence of published work [11], lack of agreement of results obtained by different researchers [12], inadequacy of theoretical understanding of the mechanisms responsible for changes in properties [13], high costs of production especially on a large scale, Insufficient understanding of the forces that act on the nanoparticles during and after suspension [14]. There is a number of published articles on thermal conductivity [14-16] but less attention is given to specific heat capacity and use of surfactants, To date, there is no more than 20 publications [17] with the topic 'activated carbon nanofluids'. Therefore, the aim of this paper is to analyse physical property measurements of activated carbon nanofluids. This work focuses on viscosity, specific heat capacity, stability and the overall rheological behaviour of nanofluids with different stabilising agents.

Nanofluids Preparation

The two-step method [18, 19] was used in nanofluids preparation. This involved purchasing commercially available activated carbon nano-powder and suspension in selected fluids. The percentage volume concentration of the nanoparticles was 1.38 vol.% for C/H_2O, 1.5 vol.% for C/EG and 1.0 vol. % for C/C_6H_{14}. Table 1 describes the characteristics of nanoparticles used in this study.

Table 1 Physical characteristics of nanoparticles.

Nanomaterial	*Average particle size (nm)*	*Bulky density ($kg.m^{-3}$)*	*Specific surface area ($m^2.kg^{-1}$)*	*Purity (%)*
Activated carbon	50	3020 - 3300	500000	99.5

Nanoparticles were weighed and then suspended in sample bottles containing base fluid (water or ethylene glycol or hexane). There is no doubt that during thermal transport, nanofluids experience inter-particle forces that result in sedimentation [14]. Therefore, surfactants were added to the nanofluid to lower the inter-particle forces and immediately the solution was stirred before it was transferred to an ultrasonic device as shown in Fig. 1. Nanofluids were kept under ultra-sonication for 1 hour with the micro-tip probe amplitude and the pulse set to 20% and 10 seconds respectively. The mechanical vibration from the micro-tip probe during ultrasonication creates microscopic bubbles that collapse and breaks apart the nanofluid molecules thus forming homogenous and stable solutions.

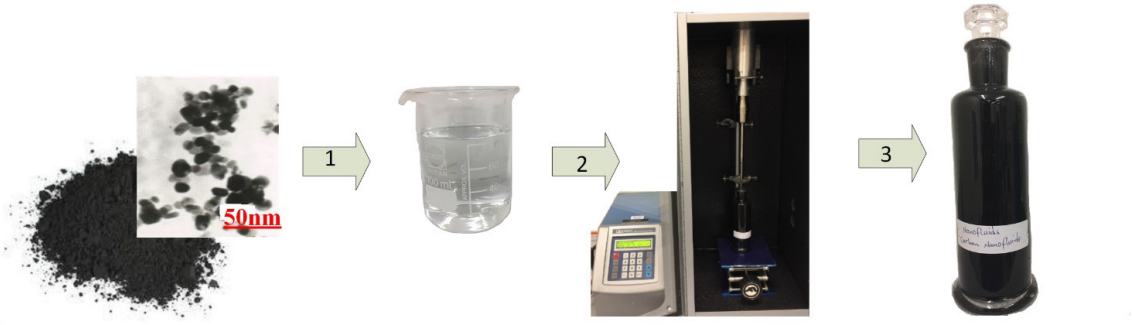

Fig. 1 Nanofluids preparation process.

Measurements

Nanofluid stability was determined qualitatively by monitoring and observing sedimentation of nanoparticles of sample bottles containing nanofluids at regular intervals.

Viscosity measurements were conducted using Anton Paar digital viscometer (DV - 1P) Fig. 2(a). This viscometer measured the torque created by the rotation of a spindle at constant speed from which dynamic viscosity is obtained as a value proportional to the measured torque. The linear velocity 'V' and shear rate 'γ'were calculated using Eqs. 1-3

$$V = \omega r \tag{1}$$

$$\omega = 2\pi * RPS \tag{2}$$

$$\dot{\gamma} = 2\left(\frac{r^2}{r^2 - 1}\right) \tag{3}$$

Where 'ω' and 'r' are the angular velocity and the radius of the spindle respectively.

Prior to starting measurements, the flow jacket that housed the sample chamber was connected to the water bath flow loop to maintain steady temperatures of the nanofluids in question. The low viscosity adapter 'LCP spindle' was selected throughout the entire investigation because it allows accurate measurements and most importantly where low shear rates values are obtained. The spindle was lowered into the sample chamber and the viscometer was perpendicularly levelled for accurate measurements.

The water bath was set at 25 °C, the viscometer spindle was set to rotational speeds that ranged from 50 to 100 revolutions per minute (RPM). The viscometer accuracy and repeatability of the full-scale range of the measurements values from the user manual was ± 1% and ± 0.2% respectively. The viscosity was obtained as an average of three viscosity readings from display with a minute time interval between each reading.

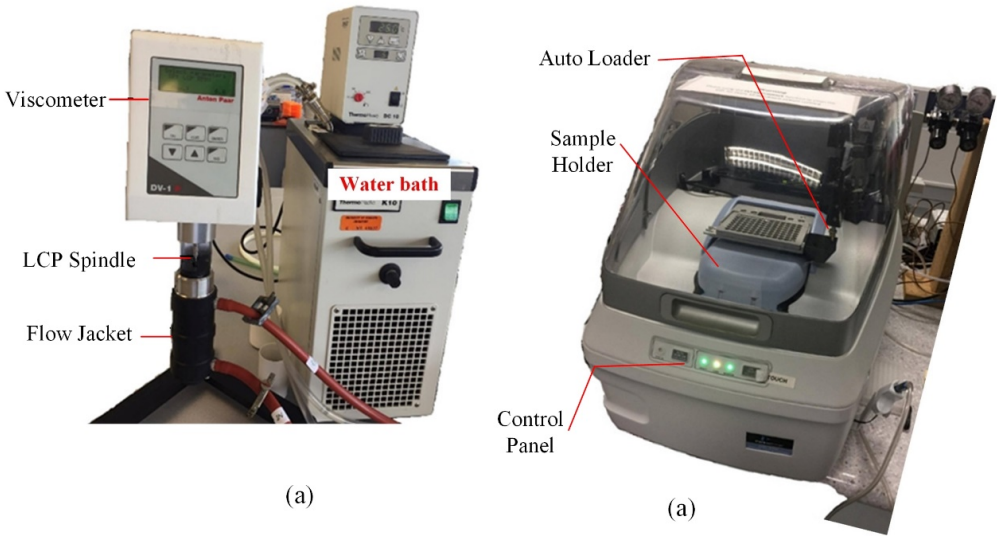

Fig. 2 Viscometer and water bath (a) and (b) Differential scanning calorimeter.

Specific heat capacity was measured by a differential scanning calorimeter (Perkin Elmer DSC - 8500) Fig. 2(b). Prior to starting the DSC operations, empty aluminium pans were prepared as a reference for the sample measurements. The samples that ranged from 11.5 to 23.7 mg in mass were spread evenly along the base of the aluminium pans. The weight of the pan and sample was measured using an electronic balance (Mettler Toledo AG204) with a precision and maximum range of ±0.003% mg and 210.0 mg respectively. The sample holder cell initial and maximum temperature were set at 30 °C and 80 °C respectively. In order to achieve the DSC signal stability, the sample was maintained at the initial temperature for 60 seconds. Hu et al. [20] explained that the uncertainties in the experimental results are dependent on the measurement deviations for each of the parameters, including mass and heat flow. Therefore, the specific heat capacity was obtained using Eq. (4) where C_p is the specific heat capacity, q is the heat flow, *'m'* is the weight, and the subscripts *'s'* and *'z'* denote sample and water.

$$C_{p,s} = C_{p,z}\left[\frac{\Delta q_s * m_z}{\Delta q_z * m_s}\right] \quad (4)$$

The propagation of uncertainties was calculated using the root-sum-square method [21] Eq. (5), where *'Q'* is given as any defined function of independent variables *'V'*. Finally, the uncertainty *'δQ'* of the function is as follows

$$\delta Q = \sum_{i=1}^{n}\left|\frac{\delta Q}{\partial V_i}\right|\delta V_i \quad (5)$$

The average heat flow and its uncertainty was 27.8mW and ±0.2 respectively.

Stability is one of the most discussed characteristics of nanofluids. For instance, Sánchez et al. [22] claimed that nanoparticles in nanofluids show a tendency to agglomerate due to van der Waals attractive forces and are prone to sedimentation because of the big difference in density between the nanoparticles and the base fluid. However, surfactants are capable of altering the polar component of liquid molecules thus improving stability [23]. Mucalo et al. [24] explained that ARB is highly soluble in water, capable of being prepared with high purity and not settling out insoluble material over time. Likewise, ionic and non-ionic surfactants such as SDS and TritonX-114 respectively are efficient solubilizers [25], less viscous, lower toxicity and cost effective [26]. Therefore, the stability of activated carbon nanofluid with ARB or SDS or TritonX-114 surfactants was observed.

Results and Discussion

Stability observations

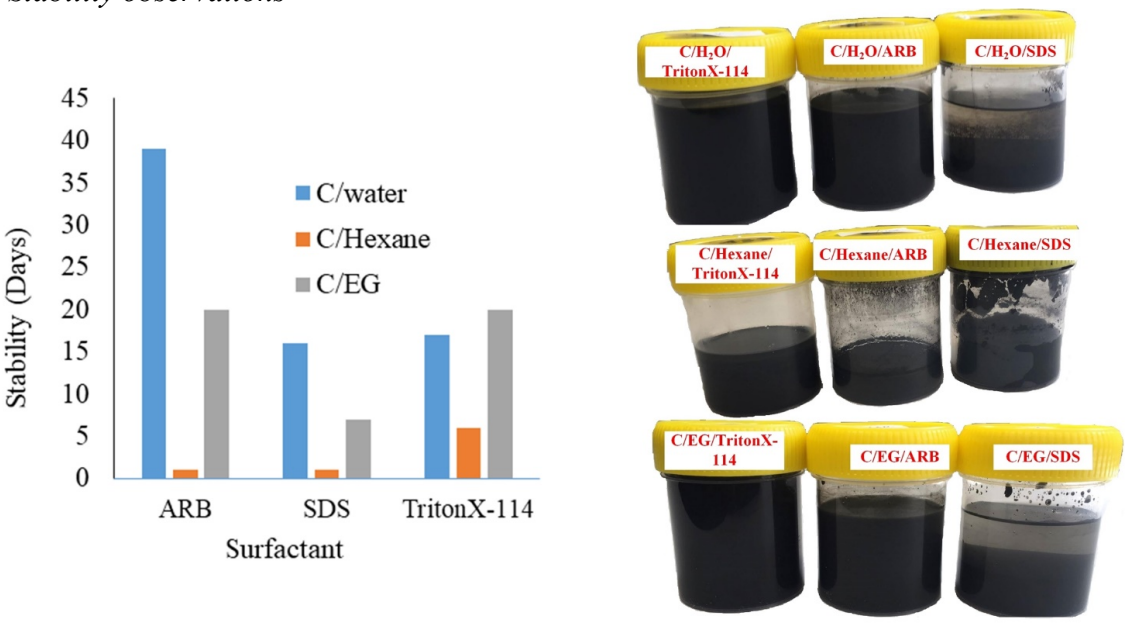

Fig. 3 Stability timeline (a) and (b) samples of nanofluid with varying surfactants.

Figure 3a shows that the addition of ARB to C/H_2O nanofluids sustained particle stability for 39 days compared to SDS and TritonX-114. In the same way, ARB and TritonX-114 showed better results by keeping the C/EG nanofluid stable for 20 days. Moreover, TritonX-114 produced better stability for C/C_4H_{16} nanofluid compared to SDS and ARB surfactants.

Figure 3b shows clear layers that mark separations between the nanoparticles and base fluids in the samples. Surprisingly, a remarkable evaporation of hexane was observed when ARB and SDS were added as surfactants. Nanoparticles agglomerate and later sediment at the bottom of the sample bottle to form a thick solution. It is worth noting that the chemical properties, affordability, non-pollutant and thermal stability of hexane makes it an excellent refrigerant for two-phase heat transfer applications. However, this observation (evaporation and viscous) is an absolute limitation

specifically as a nano-refrigerant. Kaggwa and Wang. [27] mentioned that refrigerants with high viscosities increase pressure drop that requires high compressor work and power consumption, which in return lowers the overall coefficient of performance of systems.

The Effect of shear rate and velocity on viscosity measurement

Figure 4a shows that the viscosity of carbon-water (C/H_2O) nanofluids was significantly higher compared to that of carbon-hexane (C/C_6H_{14}) specifically at low velocities ranging from 0.07 to 0.09 m/s.

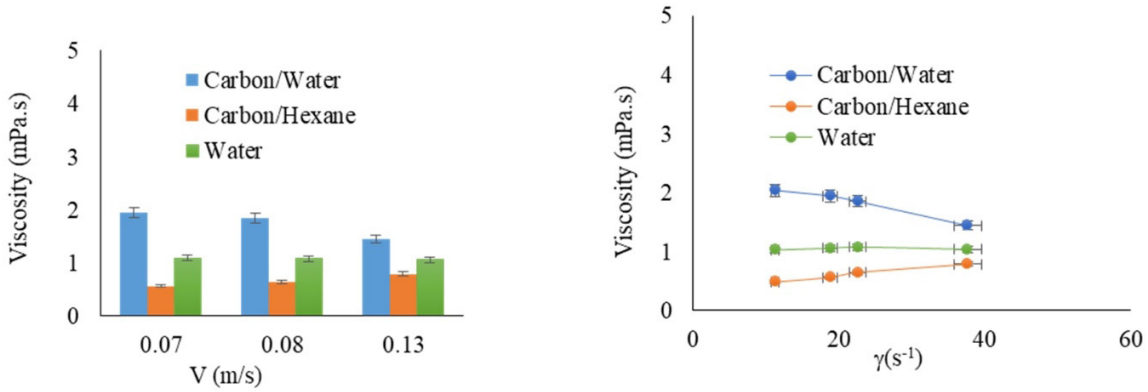

Fig. 4 Viscosity as a function of linear velocity (a) and (b) the effect of shear rate on hexane and water carbon nanofluids.

Newtonian fluids are independent of shear rate because their viscosity remains constant at specified temperatures and pressures. Therefore, water being a Newtonian fluid was used as a reference to study the impact of shear rate on viscosity measurements of C/H_2O and C/C_6H_{14} nanofluids. The results in Fig. 4b demonstrate that C/H_2O nanofluid viscosity decreases with an increase in shear rate. In contrast, C/C_6H_{14} viscosity increases with the increase in shear rate. The results are similar to those of Afrand et al. [28] where they explained that factors such as nanoparticles concentration, the complexity in the interactions between the base fluid molecules and nanoparticles can be the reasons for the shear thinning and thickening under the influence of increasing shear rate.

The effect of nanoparticles and surfactant on specific heat capacity

During specific heat measurements, similar procedures were adopted from Hu et al. [20] except in this study sapphire was replaced by water as a reference material. The enhancement ratio was calculated using Eq. (6) as an attempt to clearly asses the performance of activated nanofluids with varying fillers.

$$E_{\%} = \left[\frac{cp_{nf} - cp_{water}}{cp_{water}} \right] * 100 \tag{6}$$

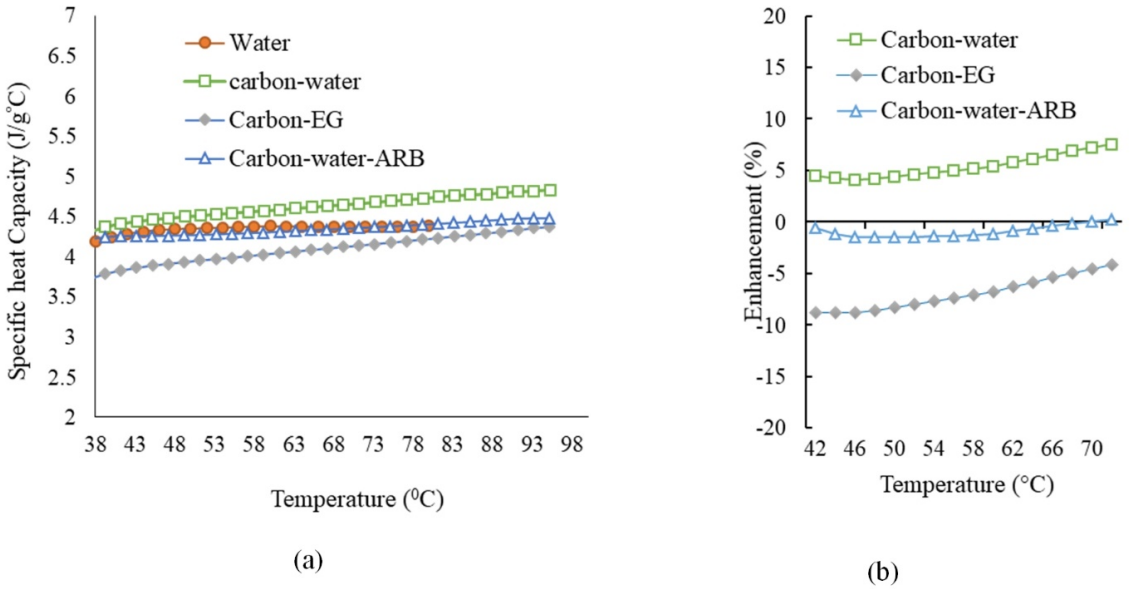

Fig. 5 Effect of activated carbon nanoparticles and surfactant on heat capacity (a) and (b) enhancement ratio as a function of temperature.

Figure 5a shows that C/H_2O nanofluids heat capacity was enhanced by an average of 6.1% compared to water. By contrast, an average decrease of 6.3% heat capacity was noticed for C/EG nanofluid. Equally important, Fig. 5b shows a slight average decrease of 0.21% in heat capacity for nanofluids with ARB surfactant. Tiznobaik et al. [9] pointed out that exceptionally large specific surface area can significantly increase the effect of surface energy on the effective specific heat capacity. He et al. [29] believes that if the heat capacity of the nanoparticles is less than that of the base fluid, then the specific heat of the nanofluid will decrease and vice versa. Likewise, Wang et al. [30] explained that the lager specific surface area of nanoparticles together with their surface free energy has a greater proportion in the system capacity that affect the specific heat of composite materials thus leading to the change of solid-liquid interfacial free energy of the suspended nanoparticles.

Despite the fact that surfactants generally play a significant role in the stabilisation of suspended nanoparticles, Fig. 5b also proves that they affect specific heat capacity during heat transfer enhancement. In summary, both base fluids and surfactants have an impact on specific heat capacity of nanofluids and the overall heat transfer enhancement.

From heat transfer standpoint, it appears that C/H_2O would be the best choice as a working fluid of the three considered nanofluids. However, stability is still a challenge because ARB lowers the heat capacity much as it sustains stability of the suspended nanoparticles compared to other surfactants investigated. Further experimental investigations need to be carried out with optimal pairings of nanoparticles, base fluids and surfactants.

Conclusion

This paper investigated physical properties of activated carbon nanofluids and the major conclusions are as follows;

1. The addition of ARB to C/H_2O nanofluids yield better stability up to 39 days. However, ARB decreased the heat capacity of C/H_2O by an average of 0.21%.
2. C/H_2O nanofluid viscosity decreased with an increase in shear rate. In contrast, C/C_6H_{14} viscosity increased with the increase in shear rate specifically for high values of shear rate.
3. Low velocities ranging from 0.07 to 0.09 m/s yielded better viscosity measurements.
4. C/H_2O heat capacity was enhanced by an average of 6.1% compared to C/EG that decreased by an average of 6.3%.

References

[1] P. Simon, Y. Gogotsi, Materials for electrochemical capacitors, Nat. Mater. 7 (2008) 845–854. doi:10.1038/nmat2297.

[2] D. Yang, F. Yang, J. Hu, J. Long, C. Wang, D. Fu, Q. Ni, Hydrophilic multi-walled carbon nanotubes decorated with magnetite nanoparticles as lymphatic targeted drug delivery vehicles, Chem. Commun. (2009) 4447–4449. doi:10.1039/b908012k.

[3] L. Léal, M. Miscevic, P. Lavieille, M. Amokrane, F. Pigache, F. Topin, B. Nogarède, L. Tadrist, An overview of heat transfer enhancement methods and new perspectives: Focus on active methods using electroactive materials, Int. J. Heat Mass Transf. 61 (2013) 505–524. doi:10.1016/j.ijheatmasstransfer.2013.01.083.

[4] J.A. Eastman, S.U.S. Choi, S. Li, W. Yu, L.J. Thompson, Anomalously increased effective thermal conductivities of ethylene glycol-based nanofluids containing copper nanoparticles, Appl. Phys. Lett. 78 (2001) 718–720. doi:10.1063/1.1341218.

[5] K.S. Suganthi, K.S. Rajan, Metal oxide nanofluids: Review of formulation, thermo-physical properties, mechanisms, and heat transfer performance, Renew. Sustain. Energy Rev. 76 (2017) 226–255. doi:10.1016/j.rser.2017.03.043.

[6] S.U.S. Choi, J.A. Eastman, Enhancing thermal conductivity of fluids with nanoparticles, ASME Int. Mech. Eng. Congr. Expo. 66 (1995) 99–105. doi:10.1115/1.1532008.

[7] O.A. Alawi, N.A.C. Sidik, H.W. Xian, T.H. Kean, S.N. Kazi, Thermal conductivity and viscosity models of metallic oxides nanofluids, Int. J. Heat Mass Transf. 116 (2018) 1314–1325. doi:10.1016/j.ijheatmasstransfer.2017.09.133.

[8] G. Colangelo, E. Favale, P. Miglietta, M. Milanese, A. De Risi, Thermal conductivity , viscosity and stability of Al 2 O 3 -diathermic oil nano fl uids for solar energy systems, Energy. 95 (2016) 124–136. doi:10.1016/j.energy.2015.11.032.

[9] H. Tiznobaik, D. Shin, Enhanced specific heat capacity of high-temperature molten salt-based nanofluids, Int. J. Heat Mass Transf. 57 (2013) 542–548. doi:10.1016/j.ijheatmasstransfer.2012.10.062.

[10] J. Seo, D. Shin, Size effect of nanoparticle on specific heat in a ternary nitrate (LiNO3-NaNO3-KNO3) salt eutectic for thermal energy storage, Appl. Therm. Eng. 102 (2016) 144–148. doi:10.1016/j.applthermaleng.2016.03.134.

[11] M.H. Hamzah, N.A.C. Sidik, T.L. Ken, R. Mamat, G. Najafi, Factors affecting the performance of hybrid nanofluids: A comprehensive review, Int. J. Heat Mass Transf. 115 (2017) 630–646. doi:10.1016/j.ijheatmasstransfer.2017.07.021.

[12] A.A. Minea, Challenges in hybrid nanofluids behavior in turbulent flow: Recent research and numerical comparison, Renew. Sustain. Energy Rev. 71 (2017) 426–434. doi:10.1016/j.rser.2016.12.072.

[13] L. Yang, Y. Hu, Toward TiO2 Nanofluids—Part 2: Applications and Challenges, Nanoscale Res. Lett. 12 (2017) 446. doi:10.1186/s11671-017-2185-7.

[14] H. Farzaneh, A. Behzadmehr, M. Yaghoubi, A. Samimi, S.M.H. Sarvari, Stability of nanofluids: Molecular dynamic approach and experimental study, Energy Convers. Manag. 111 (2016) 1–14. doi:10.1016/j.enconman.2015.12.044.

[15] S.M.S. Murshed, K.C. Leong, C. Yang, Enhanced thermal conductivity of TiO2 - Water based nanofluids, Int. J. Therm. Sci. 44 (2005) 367–373. doi:10.1016/j.ijthermalsci.2004.12.005.

[16] M. Kole, T.K. Dey, Investigation of thermal conductivity, viscosity, and electrical conductivity of graphene based nanofluids, J. Appl. Phys. 113 (2013). doi:10.1063/1.4793581.

[17] W. of S. [v.5.27.2], Web of Science Core Collection Citation Report, (2018) Activated carbon. Apps.webofknowledge.com,.

[18] N.A.C. Sidik, H.A. Mohammed, O.A. Alawi, S. Samion, A review on preparation methods and challenges of nanofluids, Int. Commun. Heat Mass Transf. 54 (2014) 115–125. doi:10.1016/j.icheatmasstransfer.2014.03.002.

[19] Z. Haddad, C. Abid, H.F. Oztop, A. Mataoui, A review on how the researchers prepare their nanofluids, Int. J. Therm. Sci. 76 (2014) 168–189. doi:10.1016/j.ijthermalsci.2013.08.010.

[20] Y. Hu, Y. He, Z. Zhang, D. Wen, Effect of Al2O3 nanoparticle dispersion on the specific heat capacity of a eutectic binary nitrate salt for solar power applications, Energy Convers. Manag. 142 (2017) 366–373. doi:10.1016/j.enconman.2017.03.062.

[21] S. Bell, A Beginner's Guide to Uncertainty of Measurement, Meas. Good Pract. Guid. (1999) 41. doi:10.1111/j.1468-3148.2007.00360.x.

[22] A. Sánchez-Coronilla, J. Navas, T. Aguilar, E.I. Martín, J.J. Gallardo, M.R. Gómez-Villarejo, M.I. Carrillo-Berdugo, R. Alcántara, C. Fernández-Lorenzo, J. Martín-Calleja, The Role of Surfactants in the Stability of NiO Nanofluids: An Experimental and DFT Study, ChemPhysChem. 18 (2017) 346–356. doi:10.1002/cphc.201601161.

[23] A.R. Harikrishnan, S.K. Das, P.K. Agnihotri, P. Dhar, Particle and surfactant interactions effected polar and dispersive components of interfacial energy in nanocolloids, J. Appl. Phys. 122 (2017). doi:10.1063/1.4997123.

[24] M.R. Mucalo, C.R. Bullen, M. Manley-Harris, T.M. McIntire, Arabinogalactan from the Western larch tree: A new, purified and highly water-soluble polysaccharide-based protecting agent for maintaining precious metal nanoparticles in colloidal suspension, J. Mater. Sci. 37 (2002) 493–504. doi:10.1023/A:1013757221776.

[25] M. Le Maire, P. Champeil, J. V. Møller, Interaction of membrane proteins and lipids with solubilizing detergents, Biochim. Biophys. Acta - Biomembr. 1508 (2000) 86–111. doi:10.1016/S0304-4157(00)00010-1.

[26] K. Szymczyk, A. Taraba, Aggregation behavior of Triton X-114 and Tween 80 at various temperatures and concentrations studied by density and viscosity measurements, J. Therm. Anal. Calorim. 126 (2016) 315–326. doi:10.1007/s10973-016-5631-3.

[27] A. Kaggwa, C. Wang, Investigation of Thermal-Hydrodynamic Heat Transfer Performance of R-1234ze and R-134a Refrigerants in a Microfin and Smooth Tube., J. Enhanc. Heat Transf. 23 (2016) 221–239. doi:10.1615/JEnhHeatTransf.2017019585.

[28] M. Afrand, D. Toghraie, B. Ruhani, Effects of temperature and nanoparticles concentration on rheological behavior of Fe3O4-Ag/EG hybrid nanofluid: An experimental study, Exp. Therm. Fluid Sci. 77 (2016) 38–44. doi:10.1016/j.expthermflusci.2016.04.007.

[29] Q. He, S. Wang, M. Tong, Y. Liu, Experimental study on thermophysical properties of nanofluids as phase-change material (PCM) in low temperature cool storage, Energy Convers. Manag. 64 (2012) 199–205. doi:10.1016/j.enconman.2012.04.010.

[30] B.-X. Wang, L.-P. Zhou, X.-F. Peng, Surface and Size Effects on the Specific Heat Capacity of Nanoparticles, Int. J. Thermophys. 27 (2006) 139–151. doi:10.1007/s10765-006-0022-9.

Appendix B
Characterisation and physical property measurements

B.1 Introduction

This Appendix discusses additional information on stability and physical property measurements of nanofluids.

B.2 Stability

The first results on stability were conducted focusing only on activated carbon nanoparticles with various surfactants including ARB, SDS and TritonX-114. Water, ethylene glycol and hexane were selected as base fluids. The main objective for the aforementioned materials for the first observational tests was to select the best matches between base fluids and surfactants after a period of 40 days. Table B.1 shows quantity and the volume of concentration of nanoparticles. The observations and conclusions are as below.

Table B.1. Concentration of nanoparticles in nanofluids.

Nanofluid	Nanoparticles (kg)	Volume of concentration (vol. %)
C/H_2O	0.002	1.45
C/EG	0.002	1.59
C/C_6H_{14}	0.002	0.91

Figure B.1(a) shows that the addition of ARB to C/H_2O nanofluids sustained particle stability for 39 days compared to SDS and TritonX-114. In the same way, ARB and TritonX-114 showed better results by keeping the C/EG nanofluid stable for 20 days. Moreover, TritonX-114 produced better stability for C/C_4H_{16} nanofluid compared to SDS and ARB surfactants.

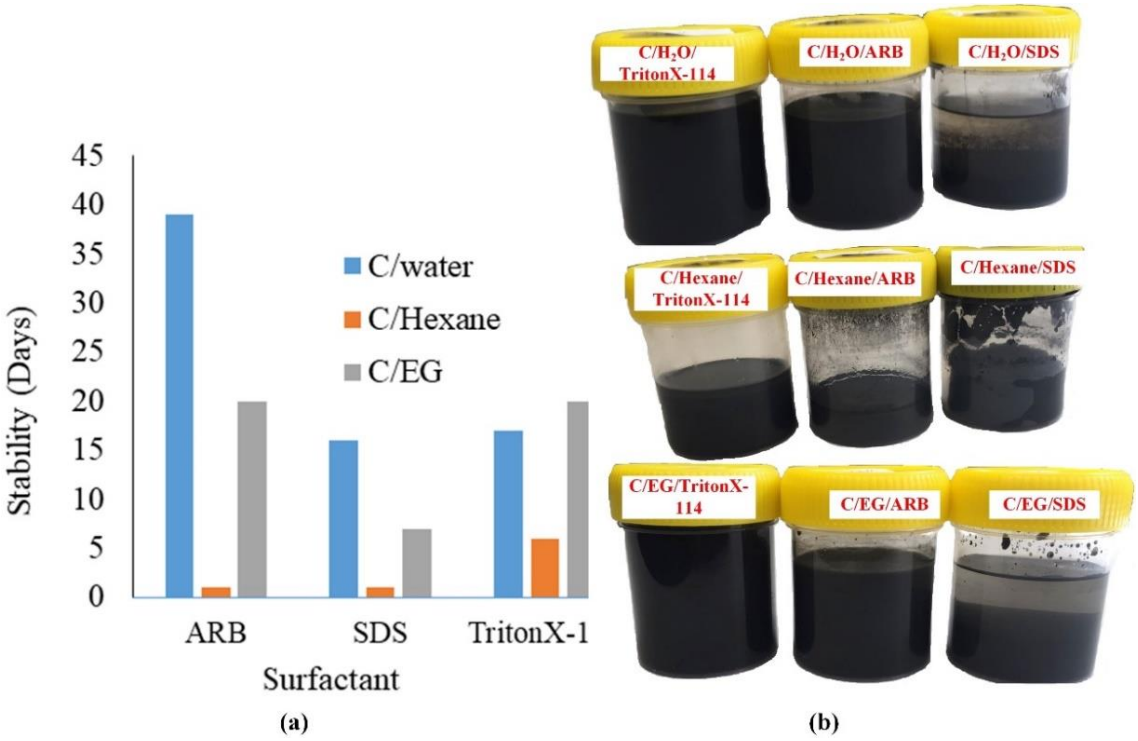

Figure B.1 Stability timeline (a) and (b) samples of nanofluid with varying surfactants after 40 days.

Figure B.1(b) shows clear layers that mark separations between the nanoparticles and base fluids in the samples. Surprisingly, a remarkable evaporation of hexane was observed when ARB and SDS were added as surfactants. For that reason, hexane was discontinued from further investigation as a base fluid.

B.3 Viscosity

Figure B.2 shows that the viscosity of carbon-water (C/H_2O) nanofluids was significantly higher compared to that of carbon-hexane (C/C_6H_{14}) specifically at low velocities ranging from 0.07 to 0.09 m/s.

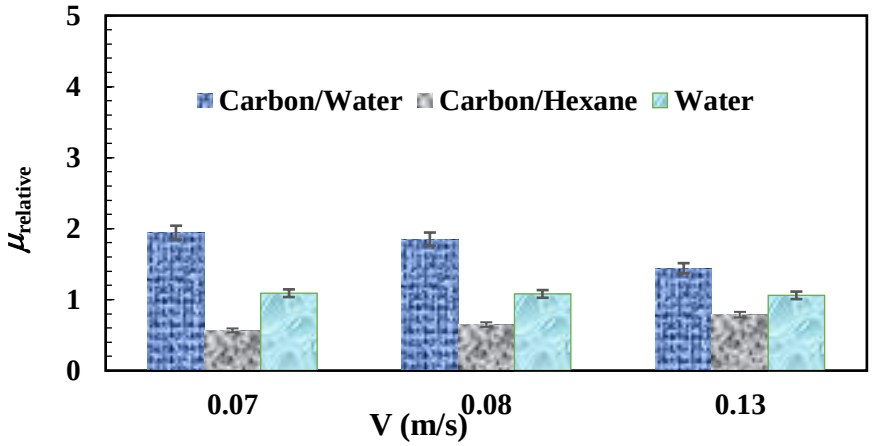

Figure B.2 Viscosity as a function of linear velocity.

Newtonian fluids are preferred in thermal systems because they have constant viscosity at a particular temperature and pressure; and are independent of shear rate (Stewart 2016b). Therefore, water being a Newtonian fluid was used as a reference to study the impact of shear rate on viscosity measurements of C/H_2O and C/C_6H_{14} nanofluids. The results in Fig. B.3 demonstrate that C/H_2O nanofluid viscosity decreases with an increase in shear rate. In contrast, C/C_6H_{14} viscosity increases with the increase in shear rate. The results are similar to those of Afrand et al. (Afrand, Toghraie, and Ruhani 2016) where they explained that factors such as nanoparticles concentration, the complexity in the interactions between the base fluid molecules and nanoparticles can be the reasons for the shear thinning and thickening under the influence of increasing shear rate.

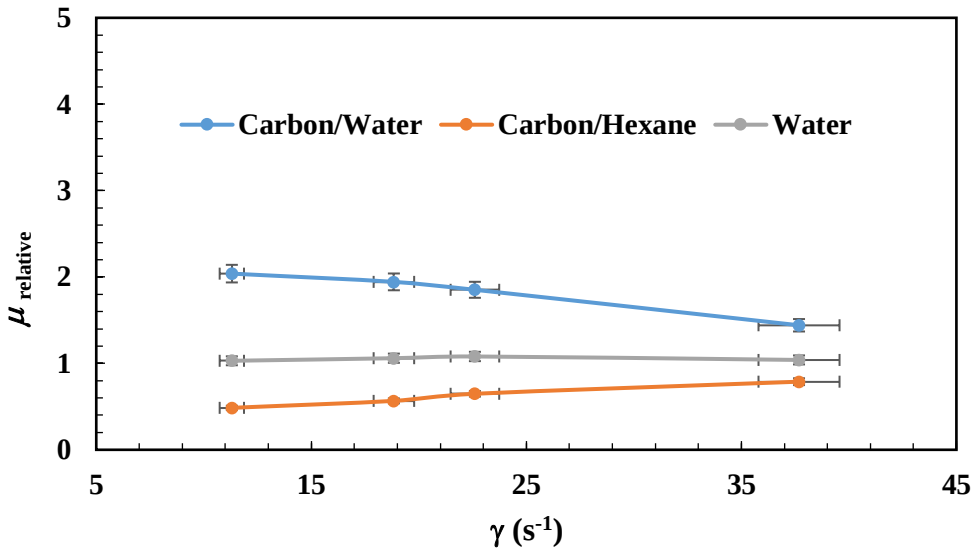

Figure B.3 The effect of shear rate on hexane and water carbon nanofluids.

Figures B.4a and B.4b, indicate that in most cases the surfactants had no significant impact on either shear stress or shear-rate dependence of nanofluids except for ARB and CTAB that demonstrated shear-thinning behaviour for C/H_2O and Al_2O_3/H_2O nanofluids respectively.

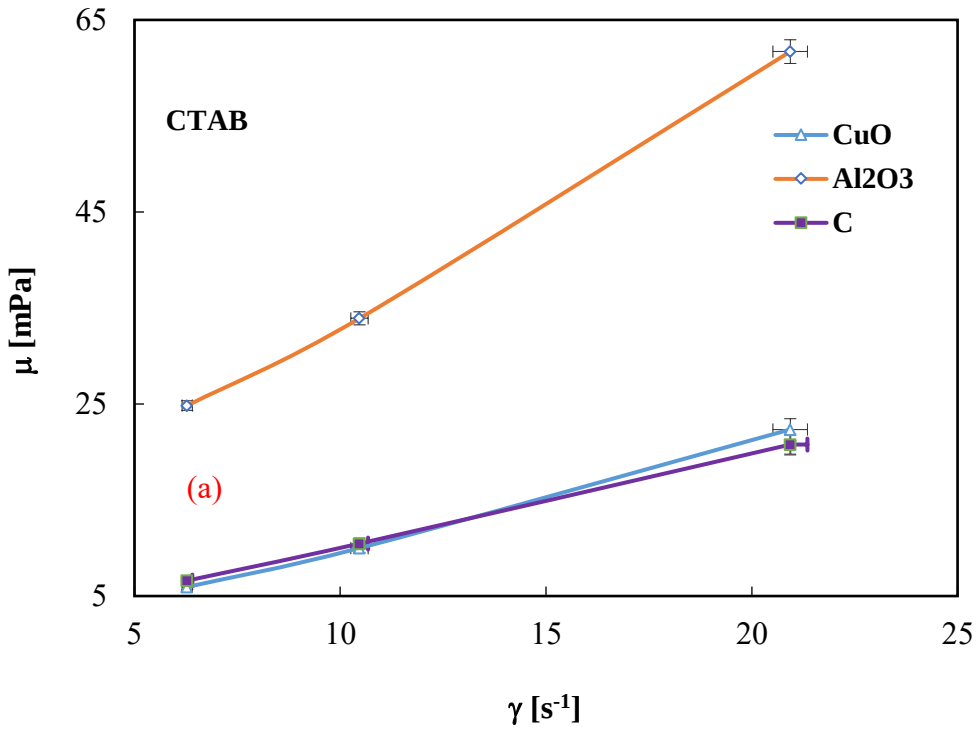

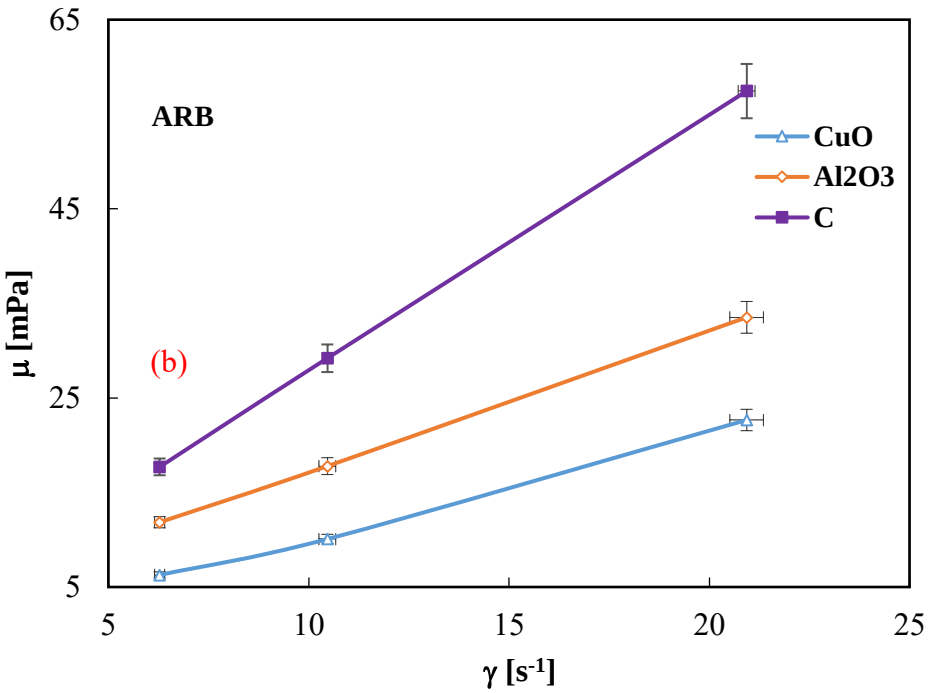

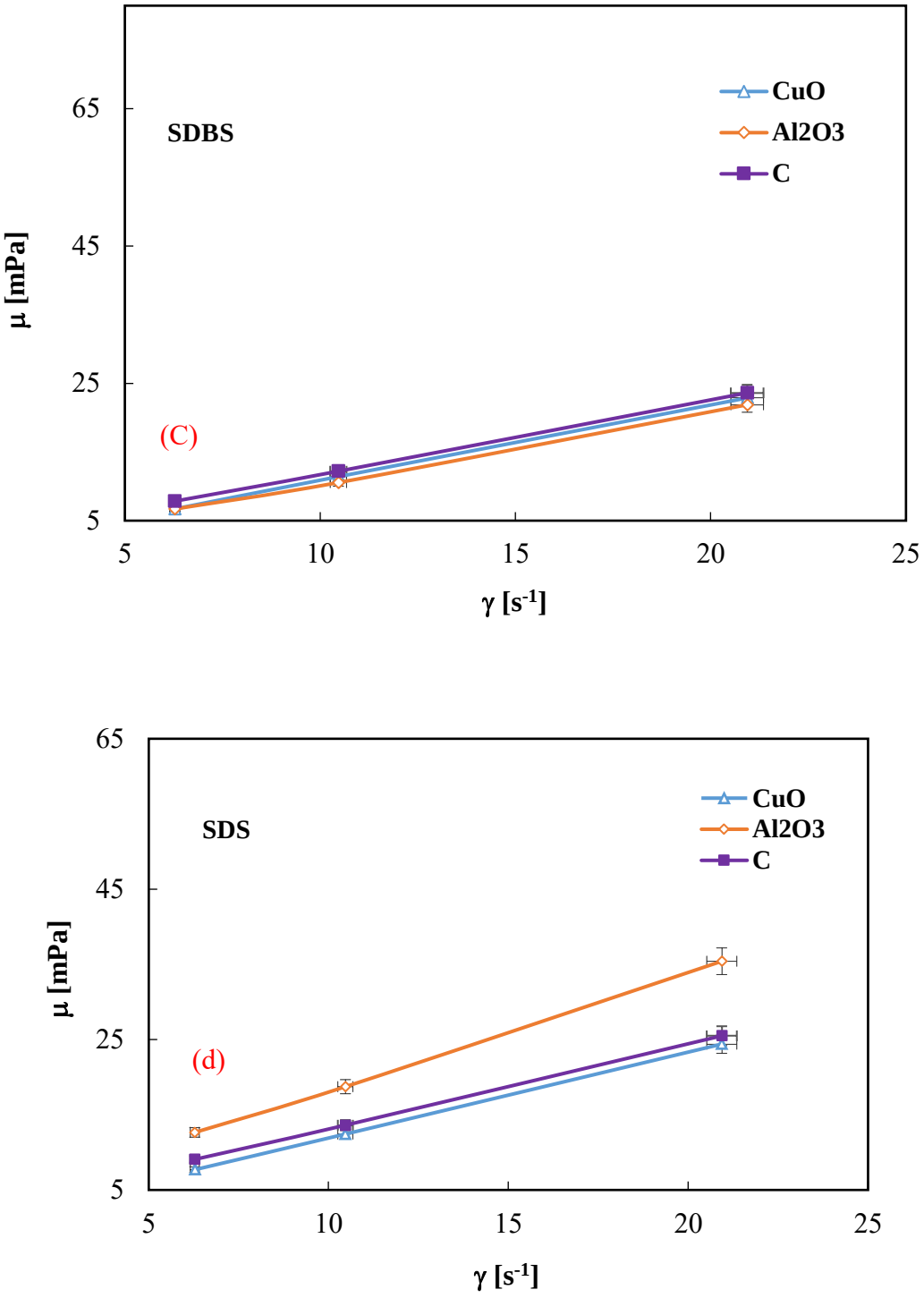

Figure B.4 Comparison of shear stress against shear rate of nanofluids with various surfactants at T=25 ÁC.

B.4 Specific heat capacity

Specific heat capacity was measured by a differential scanning calorimeter (Perkin Elmer DSC - 8500) Fig. B.5, equipped with a liquid nitrogen cooling system. Prior to starting the DSC operations, empty aluminium pans were prepared as a reference for the sample measurements.

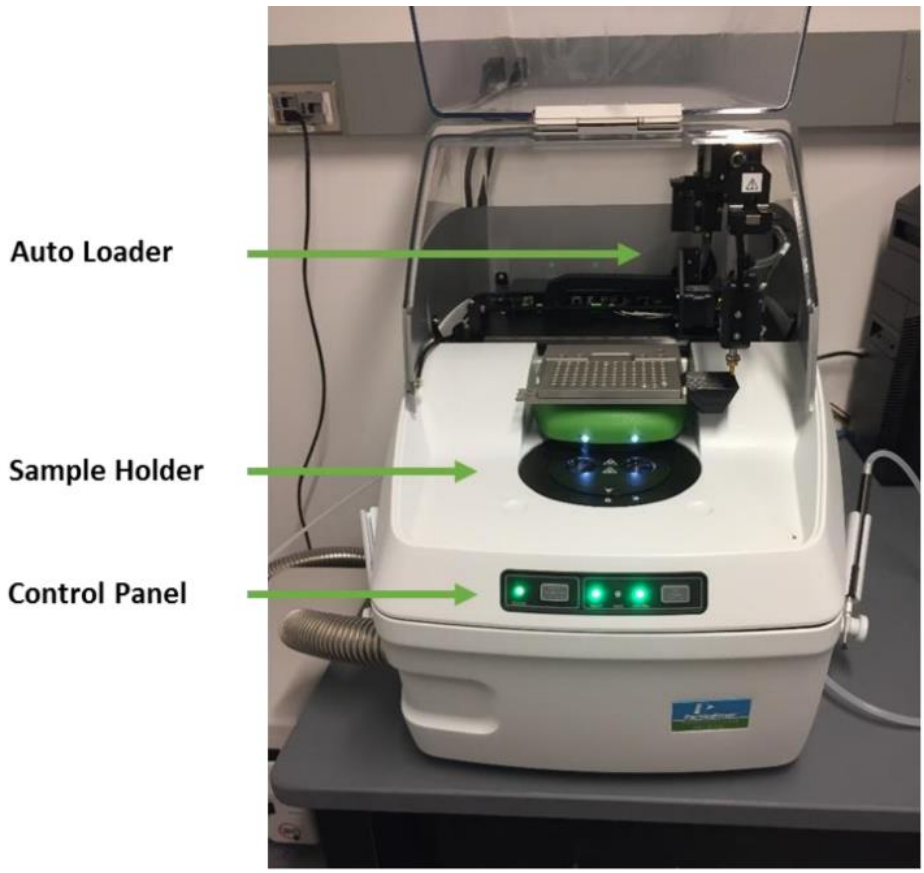

Figure B.5 Differential scanning calorimeter.

The samples that ranged from (11.5 to 23.7 mg) in were placed and spread evenly along the base of the aluminium pans. Aluminium cover was placed on top and sealed. The weight of the assembly (pan, cover and sample) was measured using an electronic balance (Mettler Toledo AG204) with a precision and maximum range of ± 0.003 % mg and 210.0 mg respectively. The sample holder cell initial and maximum temperature were set at 30 $^{\circ}$C and 80 $^{\circ}$C respectively. In order to achieve the DSC signal stability, the sample was maintained at the initial temperature for 60 seconds and nitrogen purge gas used was kept at a rate of 50 mL/ min.

Hu et al. (Hu et al. 2017) explained that the uncertainties in the experimental results are dependent on the measurement deviations for each of the parameters, including mass and heat flow. Therefore, the specific heat capacity was obtained using Eq. (B.1) where C_p is the specific heat capacity, q is the heat flow, *'m'* is the weight, and the subscripts *'s'* and *'z'* denote sample and water.

$$C_{p,s} = C_{p,z}\left[\frac{\Delta q_s * m_z}{\Delta q_z * m_s}\right] \tag{B.1}$$

The propagation of uncertainties was calculated using the root-sum-square method [21] Eq. (B.2), where *'Q'* is given as any defined function of independent variables *'V'*. Finally, the uncertainty *'δQ'* of the function is as follows

$$\delta Q = \sum_{i=1}^{n}\left|\frac{\delta Q}{\partial V_i}\right|\delta V_i \tag{B.2}$$

The average heat flow and its uncertainty was 27.8mW and ± 0.2 respectively.

$$E_{\%} = \left[\frac{cp_{nf} - cp_{water}}{cp_{water}}\right] * 100 \quad \text{..... (B.3)}$$

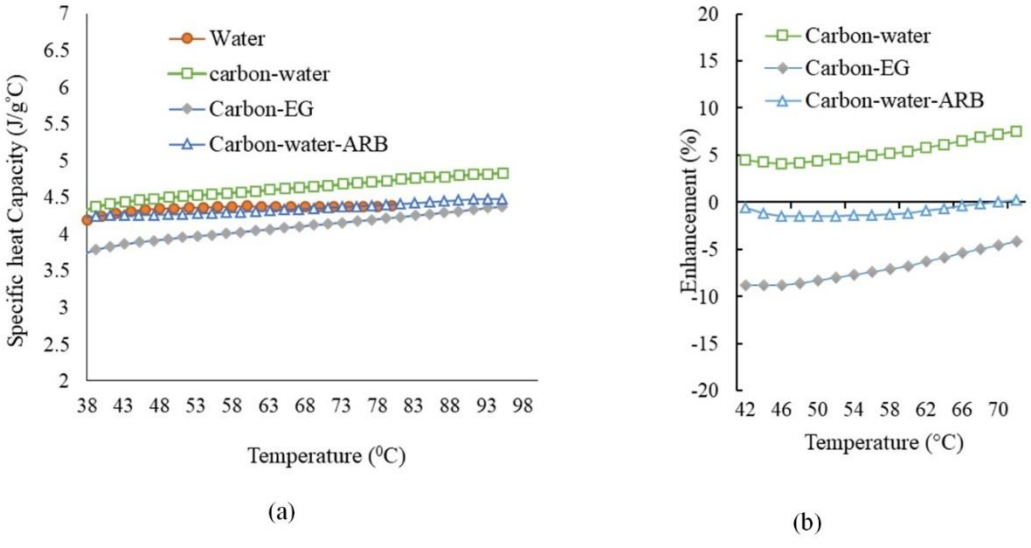

Figure B.6 Effect of activated carbon nanoparticles and surfactant on heat capacity (a) and (b) enhancement ratio as a function of temperature.

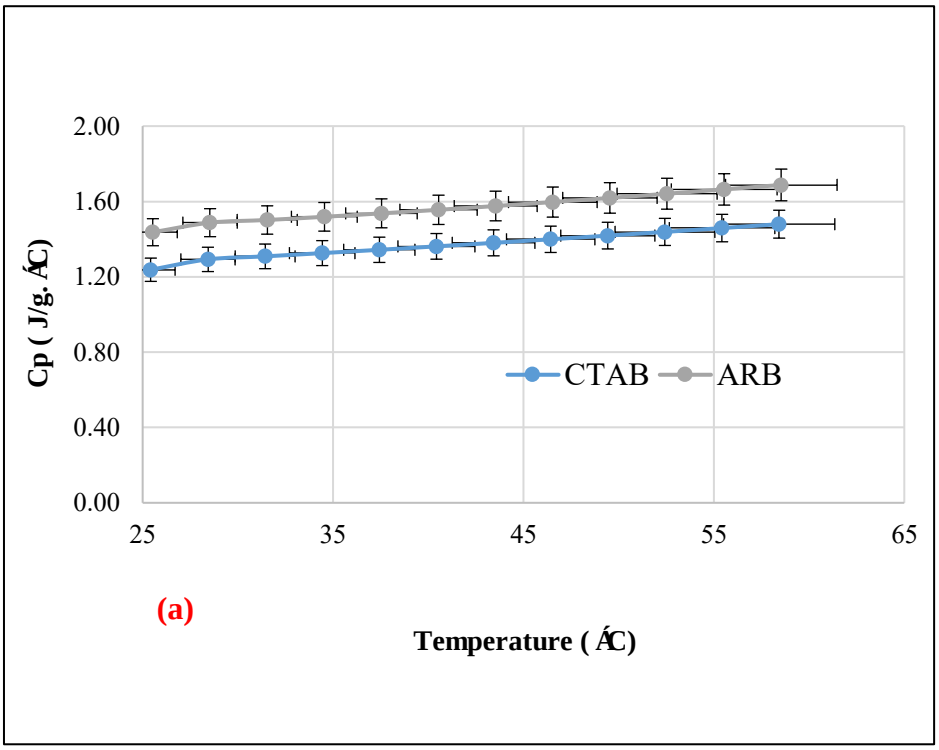

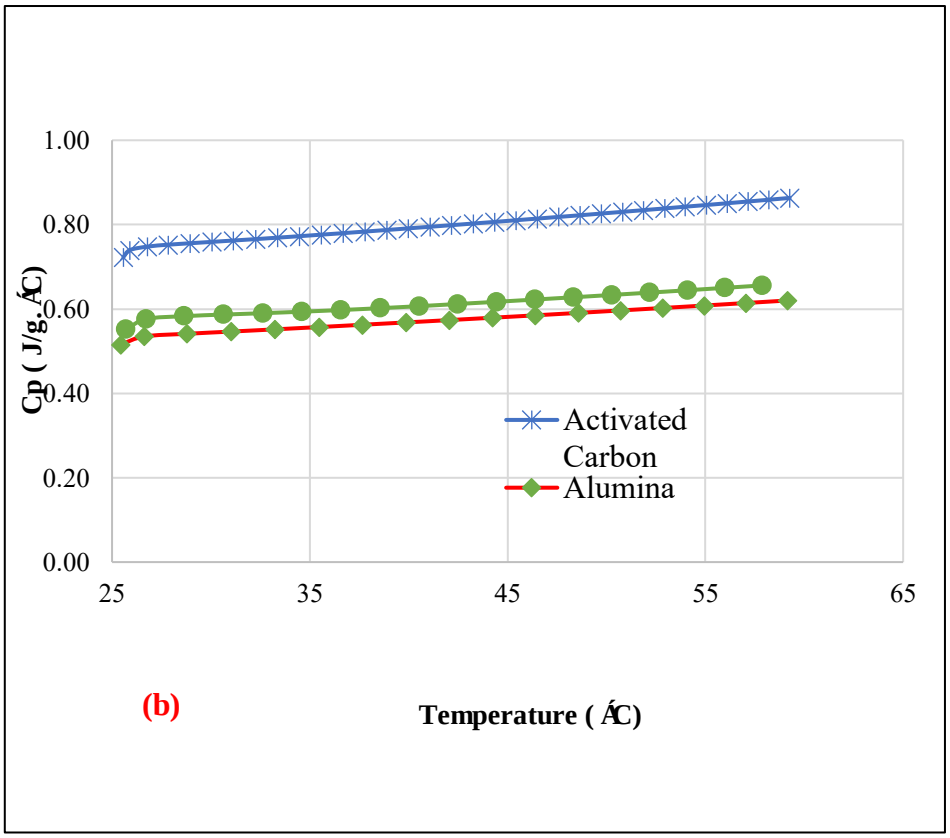

Figure B.7 Specific heat capacity measurements for surfactants (a) and (b) nanoparticles using a DSC

Appendix C

Experimental devices and calibration

C.1 Introduction

This Appendix presents additional information on calibration of devices used to build the test rig in Chapter 5; that was used to investigate heat transfer analysis of nanofluids.

C.2 Thermocouples

All thermocouples used to measure the temperatures from the test rig were T-type thermocouples and their temperature measurement range is from –270 to +370 °C. The thermocouples were calibrated using a temperature-controlled circulating water bath for temperatures in the range 0 °C to 65 °C and the ice point to provide an absolute calibration. The thermocouple temperatures were monitored using a Picolog TC-08 eight channel thermocouple DAQ system connected to a computer via the USB interface and manually recorded. The average standard deviation for the thermocouples was 0.3 °C. Considering the thermocouples accuracy which is ± 1.0 °C, the uncertainty of the temperature sensors was conservatively taken to be ± 1.3 °C.

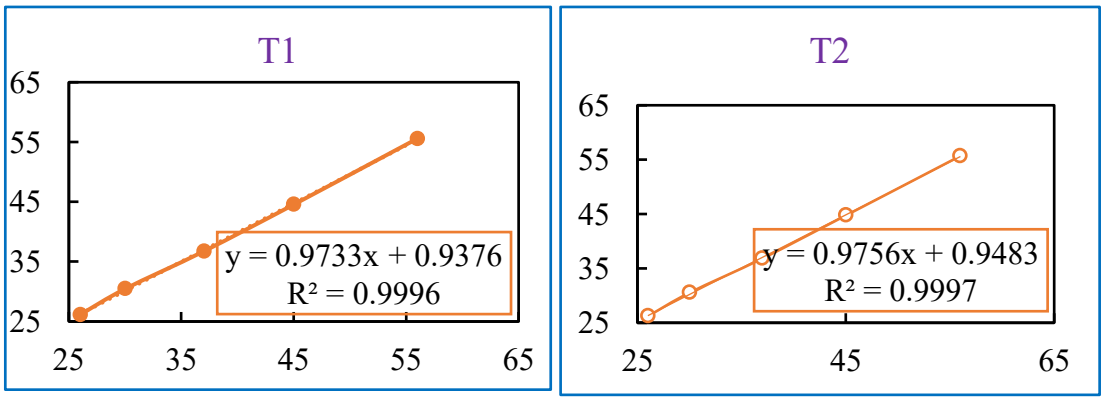

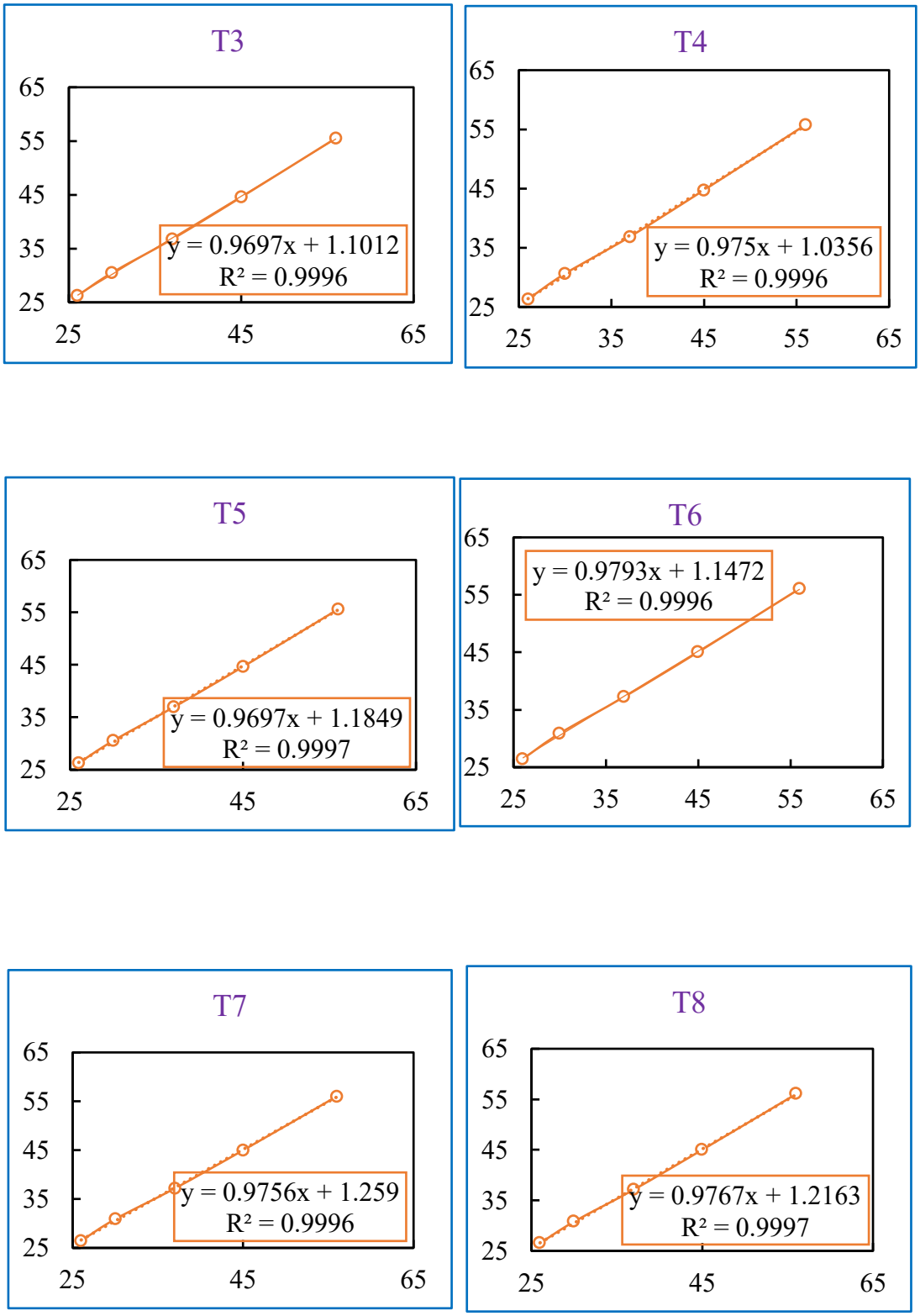

Figure C.1 Plotted graphs indicating thermocouple gain and offset from calibration.

C.3 Flow meters

Prior to test measurements, calibrations were conducted to validate the accuracy of the flow rates and this was achieved by using the bucket and stopwatch method. A total of 3 trials results showed a good agreement between the volume outputs against time as shown in Fig. C.3 and C.4 for tube and annulus side respectively. The standard deviation for this was found to be approximately 3 % of the measurement.

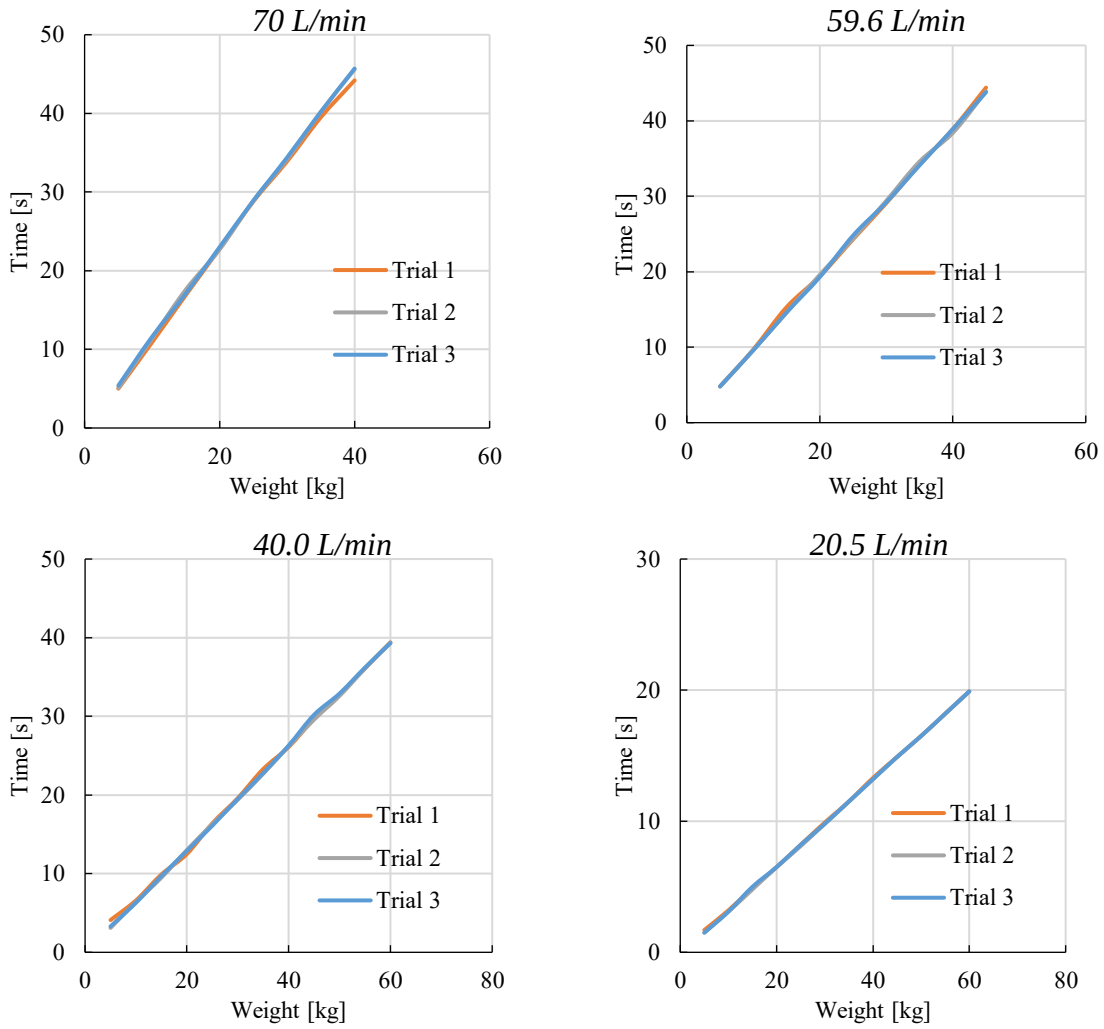

Figure C.2 Tube side flow meter calibration

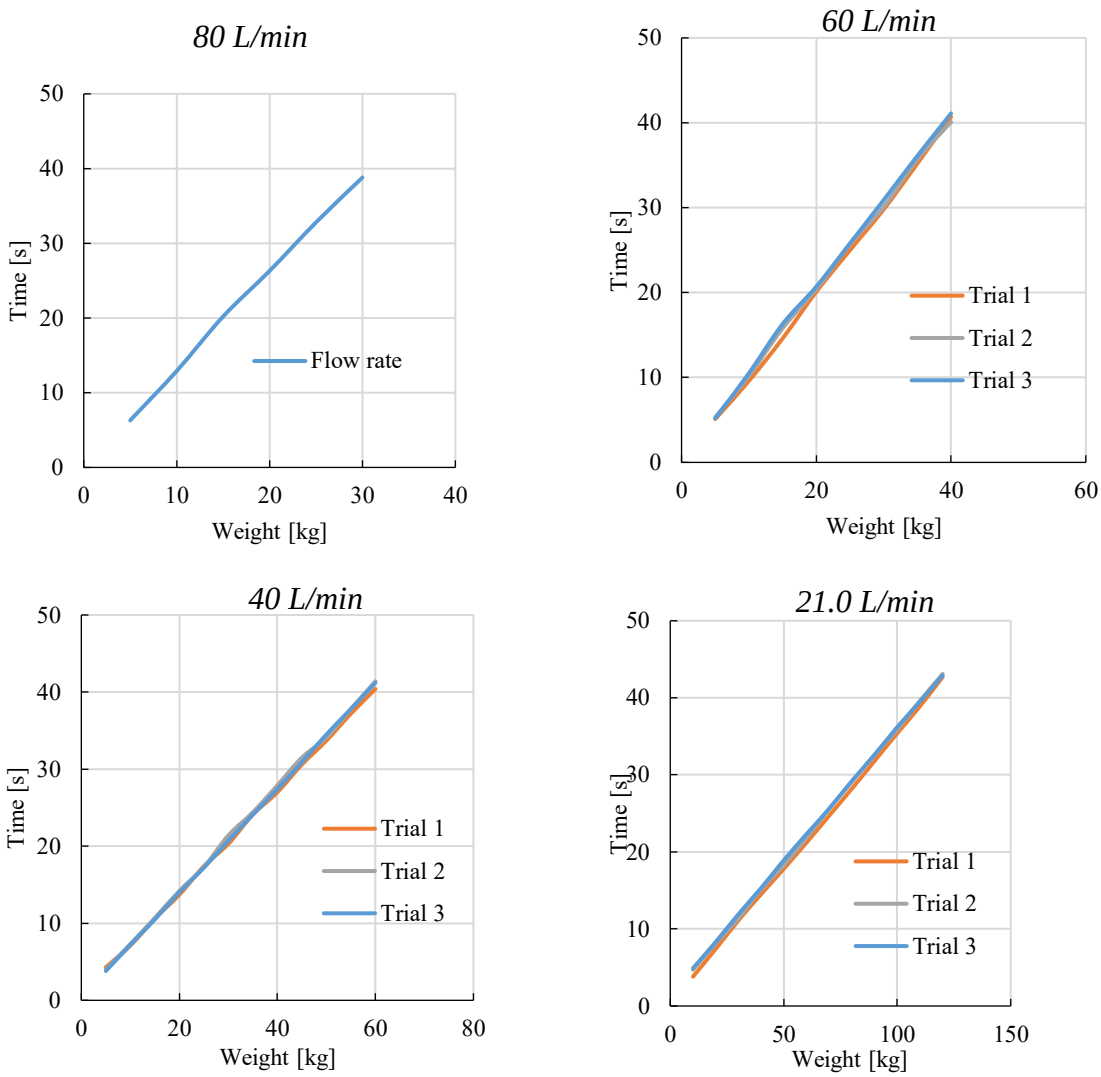

Figure C.3 Annulus side flow meter calibration

C.4 Pressure differential transmitter

The differential pressure transmitter was calibrated by connecting the high range value port to a hand pump to supply pressure while the lower range value port was left open to the atmosphere. The transmitter was spanned from 0 % to 100 % so that 1~ 5 V corresponded to 0 ~145 kPa respectively. Measured pressure was then compared with the gauge readings. Finally, graphs showing output signal against measured pressure and gauge readings are presented in Fig. C.4.

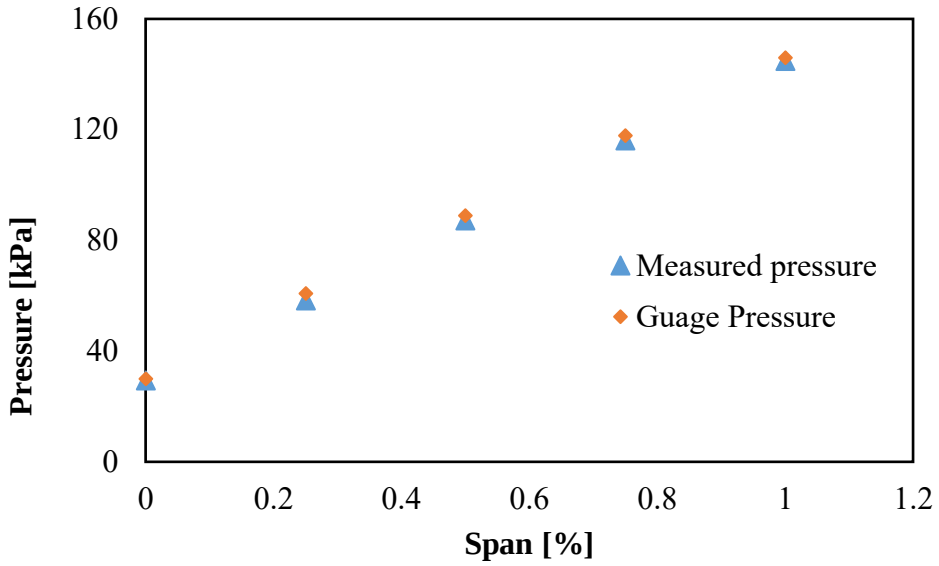

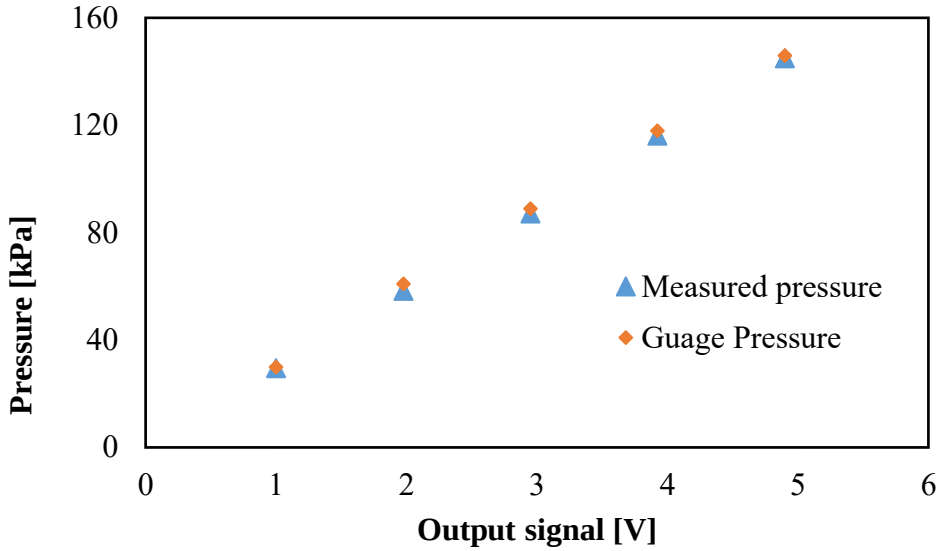

Figure C.4 Comparison between measured and gauge pressure

C.5 Heat exchanger

While using the double pipe heat exchanger, the flow pattern through a heat exchanger affects the required heat exchanger surface (Bengtson n.d.). For that reason, counter-current flow was opted to parallel flow. In counter-current flow, the fluid in the outer tube (annulus) flows in the opposite direction to that in the inner tube. This allows temperature difference of the fluids in the whole assembly of the heat exchanger to closely remain constant Fig. C.5, which allows more heat to be transferred thus increasing the efficiency of the system.

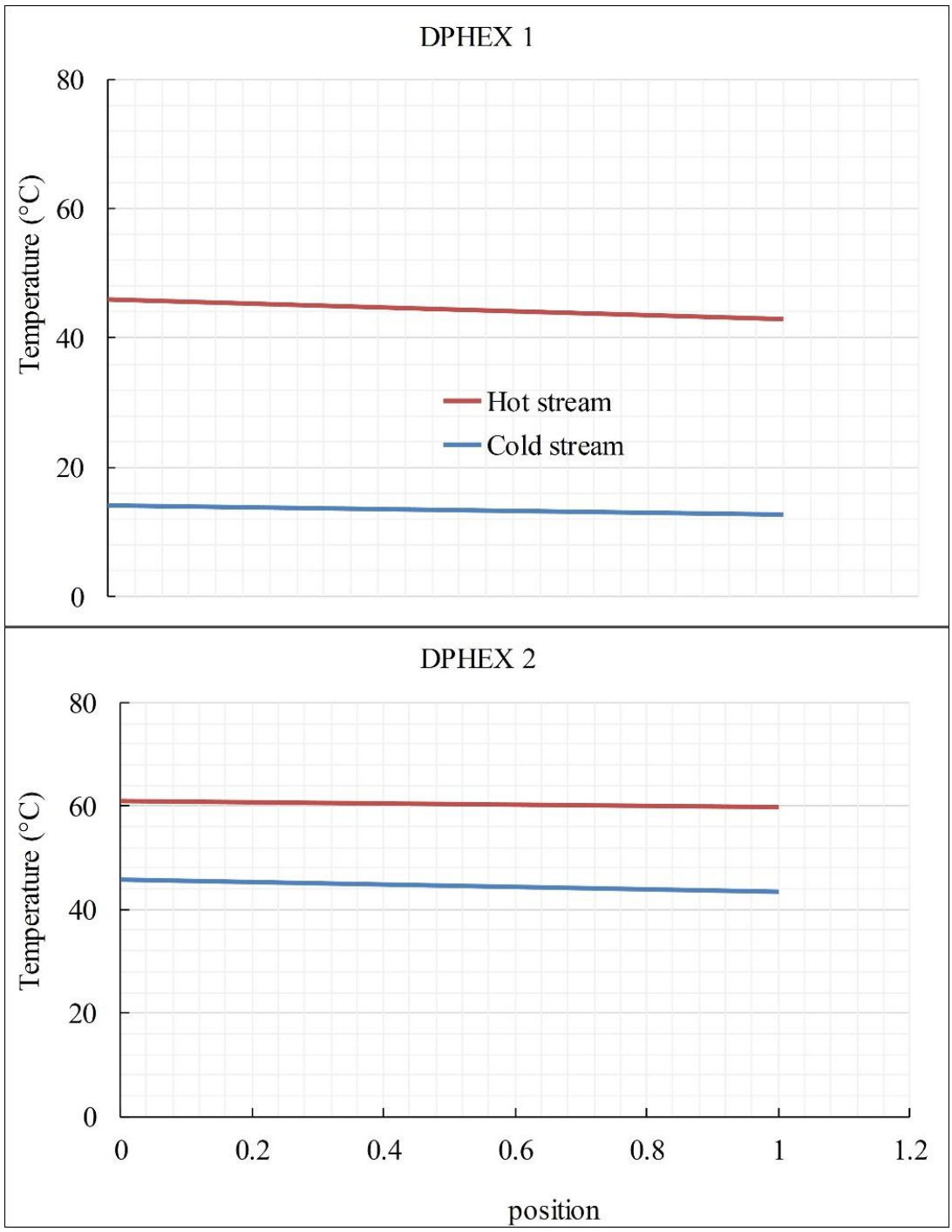

Figure C.5 Temperature profile for counter-current flow in the heat exchanger.

C.6 Rig support stand construction

A frame of 1.7 m high, 2.0 m length and 0.8 m wide was built using steel rods. Later, plywood was screwed on the frame to provide enough platform for the installation of all the instruments and devices on the stand (Fig. C.6). Four swivel wheel casters were fixed to the base to allow easy mobility of the rig and for future educational purposes.

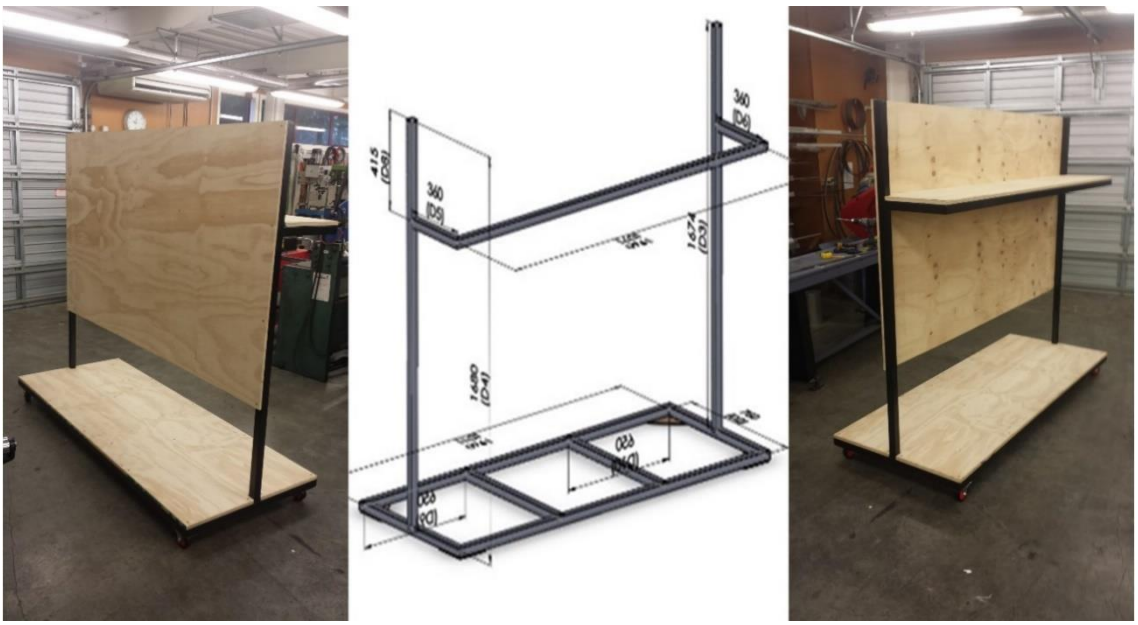

Figure C.6 Rig support stand and its dimensions.

Appendix D

Measurement procedure

D.1 Introduction

This part of the appendix presents additional information in Chapter 5 about how experimental data was obtained from the test rig and later processed on a spread sheet. It also details the uncertainty analysis and finally the standard operation procedure for running the constructed test rig used to evaluate heat transfer enhancements of nanofluids.

D.2 Data procedure and processing

This was done following steps below: First, we had to make sure that all connected devices are detected and readable by the logger. This was done by assigning devices to the correct channels. Later, the channels were configured to the correct parameters and units as illustrated in Fig. D.1 That is to say, the first 8 channels were specifically assigned to T-type thermocouples. Since this DAQ was limited to only to direct-current channels, 2 flow meters were assigned to those, and we employed a shunt resistor to convert 2 extra channels to allow the reading of direct voltage from other transmitters. Lastly, the gain and the offset from calibrations were set to respectful channels.

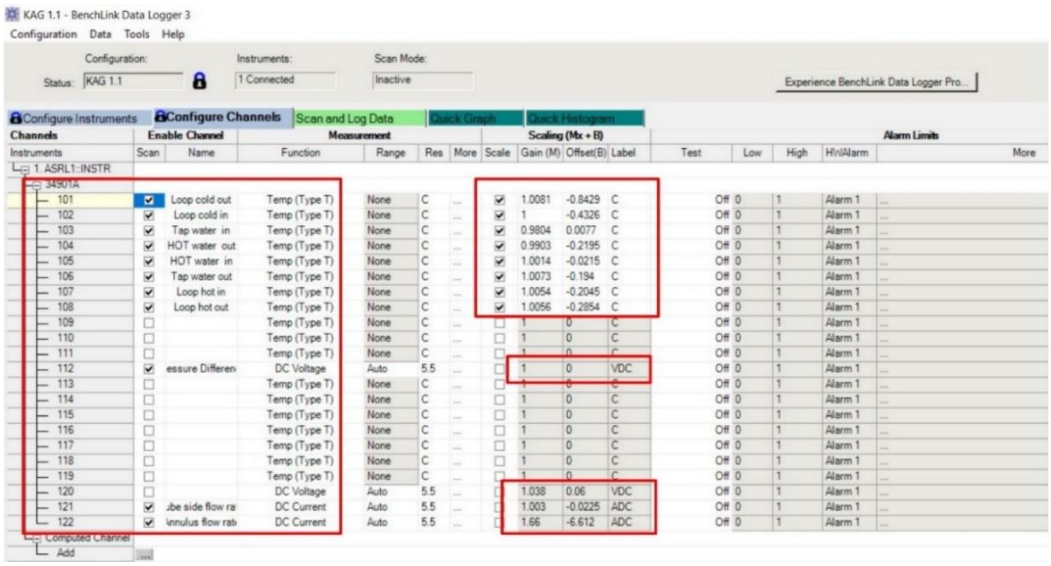

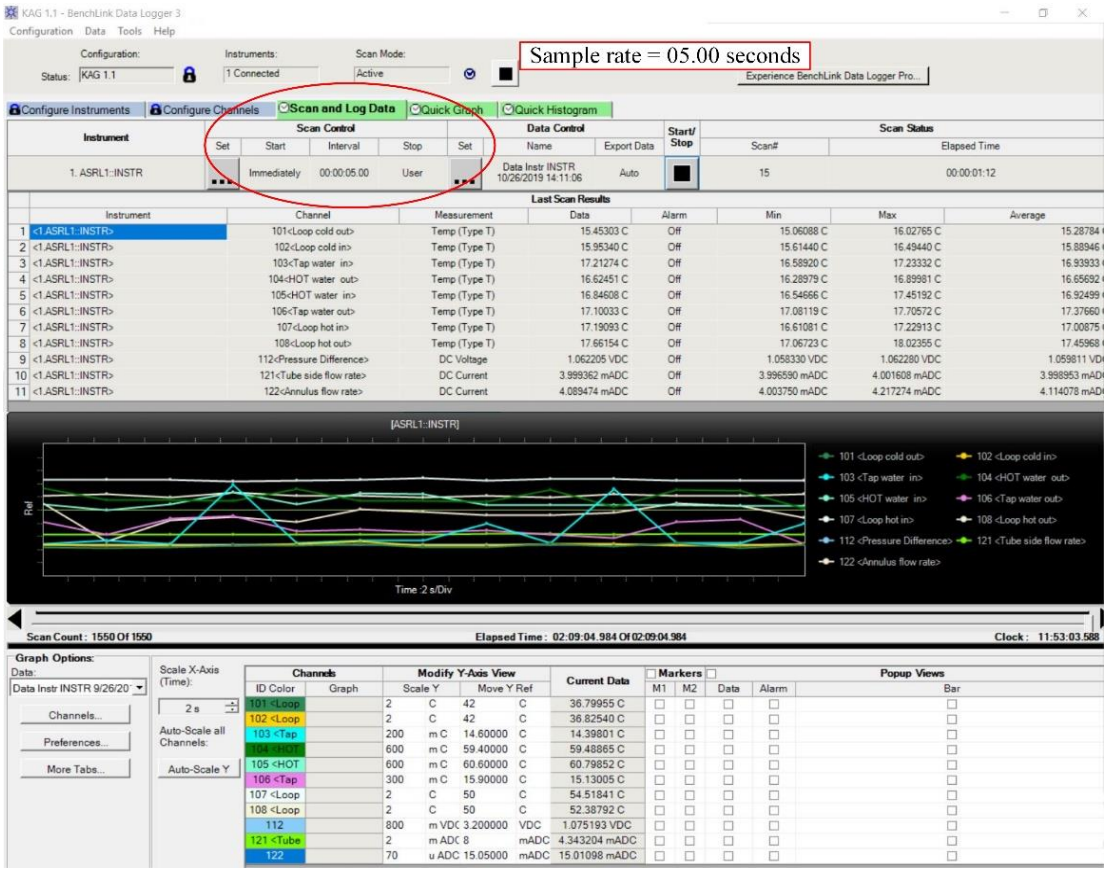

Figure D.1 Configuration of channels on DAQ

Secondly, a preferred sample rate of 5 seconds was considered. Since the signals from connected devices to the logger change rapidly in a short time, it was necessary to set a faster sample rate (Fig. D.2) for reliable data. With that in mind, the logger's internal timer was set to automatically scan data every after 5 seconds.

Immediately after scanning data for a duration of 5 to 6 hours, the next step was to process the data. The data-logger creates a comma separated values file (*CSV), but also allows the exportation of its CSV file to a selected folder and there is an option to be converted to an excel format as pictured in Fig. D.3.

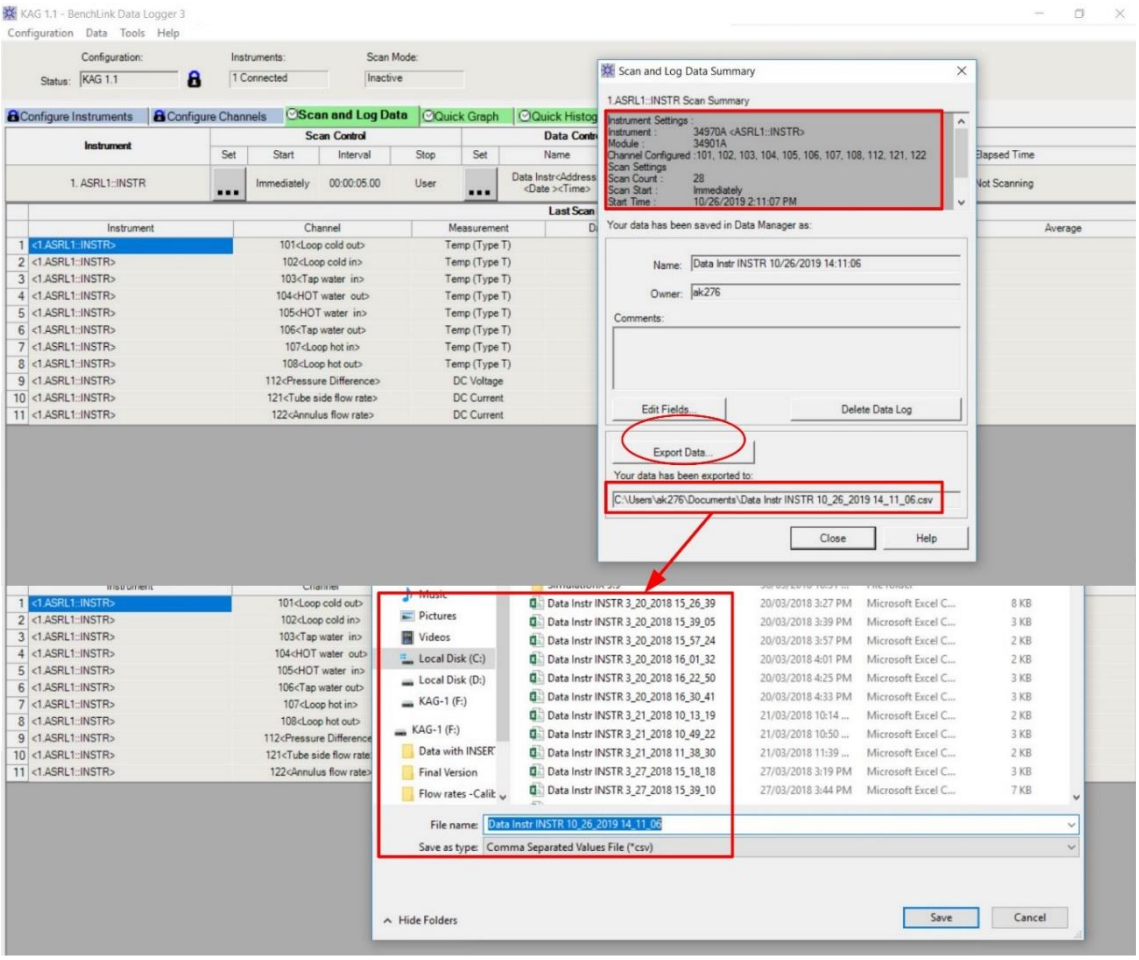

Figure D.2 Exportation of data prior to processing.

At the end of an experimental run, an Excel™ spreadsheet was created to process recorded data (see Fig. D.3). The recorded temperatures were automatically produced in degrees Celsius. However, pressure and flow rates were converted manually from electric signals to kPa and litres per minute respectively. On the same spreadsheet, further processing was done by creating several sheets; where individual data belonging to similar flow rate was processed. Thereafter, equations or formulas were used to calculate Reynolds number, local heat transfer coefficients and friction factor and their corresponding graphs were drawn.

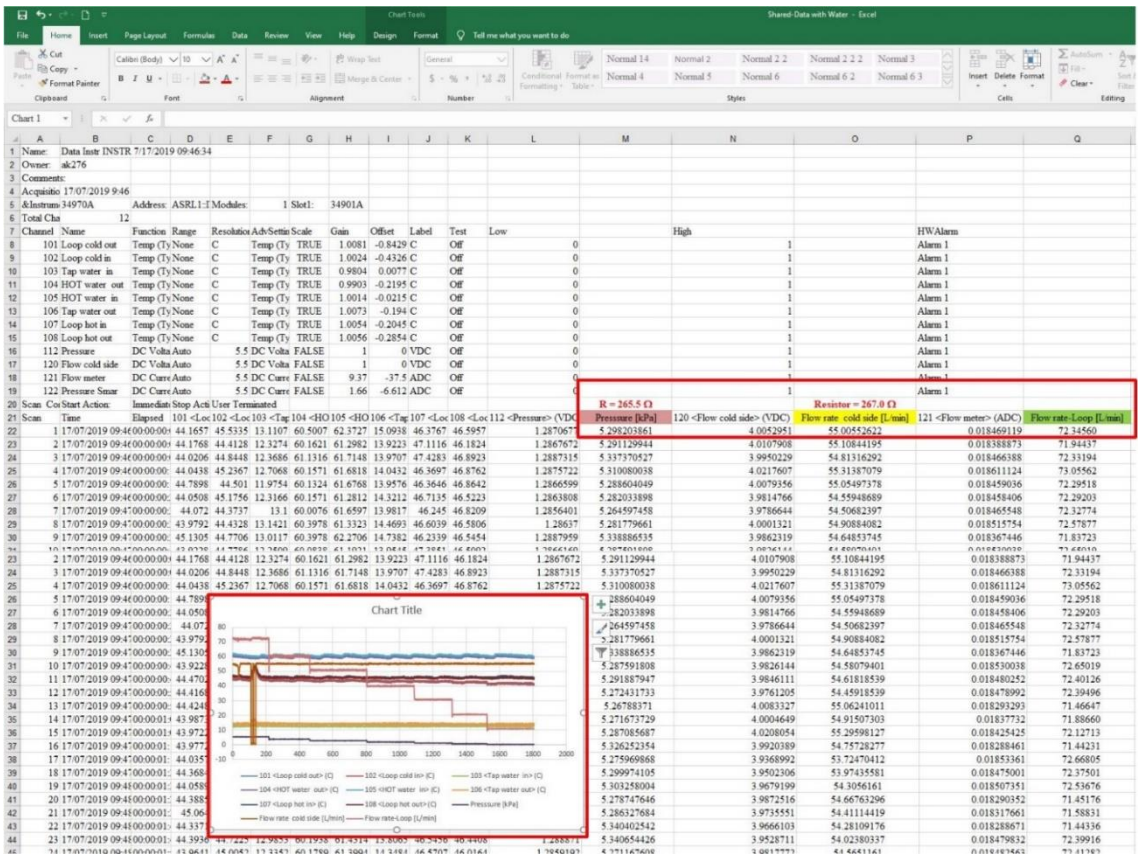

Figure D.3 Excel spreadsheet with processed data.

D.3 Uncertainty analysis

In this thesis a root-sum-square approach Eq. D.1 proposed by Kline and McClintock (McClintock 1953) was used to calculate the uncertainties.

$$\partial R = \left[\sqrt{\left(\frac{\partial a}{a}\right)^2 + \left(\frac{\partial b}{b}\right)^2 + \cdots + \left(\frac{\partial z}{z}\right)^2}\right] R \qquad \text{(D.1)}$$

Where 'R' is given as any defined function of independent variables (a, b and z). The uncertainty of each independent variable (e.g., ∂a) is obtained as

$$\partial a = \frac{\sigma}{\sqrt{n}} \qquad \text{(D.2)}$$

Where "σ" is the standard deviation and "n" is the number of measurements.

D.4 Uncertainty in heat transfer rate measurements

When determining the uncertainty in heat transfer rate ($\dot{Q}$), the heat transfer rate on the tube and shell-side is a function of mass flow rate ($\dot{m}$), specific heat capacity (Cp), and the temperature difference (ΔT) as shown in Eq. D.3

$$\dot{Q} = \dot{m} Cp \Delta T \tag{D.3}$$

Assuming that the uncertainty in the specific heat capacity is zero. The uncertainty of mass flow rate is given by Eq. D.4 as:

$$\frac{\partial \dot{m}}{\dot{m}} = \left[\left(\frac{\partial v}{v} \right)^{1/2} + \left(\frac{\partial \rho}{\rho} \right)^{1/2} \right]^{1/2} \tag{D.4}$$

The uncertainty in the inlet and outlet temperature difference on the tube-side ($\partial \Delta T_i$) and shell-side ($\partial \Delta T_o$) is obtained as:

$$\partial \Delta T_i = [(\partial T_1)^2 + (\partial T_7)^2]^{1/2} \tag{D.5}$$

$$\partial \Delta T_o = [(\partial T_3)^2 + (\partial T_6)^2]^{1/2} \tag{D.6}$$

By substituting the values of the measurements and the associated uncertainty ($\partial \dot{m}$, $\partial T\Delta_i$ and $\partial \Delta T_o$) in Eq. D.7, the uncertainty in tube-side heat transfer rate was found to be approximately ± 6 %.

$$\frac{\partial \dot{Q}}{\dot{Q}} = \left[\left(\frac{\partial \dot{m}}{\dot{m}} \right)^2 + \left(\frac{\partial Cp}{Cp} \right)^2 + \left(\frac{\partial \Delta T}{\Delta T} \right)^2 \right]^{1/2} \tag{D.7}$$

The energy balance ratio ($\propto$) was determined by comparing the heat transferred by the fluid in the shell-side (Q_o); with the thermal energy removed by the fluid in the tube-side of the heat exchanger (Q_i). The energy balance ratio presented in Fig. D.8 was defined as:

$$\propto = \frac{Q_i}{Q_o} \tag{D.8}$$

The average energy balance ratio was within approximately ± 9 %.

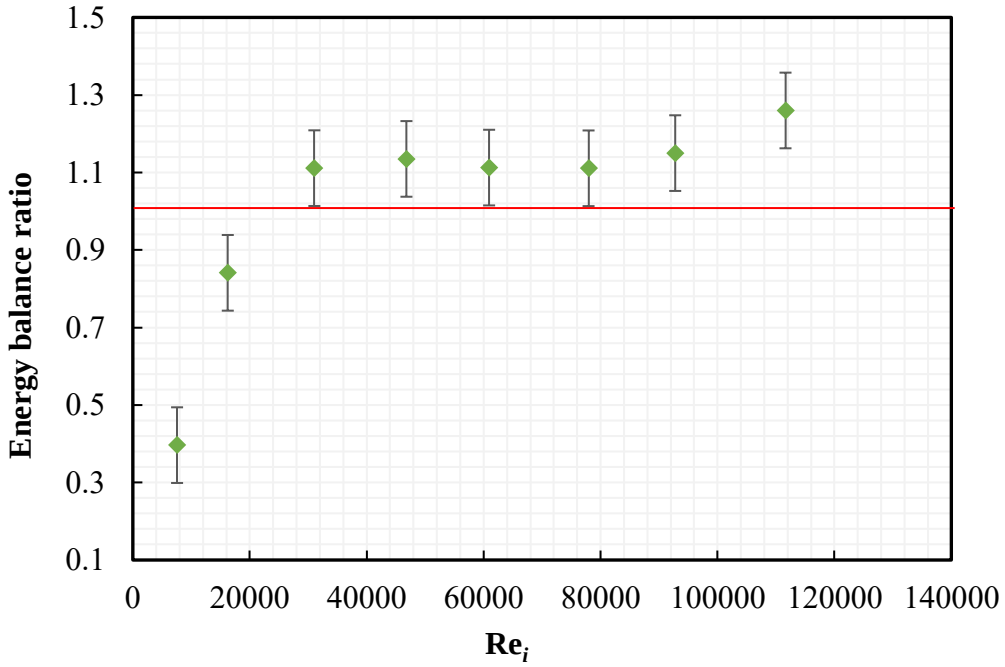

Figure D.4 The energy balance ratio of the test closed-loop for the testing system.

D.5 Uncertainty in overall heat transfer measurements

The overall heat transfer coefficient (U) is defined as a function of average heat transfer rate ($\dot{Q}_{avg}$), heat transfer area (A) and the logarithmic Mean Temperature Difference (ΔT_{LMD}) as shown in Eq. (D.9):

$$U = \frac{\dot{Q}_{avg}}{A\Delta T_{LM}} \tag{D.9}$$

The uncertainty in the overall heat transfer coefficient was determined from:

$$\frac{\partial U}{U} = \left[\left(\frac{\partial \dot{Q}_{avg}}{\dot{Q}_{avg}}\right)^2 + \left(\frac{\partial A}{A}\right)^2 + \left(\frac{\partial \Delta T_{LMD}}{\Delta T_{LMD}}\right)^2\right]^{1/2} \tag{D.10}$$

Where the uncertainty in the average heat transfer rate is given as:

$$\frac{\partial \dot{Q}_{avg}}{\dot{Q}_{avg}} = \left[\left(\frac{\partial \dot{Q}_i}{\dot{Q}_i}\right)^2 + \left(\frac{\partial \dot{Q}_o}{\dot{Q}_o}\right)^2\right]^{1/2} \quad \text{(D.11)}$$

The uncertainty in logarithmic Mean Temperature Difference (ΔT_{LMD}) was determined from the following expressions:

$$\partial \Delta T_A = [(\partial T_7)^2 + (\partial T_6)^2]^{1/2} \quad \text{(D.12)}$$

$$\partial \Delta T_B = [(\partial T_1)^2 + (\partial T_3)^2]^{1/2} \quad \text{(D.13)}$$

$$\frac{\partial \Delta T_{LMD}}{\Delta T_{LMD}} = \left[\left(\frac{\partial \Delta T_A}{\Delta T_A}\right)^2 + \left(\frac{\partial \Delta T_B}{\Delta T_B}\right)^2\right]^{1/2} \quad \text{(D.14)}$$

Where ΔT_A represent the temperature difference between inlet fluid temperatures on the tube-side (T_7) and outlet fluid temperatures from the shell-side. Whereas, ΔT_B represent the temperature difference between outlet fluid temperatures from the tube-side (T_1) and inlet temperatures of the fluid in the shell-side (T_3).

Assuming that the uncertainty in the heat transfer area (A) is zero, then substituting the values of the measurements and the associated uncertainty from Eqs. D.11 and D.14 in Eq. (D.10) the uncertainty for overall heat transfer was found to be approximately ± 17 %.

D.6 Uncertainty in friction factor

The friction factor (f) is a function of measured pressure drop (ΔP), inside tube diameter (D_i), the tube length (l), the fluid density (ρ) and the velocity of the fluid (v) as shown in Eq. D.15:

$$f = \frac{D_i}{l}\left(\frac{\Delta P}{\frac{1}{2}\rho v^2}\right) \tag{D.15}$$

Assuming the uncertainty in the inside tube diameter, the tube length and the fluid density is zero. The uncertainty in measured pressure drop was approximately ± 4 % whereas the uncertainty in fluid velocity was approximately ± 2 %. Therefore, by substituting the values of the measurements and the associated uncertainty in Eq. D.16, the uncertainty in friction factor was found to be approximately ± 0.5 %.

$$\frac{\partial f}{f} = \left[\left(\frac{\partial \Delta p}{\Delta p}\right)^2 + \left(\frac{\partial L}{L}\right)^2 + \left(\frac{\partial D_i}{D_i}\right)^2 + \left(\frac{2(\partial v)}{v}\right)^2\right]^{1/2} \tag{D.16}$$

D.7 Standard operation procedure

D.7.1 Starting the test rig

1. Open the charging valve and fill the fluid (water or nanofluids) into the system through a valve opening between the DPHEX 1.
2. Close the charging valve and monitor the closed loop to ensure that there is no leakage.
3. Turn on the pumps, flow meters, data-logger and the computer.
4. Control the test loop flow rates using a valve upstream the pump in the loop.
5. Steam is tapped from the wall to heat water in the tank. Therefore, open the valve from the wall to let steam run through the coil in the tank.
6. Open the valve under the hot water tank to let hot water circulate back and forth (recycled) through the annulus side of DPHEX 2.
7. Open the valve from the wall to let cold tap water circulate through the annulus side of DPHEX 1.
8. Wait until temperatures and the flow rates stabilise (achieve steady state). You can achieve this by monitoring the temperatures and the flow rates on the computer.
9. Record data using a data-logger attached to the computer for a desired duration.

10. Export the obtained data on an excel spreadsheet for further processing and analysis.
11. Repeat steps 4, 9, 10 and 11 to obtain different flow rates and other related parameters.

D.7.2 Shutting down the test rig

12. Safely close the steam valve on the wall.
13. Close the valve under the hot water tank.
14. Turn off the pumps and close the cold tap water valve on the wall.
15. Turn off all other devices (data-logger, computer and flow meters).
16. Open the Drain valve (downstream the pump) to empty the loop.

"A theory can be proved by experiment, but no path leads from experiment to the birth of a theory."

- Albert Einstein -

END